Decadal to centennial variability of (sub-) Arctic sea ice distribution and its paleoenvironmental significance

Kumulative Dissertation

zur Erlangung des akademischen Grades
eines Doktors der Naturwissenschaften

-Dr. rer. nat.-

an der Fakultät für Geowissenschaften
der Universität Bremen

vorgelegt von

Henriette Marie Kolling

Bremen, 15.11.2017

Gutachter der Dissertation

Prof. Dr. Rüdiger Stein
Prof. Dr. Michal Kucera

Erklärung

Hiermit versichere ich, dass die vorliegende Dissertation ohne unerlaubte fremde Hilfe angefertigt wurde, keine anderen als die von mir angegebenen Quellen und Hilfsmittel benutzt wurden und die den benutzen Werken wörtlich oder inhaltlich entnommenen Stellen als solche kenntlich gemacht wurden.

Affirmation

I affirm that I wrote the presented thesis independently and without illicit assistance from third parties, I used no sources other than those indicated nor aids other than those permissible, I appropriately referenced any text or content from other sources.

Bremen, 14.11.2017

Henriette Marie Kolling

Colloquium

Proxy reconstructions of modern and late Holocene sea ice conditions in the Baffin Bay

21. December 2017

“Where I live, the sea ice never stops. It's a living thing.”

Jayko Oweetaluktuk, Inukjuak, Nunavik, Labrador, Canada

Contents

List of Figures

List of Abbreviations

AIW	Atlantic Intermediate Water
AMO	Atlantic Multidecadal Oscillation
AMOC	Atlantic Meridional Overturning Circulation
ASE	Accelerated Solvent Extractor
AWI	Alfred Wegener Institute, Helmholtz Centre for Polar and Marine Research
BG	Beaufort Gyre
BIC	Baffin Island Current
BP	Before Present (1950)
BSTAF	bis-trimethylsilyl-trifluoroacet-amide
CCA	Correspondence Analysis
CE	Common Era (starting 1950)
DACP	Dark Ages Cold Period
DCA	Detrended Correspondence Analysis
DFG	Deutsche Forschungsgemeinschaft
DIP_{25}	Ratio of HBI II and IP_{25}
EGC	East Greenland Current
GC	Gravity Core
GC-MSD	Gas Chromatograph coupled with a Mass Selective Detector
GIS	Greenland Ice Sheet
GKG	Box Core
GSA	Great Salinity Anomaly
HBI	Highly Branched Isoprenoid
HTM	Holocene Thermal Maximum
IC	Irminger Current
IP_{25}	Ice Proxy with 25 carbon atoms
IPCC	Intergovernmental Panel on Climate Change
$IPSO_{25}$	Ice Proxy with 25 carbon atoms for the Southern Ocean
IRD	Ice Rafted Debris
LC	Labrador Current
LIA	Little Ice Age
MAT	Modern Analogue Technique
MCA	Medieval Climate Anomaly
MIS	Marine Isotope Stage
MUC	Multi Core
MWP	Medieval Warm Period
NAC	North Atlantic Current
NADW	North Atlantic Deep Water
NAO	North Atlantic Oscillation
NC	Norwegian Current
ODV	Ocean Data View (software)
PIP_{25}	Phytoplankton - IP_{25} sea ice index
RAC	Return Atlantic Current
RDA	Redundancy Analysis
RWP	Roman Warm Period
SIM	Selected Ion Mode

SiO_2	Silicon Dioxide
SPG	Subpolar Gyre
SST	Sea Surface Temperature
THC	Thermohaline Circulation
TIC	Total Ion Current
TOC	Total Organic Carbon
TPD	Transpolar Drift
US	Sonication
WGC	West Greenland Current
WSC	West Spitsbergen Current
YD	Younger Dryas

Abstract

Arctic sea ice has major impact on the global climate as it affects the energy budget of the Earth and its export from the Arctic towards the North Atlantic has direct influence on the global ocean circulation. The observed modern sea ice loss, mainly associated with anthropogenic greenhouse gas emissions, has raised the concern about the role and natural variability of sea ice and its relation to short term changes in the climate system. The reconstruction of past sea ice changes based on sediment cores and analyses of specific proxies provides vital knowledge about the natural variability of sea ice in pre-industrial times. Moreover it helps to understand the present changes and may improve estimates for future changes and consequences.
Particular important areas for sea ice reconstructions are the shelves around Greenland. They connect the Arctic Ocean to the North Atlantic and underlie the major outflow of freshwater and sea ice from the Central Arctic. In this context, a specific interval of interest for climate reconstructions is the late Holocene, as it exhibits modern boundary conditions, i.e., oceanography and geography, and encompasses several well-known short-term climate events, e.g., the Medieval Warm Period and Little Ice Age.

For past sea ice conditions and open water phytoplankton production, the application of specific biomarkers, i.e., highly branched isopenoids (IP_{25}, HBI III) and sterols (brassicasterol and dinosterol) have proven as useful and reliable proxies. However, their applicability, especially in regard to HBI III, is mostly confirmed on regional scales so far. The PIP_{25} index, the ratio of IP_{25} to an open water phytoplankton biomarker, is used for a more quantitative sea ice reconstructions.

Aim of this study is to confirm the IP_{25}/PIP_{25} approach in surface sediments on an over-regional scale and for specific regions, i.e., the Baffin Bay, by comparing them to satellite-derived modern sea ice concentrations. Further the PIP_{25} approach is compared to other common microfossil methods, i.e., dinocysts and diatoms, for sea ice reconstructions. Following this, two well-dated cores from the East Greenland Shelf (PS2641-4/PS2641-5) and the West Greenland Shelf (MSM05/3-

343310) covering the last 5.2 and 2.2. kyr BP, respectively, were analysed for their biomarker content.

By analysing a nearly circum-Arctic surface sediment database that combines new and published data, the distribution of IP_{25} and specific open water phytoplankton sterols (brassicasterol, dinosterol) could be related to modern, satellite derived sea ice conditions in (sub-)Arctic regions. In regard to the phytoplankton marker HBI III, we find promising results in its distribution in relation to sea ice, however some regions remain unclear. The circum-Arctic distribution of the sea ice index PIP_{25}, (i.e., P_BIP_{25}, P_DIP_{25} and $P_{III}IP_{25}$) can be related to the modern spring sea ice distribution. However, the direct correlation to modern sea ice concentrations remains difficult for specific areas, i.e., the Central Arctic Ocean and the Russian shelves, which may be related to complex environmental conditions.

A regional comparison of the PIP_{25} and MAT dinocyst reconstructions in the Baffin Bay revealed that both methods show a positive correlation with modern sea ice concentrations, with slightly higher correlations of the $P_{III}IP_{25}$ index. Further, diatom assemblages from the Baffin Bay, show highest correlations to modern spring sea ice, however the over regional application remains questionable.

In regard to the paleo sea ice reconstructions we find specific variabilities on the East and West Greenland shelves.
A mid- to late Holocene (last 5.2 kyr BP) sea ice reconstruction from the East Greenland Shelf revealed that IP_{25}/PIP_{25} index based sea ice reconstructions do not reflect the wide-spread late Holocene Neoglacial cooling trend that follows the decreasing solar insolation pattern. This may be related to the strong influence of the polar East Greenland Current on the East Greenland Shelf and interactions with the adjacent fjord system throughout the studied time interval. However, several oscillations with increasing/decreasing sea ice concentrations that are linked to the known late Holocene climate cold/warm phases, i.e., the Roman Warm Period, Dark Ages Cold Period, Medieval Climate Anomaly and Little Ice Age, were revealed. The observed changes seem to be related to general ocean/atmosphere circulation changes, possibly related to North Atlantic Oscillation and Atlantic Multidecadal Oscillation regimes.

On the West Greenland Shelf, at the mouth of Disko Bugt, however, biomarker sea ice reconstructions from the late Holocene indicate a gradual expansion of sea ice over the past 2.2 kyr following the Neoglacial cooling. Maximum sea ice conditions were reached during the Little Ice Age and we find evidence for the presence of a stable spring ice edge around 0.2 kyr BP. The Disko Bugt record revealed no other clear evidence for sea ice changes related to late Holocene climate events. However, superimposed on the general trend, a short-term oscillation in open water primary production and terrigenous input may be related to changes in the Atlantic Multidecadal Oscillation and solar activity as trigger mechanism.

Within this thesis the nearly Arctic wide application of IP_{25} as sea ice proxy and the regional correlation of the PIP_{25} index with modern sea ice concentrations was further approved. The studies revealed substantial differences between East and West Greenland Shelf sea ice conditions during the Holocene. The studied location on the East Greenland Shelf was highly sensitive for small-scale Holocene climate events whereas the West Greenland Shelf reflected the general Neoglacial cooling trend.
Further studies will improve the knowledge on the application of the biomarker sea ice reconstruction approach and the relationship of East and West Greenland sea ice development in late Holocene times.

Kurzfassung

Die Meereisbedeckung im Arktischen Ozean hat großen Einfluss auf das globale Klima der Erde, denn es beeinflusst ihr Energiebudget. Des Weiteren hat der Export von Meereis aus der Arktis in den Nordatlantik direkten Einfluss auf die globale Ozeanzirkulation.

Die in den letzten Dekaden beobachtete Abnahme der arktischen Meereisbedeckung, die mit dem gestiegenen anthropogenen Treibhausgasausstoß in Verbindung gebracht wird, hat die Aufmerksamkeit und das Interesse an den natürlichen Schwankungen und deren Einfluss auf kurzfristige Klimaschwankungen erhöht.

Durch die Rekonstruktion von vergangenen Meereisschwankungen anhand der Analyse spezifischer Proxies in Sedimentkernen können wichtige Informationen über die natürliche Meereisvariabilität in vorindustriellen Zeitspannen gewonnen werden.

Des Weiteren tragen diese Rekonstruktionen dazu bei, die gegenwärtigen Veränderungen zu verstehen und zukünftige Veränderungen und die damit verbundene Konsequenzen besser vorherzusagen.

Die Kontinentalschelfe von Grönland sind ideale Gebiete für die Rekonstruktionen von vergangenen Meereisschwankungen. Sie formen die Verbindung des Arktischen Ozeans mit dem Nordatlantik und liegen unter dem Hauptstrom von Süßwasser und Meereis aus der zentralen Arktis.

In diesem Zusammenhang sind für Klimarekonstruktionen bestimmte Zeitintervalle, wie das Spät-Holozän, von besonderem Interesse, da in diesen Intervallen bereits die modernen Rahmenbedingungen, wie Ozeanographie und Geographie, bestanden und in diesen bestimmte, weitbekannte kurzzeitige Klimaereignisse stattfanden, wie z.B. die Mittelalterliche Klimaanomalie und die Kleine Eiszeit.

Um vergangene Meereisbedingungen und Phytoplanktonproduktion zu rekonstruieren, haben sich bestimmte Biomarker, sogenannter hochverzweigte Isoprenoide (IP_{25}, HBI III) sowie Sterole (Brassicasterol und Dinosterol), als nützliche und verlässliche Proxies erwiesen. Indes ist ihre Anwendung, besonders im Bezug auf das HBI III, weitgehend nur regional bestätigt.

Der aus dem Verhältnis von IP_{25} und einem Phytoplanktonbiomarker errechnete PIP_{25} Meereisindex kann für qualitativere Aussagen über Meereisbedingungen angewendet werden.

Im Rahmen dieser Dissertation soll durch den Vergleich von modernen, durch Satelliten gemessenen Meereiskonzentrationen die Anwendbarkeit des Meereisbiomarkers IP_{25} und des PIP_{25} Meereisindizes in bestimmten Regionen, wie der Baffin Bay, bestätigt werden.

Des Weiteren soll der PIP_{25} Meereisindex mit anderen gebräuchlichen Meereisrekonstruktionen basierend auf Mikrofossilien, wie Dinozysten und Diatomeen, verglichen werden. Nachfolgend, werden zwei gut datierte Sedimentkerne vom Ostgrönlandshelf (PS2641-4/PS2641-5) sowie vom Westgrönlandshelf (MSM05/3-343310), die jeweils die letzten 5.2 und 2.2. kyr BP repräsentieren, auf ihren Biomarkergehalt analysiert.

Durch die Analyse eines nahezu zirkumarktischen Oberflächensedimentdatensatzes, der neue und bereits publizierte Daten miteinander verbindet, konnte die Verteilung von IP_{25} und spezifischen Phytoplanktonsterolen mit den modernen, satellitenbasierten Meereisbedingungen in (sub-)arktischen Regionen verknüpft werden. Die Verteilung des relativ neuen Phytoplanktonbiomarkers HBI III zeigt im Bezug auf die Meereisbedingungen im zirkumarktischen Vergleich vielversprechende Ergebnisse. Für bestimmte Regionen bleibt der direkte Zusammenhang jedoch schwierig.

Die überregionale Verteilung des Meereisindizes PIP_{25} (P_BIP_{25}, P_DIP_{25} und $P_{III}IP_{25}$) reflektiert die modernen Meereiskonzentrationen relativ gut. Die direkte Korrelation mit den modernen Meereiskonzentrationen bleibt jedoch für bestimmte Regionen, wie die zentrale Arktis und die russischen Schelfmeere, schwierig. Dies scheint durch komplexe Umweltbedingungen in diesen Regionen begründet zu sein.

Der regionale Vergleich von Meereisrekonstruktionen basierend auf PIP_{25} und MAT Dinozysten aus der Baffin Bay zeigte, dass beide Methoden positiv mit den modernen Meereiskonzentrationen korrelieren, wobei die höchsten Korrelationen

für den $P_{III}IP_{25}$ Index gefunden wurden. Des Weiteren zeigen Diatomeengesellschaften in der Baffin Bay hohe Korrelationen mit den modernen Frühlingsmeereiskonzentrationen, indes bleibt eine überregionale Anwendbarkeit dieser Methode offen.

Bezüglich der Rekonstruktion vergangener Meereisbedingungen auf den Schelfen von Ost- und Westgrönland konnten konkrete Unterschiede in der Entwicklung der spätholozänen Meereisbedeckung gefunden werden.
Die Meereisrekonstruktion des mittleren und späten Holozäns (die letzten 5.2 kyr BP), basierend auf IP_{25} und PIP_{25} Index, deutet darauf hin, dass das weitverbreitete spätholozäne Neoglazial, welches mit der abnehmenden Insolation verbunden wird, sich nicht in den Sedimenten des Ostgrönlandschelfes widerspiegelt. Diese Ergebnisse werden für den untersuchten Zeitraum, mit dem starken Einfluss des Ostgrönlandstroms sowie des nahegelegenen Fjordsystems auf den Ostgrönlandshelf in Verbindung gebracht. Indes konnten kurzfristige Schwankungen in der Meereisbedeckung mit bekannten spätholozänen Warm-/Kaltphasen, wie dem Klimaoptimum der Römerzeit, den Dunklen Jahrhunderten, der Mittelalterlichen Warmzeit und der Kleinen Eiszeit, in Verbindung gebracht werden. Die beobachteten Schwankungen scheinen mit großräumigen ozeanographischen und atmosphärischen Veränderungen, wie etwa der Nordatlantischen Oszillation und der Atlantischen Multidekaden-Oszillation, einher zu gehen.

Auf dem westgrönländischen Schelf, nahe der Disko Bucht, hingegen scheint die kontinuierliche Ausdehnung der Meereisbedeckung während der letzten 2.2 kyr dem Neoglazial zu folgen. Die maximale Ausdehnung des Meereises wurde während der Kleinen Eiszeit erreicht. Diesbezüglich wurden Hinweise für die Entwicklung eines stabilen Eisrandes an/nahe der Kernlokation um 0.2 kyr BP gefunden wurden. Die Ergebnisse aus der Disko Bucht deuten nicht auf kleinskalige Veränderungen der Meereisbedeckungen in Bezug auf spätholzäne Klimaereignisse hin. Indessen deuten kurzfristige Schwankungen innerhalb der Primärpoduktion und des terrigenen Eintrages auf einen Zusammenhang mit der Atlantischen Multidekaden Oszillation, die durch Sonnenaktivität verursacht wurden, hin.

Im Rahmen dieser Dissertation wird die nahezu arktisweite Korrelation des Meereisproxies IP_{25} und die regionale Anwendbarkeit des Meereisindexes PIP_{25} neuerlich bestätigt. Die Meereisrekonstruktionen von Ost- und Westgrönlandshelf zeigen deutliche Unterschiede in der Meereisbedeckung während des späten Holozäns. Die untersuchte Lokation auf dem Ostgrönlandschelf zeigt kleinskalige Schwankungen, die mit bekannten Klimaereignissen in Verbindung zu stehen scheinen, wohingegen der Westgrönlandschelf den generellen Klimatrend des Neoglazials widerspiegelt.

Weitere Untersuchungen werden zum Verständnis der Anwendbarkeit von Biomarkern für Meereisrekonstruktionen beitragen sowie zu einem erhöhten Verständnis über die Zusammenhänge zwischen Ost- und Westgrönlandshelf während des Holozäns beitragen.

Acknowledgements

During the time of my PhD I had the opportunity to gain extraordinary experiences and learn things I never dreamed of. First of all, I am deeply grateful to Prof. Dr Rüdiger Stein, who gave me the opportunity of this PhD. During the last years you rewarded me with a lot of trust, time, support and experiences between Bremerhaven, Canada and the Arctic Ocean. I would like to thank you especially for your support and patience with publishing papers and giving me the opportunity to join two expeditions.

I want to thank my second supervisor, Prof. Dr. Michal Kucera, for reviewing my thesis and also for continuous input and support during my committee meetings and other ArcTrain meetings.

Very special and heartfelt thanks to Kirsten Fahl, who was and is a continuous support in the field of geochemistry, paper writing and publishing, and a constant source of positivity – even if not present there was always a box of 'positivity' on her desk which helped me through some late-night shifts at AWI.

I would also like to express my gratitude to Anne de Vernal who completed my thesis committee and made my time at UQAM, Montreal a very pleasant and fruitful research stay.

My deepest appreciation goes to Kerstin Perner and Matthias Moros, who provided samples, helped me to sort the puzzle pieces of our different proxies and assisted with publishing papers. I would also like to thank Jens Matthiessen, Henning Bauch and Andrea Jaeschke for help and lively discussions.

This thesis was part of the ArcTrain programme, to which I owe a very important dept. It enabled me to participate in conferences and take part in unique experiences during the 2015 Summer School in the Torngat Mountains and during the three wonderful summer schools. I want to thank my fellow ArcTrain PhDs for this wonderful time. Special thanks to Mischa (for helping with sea ice data) and of course Annegret, Tilia, Kerstin and Andrea – we shared so many beautiful moments, you welcomed me Bremen and made me feel at home wherever we were.

To my office mates and PhD 'sisters', Anne and Tanja, and our 'Norwegian guests' Caro and Henrik: you made our office and lab (and wherever we were) a happy place, thank you for all the fun, help and comfort. You made going to work fun! Also, many thanks to Thomas, Verena, Nadine, Nicole, Kevin, Jeetendra, Junjie, Xiaotong, Marc, Nele and Elena.

In 2014 and 2015, I was allowed to join two unique expeditions to the Central Arctic and the Baffin Bay, I had such a great time during PS87 and MSM44 thanks to Onkel Robert, Matze, Lina, and Maren.

Lieber Walter, vielen Dank für deine Unterstützung, Hilfe und Geduld im Labor! Es war eine wirklich schöne Zeit mir dir. Ich möchte außerdem Santi für deine tolle Hiwi-Arbeit und Rita Froehlking-Teichert, Susanne Wiebe und Michael Seebeck für eure Hilfe im Labor danken.

Vielen lieben Dank an Catherine, Laura und Ina.

Zu guter Letzt danke ich von ganzem Herzen meiner Familie: meinem Bruder Jakob und meinen Eltern, ihr habt an mich geglaubt, wenn ich es nicht getan hab. Danke für eure Unterstützung!

1. Introduction

1.1. Sea ice - modern distribution, variability and significance

Throughout the recent geological epoch, the Holocene (11.7 kyr - present), the Arctic Ocean and parts of its adjacent seas have been covered by sea ice, which influenced the climate and thereby the population history and the development of our modern culture in the Northern Hemisphere.

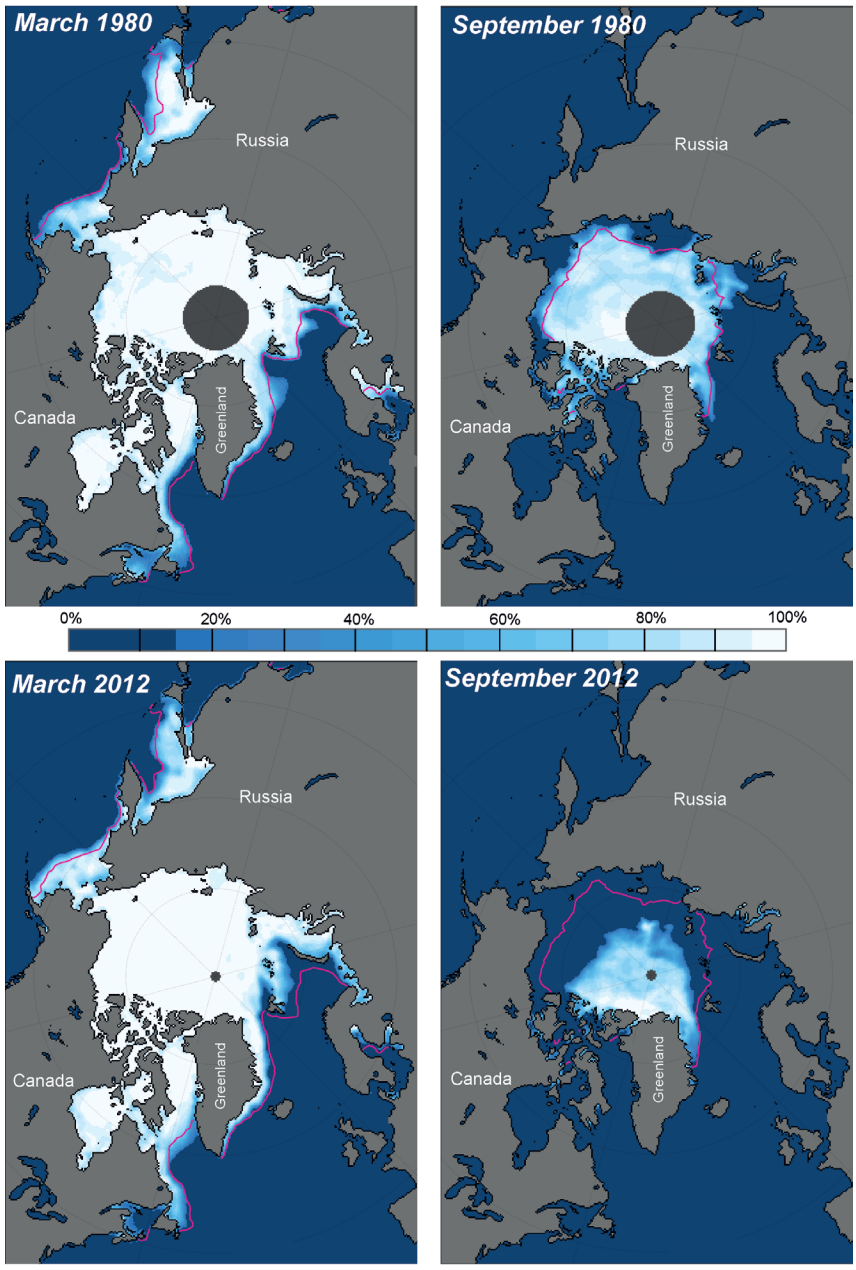

Fig 1. 1 Satellite derived Arctic sea ice extent in March and September 1980, which represent an average sea ice extent for the time period between 1979-2000. And the sea ice extent in March and September 2012, during which the lowest sea ice extent has been observed so far. The pink line represents the average sea ice extent for the corresponding months from 1979-2000. The grey dot around the North Pole indicates areas not covered by satellite measurements. Figures adapted from *nsidc.org*

The Arctic sea ice has declined rapidly throughout the last decades, which is most likely caused by anthropogenic greenhouse gas emissions *(IPCC, 2014; Swart, 2017)*. This reduction in Arctic sea ices and has become the symbol of anthropogenic climate change and is a prominent topic in public media. The public concern is mainly with the fate of this unique ecosystem and the consequences for the highly adapted animals relying on the presence of sea ice, e.g., polar bears. On the other hand, economic interest towards the Arctic is increasing due to newly developing shipping routes, fishing grounds as well as new accessible fossil and mineral resources. This development has raised a debate on ownership claims and the ecological risks of such activities in the Arctic Ocean.

Alongside the probable anthropogenic sea ice decline, (sub-)Arctic sea ice is subject to strong natural changes in temporal and spatial extent. Modern conditions are characterized by a maximum extent after the Northern Hemisphere winter, in early spring in February/March with an average extent (from 1981-2010) of 15.64 x 10^6 km^2 (Fig 1.1; *National Snow and Ice Data Centre, NSIDC*). Minimum conditions are reached at the end of the melt season during September with an average extent of 6.22 x 10^6 km^2 (from 1981-2010; Fig 1.1; *NSIDC*). During these minimum conditions only parts of the central Arctic Ocean remain ice covered by thick (several meters) perennial multi-year ice (Fig 1.2).

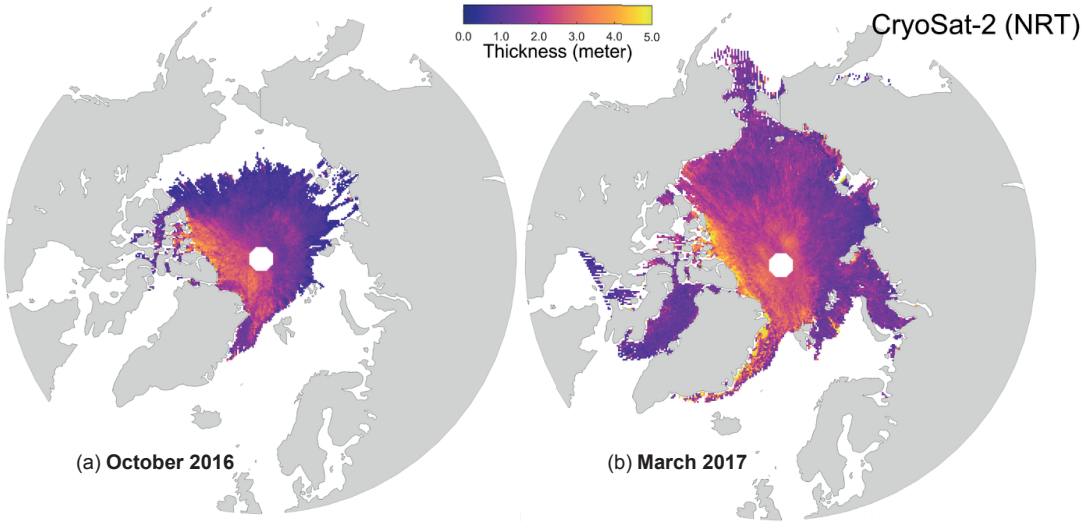

Fig 1.2. Seasonal variability of sea ice thickness in the Arctic Ocean (a) in October 2016 and (b) in March 2017 measured with the CryoSat-2 satellite. Adapted from *meereisportal.de*.

New first year ice (0.5 m; *Eicken, 2003*) is formed in winter. During its formation, surface water cools and freezes, which is accompanied by brine formation (the

rejection of salt) causing a strong stratification with relatively warm and saline waters at the bottom and a partly frozen, fresh surface water lens *(Rudels & Quadfasel, 1991; Dieckmann & Hellmer, 2003)*. In case of the Arctic shelves, strong riverine freshwater input from Canadian and Russian rivers contributes to a pronounced stratification favouring the formation of sea ice *(Aagaard & Carmack, 1989; Macdonald et al., 2004)*. Large amounts of sea ice formed in the Arctic are moved along the Arctic Ocean and exported by the Transpolar Drift (TPD) through the Fram Strait (~30.000 km^2 mean annual export from the year 1950 to 2000; *(Kwok, 2004)*. This sea ice is transported southward by the East Greenland Current (EGC) along the East Greenland Shelf through Denmark Strait and around Cape Farewell towards the Baffin Bay *(Aagaard & Coachman, 1968a, b; Hopkins, 1991; Johannessen et al., 2004; Tang et al., 2004)*. In addition to the cold and low salinity Arctic waters of the EGC, the interplay of locally formed sea ice and meltwater from melting sea ice and adjacent glaciers affects the shelves around Greenland.

The seasonal melting of Arctic sea ice and the associated increase of meltwater play a major part in the global thermohaline overturning circulation *(Aagaard et al., 1985; Häkkinen, 1995, 1999; Holland et al., 2001; Arzel et al., 2008)*. The influence of Arctic freshwater on European climate became especially evident during the Great Salinity Anomaly (GSA) between 1960 and 1970, during which enhanced freshwater and sea-ice flux reduced the deep convection and thermohaline circulation (THC) in the Labrador Sea, which lead to a cooling in the North Atlantic area *(Curry et al., 1998; Dickson, 1999; Dima & Lohmann, 2007; Sundby & Drinkwater, 2007)*.

The effect of Arctic sea ice on Earth's climate exceeds its effect on ocean circulation. The high albedo of the bright surface of sea ice affects the global energy budget by reflecting high amounts of the incoming solar radiation and prevents the absorption of external heat (Fig 1.3). The so-called 'ice albedo feedback' *(Barry, 1996)* denotes the amplification of global warming caused by the loss of Arctic sea ice, an increase in energy uptake of the Oceans and an subsequent increase of Arctic sea surface temperatures (SST; *Manabe et al., 1992; Randall et al., 1998; Screen & Simmonds, 2010*), as the areas covered by bright snow and ice are replaced by dark ocean surface. Further, the sea ice affects the exchange of heat and moisture between ocean and atmosphere (Fig 1.3; *Dieckmann and Hellmer, 2003*).

Increased incoming solar radiation may act as a trigger for the negative sea ice albedo feedback. Further, modelled reconstructions of the North Atlantic Oscillation (NAO; *Nesje et al., 2001; Jackson et al., 2005; Funder et al., 2011; Darby et al., 2012; Olsen et al., 2012*) suggest a connection between the positive (negative) NAO mode and increased (reduced) northward advection of Atlantic water and a decrease (increase) in sea ice in the Arctic (*Dickson et al., 1996; Thompson and Wallace, 1998*).

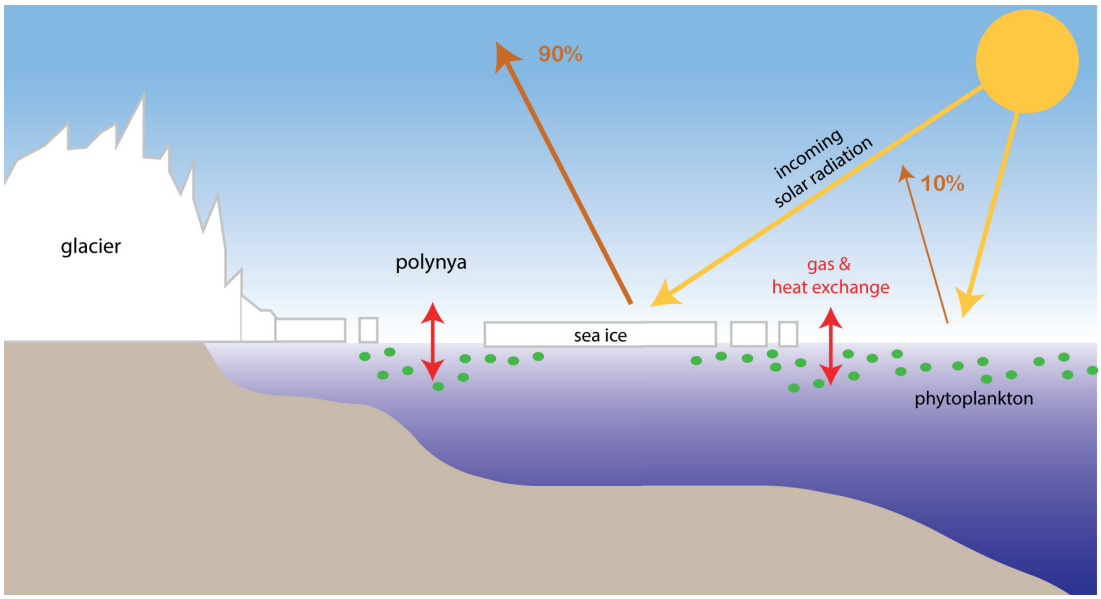

Fig 1. 3 Schematic illustration of the influences of sea ice on the Earth's energy budget and gas and heat exchange between atmosphere and ocean. Adapted after *npolar.no* and *Tsamados et al., 2015*.

Alongside its climatic influence, Arctic sea ice provides a unique habitat for marine organisms and controls marine productivity to a great extent. Its thickness greatly controls light conditions and hence limits productivity of photosymbiontic organisms *(Cremer, 1999; Belchansky and Douglas, 2002)*. Ice algal blooms are one of the foundations of the Arctic food web and influence the production of biomass and carbon release of the Arctic Ocean *(Goesselin et al., 1997; Gradinger, 2009)*.

In summary, sea ice has vital effects on the Earth's energy budget, atmospheric and oceanic circulation and may act as an amplifier for global warming.

During the last decade, a reduction of Arctic sea ice has been observed, which exceeded any predictions made by climate models (Fig 1.4; e.g., *Cavalieri et al.,*

1997; Johannessen et al., 2004; Francis et al., 2005; Stroeve et al., 2007; Comiso et al., 2008; Serreze and Barry, 2011).

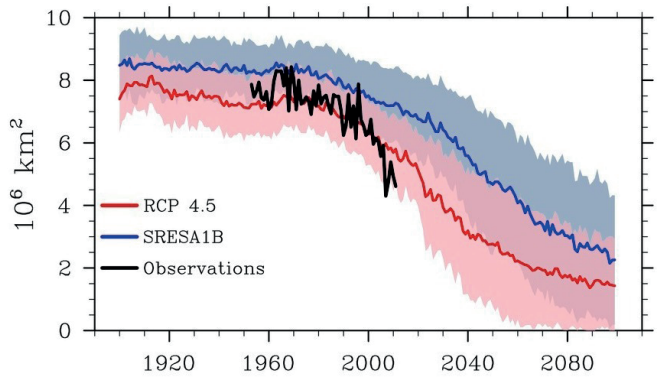

Fig 1. 4 For the 4th assessment report of the Intergovernmental Panel on Climate Change (IPCC) compared observed September Arctic sea ice extent (1952-2011; black curve) to model output (blue and red curves). SRESA1B: greenhouse gas emissions scenario, RCP 4.5: Representative Concentration Pathways of greenhouse gases in relation to the estimated radiative forcing in 2100. Pink and blue shadings show the +/- 1 standard deviation of the different model runs. Source: nsidc.org; *Stroeve et al., 2012*.

Since sea ice satellite remote sensing started in 1978, the Arctic sea ice maximum extent has decreased by 2.8 % per decade, whereas the summer minimum decreased much more severely by 13.5% per decade (*NSIDC*). So far, the lowest sea ice extent was recorded in September 2012 (3.41 x 10^6 km^2; Figs 1.1., 1.5.) showing 49% less sea ice than the average minimum extent from 1979-2000; *NSIDC*). Besides the spatial loss of sea ice, a loss of thick multi-year ice and an increase in thin first-year ice is observed (Fig 1.6; *Maslanik et al., 2007; Serreze et al., 2007; Stroeve et al., 2007, 2012).*

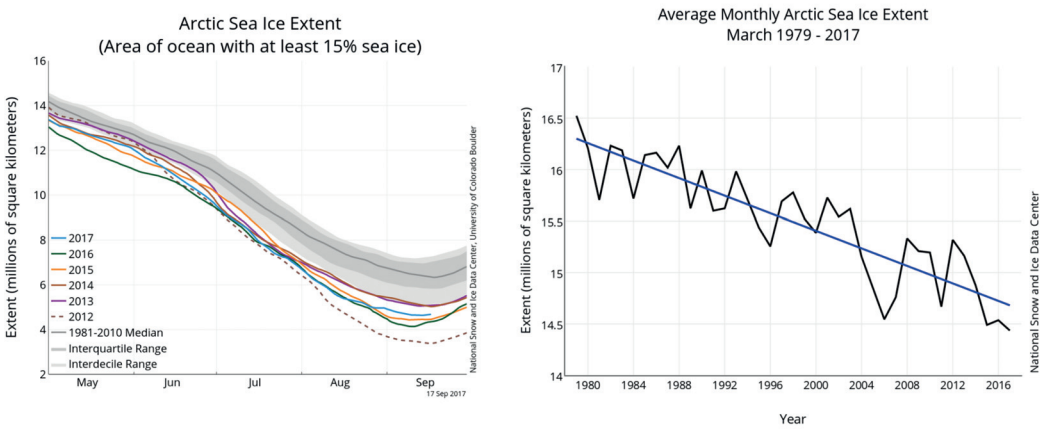

Fig 1. 5 Observations of the recent reduction of Arctic ice extent (in millions of square kilometres) for each year from 2012-2017 and the 1981-2010 median. The monthly sea ice extent in March for each year from 1979 to 2017 displays the continuous decrease in Arctic sea ice extent. Source: *nsidc.org*.

An average sea ice volume loss of ~500 km^3/yr or a decrease of thickness by 0.075m/yr has been observed by satellite measurements since 1983 (Fig 1.6*; Laxon*

et al., 2013). Further, the amount of multi-year sea ice in the Arctic Ocean has declined strongly, i.e., from 20% in 1983 to ~2% in 2013 of the Arctic sea ice cover (Fig 1.6; *NSIDC*). This loss of sea ice volume makes Arctic sea ice more susceptible to changes in oceanic and atmospheric temperatures *(Comiso, 2012)*.

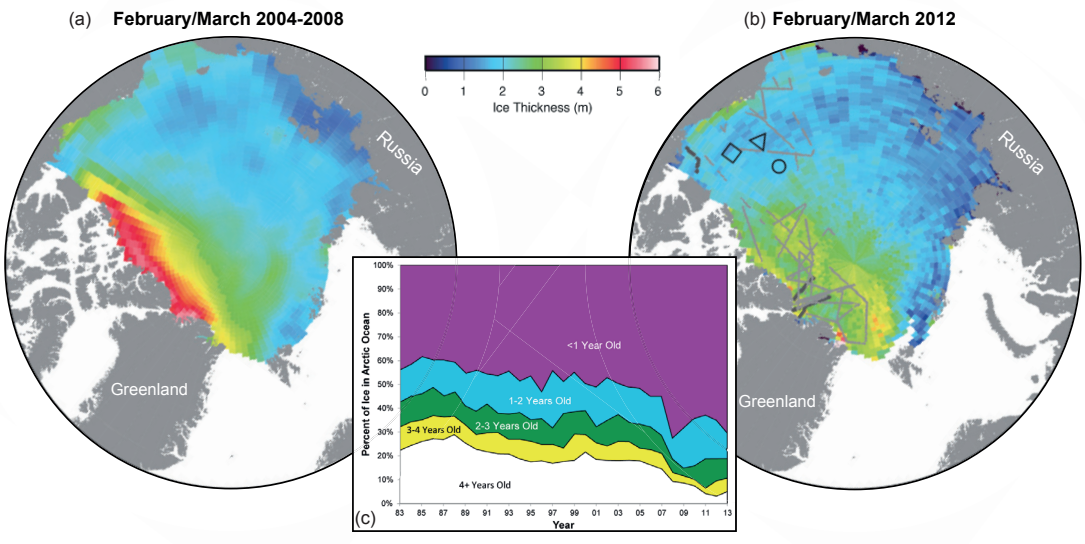

Fig 1.6. Comparison of (a) the average sea ice thickness in February/March 2004-2008 and (b) February/March 2008 showing the decline in thick, multi-year sea ice (adapted from *Laxon et al., 2013*). (c) The age composition of Arctic sea ice shows a reduction of multi-year ice (4+years) from 1983 to 2013. Adapted from *nsidc.org*, Madlanik and Tschudi, University of Colorado.

The underestimation of the recent sea ice loss of climate models displays the lack of knowledge about the natural processes driving sea ice variability *(Stroeve et al., 2007, 2012;* Fig 1.4). Reconstructions of pre-industrial sea ice changes, their driving mechanisms and ecological consequences will greatly contribute to improve climate models and increase the quality of future predictions.

1.2. Modern oceanographic setting

The modern Arctic Ocean circulation is characterized by the wind-driven, clockwise flowing Beaufort Gyre in the western and the Transpolar Drift in the eastern Arctic Ocean *(*Fig 1.7; *Thorndike, 1986; Gow and Tucker, 1987*). These current systems drive the Arctic export of low-saline surface waters alongside sea ice via Fram Strait and the Canadian Arctic Archipelago (Fig 1.7; *Jones et al., 2001; Jakobsson et al., 2004; Schauer et al., 1997)*. Changes in Arctic Ocean circulation patterns strongly affect the Arctic sea ice extent, freshwater and sea ice export via Fram Strait *(Carmack, 2000)*. One factor controlling circulation and sea ice formation in the Arctic is freshwater input from adjacent rivers, i.e., Yenisei, Ob and Lena *(Aagaard*

and Carmack, 1989).

Most of the riverine inflow occurs to the Eurasian shelves, i.e., in Kara and Laptev Sea, which display a strong seasonal and interannual variability in sea ice, fast ice and polynyas *(Pfirman et al., 1995; Parkinson et al., 1999)*. A smaller proportion of Arctic waters are exported through the Canadian Arctic Archipelago towards the Baffin Bay through Nares Strait, Jones Sound and Lancaster Sound and forms the Baffin Island Current (BIC) that flows southwards along the Canadian Shelf *(Drinkwater, 1986)*.

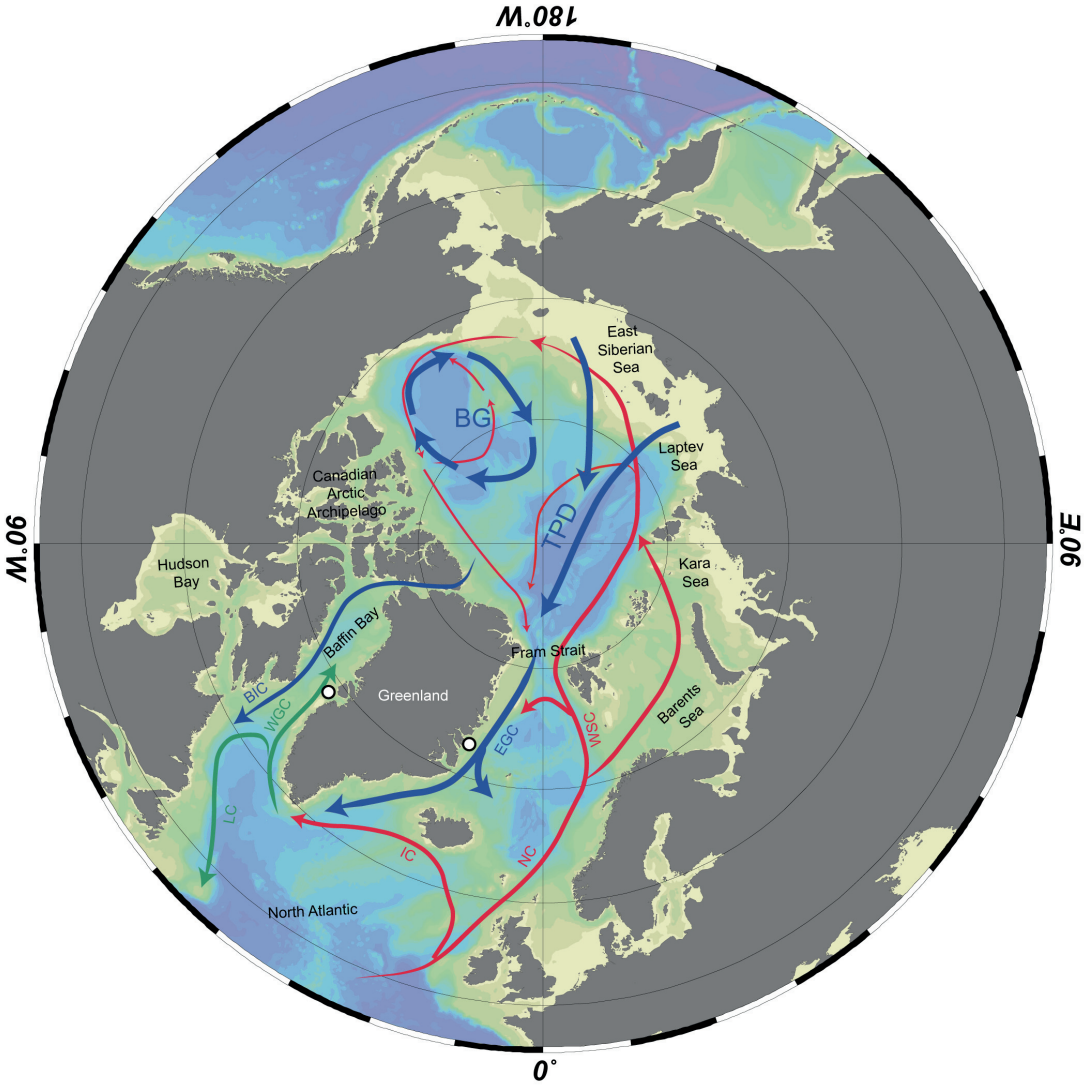

Fig 1. 7 Modern surface circulation in the Arctic Ocean and adjacent regions (adapted after *Macdonald et al., 2003*). White dots indicate the location of studied sediment cores on the East and West Greenland Shelf. Abbreviations are as follows: BIC = Baffin Island Current; BG = Beaufort Gyre; EGC = East Greenland Current; IC = Irminger Current; LC = Labrador Current; NC = Norwegian Current; TPD = Transpolar Drift; WGC = West Greenland Current; WSC = West Spitsbergen Current. The bathymetry is based on the IBCAO V3 gird (*Jakobsson et al., 2012*).

The main in- and outflow of the Arctic Ocean occurs via the only deep gateway: the Fram Strait. Warm saline waters flow along the Norwegian Coast as the Norwegian Atlantic Current (NAC) and continue as the West Spitsbergen Current (WSC), which enters the Arctic Ocean through the eastern Fram Strait and the St Anna Trough. Within the Arctic Ocean, the saline Atlantic water masses sink below the less saline Arctic waters (Fig 1.7; *Jakobsson et al., 2004*).

The warm inflow of Atlantic Waters in the eastern part of the Fram Strait is counterbalanced by cold polar water outflow in the east by the EGC, which flows southward along the East Greenland coast (Fig 1.7.; *Aagaard and Coachman, 1968)*. South of Greenland, the EGC circumnavigates Cape of Farewell to unite with the Irminger Current (IC), a westward flowing branch of the NAC. Both currents form the stratified West Greenland Current (WGC), which splits afterwards. One part flows northward along the West Greenland Shelf *(Cuny et al., 2005),* carrying a mixture of cold, less saline polar waters on the surface and warmer and more saline Atlantic waters *(Tang et al., 2004; Myers et al., 2007)*. Another part flows southward forming the Labrador Current and enters the Subpolar Gyre (SPG; *Holliday et al., 2007*). Within the Subpolar Gyre, the North Atlantic Deepwater (NADW) is formed by convective sinking. The deep mixing constitutes an important part of the Atlantic Meridional Overturning Circulation (AMOC; *Eldevik et al., 2009*). The strength and shape of the SPG controls the northward advection of Atlantic water flowing into the North Atlantic and subsequently into the Arctic *(Hátún et al., 2009)*. The SPG is to a great extent influenced by freshwater inflow into the Labrador Sea, enhanced inflow of freshwater diminishes the salinity differences between inner and outer gyre and weakens its circulation *(e.g., Born and Stocker, 2013*) and hence its contribution to the AMOC. This illustrates the significance of export of Arctic freshwater (in form of sea ice) and the importance of this area for climate reconstructions.

1.3. Holocene climate variability

The present climate interglacial, i.e., the Holocene, began 11.7 kyr ago with the termination of the Younger Dryas (YD) cold phase *(Rasmussen et al., 2006)*. The climatic transition from YD to Holocene, i.e., from Marine Isotope Stage (MIS) 2 to MIS 1, is characterized by a strong increase in stable oxygen ($\delta^{18}O$) isotope values in Greenland ice cores (Fig 1.8; *Stuiver and Grootes, 2000; NGRIP-Members, 2004;*

Alley et al., 2010). The onset of the Holocene has been related to high solar insolation in the Northern Hemisphere (Fig 1.6; *Risebrobakken et al., 2011*).

In general, the Holocene period can be divided into three phases (e.g., *Nesje and Dahl, 1993)*: The early Holocene, lasting from 11.6 to 9 kyr BP, correlates with the 'Preboreal' and the 'Boreal' chronozones (Fig 1.8; *Wanner et al., 2008*). The mid-Holocene, from 9 to 5 kyr BP, coincides with the 'Atlantic' chronozone. The 'Subboreal' and 'Subatlantic' chronozones frame the late Holocene, from 5 kyr BP to pre-industrial times (Fig 1.8; *Wanner et al., 2008*). Compared to the previous glacial period, the Holocene interglacial was, based on ice core records, considered as a relatively stable climate period (e.g., *Grootes et al., 1993)*. However, climate reconstructions revealed several high amplitude climate variations (e.g., *Bond, 1997; Mayewski et al., 2004)*. These Holocene climate variations provide important climate information, as changes occurred within the same boundary conditions (e.g., paleogeography, ocean circulation) and exhibit the natural transition from a cold to a warmer climate.

1.3.1. Early to mid Holocene

The Early Holocene was characterised by high summer solar insolation, which reached its maximum around 10 ky BP (Fig 1.8; *Laskar et al., 2004*). This insolation maximum has been related to a phase of high atmospheric temperatures from 9.5 to 5 ky BP over Greenland (*Renssen et al., 2012)* displaying temperatures possibly 1.3 – 3.5 °C warmer than the 21th century *(Stuiver et al., 1995; Koerner & Fisher, 2002; Kaufman et al., 2004; Rasmussen et al., 2006)*, termed the Holocene Thermal Maximum (HTM; Fig 1.8). The HTM has been found globally in various proxy records, however character and timing of this warming differs between regions and especially between high and low latitudes (for overview see *Renssen et al., 2012*). Warm HTM conditions have been found in the Arctic Ocean (e.g., *Polyak and Mikhailov, 1996; Pisaric et al., 2001; Andreev et al., 2009)*, the Nordic Seas (e.g., *Birks and Koç, 2002; Moros et al., 2004; Hald et al., 2007; Ślubowska-Woldengen et al., 2007; Cronin et al., 2010*) and the Baffin Bay (e.g., *Dyke, et al., 1996*).

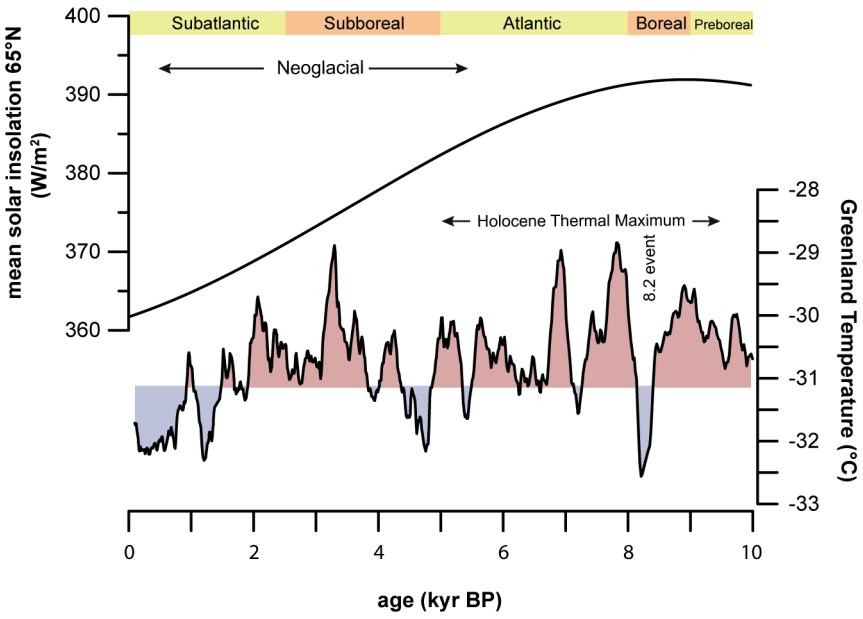

Fig 1. 8 Overview of Holocene Greenland temperatures (in °C; based on $\delta^{18}O$ on the GISP ice core; *Alley et al., 2010*) and Northern Hemisphere solar insolation *(Laskar et al., 2004)*.

The HTM warming is associated with the north-westward retreat of sea ice and oceanic fronts in the Nordic Seas possibly initiated by the advection of Atlantic Waters towards the Arctic Ocean *(Koç et al., 1993a; Ślubowska-Woldengen et al., 2007)* as well as strong retreat of Arctic sea ice *(Koerner and Fisher, 1990, 2002; Svendsen et al., 2004)*. Enhanced melting has been accounted for a strong postglacial sea level rise and the flooding of the Eurasian Arctic shelves, which contributed to the establishment of the modern ocean circulation in the Arctic Ocean and the Nordic Seas *(Bauch et al., 1999, 2001b; Stein et al., 2001; Spielhagen et al., 2005)*. In particular, the melting of the Greenland Ice Sheet (GIS; *Blaschek and Renssen, 2013*) during the HTM and its negative feedback mechanism to atmospheric warming, caused by increased solar insolation, have been related to distinct differences in the spatial and temporal extent of the HTM in the Nordic Seas (e.g., *Hald et al., 2007; Risebrobakken et al., 2010)*.

The mid-Holocene was characterized by persistent warm temperatures *(Sarnthein et al., 2003; Hald et al., 2007; Rasmussen et al., 2007)* interrupted by a prominent and global climate cooling event observed around 8.2 kyr (Fig 1.8; *Rohling & Pälike, 2005*) which was termed '8.2 kyr event'. This abrupt climatic change towards cool, dry and windy conditions was recorded in Greenland Ice Cores (Fig 1.8; *Alley et al., 2010; Kobashi et al., 2017*) and climate proxy records from the North Atlantic *(Alley et al., 1997; Hall et al., 2004; Risebrobakken et al., 2003; Moros et al., 2004;*

Kleiven et al., 2008). This relatively short cooling period has been associated to the abrupt final drainage of the proglacial lakes Agassiz and Ojibway into the Labrador Sea and North Atlantic causing a reduction in deep convection and THC *(Stuiver et al., 1995; Barber et al., 1999; Rohling and Pälike, 2005)*. During this short climate event, an increase in sea ice has been observed in Fram Strait *(Müller et al., 2012)*. Based on driftwood reconstructions *(Dyke et al., 1997)*, the modern oceanographic conditions, and with it the modern sea ice transport across the Arctic Ocean, were established around 6 kyr. From this point onwards, the southward export of Arctic sea ice was mainly controlled by the Transpolar Drift and the Beaufort Gyre (e.g., *Miller et al., 2010*).

Based on archaeological evidence, the Saqqaq people settled in West Greenland at the end of the relatively mild HTM around 4.5 kyr BP *(*Fig 1.9; *Jensen et al., 1999; Jensen, 2006*). It is assumed that seasonally open waters in Disko Bugt area favoured open water hunting and secured their survival *(Jensen, 2006)*.

1.3.2. The late Holocene

Whilst the early and mid-Holocene were characterized by relatively warm conditions and the establishment of the modern ocean circulation, the late Holocene climate was widely characterized by decreasing solar insolation (Fig 1.8; *Porter and Denton, 1967; Denton and Karlén, 1973; Wanner et al., 2011*). Based on the extensive glacier advances in Scandinavia, Svalbard and Greenland (Fig 1.9; *Tarussov, 1992; Werner, 1993; Svendsen and Mangerud, 1997; Nesje et al., 2001; Isaksson et al., 2005; Levy et al., 2017),* this phase is also referred to as Neoglacial *(Wanner et al., 2008)*. Climate reconstructions revealed a reduction of Northern Hemisphere temperatures *(Moberg et al., 2005)* and sea ice advances in the Nordic Seas (e.g., *(Koç and Jansen, 1994; Bauch et al., 2001b; Jennings et al., 2002; Andersson et al., 2003; Miller et al., 2005; Vinther et al., 2006; Seidenkrantz et al., 2007a; Sicre et al., 2008)*, a cooling/freshening of bottom waters in the Baffin Bay *(Perner et al., 2013)* and increasing influence of polar waters on the southeast Greenland Shelf *(Jennings et al., 2011)*. The characteristics of the Neoglacial cooling varies in different regions, some areas notice a gradual cooling (e.g., *Andersen et al., 2004a; Marchal et al., 2002; Müller et al., 2012)* others are characterized by a stepwise cooling (e.g., *Calvo et al., 2002; Werner et al., 2013*). A stepwise cooling has been

linked to the flooding of the Arctic shelves between 9 and 5 kyr BP *(Werner et al., 2013)*, which was associated with an increase in Arctic sea ice production *(Bauch et al., 2001a)* and an enhanced sea ice export through Fram Strait *(Dyke et al., 1997; Prange and Lohmann, 2003)*.

Furthermore, the timing of the Neoglacial cooling in the Northern Hemisphere shows strong regional differences, in some areas the onset of a cooling was recognized around 9 kyr *(Hald et al., 2007; Risebrobakken et al., 2011)* whereas in most of the Nordic Seas the 8.2 kyr event marks the onset of a climate deterioration (e.g., *Fronval and Jansen, 1997; Bauch et al., 2001b; Sarnthein, 2003; Andersen et al., 2004a)*. Despite these differences in timing and character, various environmental reconstructions from the Fram Strait, Laptev and Chuckchi Sea and the Canadian Arctic Archipelago find evidence for an overall strengthening of the EGC *(Moros et al., 2006a)* and increases in sea ice that were associated to the Neoglacial *(e.g., Vare et al., 2009; Müller et al., 2012; Hörner et al., 2016; Stein et al., 2017a)*.

A solar minimum between 3 and 2.5 kyr BP promoted the cooling in the Nordic Seas (Fig 1.9; *Renssen et al., 2006*), reflected in reduced SSTs, primary production and an increase of polar water outflow to the Nordic Seas *(Koç et al., 1993; Calvo et al., 2002; Andersen et al., 2004b; Cabedo-Sanz et al., 2016)*. Further, an increase in drift ice around 3 kyr BP (e.g., *Bond et al., 2001; Müller et al., 2012*) seems to have influenced the water column stratification in the North Atlantic and led to a reduction in Atlantic Meridional Overturning Circulation (AMOC; *Hall et al., 2004)*. This reduction has been observed in decreases in stable carbon isotopes ($\delta^{13}C$) of planktic foraminifera (e.g., *Bauch et al., 2001b; Sarnthein, 2003; Risebrobakken et al., 2011; Werner et al., 2013*).

This general cooling and increase in sea ice conditions, which is likely to have aggravated open water hunting, has been linked with the abandonment of West Greenland settlements of the Saqqaq people *(Meldgaard, 2004)*. On the other hand, these conditions are thought to be favourable for the Dorset people, who settled in West Greenland from 2.8 – 2.2 kyr BP, which were highly adapted to ice hunting and cold conditions *(Jensen et al., 1999; Jensen, 2006)*.

Superimposed on the general solar induced cooling trend of the late Holocene, several climate fluctuations have been recorded all over the North Atlantic region.

These events are of particular interest for climate reconstructions, as they present the latest equivalents for pre-industrial climate oscillations *(Jones and Mann, 2004; Ljungqvist, 2010; IPCC, 2014)*. In addition, these events can be related to the population history of northern Europe and Greenland (Fig 1.9; *McGovern, 1991; McGhee, 1996; Jensen, 2006; Kuijpers et al., 2014)* and provide unique examples how human life is related to relate consequences of climate change. However, the forcing mechanisms causing these oscillations remain uncertain as well as the role and reaction of (sub-) Arctic sea ice. These short-term fluctuations are introduced briefly in the following chapters.

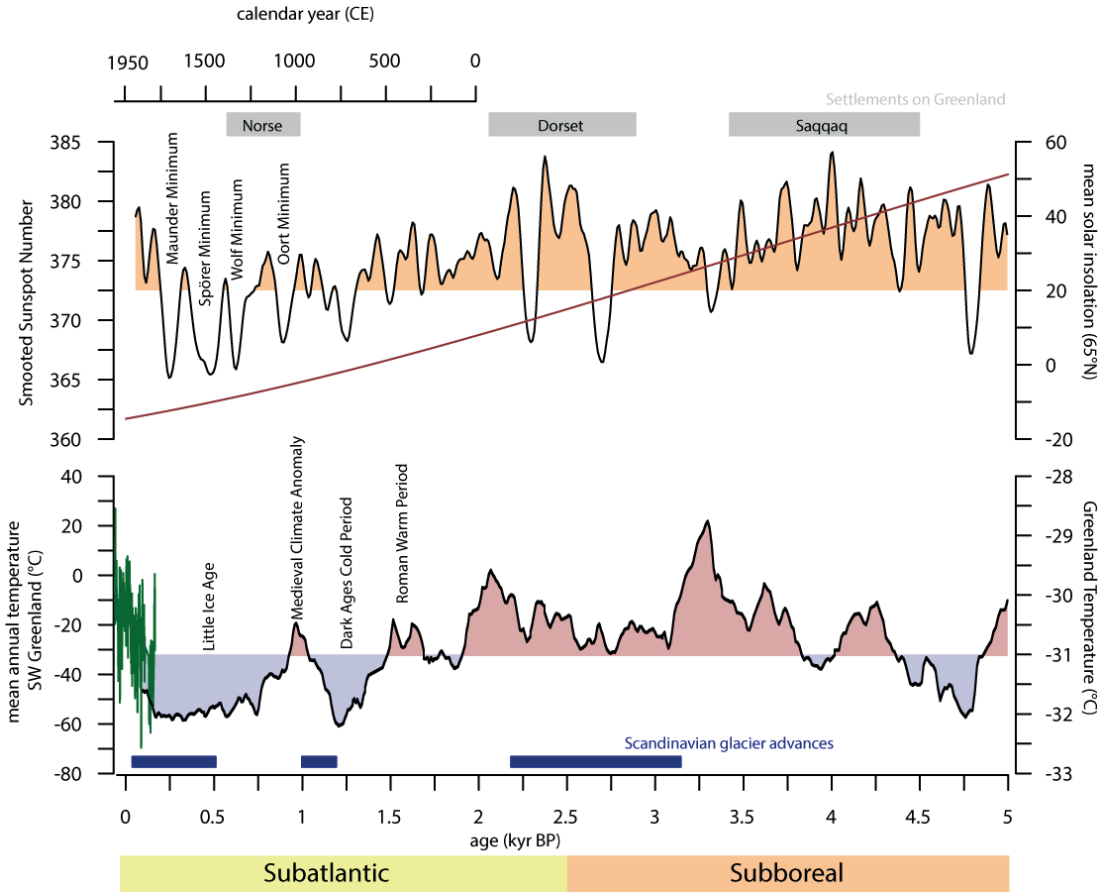

Fig 1. 9 Overview over the last 5 kyr BP. Fluctuations of Greenland temperatures (°C; based on $\delta^{18}O$ from the GISP2 ice core; *Alley et al., 2010*) and observed atmospheric temperatures from SW Greenland covering the years 1880 – 2010 (green curve; *Cappelen and Vinther, 2014)*. Specific climate events correlate with temperature reconstructions of Greenland atmospheric temperatures. Blue bars indicate glacier advances in Scandinavia *(Nesje et al., 2001)*. Further, the number of sunspots and specific sunspot minima *(Stuiver, 1961; Bond et al., 2001; Solanki et al., 2004)* are shown, compared to the solar insolation *(Laskar et al., 2004)*. Known settlements of the Saqqaq, Dorset and the Norse on Greenland are indicated by grey bars *(Jensen et al., 1999; Meldgaard, 2004; Jensen, 2006; Kuijpers et al., 2014)*. An additional age scale, showing calendar years CE, is given.

1.3.2.1 The Roman Warm Period

The Roman Warm Period (RWP) was a phase of atmospheric warmth over northwest Europe around 1.8 kyr BP (i.e., CE 150; *Ljungqvist, 2010*) and Greenland (Fig. 1.9; e.g., *Alley et al., 2010; Kobashi et al., 2017*). Distinct changes of oceanographic warming and a reduction in sea ice have been recorded across East Greenland and the northern North Atlantic *(e.g., Jennings et al., 2002; Giraudeau et al., 2004; Jiang et al., 2005; Sicre et al., 2008; Werner et al., 2015; Cabedo-Sanz and Belt, 2016; Perner et al., 2017*) as well as in the Baffin Bay (e.g., *Erbs-Hansen et al., 2013; Larsen et al., 2015; Nørgaard-Pedersen and Mikkelsen, 2009; Seidenkrantz et al., 2008*) and the Canadian Arctic Archipelago *(Belt et al., 2010)*. The shift towards warmer RWP conditions correlated with a change in the North Atlantic Oscillation (NAO) to a more positive mode *(Funder et al., 2011; Darby et al., 2012; Olsen et al., 2012)* which has been related to an intensification of westerly winds favouring the northward advection of Atlantic waters towards the Arctic.

1.3.2.2 The Dark Ages Cold Period

The RWP is followed by a climate deterioration in north-western Europe from 1.5 – 1.3 kyr BP, termed the Dark Ages Cold Period (DACP; also: Dark Ages; Fig. 1.9; *Lamb, 1995*). A prominent layer of ice-rafted debris (IRD) deposited in the North Atlantic around 1.4 kyr BP has been associated with increased iceberg drift *(Bond, 1997)*. Colder conditions and increases of sea ice have been documented roughly around this period in the Fram Strait *(Werner et al., 2013; Cabedo-Sanz and Belt, 2016)*, the North Iceland Shelf *(Cabedo-Sanz et al., 2016)* and south Greenland *(Jensen et al., 2004)*. In the Baffin Bay and on the East Greenland Shelf changes to colder conditions were related to a general increase in EGC influence (*Moros et al., 2006a; Seidenkrantz et al., 2008; Jennings et al., 2011; Perner et al., 2013, 2011; Ouellet-Bernier et al., 2014; Sha et al., 2017*). However, in some records from West Greenland a warming was recorded *(Andresen et al., 2010; Ribeiro et al., 2012)*. The atmospheric and oceanic cooling in the North Atlantic and over Europe during the DACP have previously been associated with a shift in the mode of NAO, that may have been triggered by reduced solar activity (Fig 1.9; *Gray et al., 2010; Helama et al., 2017)*. An anti-correlation of West Greenland to the North Atlantic is known from instrumental climate observations since the mid 19th century *(Jones et al.,*

2014). Despite the wide spatial distribution of this event the exact timing and forcing mechanisms remain uncertain (see *Helama et al., 2017* for a review).

1.3.2.3 The Medieval Climate Anomaly

The Medieval Climate Anomaly (MCA; or Medieval Warm Period, MWP) was a phase of relative atmospheric warmth over northwest Europe from 0.1 – 0.75 kyr BP (Fig. 1.9; *Lamb, 1965, 1977)*. This phase was characterized by warm temperatures over Greenland *(Alley et al., 2010; Kobashi et al., 2017)*, enhanced northward advection of Atlantic Water towards the Arctic (*Spielhagen et al., 2011*), a reduction in sea/drift ice *(Andrews et al., 2009; Kinnard et al., 2011; Cabedo-Sanz et al., 2016; Moros et al., 2006b)* and warmer SSTs *(Helama et al., 2010; Mernild et al., 2012)*. In the Baffin Bay, the MCA was characterized by a subsurface warming *(Perner et al., 2011)* whereas surface waters experienced a cooling *(e.g., Moros et al., 2006b; Seidenkrantz et al., 2008; Ribeiro et al., 2012; Krawczyk et al., 2013)*. Other microfossil records from Disko Bugt and West Greenland covering the late Holocene found an anti-phase correlation to the NAO modes of the North Atlantic, i.e., a cooling during the positive NAO mode associated with the MCA and a warming during the negative NAO mode correlating with the Little Ice Age (*Seidenkrantz et al., 2008; Krawczyk et al., 2010, 2013; Ribeiro et al., 2012)*. However, it should be noted that comparative approaches of *Dawson et al. (2003)* and *Seidenkrantz et al. (2008)* could not identify a direct seesaw pattern between the North Atlantic and West Greenland during the late Holocene.

Nevertheless, it has been suggested that a shift from more negative to a strong positive NAO regime has triggered the transition from DACP to MCA *(e.g., Kuijpers and Mikkelsen, 2009; Mann et al., 2009; Trouet et al., 2009; Faust et al., 2016)*. Associated stronger westerly winds and enhanced AMOC and northward advection of Atlantic waters during this mode may have caused a general warming during this time *(Trouet et al., 2009)*. The warm conditions corresponding to the MCA correlate with the migration of the Norse to West Greenland around 1.0 kyr BP *(Kuijpers et al., 2014)*.

1.3.2.4 The Little Ice Age

The general Neoglacial cooling trend peaked in the Little Ice Age (LIA) cold phase, around 0.3 kyr BP *(Jones and Mann, 2004; Ljungqvist, 2010)* associated with an

atmospheric and oceanic cooling in the Northern Hemisphere (Fig. 1.9; *Denton and Karlén, 1973; Nesje and Dahl, 2003; Matthews and Briffa, 2005; Wanner et al., 2008; Alley et al., 2010)*. The LIA is a widespread phenomenon in marine and terrestrial records around the North Atlantic *(e.g., Hass and Kaminski, 1995; Jennings and Weiner, 1996; Nesje et al., 2000; Seppä and Birks, 2002; Andersson et al., 2003; Cronin et al., 2003; Roncaglia and Kuijpers, 2004; Massé et al., 2008; Vare et al., 2009; Spielhagen et al., 2011; Werner et al., 2011; Jansen et al., 2016)*. The onset of the LIA coincides with a shift of NAO towards a more negative mode *(Andersen et al., 2004b; Mann et al., 2009; Trouet et al., 2009; Miller et al., 2011; Faust et al., 2016)* and several volcanic eruptions in the tropics *(Eddy, 1976; Wanner et al., 2008)*. Moreover, the Wolf solar minimum (0.67 kyr BP; Fig 1.9; *Miller et al., 2011*) may have favoured further atmospheric cooling leading to the onset of the LIA around 0.7 kyr BP *(Ljungqvist, 2010)*. The cooling related to the LIA has been assumed as a possible trigger of the abandonment of Norse settlements on Greenland around 0.65 kyr BP *(Kuijpers et al., 2014)*. Enhanced sea ice and colder atmospheric conditions are thought to have impeded agriculture and trade on which the Norse were relying *(Kuijpers et al., 2014)*.

1.3.4 Holocene climate cyclicity

In the 18th century, the Danish missionary Hans Egede Saabye was the first to report an opposite climate pattern between West Greenland and Europe: 'In Greenland, all winters are severe, yet they are not alike. The Danes have noticed that when the winter in Denmark was severe, as we perceive it, the winter in Greenland in its manner was mild, and conversely' *(Saabye, 1942; van Loon and Rogers, 1978)*. From further historical and modern climate records a coherent climate oscillation in the Northern Hemisphere named the North Atlantic Oscillation (NAO) was recognized (Fig. 1.10; *Rogers, 1984; Hurrell, 1995; Portis et al., 2001; Hanna and Cappelen, 2003)*.

This climate pattern influences atmospheric and oceanographic circulation patterns (e.g., *Buch, 2002*). A positive (negative) mode of the NAO is associated with increased (reduced) northward advection of Atlantic water and a decrease (increase) in sea ice in the Arctic caused by a dominant northward (eastward) direction of winter storms (Fig. 1.10; *Dickson et al., 1996; Thompson and Wallace, 1998)* .

Based on these modern observations, *Nesje et al. (2001)* assumed that the NAO pattern may have persisted back in time and may be accounted for general climate shifts. Yet, it remains speculative what causes the observed NAO shifts and whether they follow a specific cyclicity.

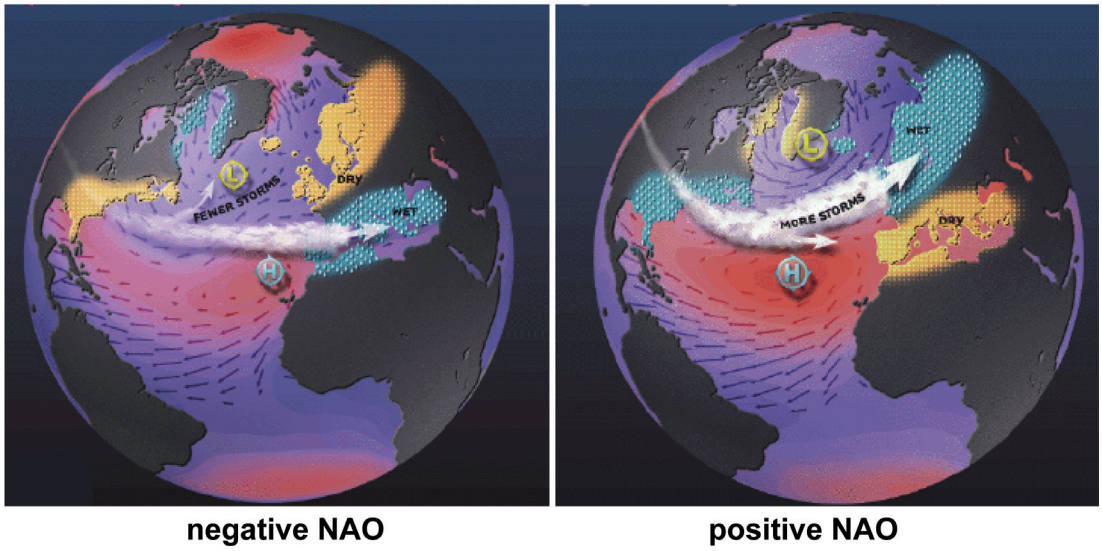

Fig 1. 10 Modern observations of the different modes of the North Atlantic Oscillation. The negative mode is characterised by a weak subtropical high and a weak Icelandic low causing a west-eastward winter storm track. Storms are generally weaker and fewer. They carry dry and cold air to Europe. Greenland experiences milder winter temperatures. The positive mode is characterised by a strong pressure gradient between Icelandic low and subtropical high, with enhanced winter storm intensity and a more northward orientation. This causes warm and wet winters in Europe and cold and dry winters in Greenland. Source: *ldeo.columbia.edu/res/pi/NAO/ by Martin Visbeck*.

In a comparative approach, a global synchronicity between specific climate alterations has been observed during the Holocene (see *Wanner et al., 2008* for summary). *Bond et al. (1997, 2001)* related periods of reduced solar activity with increasing iceberg discharge, indicated by increases in IRD, to the Nordic Seas with a cyclicity of 1.5 kyr. This millennial-scale cyclicity of solar output affecting drift ice and the North Atlantic Deep Water formation could not be sustained by later studies (e.g., *Andersson et al., 2003; Risebrobakken et al., 2003; Andrews et al., 2006; Polyak et al., 2009)*. Other studies related these changes to several internal driving mechanisms, e.g., volcanic activity or oceanic and atmospheric circulation changes *(Kinnard et al., 2011)*. However, no clear evidence for persistent climate cyclicity during the Holocene could be identified (e.g., *Schulz et al., 2004; Wanner et al., 2008*) and no exact timing for most of the late Holocene events could be found. This may partly be caused by different proxies reflecting various depth habitats *(Andersson et al., 2010*) and responding differently to the changing environment.

Further, the Nordic Seas circulation has been associated with a 'see-saw' effect *(van Loon and Rogers, 1978)* throughout the Holocene (e.g., *Seidenkrantz et al., 2007b, 2008)* which may have contributed to the observed differences in climate reconstructions.

1.4. Approach

1.4.1. Common proxies for sea ice reconstructions

Present sea ice observations are mainly based on satellite passive microwave measurements (since 1978; e.g., *Comiso et al., 2008; Parkinson, 2014)* as well as historical ship and aerial observations *(Rothrock et al., 1999; Walsh & Chapman, 2001; Rayner et al., 2003)*. To gather information about past sea ice extent further back in time sedimentary parameters such as IRD (e.g., *Vogt et al., 2001; Polyak et al., 2010; Andrews et al., 2014)* and geochemical proxies such as stable isotopes of microfossils (e.g., $\delta^{18}O$ of foraminifera; *Hillaire-Marcel & de Vernal, 2008; Dokken et al., 2013; Gibb et al., 2014*) have been applied for sea ice reconstructions. Apart from that, assemblages and transfer functions of specific microfossils have been used to gather information about sea ice conditions, as described in the following.

Foraminifera

The specific composition of paleo-communities of foraminifera have been associated with specific water mass characteristics (i.e., temperature and salinity), food availability (i.e., surface productivity; e.g., *Murray, 1991; Rytter et al., 2002; Sejrup et al., 2004)* and have been used as proxies for sea ice variability (e.g., *Schröder-Adams et al., 1990; Jennings et al., 2002; Scott et al., 2009, 2008*). A foraminiferal assemblage transfer function, i.e., the Similiarity Maximum Modern Analogue Technique (SIMAXX), has been established as a tool for past sea surface temperatures reconstructions *(Pflaumann et al., 2003; Sarnthein, 2003)* that is widely applied in the Arctic Ocean and adjacent seas *(e.g., Cronin et al., 2013; Telesiński et al., 2015; Werner et al., 2016)*. However, the precision of this approach in low temperature regimes remains difficult *(e.g., Telesiński et al., 2015*).

The sea ice sensitivity of benthic foraminifera is based on their general sensitivity to food and oxygen availability at the sea floor *(Seidenkrantz, 2013)*. These factors are only partly influenced by sea ice, the tolerances of foraminifera to certain

environmental changes are not yet fully understood and seem to follow a complex combination of environmental mechanisms (see *Seidenkrantz, 2013* for a review). So far, no foraminiferal species has been identified as a specific sea ice species *(Seidenkrantz, 2013)*. Hence, this approach can only give indirect information about past sea ice changes. Further, the preservation of foraminifera is problematic in certain regions, i.e., the Arctic Ocean *(Wollenburg et al., 2001, 2004)* and limits its Circum-Arctic application.

Diatoms

Another common microfossil group used for environmental reconstructions, including sea ice conditions, are diatom assemblages *(Weckström et al., 2013)*. Specific diatom species could be directly linked to past sea ice variability in Arctic sea ice and are commonly applied for qualitative sea ice reconstructions in the Northern Hemisphere (*e.g., Moros et al., 2006a; Ran et al., 2006; Krawczyk et al., 2013)*. Further, diatom transfer functions have been used for more quantitative sea ice and SST reconstructions in the North Atlantic (e.g., *Jiang et al., 2001; Andersen et al., 2004b; Justwan and Koç, 2008; Berner et al., 2011; Miettinen et al., 2012*) and West Greenland *(Sha et al., 2014; Krawczyk et al., 2017)*. However, the preservation of diatoms is problematic in specific areas, e.g., the Canadian Arctic Archipelago and the Arctic Ocean *(Armand and Leventer, 2010; Pieńkowski et al., 2017)* and a number of diatoms tolerable of sea ice are also found in the surrounding cold open waters *(von Quillfeldt et al., 2003; von Quillfeldt, 2004; Lundholm and Hasle, 2010*).

Dinoflagellate Cysts

A microfossil group less affected by carbonate and opal dissolution in the (sub-) Arctic Ocean are the fossil cysts of dinoflagellates. Specific species have been found to live in sea ice (see review by *Matthiessen et al., 2005),* however, only two sea ice dwelling species have been reported to be preserved in the sedimentary record; *Islandinium minutum* and *Polarella glacialis* (cf. *Potvin et al., 2013; Heikkilä et al., 2016*). For quantitative reconstructions of environmental conditions, including sea ice, the modern analogue technique (MAT) is a widely applied method. This approach is based on a wide reference database that connects recent assemblages of dinocysts to observed environmental parameters, i.e., sea ice *(de Vernal et al.,*

2013a, 2013b). For paleoreconstructions, the principle that certain dinocyst communities are formed under specific environmental conditions is applied. However, this approach yields certain insecurities e.g., different dinoflagellates may form the same fossil dinocyst *(Zonneveld et al., 2013)* and assemblages may differ strongly between different regions and prohibit an over regional application *(Heikkilä et al., 2014)*.

Despite the wide application of these sedimentological and micropaleontological proxies for sea ice reconstructions, most of them can only be considered as indirect. For example, reconstructions from IRD cannot differentiate between icebergs or sea ice transport *(e.g., Lisitzin, 2002* and therein). Microfossils are affected by a wide range of environmental parameters, with sea ice being only one of them. Errors of transfer functions may increase within the application in paleorecords *(de Vernal et al., 2005)*. Microfossils may not be preserved in the fossil record, i.e., sea ice dwelling dinocysts. Furthermore, if deposited on the sea floor, they may be affected by dissolution such as observed for foraminifera or diatoms.

1.4.2. Biomarker proxies for sea ice

The determination of specific organic biomarkers provides essential information for ecological reconstructions of past environments *(Meyers, 1997; Stein & Macdonald, 2004; Volkman, 2006; Stein, 2008)*. These chemical fossils can be found in sediments, often even though the originating organism is not preserved in the sedimentary records or already decomposed (e.g., *Killops and Killops, 2004*).

A widely found biomarker group are **h**ighly **b**ranched, mono- and polyunsaturated **i**soprenoids (HBI). They are produced mostly by diatoms and are found in most marine and freshwater milieus and their sediments *(Rowland and Robson, 1990; Volkman et al., 1994; Belt et al., 2000; Grossi et al., 2004; Xu et al., 2006)*.

Belt et al. (2007) introduced a highly branched, monounsaturated C_{25} isoprenoid, commonly found in sediments under seasonal sea ice as a new sea ice proxy. This compound was found in Arctic sea ice and Canadian Arctic surface sediments, and has been, based on its ^{13}C isotope signature, suggested to be synthesised by diatoms living in sea ice *(Belt et al., 2008)*. The new sea ice proxy, named IP_{25} ('**I**ce **P**roxy with **25** carbon atoms': Fig 1.11), was then applied in a paleo-approach by *Massé et*

al. (2008) in sediments from the North Iceland Shelf and could successfully relate changes of IP_{25} concentration to changes in historic sea ice data over the last 2 ky. Further, *Müller et al. (2009)* could show that variabilities in IP_{25} concentrations reflect sea ice changes over glacial/interglacial time scales in the Fram Strait.

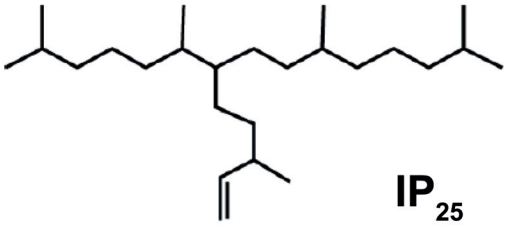

Fig 1. 11 Chemical structure of IP_{25}

The source of IP_{25} remained unknown, until *Brown et al. (2014)* identified three/four specific diatoms (*Pleurosigma stuxbergii var. rhomboides*, *Haslea kjellmanii*, *Haslea crucigeroides* and/or *H. spicula*) as its producers. These species make up only small proportions of the sea ice diatom community. Due to their small size, they are often not included in sea ice diatom assemblage studies. Further, their sedimentary preservation is expected to be low *(Shemesh et al., 1989; Leventer, 1998; Brown et al., 2014)*. Nevertheless, these taxa are distributed continuously over the Arctic, allowing an Arctic wide application of IP_{25} as sea ice proxy. In the first studies from the Canadian Arctic Archipelago and Fram Strait sedimentary IP_{25} concentrations have been related to the spring bloom (*Belt et al., 2007; Müller et al., 2011*). However, in the Central Arctic, *Fahl and Stein (2012)* found highest concentration of IP_{25} in sediment traps during summer months. In comparison to previous findings, this illustrated the regional differences of IP_{25} production, depending on seasonal light and sea ice conditions.

As pointed out by *Belt et al., (2007)*, the absence of IP_{25} may be caused either by permanent sea ice cover, with too low light penetration for sea ice algae growth or ice free conditions (Fig 1.12). In order to distinguish between these two extremes, *Müller et al. (2011)* combined IP_{25} with open water phytoplankton markers (i.e., brassicasterol and dinosterol, see Chapter 1.4.3.) in the so-called PIP_{25} index. The index is calculated using the following equation:

$$PIP_{25} = IP_{25}/(IP_{25}+(\text{phytoplankton marker x c})).$$

Due to the over proportional higher open water phytoplankton marker concentrations the balance factor *c* was introduced to compensate these concentration differences (cf. *Müller et al., 2011*)

$$c = \text{mean concentration } IP_{25} / \text{ mean concentration phytoplankton marker.}$$

The correlation of PIP_{25} values and modern satellite-derived sea ice concentration in Fram Strait has been found higher than those of IP_{25} *(Müller et al., 2011)*. Based on this correlation, *Müller et al. (2011)* ascribed sea ice concentrations to PIP_{25} values: a PIP_{25} index of 0 represents ice free conditions, values below 0.5 represent reduced sea ice conditions, values from 0.5 to 0.75 represent ice edge conditions and values above 0.75 represent permanent sea ice cover.

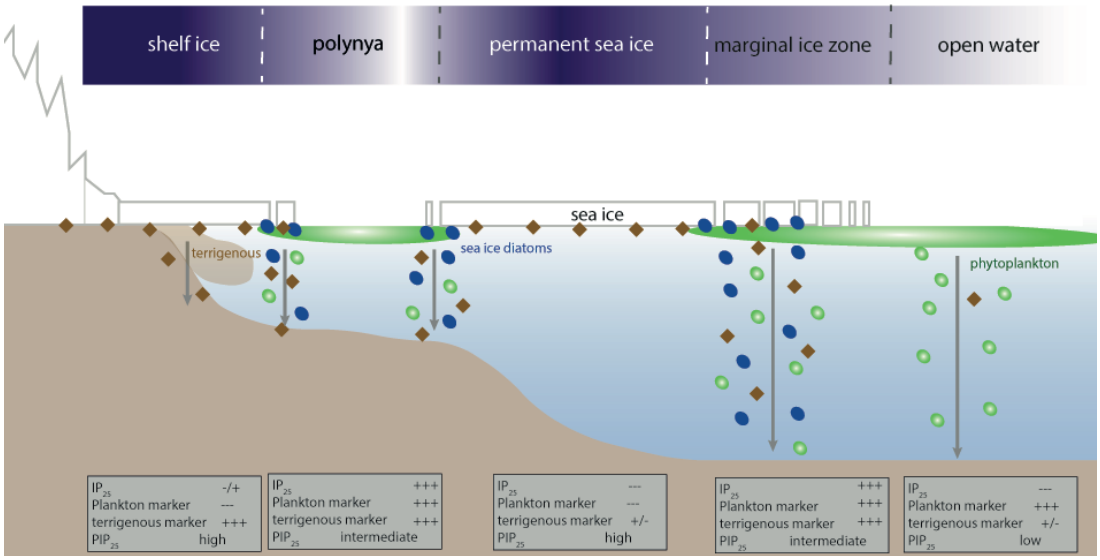

Fig 1. 12 Schematic cross section of the Greenlandic shelf, illustrating the distribution of phytoplankton and ice algae production and terrigenous input mechanisms. The sedimentary content of associated biomarkers and the resulting range of the PIP_{25} index is indicated in grey boxes. Figure modified from *Müller et al. (2011)* and *Stein et al. (2016)*.

In additional studies covering the central Arctic Ocean, the Siberian marginal seas, the Barents Sea and Svalbard area, the relationship of the PIP_{25} index to modern sea ice concentrations was confirmed *(Navarro-Rodriguez et al., 2013; Xiao et al., 2013, 2015a; Belt et al., 2015)*. However, the limits of this correlation became obvious within the extreme conditions on the Siberian shelves, i.e., river runoff and ice massifs *(Xiao et al., 2013, 2015a)*.

The IP_{25} approach still yields certain insecurities, i.e., the ecological factors

controlling IP_{25} accumulation, export and preservation are not fully understood as well as the influence on freshwater and sea ice structure on sea ice algae productivity *(Brown et al., 2011; Stein et al., 2012, 2017a, b; Belt and Müller, 2013; Weckström et al., 2013; Xiao et al., 2013, 2015a)*. Further, within the PIP_{25} approach the balance factor is discussed as one of the uncertainties *(Belt et al., 2015; Smik et al., 2016)*. These aspects need to be taken into account when interpreting biomarker sea ice records, and further surface studies of specific areas will certainly contribute to the applicability and reliability of this method.

Nevertheless, the IP_{25} and PIP_{25} approach was applied successfully in the late Holocene (e.g., *Massé et al., 2008; Belt et al., 2010; Müller et al., 2011; Cabedo-Sanz et al., 2016; Pieńkowski et al., 2017*) and on longer time scales within the Quaternary *(e.g., Fahl and Stein, 2012; Cabedo-Sanz et al., 2013; Stein and Fahl, 2013; Müller and Stein, 2014; Hoff et al., 2016; Hörner et al., 2017; Stein et al., 2017a; Xiao et al., 2017)*. So far, IP_{25} could be successfully used even in 15 Ma old sediments from the Lomonosov Ridge to reconstruct sea ice conditions *(Stein et al., 2016)*. The comparability of results from the analytical procedure of nine different laboratories was confirmed in an intra-laboratory study *(Belt et al., 2014)*.

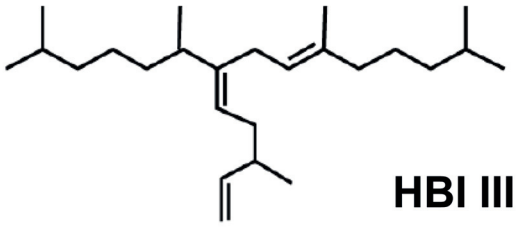

Fig 1. 13 Chemical structure of HBI III.

As mentioned above, the PIP_{25} approach and the applied balance factor remains one of its uncertainties. Recently, *Smik et al. (2016)* have modified the PIP_{25} approach by introducing a tri-unsaturated HBI alkene (HBI III, $C_{25:3,}$ Z-isomere; Fig 1.13), probably associated to ice margin productivity, as open water phytoplankton biomarker, which seem to not require a balance factor *(Belt et al., 2015)*. HBI III is produced by marine diatoms of the genera *Pleurosigma* and *Rhizosolenia (Rowland et al., 2001; Belt et al., 2017)*, which may be beneficial for environmental reconstruction as it is produced by a smaller group of organisms than brassicasterol and dinosterol and may yield a higher ecological sensitivity *(Belt et al., 2015)*. Its applicability has only been tested in the Barents Sea and Svalbard region *(Belt et al.,*

2015; Smik et al., 2016; Smik and Belt, 2017) and a wider spatial distribution of this approach is strongly needed to verify its use as an over regional proxy.

Another sea ice related compound seems to be the di-unsaturated HBI alkene (HBI II, $C_{25:2}$; Fig 1.14), which has been identified in the Arctic and Antarctic sediments *(Belt et al., 2007; Vare et al., 2009; Massé et al., 2011)*. In sedimentary records from the Canadian Arctic Archipelago and around the Antarctic, HBI II has been found in ice-covered areas and with similar variability as IP_{25} *(Vare et al., 2009; Massé et al., 2011)*.

Following *Rowland et al. (2001)*, who found a relationship between the degree of unsaturation in HBI molecules and temperature, the ratio of the HBI II to IP_{25} (termed DIP_{25}-index; *Cabedo-Sanz et al., 2013*) has been suggested as a possible index for sea surface temperature *(Fahl & Stein, 2012; Stein et al., 2012; Cabedo-Sanz et al., 2013; Xiao et al., 2013; Müller & Stein, 2014)*. Despite the good correlations in some regions, other studies could not find such a correlation with temperature and proposed the DIP_{25} index as indicative for sea ice stability rather than sea surface temperatures *(Cabedo-Sanz et al., 2013)*. Contradictory to these findings, HBI II has also been found in warmer, ice free regions such as the Everglades in Florida *(Barrick et al., 1980; Volkman et al., 1983; Yruela et al., 1990; Summons et al., 1993; He et al., 2016)*. Hence, the relation of HBI II and sea ice remains unclear in the Northern Hemisphere.

In the Southern Hemisphere, *Belt et al. (2016)* identified the HBI II as a proxy for landfast ice, termed $IPSO_{25}$, and stated that it may be produced by sea ice dwelling diatoms, living in landfast ice close to the coast.

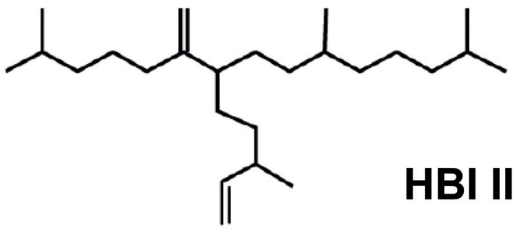

Fig 1. 14 Chemical structure of HBI II.

1.4.3. Indicators for organic carbon sources

For the identification of organic carbon sources, organic geochemical bulk parameters (e.g., C/N ratios, $\delta^{13}C_{org}$ values), maceral composition and biomarkers can be used (e.g., *Meyers 1997; Stein & Macdonald, 2004*). Especially biomarkers may give precise information about these sources (for an overview see *Stein & Macdonald, 2004*). For input from terrestrial sources, long chain n-alkanes, (C_{25}, C_{27}, C_{29}, C_{31}) and lignin, originating in vascular plants, have been established as reliable proxies (e.g., *Prahl & Muehlhausen, 1989; Yunker, et al., 1995)*. Specific short chain n-alkanes (C_{17}, C_{19}; *Blumer et al., 1971; Prahl & Muehlhausen, 1989; Yunker et al., 1995)* and short chain fatty acids (e.g., *de Leeuw et al., 1983; Fahl & Stein, 1997; Nichols et al., 1984; Volkman et al., 1993*) are produced by marine organisms and are established proxies for marine organic matter production. The production and accumulation of these biomarkers in sediments is strongly affected by environmental conditions, which makes them useful tools for paleoenvironmental reconstructions.

For this thesis, specific sterols (Fig 1.15) are used as indicators for terrigenous input from higher land plants and marine primary production (e.g., *Meyers, 1997; Fahl & Stein, 1999, 2007*). Brassicasterol and dinosterol, produced by a wider range of marine diatoms and dinoflagellates, have been established as biomarkers for marine phytoplankton productivity (e.g., *Volkman, 1986; Volkman et al., 1993*). However, the application of brassicasterol should be considered with caution, as it may partly synthesised by limnic diatoms *(Yunker et al., 1995)* and possibly to a minor extent by sea ice diatoms *(Belt et al., 2013)*. Hence, the application of brassicasterol for marine open water productivity is restricted by ecological conditions such as riverine freshwater input, as observed on the Siberian shelves *(Fahl & Stein, 1999; Fahl et al., 2003; Hörner et al., 2016)*.

β-sitosterol and campesterol have been proven as a useful biomarker proxies for higher land plants, i.e., terrigenous organic matter input *(e.g., Huang & Meinschein, 1979; Volkman et al., 1993)*. Despite that, these sterols have also been found in marine organisms *(Volkman et al., 2008; Rontani et al., 2014)*. However, they have been successfully applied in marine sediment records to reconstruct terrigenous input to the Arctic Ocean (e.g., *Fahl & Stein, 1997, 1999, 2007; Xiao et al., 2013, 2015a)*.

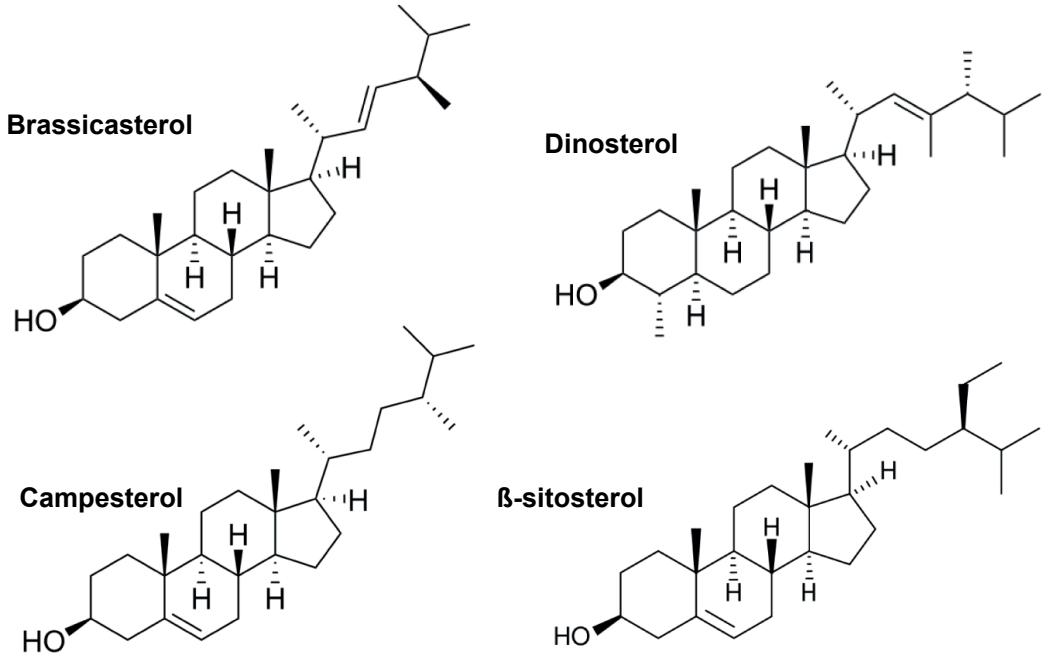

Fig 1. 15 Chemical structures of the sterols used in this study for organic carbon sources.

1.5. Rationale and key questions of this thesis

The Arctic Ocean plays an important role in Earth's climate; especially the role of sea ice, its dynamics and variability are of crucial interest in the reconstructions of past environmental changes. Due to its high sensitivity and internal feedback mechanisms sea ice has active influence on climate developments on short as well as long time scales.

Correlations of instrumental climate records with signals recorded in modern surface sediments create a framework to ground truth proxy signals and provide a vital baseline to understand their paleorecords. So far, the sea ice biomarker approach (i.e., IP_{25} and related PIP_{25} index) has mainly concentrated on specific areas, i.e., Fram Strait and East Greenland Shelf, Barents Sea, the Bering Sea and the Central Arctic and Russian Shelf Seas. Further, the relatively new approach to use HBI III as phytoplankton biomarker has so far only been correlated to satellite observed sea ice concentrations in the Barents Sea region. Hence, it is important to extend the biomarker surface database quantitatively and spatially to answer the following questions:

How reliable is the biomarker sea ice approach? How well do biomarker sea ice proxies reflect recent circum-Arctic sea ice conditions?

Several microfossil proxies are commonly used to reconstruct sea ice, i.e., foraminifera (e.g., *(Aagaard-Sørensen et al., 2010; Werner et al., 2011; Seidenkrantz, 2013)*, ostracods (e.g., *Cronin et al., 2013)*, diatoms (e.g., *Justwan & Koç, 2008*), organic walled dinocysts (e.g., *de Vernal et al., 2005; Bonnet et al., 2010*). However, only few multi-proxy studies have compared and correlated the outcome of these different indirect sea ice reconstruction approaches *(Weckström et al., 2013; Berben et al., 2014; Pieńkowski et al., 2017)* and evaluated their accuracy and response to specific ecological settings. This leads to the following research question:

Do biomarker sea ice proxies correlate with other more commonly used microfossil sea ice proxies (i.e., foraminifera, diatoms and dinocysts)?

Once the applicability of the biomarker approach is tested in an (over-) regional approach, it is possible to reconstruct past sea ice conditions in high-resolution biomarker studies in key areas, such as the shelves of Greenland. These areas are located in a highly sensitive climate region, as they directly underlie the pathway of low saline polar waters and sea ice exported from the Arctic Ocean. Further, they are closely located to the GIS, the biggest freshwater reservoir in the Northern Hemisphere. Despite the importance of these regions, only few studies have reconstructed past sea ice changes in these regions with a direct biomarker approach *(e.g., Müller et al., 2012; Cormier et al., 2016)* . These relatively low-resolutions studies could only resolve the general Holocene climate trend, but not the short-term variability. This leads to the following research question:

How did sea ice conditions change over the last 5 kyr on the East and West Greenland Shelves? Are specific late Holocene short-term oscillations recorded in biomarker sea ice records from these areas?

Special emphasis will be laid on the 'Neoglacial'. This general cooling, related to a decrease in solar insolation *(Wanner et al., 2011)*, is accompanied by an increase of

sea ice and has been recorded in several archives in the Northern Hemisphere (North Atlantic sediments: e.g., *Marchal et al., 2002; Jennings et al., 2002, 2011; Sicre et al., 2008; Andresen et al., 2012; Telesiński et al., 2014; Cabedo-Sanz et al., 2016;* Greenland: *Gowan et al., 2003; Anderson & Leng, 2004; Olsen et al., 2012)*. So far, *Müller et al. (2012)* found an increase in sea ice in the eastern Fram Strait, that followed the solar insolation decrease. In the same study, no evidence for a response of sea ice on the East Greenland Shelf to the reduction in solar insolation was found. This leads to the following research question:

Is the Neoglacial cooling reflected in sea ice records on the Greenland Shelves?

Further, modern climate observations recorded an opposing climate pattern between Europe and West Greenland *(Saabye, 1942; van Loon & Rogers, 1978)*. The anti-correlation of these areas has been related to the Northern Hemisphere climate pattern of the NAO *(Rogers, 1984; Hurrell, 1995; Portis et al., 2001; Hanna & Cappelen, 2003)*. Late Holocene climate events such as the MCA and LIA have been linked to general shifts in this mode and suggest that the opposing signals between East and West Greenland were also distinctive on centennial to millennial time scales *(Keigwin & Pickart, 1999; Seidenkrantz et al., 2007a, 2008)*. In paleoclimate records from the North Atlantic specific oceanographic changes could be associated with shifts in the NAO mode *(e.g., Sicre et al., 2008; Müller et al., 2012)*, whereas on the West Greenland side the relation of changes to modes of the NAO are less consistent and seem to follow a more complex pattern *(Seidenkrantz et al., 2008; Ribeiro et al., 2012; Krawczyk et al., 2013)*. This leads to the following research question:

Is there an evident anti-phase relationship/seesaw pattern of sea ice conditions between the East and West Greenland Shelf?

1.6. Concept of this thesis

In order to further assess its applicability, the biomarker sea ice reconstruction approach, i.e., IP_{25} and PIP_{25} index, is tested on an extended set of surface sediments. By this, biomarker concentrations and sea ice indices are compared to modern sea ice observations (derived from satellite passive microwave measurements) in a circum-Arctic approach. To widen the spatial distribution, previously published surface biomarker data were combined with our new surface data. To test the applicability of the biomarker sea ice index PIP_{25} and the reliability of different phytoplankton markers used in its calculation, the different indices are compared to modern satellite derived sea ice concentrations in key areas, i.e., the Baffin Bay/Labrador Sea and the Fram Strait/Barents Sea.

Besides the study of surface sediments, sea ice conditions and open water phytoplankton production are reconstructed for pre-industrial times on well-dated sediment cores using the same biomarker approach. One of the goals of this thesis is to compare sea ice variability on the East and West Greenland Shelves. For this purpose, cores from these regions were selected, i.e., from the mouth of Foster Bugt (East Greenland) and from the mouth of Disko Bugt (West Greenland). One specific selection criterion for these cores was a high resolution of the mid- and late Holocene in order to detect short-term variability and specific climate events within the late Holocene. In addition, biomarker results were compared to previously published microfossil records (i.e., foraminifera, diatoms and dinocysts) from the same samples. This approach enables the evaluation of the sensitivity of each proxy to sea ice and provides a better understanding of the ecological system and changes.

In Chapter 1 the significance of the (sub-)Arctic Ocean and its sea ice cover are introduced. The global effect and environmental as well as social consequences of changes in (sub-)Arctic sea ice cover are pointed out. Within this context, key scientific questions that should be addressed in this thesis are developed. A strategy to address these questions is presented.

In Chapter 2 the analysed sediment material and applied methods are presented.

Chapters 3 to 5 include three individual studies in order to address the previously

stated research questions (see Chapter 1.5).

Chapter 3 (Paper I) presents a study of surface sediments comparing biomarker sea ice reconstructions with modern sea ice conditions in key areas, i.e., Central Arctic, Fram Strait, Barents Sea and Baffin Bay. Moreover, other commonly used microfossil sea ice proxies (i.e., diatoms and dinocysts) are compared to the biomarker sea ice reconstructions. Relatively good correlations of the PIP_{25} index to modern sea ice conditions verify the biomarker approach for paleo sea ice reconstruction. However, in some regions the correlation remains unclear.

The first high-resolution biomarker sea ice reconstruction from the East Greenland Shelf over the past 5 kyr is presented in Chapter 4 (Paper II). One aim of this study is to gain insight into the sensitivity of sea ice on the East Greenland Shelf and its relation to oceanographic and atmospheric changes. The sea ice record from the East Greenland Shelf seems to be mainly influenced by a combination of processes in the adjacent fjord and a constant influence of the EGC. Hence it does not reflect the over-regional Neoglacial cooling trend. However, over the past 2 kyr reconstructions reveal a high sensitivity to short-term climate variability, which is reflected in sea ice and phytoplankton biomarker proxies.

In Chapter 5 (Paper III), a late Holocene, i.e., the last 2.2 kyr, sea ice reconstruction from Disco Bugt, West Greenland is presented. The intention of this study is to provide a more direct insight into the sea ice variability on the West Greenland Shelf during the late Holocene and compare it to previously published proxy records (for overview see *Moros et al., 2016*). Further, with the new biomarker record we aim to provide new insights into a possible anti-phase correlation of sea ice conditions compared to the NAO mode.
Our biomarker record indicates a spatial expansion of the sea ice cover in the Baffin Bay with the establishment of ice edge conditions during the Little Ice Age, around 0.3 kyr BP. It seems that NAO mode shifts are not reflected in the sea ice record from Disko Bugt, but the gradual sea ice increase seems to follow the Neoglacial reduction in solar insolation. A multi proxy comparison of previously published geochemical and microfossil proxies to this new biomarker record confirms that different proxies are strongly affected by the strong seasonality and stratification of

the Disko Bugt area.

A comparison of microfossil sea ice proxies to the new biomarker record supports the biomarker approach as a reliable sea ice proxy, microfossils associated with sea ice seem strongly affected by other environmental factors, e.g., meltwater, nutrient availability and atmospheric temperatures.

Finally, Chapter 6 provides a conclusion of the findings from the individual studies in order to address the key questions (see Chapter 1.5). Further, remaining questions and possible strategies are specified.

1.7. Declaration of author's contribution

This thesis has been carried out within the framework of the International Research Training Group ArcTrain under the supervision of Prof. Dr. Rüdiger Stein. Funding was provided by the Deutsche Forschungsgemeinschaft (DFG). The Alfred Wegener Institute (AWI) - Helmholtz Centre for Polar and Marine Research, section Marine Geology (Department of Geosciences) provided laboratories and technical support. The thesis is written cumulatively, composed of three joint-authorship papers that have been or will be published in peer-reviewed journals.

Paper I (Chapter 3): Henriette M. Kolling, Anne de Vernal, Rüdiger Stein, Kirsten Fahl, Taoufik Radi, Estelle Allan, Xiaotong Xiao, Diana W. Krawczyk; 'Proxy reconstructions of modern Artic sea ice cover – IP_{25}, dinocysts and diatoms'; *in preparation*.

The concept of this study was developed by myself in discussion with Anne de Vernal and Rüdiger Stein. I performed the organic geochemical analyses (biomarkers and TOC) on new surface samples presented in this chapter. Anne de Vernal analysed 77 samples for dinocysts and MAT sea ice reconstructions. Statistical analyses were performed by Anne de Vernal, Estelle Allan and Taoufik Radi. Anne de Vernal wrote Chapters 3.3.3, 3.3.4 and 3.3.5 concerning the Dinocyst methods and statistical approach. All other parts of the manuscript and figures were written and produced by me with contributions by Rüdiger Stein. Diana W. Krawczyk contributed sea ice diatom assemblages. Anne de Vernal, Kirsten Fahl and Rüdiger Stein and contributed to the interpretation of the data and the final manuscript.

Paper II (Chapter 4): Henriette M. Kolling, Rüdiger Stein, Kirsten Fahl, Kerstin Perner, Matthias Moros (2017). 'Short-term variability in late Holocene sea ice cover on the East Greenland Shelf and its driving mechanisms'. *Palaeogeography, Palaeoclimatology, Palaeoecology, Vol. 485, pp. 336-350.*

I performed all organic geochemical analyses used in this chapter. I wrote the first version manuscript and elaborated the figures. The revised version of the manuscript and the interpretation of the data benefited from the input by Rüdiger Stein. All co-authors contributed to the final version manuscript and the discussion.

Paper III (Chapter 5): Henriette M. Kolling, Rüdiger Stein, Kirsten Fahl, Kerstin Perner, Matthias Moros. ‚New insights into sea ice changes over the past 2.2 kyr in Disko Bugt, West Greenland' *Submitted to 'PAST Gateways special issue of arktos - The Journal of Arctic Geosciences', November 2017*

I developed the concept of the manuscript in discussion with the co-authors. I performed all organic geochemical analyses used in this chapter, except for 33 samples, which were analysed by Walter Luttmer. I interpreted the biomarker results, in discussion with the co-authors. I wrote the first version of the manuscript and produced all figures. The revised version of the manuscript benefitted from helpful contributions from Rüdiger Stein. All co-authors contributed to the final version of the manuscript.

2. Material and organic geochemistry

2.1. Material

2.1.1. Surface sediments

Surface sediments selected for this thesis were collected between 2008 and 2015 during several campaigns from a variety of cruises between 53° and 90° N and 74° W and 172° E. In total, 132 samples have been collected from the Baffin Bay (*Dorschel et al., 2014)* and the West Greenland Shelf (n = 65; *Krawczyk et al., 2017*), Hudson Strait (n = 5; *Pollehne et al., 2015)*, the Gulf of St Lawrence (n = 6; *Pollehne et al., 2015*), Fram Strait and East Greenland Shelf (n = 17; *Geissler, 2013; Stein, 2015, 2016*) and Barents Sea (n = 24; *Hanebuth, 2013)* as well as the Central Arctic Ocean (n = 12; *Hanebuth, 2009; Stein, 2015*). The wide geographical range of this sample set required the use of different sampling methods, i.e., multi corer, box corer and grab. Depending on local sedimentation rates and bioturbation some of these surface sediments (0 – 2 cm) may represent time periods varying between several years up to several millennia *(e.g., Stein et al., 1994; Stein, 2008; Ternois et al., 2001 and references therein)*. For most of the surface sediments no exact age control is provided, however, selected sediment samples from the *R/V Paaimut* expedition from the West Greenland Shelf were analysed for natural ^{210}Pb and artificial ^{137}Cs radionuclides (emitted during nuclear bomb testing in the 1950s; *Krawczyk et al., 2017*). 20 of the 46 samples from the West Greenland Shelf were confirmed as modern, i.e., deposited after 1950.

2.1.2. Sediment Core PS2641 from the East Greenland Shelf

For the study on the East Greenland Shelf gravity core PS2641-4 and box core PS2641-5 were combined into a continuous record, referred to as ‘Core PS2641’. These cores were obtained on the East Greenland Shelf (73°09.35’N, 19°29.00’W; water depth: 469 m), during the *R/V Polarstern* Expedition ARK-X/2 in 1994 *(Hubberten, 1995)*. Gravity core PS2641-4 provides a 700 cm continuous record, of which the upper 251 cm were selected for this thesis. Sediments were sampled in 1 cm steps. Box core PS2641-5 provides a continuous 44 cm long record of the uppermost undisturbed sediments, which were sampled in 0.5 cm steps. A first description of the lithology of both cores was given by *Hubberten (1995)* and later in

more detail by *Evans et al. (2002)*. A brief summary of the lithology of both cores is given in Fig 2.1 and Chapter 4.

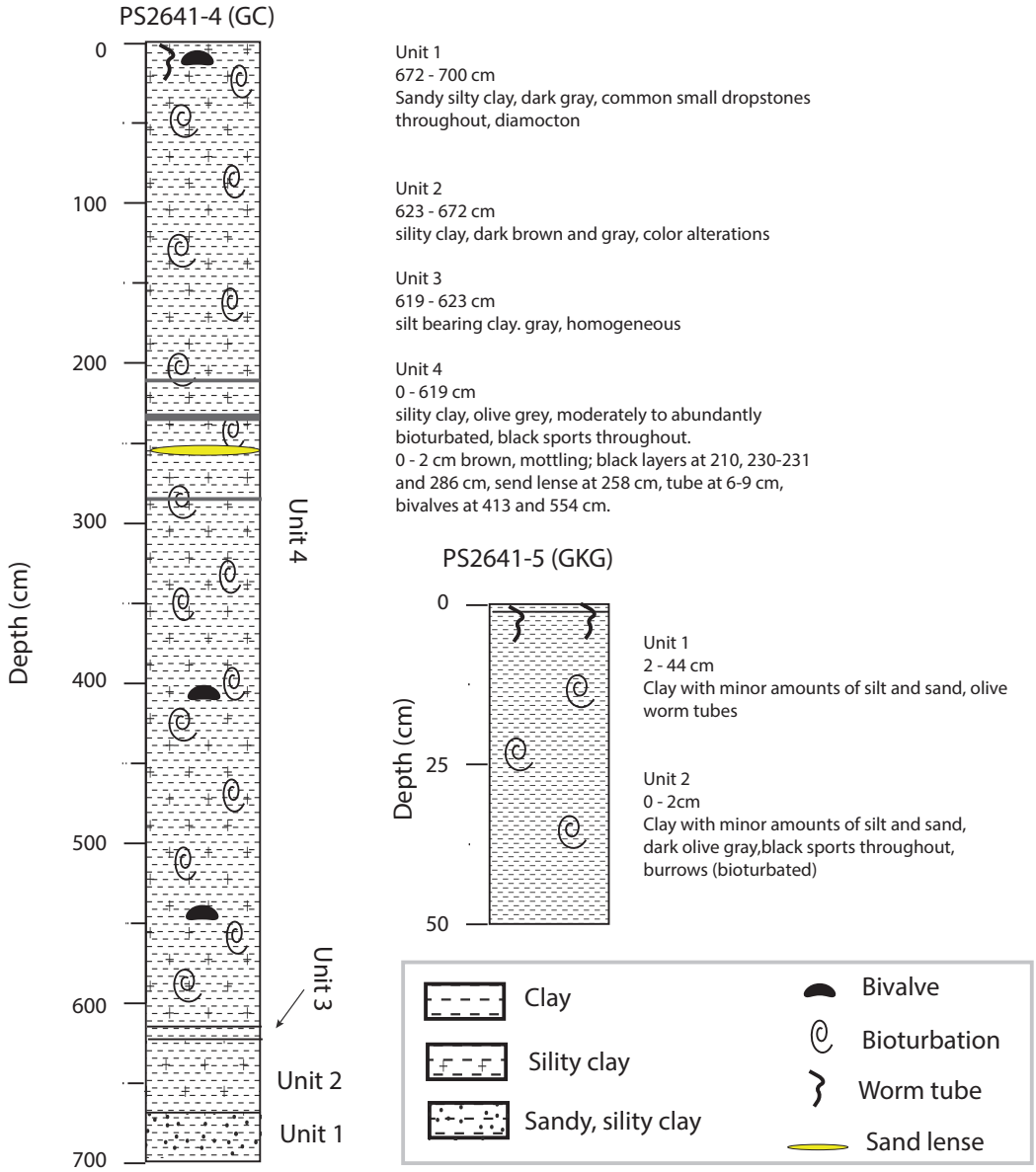

Fig 2. 1 Schematic illustration of the lithology of sediment Cores PS2641-4 (Gravity Core, GC) and PS2641-5 (Box Core, GKG), adapted after *Hubberten, 1995, Evans et al., 2002*.

2.1.3. Sediment Core 343310 from Disko Bugt, West Greenland

To study the Disko Bugt region, a gravity and a multi core from station 343310 were selected. They were obtained from Ededesminde Dyp, southwestern Disko Bugt (68° 38' N, 53°49' W, water depth: 855 m) during the *R/V Maria S. Merian* expedition MSM05/03 *(Harff et al., 2007)*. The gravity core provides a 940 cm continuous record, of which the upper 580 cm were analysed for this thesis. Sediments were sampled in 1 cm steps. The multi core provides a continuous 32 cm long record of

the uppermost undisturbed sediments, which were sampled in 0.5 cm steps, of which six specific sampled were selected for biomarker analysis. A brief summary of the lithology of gravitiy core 343310-5-1 is given in Fig 2.2 and Chapter 5.

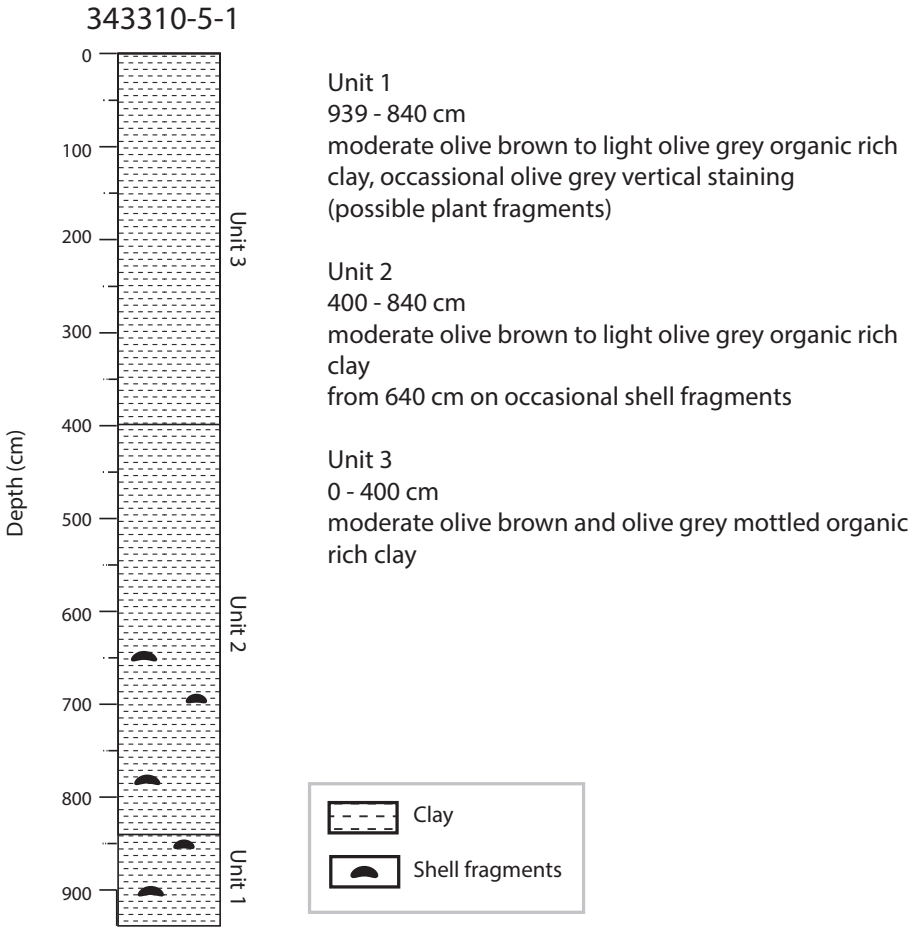

Fig 2. 2 Schematic illustration of the lithology of gravity core 343310-5-1 after *Harff et al., 2007*.

2.2. Organic Geochemistry

2.2.1. Elemental Analysis – Bulk Parameter

Total organic carbon (TOC) was measured on samples that were frozen at -20°C, subsequently freeze-dried and homogenized beforehand. Carbonates were removed by adding hydrochloric acid (500 µl). TOC was then measured on 100 µg sedimentary material with a carbon-sulphur analyser (ELTRA CS-125CS-125).

2.2.2. Chemical processing

For organic geochemical analyses, 5 g of freeze-dried and homogenized sediment was used. The following internal standards have been added for quantification purposes prior to extraction: androstanol (5α-androstan-3β-ol, 20 µl/sample), squalane (100 µl/sample), 7-HND (7-hexylnonadecane, 20 µl/sample), cholesterol-D_6 (cholest-5-en-3β-ol-D_6, 20 µl/sample) and 9 OHD (9-octylheptadec-8-ene, 20 µl/sample).

Within this thesis two extraction methods were applied. For the sediment cores for Paper I and II (Chapters 4 and 5) an Accelerated Solvent Extractor (DIONEX, ASE) was used for biomarker extraction. With this method, the following temperature-pressure programme was applied: 200 °C, 1000 psi, 5 min; 100 °C, 5 min, 1000 psi. Using this method, dichloromethane:methanol (2:1 vol/vol) was used as solvent as well.

Biomarker extraction of surface sediments used in Chapters 3 and 5 was carried out by sonication. For this method 30 ml of dichloromethane:methanol (2:1 vol/vol) was added to the sample which was then sonicated for 15 min. Following, sediment and solvent were centrifuged for 3 min (2000 rotations/min) and the solvent was decanted. This procedure was repeated three times, the collected extract was kept for further treatment.

During the following procedure, the total liquid extracts from both extraction methods were treated identically. Extracts were separated in different fractions by open-column chromatography, using SiO_2 as stationary phase. *N*-hexane (5 ml) was used as solvent for IP_{25}, and ethylacetate:*n*-hexane (2:8 vol/vol; 7-9 ml) for sterols.

The sterol fraction was derivatized with 200 µl BSTFA (bis-trimethylsilyl-trifluoroacet-amide) by heating the fraction to 60°C for 2 two hours.

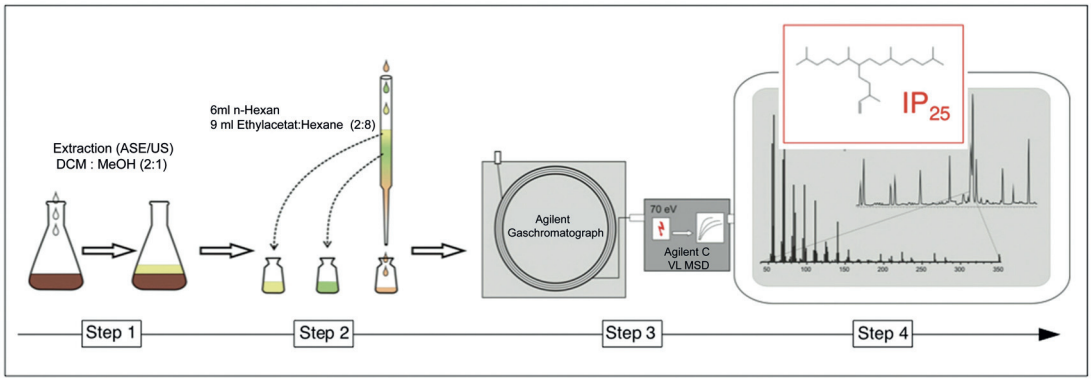

Fig 2. 3 Schematic illustration of the chemical processing and analytical methods for biomarker analysis. Step 1: Extraction with ASE or sonication (US). Step 2: Extracts are separated into hydrocarbon and sterol fractions by open column chromatography. Step 3 and 4: Both biomarker fractions are analysed with Gas Chromatography-Mass Spectrometry (GC-MS). Source: *Stein et al., 2012.*

2.2.3. Biomarker identification

Hydrocarbon concentrations were identified with a gas chromatograph Agilent Technologies 7890 GC (30 m HP-1MS column, 0.25 mm I.d. and 0.25 µm film thickness) coupled to an Agilent Technologies 5977 A mass selective detector (Triple-Axis Detector, 70eV, constant ionization potential, Scan 50-550m/z, 1scan/s, ion source temperature 230°C) with a detection limit of 5 ng/ml (i.e., 0.05 ng/gSed). Sterol concentrations were identified with a gas chromatograph Agilent Technologies 6850 GC (30 m HP-1MS column, 0.25 mm I.d. and 0.25 µm film thickness) coupled to an Agilent Technologies 5975 A mass selective detector (Triple-Axis Detector, 70eV, constant ionization potential, Scan 50-550m/z, 1scan/s, ion source temperature 230°C) with a detection limit of 10 ng/ml (i.e., 0.1 ng/gSed). With both devices, the following temperature programme was applied for hydrocarbon analyses: 60 °C (3 min), 150 °C (rate: 15 °C/min), 320 °C (rate: 10 °C/min), 320 °C (15 min isothermal) and for sterols: 60 °C (2 min), 150 °C (rate: 15 °C/min), 320 °C (rate: 3 °C/min), 320 °C (20 min isothermal). For each measurement 1 µl of the sample was injected, helium was used as carrier gas. Hydrocarbon and sterol fractions were measured in full scan mode (SCAN) and additionally hydrocarbons were also measured in the selected ion monitoring (SIM) mode. Throughout the measurements, instrument stabilities were controlled by reruns of external standards several times during one analytical sequence and by replicate

analyses for random samples.

Individual hydrocarbon compounds were identified by their specific retention times with a specific reference compound and by the compound specific fragmentation pattern in the mass spectra from published data; IP_{25}: *Belt et al., 2007;* HBI II: *Johns et al., 1999*; HBI III: *Belt et al., 2000*; sterols: *Boon et al., 1979; Volkman, 1986*. In case of low molecule abundances, it was not possible to acquire a spectrum for IP_{25}. In that case, IP_{25} was quantified in the selective ion monitoring (SIM) by applying its molecular ion m/z 350. When applying the SIM method to detect lower concentrations, more than one characteristic ion of IP_{25} has to be identified to verify its identification. A Kovats index of 2086 for IP_{25}, 2084 for HBI II and 2046 for HBI III was calculated.

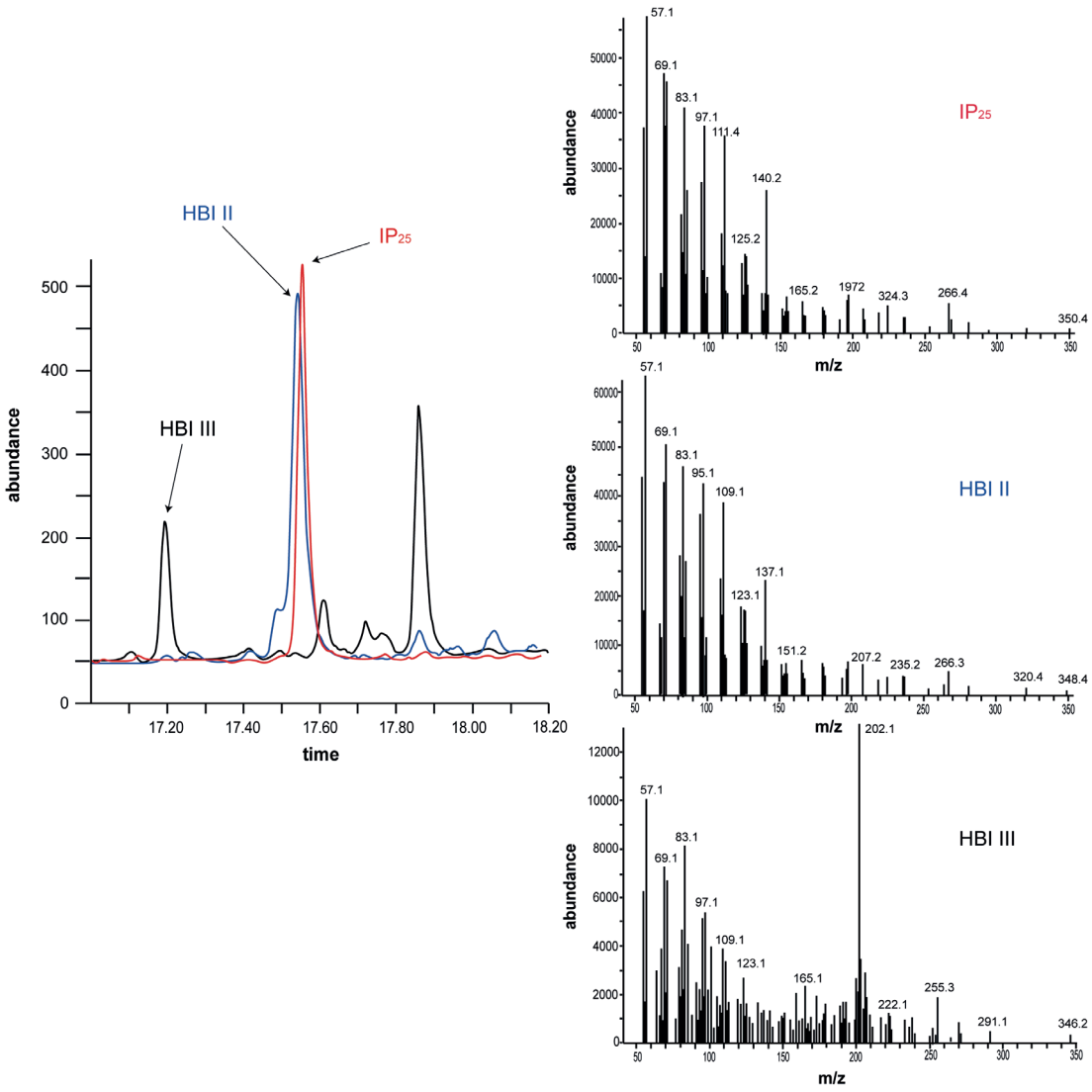

Fig 2. 4 The chromatogram (TIC) of the studied HBIs IP_{25}, HBI II and III as well as their mass spectra, taken from the surface sediments from sample GeoB19927 on the West Greenland Shelf.

2.2.4. Quantification of biomarkers

Hydrocarbons have been quantified by their molecular ion (m/z; IP_{25}: m/z =350; HBI II: m/z = 348; HBI III: m/z = 346) in relation to that of the abundant fragment ion m/z = 266 of the internal standard 7-HND in the SIM mode. In order to balance the different responses of m/z 266 of ions of the internal standard and of those of the molecular ions of specific hydrocarbons an external calibration is required. For further details see *Fahl & Stein, 2012*.

Trimethylsilyl ethers of the sterols were quantified by their molecular ions (brassicasterol: m/z = 470, campesterol: m/z = 472, β-sitosterol: m/z = 486, dinosterol: m/z = 500) in relation to the molecular ions of the internal standards cholesterol d6 (m/z = 464) or androstanol (m/z = 348). For brassicasterol, dinosterol, campesteorol and β-sitosterol, a retention time index of 1.018, 1.019, 1.042 and 1.077 were calculated respectively.

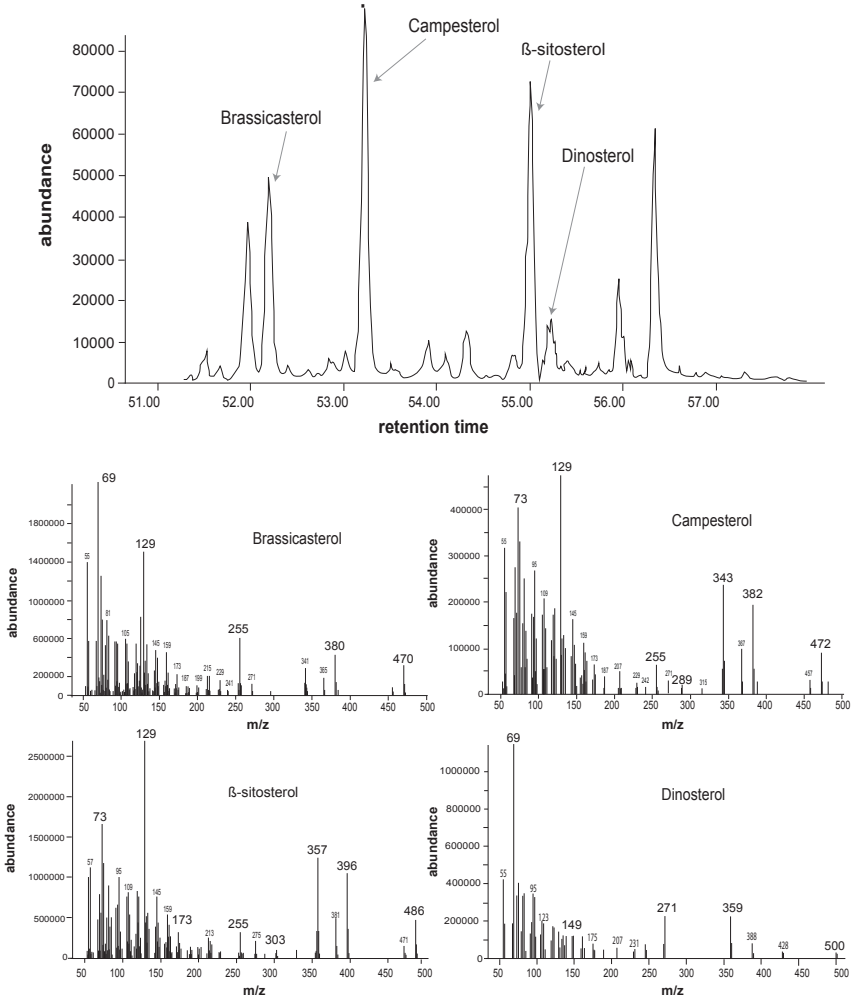

Fig 2. 5 The chromatogram (TIC) of the studied sterols: brassicasterol, campesterol, β –sitosterol and dinosterol as well as their mass spectra, taken from the surface sediments from sample GeoB19961-2 on the West Greenland Shelf

The concentrations of all biomarkers have been normalised to the extracted amount of sediment and TOC. If densities were available, accumulation rates of biomarkers were calculated.

3. Proxy reconstruction of modern Arctic sea ice cover – IP_{25}, dinocysts and diatoms

Henriette M. Kolling[a], Anne de Vernal[b], Ruediger Stein[a], Kirsten Fahl[a], Taoufik Radi[b], Estelle Allan[b], Xiaotong Xiao[c] , Diana W. Krawczyk[d]

[a] Alfred Wegener Institute, Helmholtz Centre for Polar and Marine Research, Bremerhaven, Germany

[b] Centre de rechereche en géochemie et géodynamique (Geotop), Université du Québec à Montréal, Montréal, Québec, Canada

[c] Institute of Marine Organic Geochemistry, Ocean University of China, Qingdao, PR China

[d] Greeland Climate Resreach Centre, Greenland Institute of Natural Resources, Nuuk, Greenland

Abstract

The reconstruction of past sea ice variability is crucial to understand the present sea ice development and estimate future changes. In order to understand proxy signals in paleorecords it is necessary to standardize the sedimentary signal with the comparison to modern observed environmental parameters. 132 surface sediments from key areas in (sub-) Arctic regions were analysed for specific sea ice (IP_{25}) and phytoplankton biomarkers (sterols, HBI III), additionally 73 samples were analysed for their dinocyst content. The new biomarker data obtained from the surface samples were combined with previously published biomarker surface data to a circum-Arctic database. The new circum-Arctic PIP_{25} database shows a good spatial representation of modern spring sea ice conditions and correlates relatively well with modern sea ice concentrations. The applicability of the HBI III as phytoplankton marker in the $P_{III}IP_{25}$ approach on an over-regional scale indicates promising results, however the applicability in specific areas (e.g., Laptev Sea, eastern Fram Strait) remains uncertain and requires further work. A regional comparison of sea ice reconstructions based on biomarkers, modern analogue technique dinocyst and diatom approaches revealed that all approaches provide reliable sea ice reconstructions for the West Greenland Shelf.

3.1. Introduction

Sea ice plays a crucial role in the Earth's energy budget via the sea ice albedo feedback *(Thomas & Dieckmann, 2010; Wohlfahrt et al., 2004)*. Moreover, the sea ice cover restricts heat and moisture exchange between ocean and atmosphere, whereas the formation and melting of sea ice control the thermohaline properties of the upper water column through brine formation in winter and release of freshwater in summer *(Petrich & Eicken, 2010; Thomas, 2012)*. Hence, the seasonal extend and retreat of Arctic sea ice is an important component of the global climate system. Furthermore, it is of high ecological importance, as it influences the conditions in the photic zones and thus the primary productivity *(Wassmann et al., 2011)*. Sea ice also provides habitat for polar marine mammals and birds *(Loeb et al., 1997; Stein, 2008; Dieckmann & Hellmer, 2010)*.

Satellite observation illustrate the reduction in Arctic sea ice cover extent over the last three decades *(e.g., Comiso et al., 2008; Perovich et al., 2009; Stroeve et al., 2007, 2012)* which has raised the concern about the fate of Arctic sea ice. The influence of anthropogenic greenhouse gas emission on the recent sea ice loss is very likely and the respective effect of anthropic forcing and natural variability is a matter of debate *(Swart, 2017)*. The satellite observations being of too short duration for adequate representation of the full range of sea ice variability. Thus, reconstructions of long time series are necessary to understand the observed changes and their driving mechanisms.

Since 1978, with the launch of the Nimbus7 satellite, sea ice extend has been determined from passive microwave measurements *(Comiso et al., 1997; Parkinson, 2008)*. The sea ice extent and thickness data compiled for intervals prior to 1978 come mostly from aerial and ship observations as well as historical charts *(Rothrock et al., 1999; Walsh & Chapman, 2001; Rayner et al., 2003)*. Going further back in time, sea ice reconstructions have to rely on biogenic and sedimentary proxies preserved in marine sediments *(de Vernal et al., 2013a and references therein)*. These include ice rafted detritus (e.g., *Stein et al., 1994; Vogt et al., 2001; Spielhagen et al., 2004; Andrews, 2009)*, assemblages of microfossils, such as foraminifera (e.g., *Aagaard-Sørensen et al., 2010; Werner et al., 2011; Seidenkrantz, 2013)*, ostracods (e.g., *Cronin et al., 2010*), diatoms (e.g., *Koç et al., 1993)* organic walled dinoflagellate cysts ('dinocysts'; e.g., *de Vernal et al., 2001, 2005, 2013c; Bonnet et al., 2010)* and organic biomarkers such as IP_{25} *(Belt et al., 2007; Müller et*

al., 2011).

However, most of these proxies are indirectly related to sea ice and the reconstructions are mostly qualitative *(de Vernal et al., 2013a)*. Further, dissolution of siliceous and calcareous microfossils is often occurring in Arctic and subarctic settings causing poor preservation of diatoms and foraminifera *(Wollenburg et al., 2001, 2004; Armand & Leventer, 2010)*. From this point of view, biogenic remains composed of resistant organic matters, such as the IP_{25} biomarkers *(Belt et al., 2007; Müller et al., 2011; Smik et al., 2016)* and dinocysts *(de Vernal et al., 2013b, 2013c)* provide very useful tracers of past sea ice covers. Concerning dinocysts, the development of a large standardized database in the Northern Hemisphere ($n > 1492$) permitted to demonstrate linkages between the distribution of dinocyst assemblages and specific sea-surface parameters (i.e., sea surface temperature, sea surface salinity and seasonal sea ice cover extent) and the application of the modern analogue technique (MAT; e.g., *de Vernal et al., 1997, 2001, 2005; Rochon et al., 1999)*. For the newer biomarker IP_{25} approach, studies of surface distribution in several areas provided a good spatial coverage and illustrate a relationship with satellite observed sea ice conditions at regional to over regional scales *(Müller et al., 2011; Méheust et al., 2013; Navarro-Rodriguez et al., 2013; Xiao et al., 2013, 2015a; Belt et al., 2015; Smik et al., 2016)*. However, the lack of standardization from one study to another and the spatial discontinuity of the data set prevent unequivocal calibration and the development of circum-Arctic distribution maps.

By extending the IP_{25}/PIP_{25} surface sample database in the Labrador Sea and the Baffin Bay and increasing the sample density in other areas in the Northern Hemisphere, we aim to improve the knowledge on the IP_{25} distribution and to develop correlations of the IP_{25}/PIP_{25} with modern sea ice conditions for (semi-) quantitative reconstructions. Furthermore, a set of selected samples, were also analysed for their dinocyst and diatom content in order directly compare the most common sea ice proxies, i.e., IP_{25}, (preliminary) dinocyst and diatom assemblages/MAT reconstructions. The study area for this comparison is the Baffin Bay, which covers a wide range of sea ice conditions and displays a strong annual variability. With this intercomparison, we aim to improve the understanding of sea ice proxy signals and the quality of sea ice reconstructions from sedimentary records.

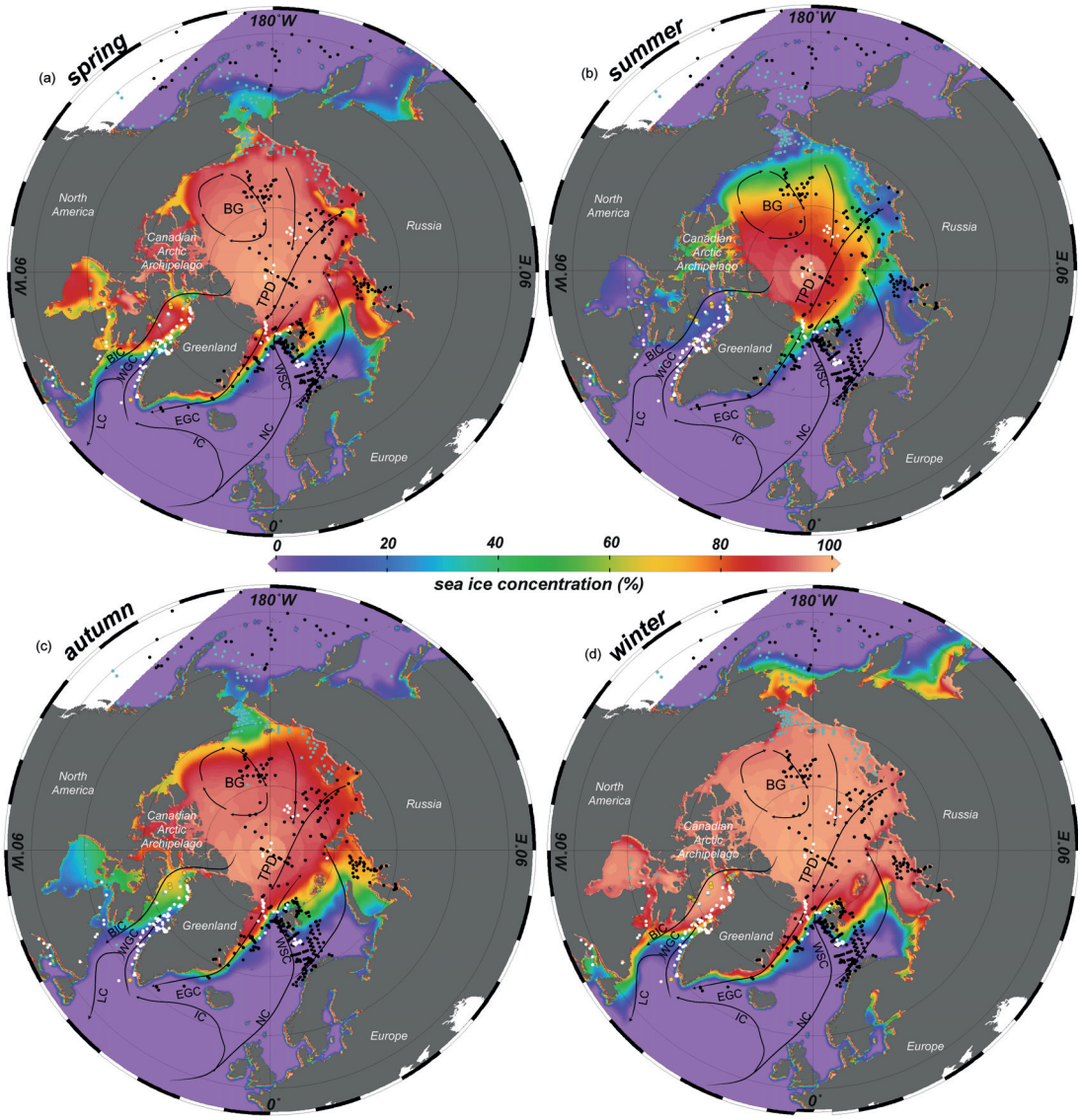

Fig 3. 1 Average sea ice concentration in ***(a)*** spring (April, May June), ***(b)*** summer (July, August, September), ***(c)*** autumn (October, November, December) from 1978 – 2015 *(Cavalieri et al., 1996; updated 2015)*. White dots indicate locations of new surface sediments, black dots indicate previously published surface samples included in this study. Blue dots indicate a surface sediments from *Stoynova et al. (2013),* that were not included in this study. Yellow dots show surface samples that will, later be included to the database. Further, dominant surface currents are indicated. Abbreviations are as follows: BG - Beaufort Gyre; BIC – Baffin Island Current; EGC – East Greenland Current; IC – Irminger Current; LC – Labrador Current; NC – Norwegian Current; TPD – Transpolar Drift; WGC – West Greenland Current; WSC – West Spitsbergen Current.

3.2. Regional Setting

The (sub-) Arctic Ocean is highly influenced by the annual expansion and retreat of sea ice. Only the Central Arctic Ocean remains covered by multi-year ice whereas the adjacent regions become mostly ice-free during the summer months (Fig 3.1; *Cavalieri et al., 1996; updated 2015)*. When sea ice expands during winter, the Arctic ice sheet extends towards Fram Strait and Barents Sea, the Canadian Arctic Archipelago and Baffin Bay. These areas are covered by either locally formed sea ice

or Arctic sea ice transported by currents and winds to these regions. The main export of Arctic sea ice occurs via western Fram Strait by the East Greenland Current (EGC), which flows south along the East Greenland Coast and carries large amounts of Arctic water masses and sea ice into the North Atlantic (Fig 3.1; *Aagaard and Coachman, 1968a, b)*. In the eastern Fram Strait sea ice conditions are less severe caused by the northward inflow of warm and saline Atlantic waters of the West Spitsbergen Current (WSC) towards the Arctic (Fig 3.1; *Rudels et al., 2005*).

Another export route of Arctic water masses and sea ice is via the Canadian Arctic Archipelago towards Baffin Bay via the Baffin Island Current (BIC), which flows south along the Canadian Shelf towards Labrador Sea (Fig 3.1; *Drinkwater, 1996*). The Canadian Arctic Archipelago remains partly ice covered during the summer months, whereas the Baffin Bay is mostly ice free during summer and covered by sea ice during winter (Fig 3.1; *Cavalieri et al., 1996; updated 2015*). Sea ice starts to form in the northwest of Baffin Bay and extends southeast (Fig 3.1). In the eastern Baffin Bay, the inflow of the West Greenland Current (WGC) strongly affects sea ice extent, as it is composed of EGC and Atlantic Irminger Current (IC) Waters (Fig 3.1; *Tang et al., 2004; Cuny et al., 2005; Myers et al., 2007)*. It may carry Arctic Sea ice and polar waters but also warm saline Atlantic waters (*Tang et al., 2004*). The interplay between the expansion of sea ice, polar outflow of polar and Atlantic derived water strongly characterizes the oceanography and extent of sea ice in (sub-) Arctic shelf Seas and Basins (e.g., *Gloersen et al., 1993; Martin and Wadhams, 1999; Årthun et al., 2012*).

3.3. Material, Methods and Approach

3.3.1. Surface sediment samples

Surface sediments were collected during numerous cruises between 2008 and 2015 of several research vessels *(Hanebuth et al., 2009; Geissler et al., 2013; Uenzelman-Neben, 2013; Dorschel et al., 2015; Pollehne et al., 2015; Stein et al., 2015, 2016; Krawczyk et al., 2017)*. Due to different sediment properties grabs, Box Cores and Multi Cores have been used to retrieve sediments in the Central Arctic (n = 12), Fram Strait and the East Greenland Shelf (n = 17), Barents Sea (n= 24) Baffin Bay and the West Greenland Shelf (n = 65) and the Gulf of Saint Lawrence (n=6), the Hudson Strait (n = 5) as well as from three fjords along the Labrador Coast (n=3) between 53° and 90° N and 74° W and 172° E. A total of 132 surface sediment

samples were analysed for biomarker content, i.e., IP_{25}, HBI III, brassicasterol, dinosterol, campesterol, β-sitosterol (see Fig 3.1). 73 of those samples were also analysed for dinocyst assemblages.

3.3.2. Biomarker approach and biogeochemistry

3.3.2.1. Biomarker approach

Information on terrigenous and marine organic matter input may be obtained by specific biomarkers such as n-alkanes, sterols, alkenones, as successfully demonstrated in paleoenvironmental reconstructions *(e.g., Fahl & Stein, 1999, 2007; Foster et al., 2015; Meyers, 1997; Moros et al., 2016; Stein et al., 2016; Yunker et al., 2011)*. For example, the distribution of β-sitosterol and campesterol have been proven as useful proxies for higher land plants, i.e., terrigenous organic matter input *(e.g., Huang & Meinschein, 1979; Volkman et al., 1993; Xiao et al., 2015a, b; Hörner et al., 2016)*. Brassicasterol and dinosterol are associated with the open water productivity of a wide range of algae groups, i.e., diatoms and dinoflagellates *(e.g., Kanazwa et al., 1971; Goad & Withers, 1982; Volkman et al., 1993)* and are established open water phytoplankton biomarker proxies *(e.g., Volkman, 1986; Volkman et al., 1993; Hoff et al., 2016; Knies et al., 2017)*.

A sea ice diatom derived highly-branched isoprenoid (HBI) alkene with 25 carbon atoms (i.e., IP_{25}; *Belt et al., 2007; Brown et al., 2014)* has been established as a direct proxy for Quaternary sea ice conditions in the Arctic and sub-Arctic *(e.g., Massé et al., 2008; Müller et al., 2009; Vare et al., 2009; Belt et al., 2010; Fahl and Stein, 2012; Hörner et al., 2016; Stein et al., 2017a, b)*. Further, IP_{25} seems to be stable on millennial time scales and has been found in Miocene and Pleistocene sediments *(Knies et al., 2014; Stein et al., 2016)*.

To avoid misleading interpretations concerning the absence of IP_{25}, which may result either from a lack of sea ice or a permanent, thick sea ice cover with too low light penetration for ice algae growth (*Horner & Schrader, 1982*), and for a more detailed understanding of sea ice conditions *Müller et al. (2011)* have combined the sea ice proxy IP_{25} with open water phytoplankton biomarkers, i.e. brassicasterol (P_BIP_{25}) and dinosterol (P_DIP_{25}), in the so-called 'PIP_{25} index' calculated after the following the following equation *(Müller et al., 2011)*:

$$PIP_{25} = IP_{25}/ (IP_{25} + (\text{phytoplankton biomarker x c})) \quad (1)$$

With c as a balance factor, being the ratio of mean IP_{25} concentration to mean sterol concentration, to counterbalance the higher concentrations of sterols compared to IP_{25}.

Recently, *Smik et al. (2016)* have modified the PIP_{25} approach by introducing a tri-unsaturated HBI alkene (HBI III, $C_{25:3,}$ z-isomere), probably associated more to ice margin productivity, as open water phytoplankton biomarker. HBI III is produced by marine diatoms of the genera *Pleurosigma* and *Rhizosolenia (Rowland et al., 2001; Belt et al., 2017)*, which may be beneficial for environmental reconstruction as it seems to be produced by a smaller group of organisms than brassicasterol and dinosterol and has been suggested to display a higher ecological sensitivity to sea ice *(Belt et al., 2015)*. So far, its applicability has only been tested in the surface sediments from the Barents Sea and Norwegian Sea region *(Belt et al., 2015; Smik et al., 2016)* and in paleorecords from the Barents Sea and Central Arctic Ocean *(Berben et al., 2017; Stein et al., 2017a)*. A wider spatial distribution of this approach is strongly needed, to verify its circum-Arctic applicability. Nevertheless, the PIP_{25} approach appears to be a promising step forward in (semi-) quantitative sea ice reconstructions as demonstrated in numerous studies (e.g., *Müller et al., 2012; Navarro-Rodriguez et al., 2013; Müller and Stein, 2014; Belt et al., 2015; Xiao et al., 2015b; Stein et al., 2017a, 2017b*).

In this study, brassicasterol, dinosterol and HBI III were used as phytoplankton biomarker to calculate the P_BIP_{25}, P_DIP_{25} and $P_{III}IP_{25}$, respectively.

3.3.2.2. Biogeochemistry

For geochemical analysis freeze-dried and homogenized surface sediments were used. On these samples total organic carbon (TOC) content and concentrations of the IP_{25} monoene, HBI III, 24-methylcholesta-5, 22-dien-3β-ol (brassicasterol), 4 α -23, 24 trimethyl-5α-cholest-22E-en-3β-ol (dinosterol), 24-ethylcholest-5-en-3β-ol (β-sitosterol) and 24-methylcholest-5en-3β-ol (campesterol) were determined.

Prior to the extraction, two internal standards, 7-HND (7-hexylnonadecane, 20 µl/sample) and androstanol (5α-androstan-3β-ol, 20 µl/sample), were added for quantification purposes. About 5 g of dried, homogenized sediment was extracted with sonication (3 x 15min) with dichloromethane:methanol (2:1 vol/vol) as solvent. The extracts were separated in different fractions by open-column chromatography, with SiO_2 as stationary phase. As solvent *n*-hexane (5 ml) was used for IP_{25}, and ethylacetate:*n*-hexane (20:80 vol/vol; 7 ml) for sterols. The sterol fraction was silylated using 200µl BSTFA (60°C, 2 h).

Hydrocarbon concentrations were identified with a gas chromatograph Agilent Technologies 7890 GC (30 m HP-1MS column, 0.25 mm I.d. and 0.25 µm film thickness) coupled to an Agilent Technologies 5977 A mass selective detector. Sterol concentrations were identified with a gas chromatograph Agilent Technologies 6850 GC (30 m HP-1MS column, 0.25 mm I.d. and 0.25 µm film thickness) coupled to an Agilent Technologies 5975 A mass selective detector. Measurement settings and identification of sterols and hydrocarbons (IP_{25}, HBI II, HBI III) were performed as described in *Fahl and Stein (2012)*. The concentrations of all biomarkers have been normalised to the extracted amount of sediment and TOC (both show nearly the same signal, we only show the data corrected against the amount of sediment referred to as µg/gSed). Instrument stability was controlled by reruns of external standards several times during one analytical sequence and by replicate analyses for random samples.

All data from this study, including environmental data, will be available on www.pangea.de upon publishing.

3.3.3. Dinocyst data

Dinoflagellates occur in all marine environments including sea ice. Hundreds of dinoflagellate taxa that have been reported from Arctic seas *(Poulin et al., 2011)*, but only a few produce cysts which preserve in sediments (e.g., *de Vernal et al., 2001; Matthiessen et al., 2005)*. The knowledge about the biology-ecology of dinoflagellates and their related cysts is incomplete. To date, no dinoflagellate yielding fossilisable cyst has been demonstrated to live in sea ice, except *Islandinium minutum* (cf. *Potvin et al., 2013*). Therefore, the relationship between sea ice cover

and dinocyst assemblages is indirect and was mostly defined from the analyses of their distribution *(de Vernal et al., 1994, 1997, 2001, 2005, 2013b; Rochon et al.,1999; Bonnet et al., 2010)*. The relationship probably rather depends upon parameters linked to sea ice conditions, such as seasonality, salinity, temperature, density and trophic level. A basic assumption is that sea ice controls the length of the living cycle of phototrophic taxa and that sea ice diatom productivity is determinant for heterotrophic taxa. Hence there are only a limited number of taxa adapted to achieve their life cycle in a short period and harsh conditions characterizing sea ice margin environments. In general, sediments from areas characterised by multiyear perennial pack-ice, where primary productivity is extremely low, are barren in dinocyst (e.g., *Rochon et al., 1999; de Vernal et al., 2013b)*. In areas characterized by seasonal sea ice, there are several dinocyst taxa routinely recovered from sediments. They include heterotrophic taxa (*Brigantedinium* spp., *Islandinium minutum*, *Islandinium*? *cezare, Echinidinium karaense, Polykrikos* sp. var. Arctic) and phototrophic taxa (*Pentapharsodium dalei, Spiniferites elongatus*, *Operculodinium centrocarpum*, *Impagidinium pallidum*). Among those, *Islandinium minutum*, *Islandinium*? *cezare, Echinidinium karaense*, *Polykrikos* sp. var. Arctic, *Spiniferites elongatus* and *Impagidinium pallidum* are often characteristic of subarctic environments characterized by seasonal sea ice. Otherwise, the majority of dinocyst taxa in the Northern Hemisphere data base (> 60 taxa) occur in warmer environments without sea ice.

The reference dinocyst database from the Northern Hemisphere was developed after standardization of the laboratory procedures with regard to sieving (10 μm) and chemical treatments avoiding oxidation techniques (see description in *Rochon et al., 1999)* and establishment of an operational standardized taxonomy. In the last published update *(de Vernal et al., 2013c)*, the database includes 1492 sites and 64 taxa after grouping. The relationship between dinocyst assemblages and sea surface conditions illustrated from multivariate analyses showing that sea ice stand out as determinant parameter, together with temperature, salinity and productivity. On these grounds, the modern analogue technique (MAT) over as expressed either in terms on number of month/year of sea ice cover > 50% or in mean annual concentration. Validation results yielded error of prediction of ±1.4 months/year of sea ice and ± 1.2/10 for concentration. One important source of error is the potential discrepency between the time interval of the reference data for the "modern" sea ice cover (1953-

2003) and the time interval represented in the surface sediment samples, which may include decades to millennia depending upon sedimentat accumulation rates (for detailed discussion, see *de Vernal et al., 2013c)*.

For the purpose of this paper, 72 surface sediment samples were analysed for their palynological content, following the standardized laboratory procedures of GEOTOP. Special attention was paid to dinocysts, which were counted and identified following the methodology adopted to develop the reference database. All results are reported here, but only the assemblages with counts > 100 cysts were used for the application of MAT.

3.3.4. Environmental dataset

Most modern environmental data used here, i.e., sea ice concentration, sea surface temperature and salinity as well as productivity are based on satellite observations. For instrumental sea ice concentration, we used the Nimbus 7 SMMR, SSM/I and SSMIS passive microwave data set *(Cavalieri et al., 1996, updated 2015)* provided by the National Snow and Ice Data Centre *(NSIDC)*. This record spans the time interval from 1978 to 2015. Another sea ice parameter considered corresponds to the number of months per year of sea ice with concentration greater than 50%. The values were based on a compilation from the NSIDC, using an interval spanning 1953 to 2003, which includes both satellite observations (post 1978) and data from charts and aerial photographs. The parameter also include the mean and the standard deviation (one sigma) of sea ice cover, which illustrate the large inter-annual variability of sea ice in the domain of winter-spring sea ice margins. The other parameters are the summer (July-August-September) sea-surface temperature (SST) and salinity (SSS) from the 2001 version of the World Ocean Atlas *(National Oceanographic Data Center, 2001)*. The mean annual productivity expressed in $gC/m^2/year$ was compiled from the MODIS satellite observation (http://modis.gsfc.nasa.gov/index.php/; cf. *Radi and de Vernal, 2008)*.

3.3.5. Statistical analysis

Distributional maps of sea ice, biomarker and dinocyst data were generated with Ocean Data View *(Schiltzer, 2017)*.

Multivariate analyses were performed with the Canoco software *(ter Braak and Šmilauer, 2002)*. The analyses included principal component analyses on dinocyst assemblages and biomarkers in addition to redundancy analyses (RDA) and canonical Correspondence Analysis (CCA) to examined the interrelationship between the different set of proxy data and the environmental parameters. Following the procedure of the software, detrended correspondence analyses (DCA) were used to identify the type of function between assemblages and environmental variables. Depending upon the length of the first axis (number of standard deviations) indicating linear (sd < 2) or unimodal-type functions (sd > 2), RDA and/or CCA were performed.

3.4. Results

Figure 3.2 shows the composite (new and previously published) surface biomarker data set. It illustrates the distribution of the single biomarkers in the (sub-)Arctic realm.

Low to absent IP_{25} concentrations are observed in the central Arctic Ocean (Fig 3.2a). Concentrations increase on the Russian Shelves, around Svalbard, along the East Greenland Shelf, in the northern Baffin Bay and in the Hudson Strait (Fig 3.2a). IP_{25} concentrations diminish in southern Barents Sea, Bering Sea and around the Cape of Farewell (Fig 3.2a).

HBI III is absent in the central Arctic Ocean and concentrations increase strongly on the Kara and Laptev Sea Shelves, the southern Chukchi Sea, west and south of Svalbard and in the Baffin Bay around 70°N (Fig 3.2b). High HBI III concentrations are also observed in the Hudson Strait and the Gulf of Saint Lawrence (Fig 3.2b).

The open water phytoplankton sterols, brassicasterol and dinosterol, are absent or show very low concentrations in the perennial ice covered Central Arctic Ocean (Figs 3.2c, d). Elevated concentrations are observed in the Fram Strait, the East Greenland Shelf and in the Baffin Bay (Figs 3.2c, d). Brassicasterol and dinosterol concentrations are highest on the Laptev and Kara Sea Shelves, in parts of the Chukchi Sea, south of Svalbard and in the Hudson Strait (Figs 3.2c, d).

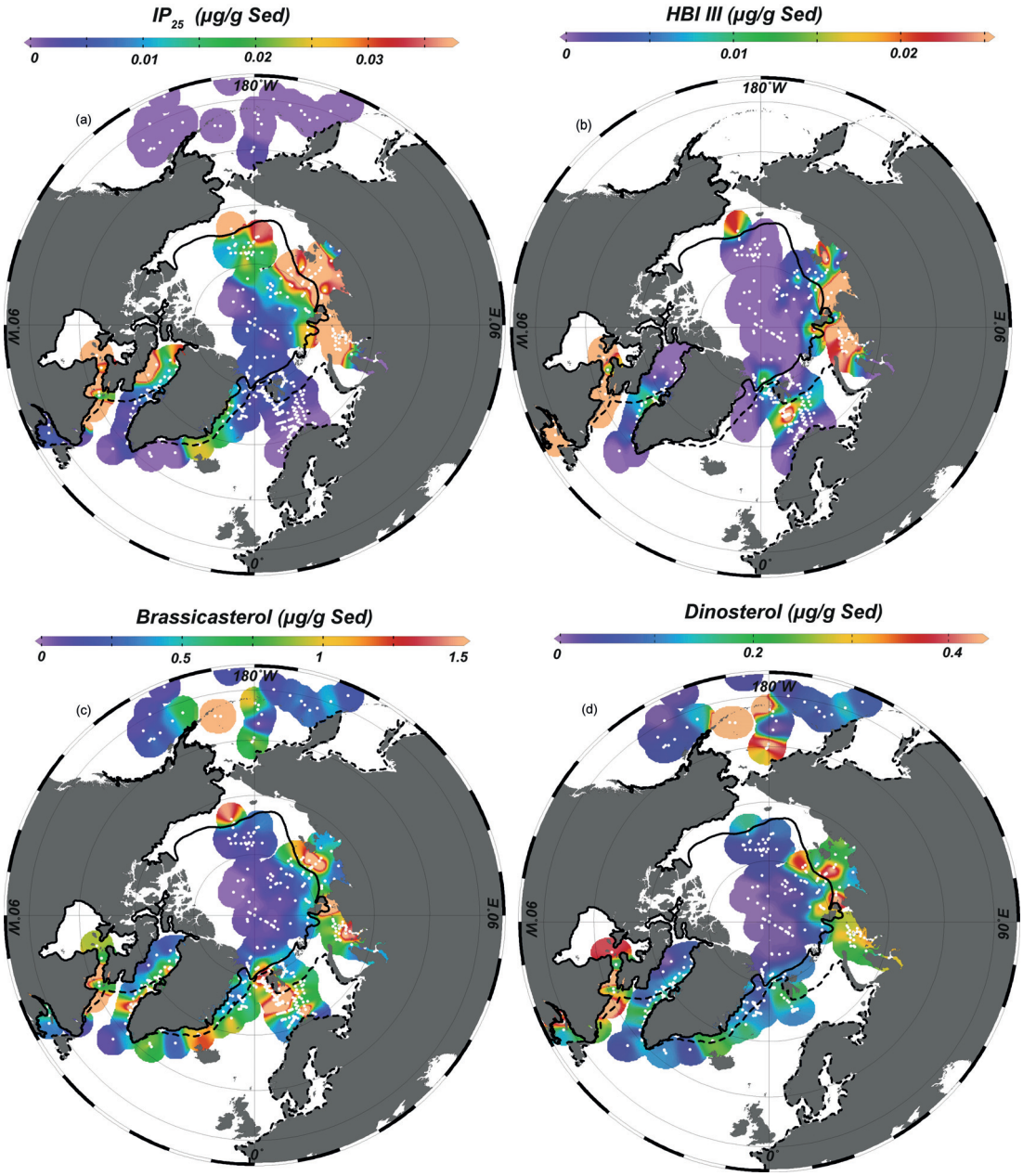

Fig 3. 2 Concentrations of ***(a)*** IP_{25}, ***(b)*** HBI III, ***(c)*** brassicasterol and ***(d)*** dinosterol (in µg/gSed) of new surface sediments and published data *(Müller et al., 2011; Méheust et al., 2013; Navarro-Rodriguez et al., 2013; Xiao, et al., 2013, 2015a; Belt et al., 2015; Smik et al., 2016)* in the Northern Hemisphere. The solid black line indicates the average minimum sea ice extent (1978-2015), the dashed line represents the average maximum spring sea ice extent (1978-2015).

The circum-Arctic distribution of the different sea ice indices is displayed in Figure 3.3. Very high P_BIP_{25}, P_DIP_{25} and $P_{III}IP_{25}$ values in the Central Arctic Ocean and in the northwestern Baffin Bay are caused by the absence/low values of phytoplankton biomarkers (i.e., brassicasterol, dinosterol, HBI III) and IP_{25} (Figs 3.3a, b, c). High IP_{25} and phytoplankton marker concentrations on the Russian and East and West Greenland Shelves lead to high to intermediate sea ice indices. Low sea ice indices,

caused by the absence of IP_{25} and high phytoplankton marker concentrations, are observed in the Bering Sea and off North Norway (Figs 3.3 a, b, c).

3.5. Discussion

Herein we present new surface sediment biomarker data from the Baffin Bay and Labrador Sea area. Further, we expand the biomarker database, especially with regard to the phytoplankton marker HBI III, in specific areas, i.e., the Fram Strait, the Barents Sea and the Central Arctic Ocean. For a detailed Arctic-wide discussion of the biomarker approach, we combine our new data with previously published surface records from the Fram Strait *(Müller et al., 2011)*, the Bering Sea *(Méheust et al., 2013)*, the Svalbard region and the Barents Sea *(Navarro-Rodriguez et al., 2013; Belt et al., 2015; Smik et al., 2016)* and the Central Arctic Ocean and adjacent Russian marginal seas *(Xiao et al., 2013, 2015a)*. These different biomarker records link together nicely and provide a nearly Arctic-wide dataset (Fig 3.2). Previously published biomarker surface data by *Stoynova et al. (2013)*, from the sub-polar North Atlantic and Pacific, display biomarker and TOC concentrations that are several magnitudes higher than observed in our Baffin Bay samples and in samples from the Barents Sea and Arctic Ocean (e.g., *Navarro-Rodriguez et al., 2013; Xiao et al., 2015a)*. As the method and laboratory used by *Stoynova et al. (2013)* were not included in an inter-laboratory study *(Belt et al., 2014)*, the reliability of their results remains unconfirmed. Hence, we did not include the surface samples of *Stoynova et al. (2013)* in our comprehensive dataset.

3.5.1. Circum-Arctic and regional biomarker distributions

Compared to the modern satellite derived sea ice conditions, the comprehensive circum-Arctic biomarker distribution reflects the regional extent of perennial and seasonal sea ice and can be related to specific current systems, which seem to affect (ice) algae production to a great extent (Figs 3.1, 3.2). Further, the circum-Arctic biomarker distributions display a wide range of concentrations (Fig 3.2). Therefore, we are precautious with comparing single extreme values and focus on trends rather than absolute concentrations.

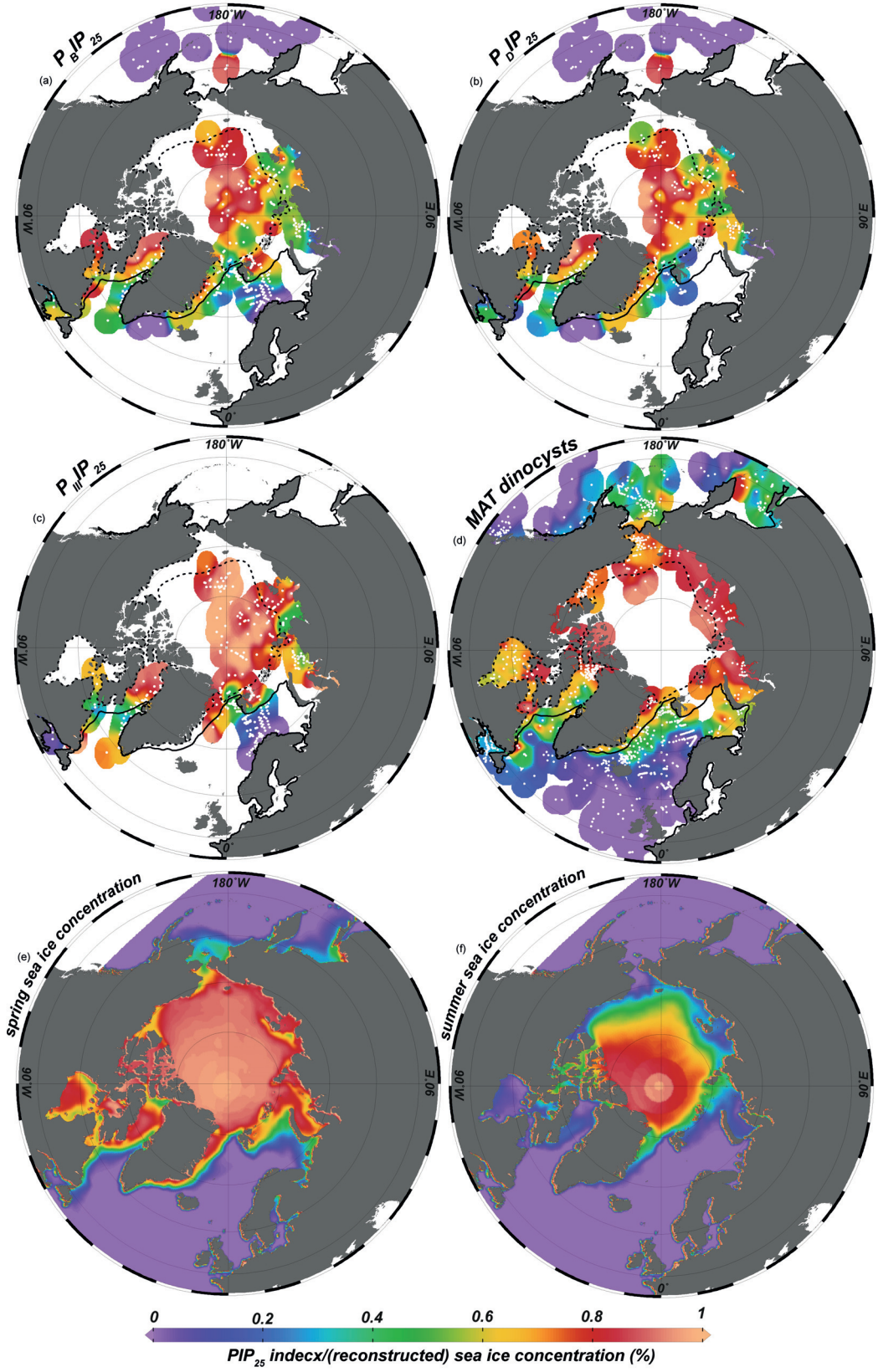

Fig. 3. 3 New and published *(Müller et al., 2011; Méheust et al., 2013; Navarro-Rodriguez et al., 2013; Xiao, et al., 2013, 2015a; Belt et al., 2015; Smik et al., 2016)* values of the PIP_{25} indices using ***(a)*** brassicasterol (P_BIP_{25}) ***(b)*** dinosterol (P_DIP_{25}), ***(c)*** HBI III ($P_{III}IP_{25}$), and ***(d)*** MAT dinocyst sea ice reconstructions *(de Vernal et al., 2013a)* compared to ***(e)*** average spring and ***(f)*** summer sea ice concentrations (1978-2015; *Cavalieri et al., 1996; updated 2015*) in the Northern Hemisphere. The solid line represents the spring sea ice extent, the dashed line the summer sea ice extent.

In general, the distribution of our new biomarker dataset supports previous findings, with IP_{25} present in seasonally ice-covered regions (i.e., Russian marginal seas, Barents Sea, Fram Strait, East Greenland Shelf, Baffin Bay) and absent in regions with perennial sea ice cover (i.e., the Central Arctic Ocean; *Xiao et al., 2015a*) as well as in ice-free regions (i.e., the Bering Sea; Fig 3.2a; *Méheust et al., 2013*).

In regard the phytoplankton biomarker HBI III, our over regional record supports findings from the Barents Sea *(Belt et al., 2015)*, as we find HBI III widely absent under perennial sea ice (Fig 3.2b). However, its relation to the marginal ice zone, as found in Barents Sea *(Belt et al., 2015)*, is less apparent in others regions of our circum-Arctic record (e.g., Fram Strait; Fig 3.2b).

In line with previous studies *(Müller et al., 2011; Navarro-Rodriguez et al., 2013; Xiao et al., 2015a, 2013)*, we find the phytoplankton sterols, brassicasterol and dinosterol absent under perennial sea ice, which restricts light and nutrient availability *(Walsh, 1989; Gosselin et al., 1997)*, and increasing concentrations in regions with seasonal ice cover and show highest concentrations along the spring ice edge (Fig 3.2c, d).

Central Arctic Ocean

Biomarker distributions in the Central Arctic Ocean seem predominantly affected by its perennial sea ice cover. Unfavourable light and nutrient conditions in this environment result in the (largely) absence of IP_{25} as well as the phytoplankton biomarkers brassicasterol, dinosterol and HBI III (Fig 3.2; *Walsh, 1989; Gosselin et al., 1997; Xiao et al., 2015a*). Thus, our dataset seems to support the use of HBI III as a phytoplankton marker for the PIP_{25} calculation *(Müller et al., 2011; Belt et al., 2015; Smik et al., 2016)*.

Russian marginal seas

High IP_{25} and open water phytoplankton sterol concentrations on the Russian shelves have been related to the annual retreat of sea ice (Fig 3.2; *Xiao et al., 2013)*. Seasonal phytoplankton and ice algae blooms in this area may be favoured by upwelling of nutrients in marginal ice zones and polynyas *(Sakshaug, 2004; Xiao et al., 2013; Willmes & Heinemann, 2016)*. High HBI III concentrations show a similar distribution pattern; it seems that parts of the seasonal ice-free regions and polynyas of the Russian shelves create favourable conditions for HBI III production (Fig 3.2b). However, HBI III concentrations are strongly reduced north of Kotelny, an area

characterized by a polynya during spring *(Dethleff et al., 1998; Xiao et al., 2013)*. In contrast, this area displays equally high IP_{25} and phytoplankton sterol concentrations (Fig 3.2a, c, d; *Xiao et al., 2013)*. A strong variability in ecological conditions and phytoplankton communities have been reported for different polynyas *(Tremblay and Smith, 2007)* and may result in the observed diminished distribution of HBI III. Brassicasterol and dinosterol are assumed to be produced by a wider range of organisms than HBI III *(e.g., Belt et al., 2017; Volkman et al., 1993)*, which may make HBI III more prone to different ecological settings. Further, HBI III concentrations reduce within the estuaries of Russian rivers (Fig 3.2b), which may support its marine origin *(Belt et al., 2017)*.

Fram Strait & East Greenland Shelf

In the Fram Strait and the Barents Sea the distribution of biomarkers seems to be closely related to the two dominant currents, the EGC and WSC.

In eastern Fram Strait and Barents Sea, the inflow of warm Atlantic waters from the WSC seems to create favourable conditions for phytoplankton blooms, reflected in high brassicasterol and dinosterol concentrations (Figs 3.2c, d; *Birgel et al., 2004; Hebbeln & Berner, 1993; Müller et al., 2011; Nöthig et al., 2015)*. Within the Barents Sea, our new HBI III data show highest concentration close to the spring ice edge, which is in line with distributions described by *Belt et al. (2015)* and *Smik et al., (2016)*.

In the western Fram Strait, within the EGC inflow, low biomarker concentrations may be related to low nutrient content of the inflowing polar surface waters and harsh sea ice conditions until summer, which may hamper phytoplankton production *(Aagaard & Coachman, 1968a, b; Hopkins, 1991; Johannessen et al., 1999; Müller et al., 2011)*. We find HBI III absent North off 75°N (Fig 3.2b), which is in line with the other phytoplankton sterol concentrations, i.e., dinosterol and brassicasterol (Figs 3.2c, d), which may be related to the long lasting sea ice cover until summer that may hamper phytoplankton productivity *(Müller et al., 2011)*. Compared to the other biomarkers, HBI III remains absent further south and southeast along the east Greenland coast (Fig 3.2). This may point towards a high ecological sensitivity, e.g., temperature, nutrients *(Nöthig et al., 2015)*, of HBI III, which is produced by a smaller group of organisms than dinosterol and brassicasterol *(Belt et al., 2015)*. However, the low sample resolution for HBI III on the East Greenland Shelf makes

further assumption difficult and displays the need to increase the sample density in this area.

Baffin Bay

In Baffin Bay, IP_{25} and phytoplankton marker concentrations seem to reflect the position of the spring ice edge (Fig 3.2). Highest IP_{25} concentrations correlate with highest sea ice concentration off Baffin Island, north of 70° N, where sea ice remains longest until July and forms first in November (Figs 3.1, 3.2a; *Cavalieri et al., 1996; updated 2015*). Vice versa, lowest phytoplankton sterol concentrations, i.e., brassicasterol and dinosterol (Figs 3.2c, d) correlate with the severe sea ice conditions in this area. Highest phytoplankton sterol concentrations seem to correlate with the position of the spring ice edge, where upwelling may favour phytoplankton blooms (Figs 3.2b, c; *Sakshaug, 2004*). The distribution of HBI III seems also closely related to the position of the spring ice edge (Fig 3.2b), however, the association to the marginal ice zone (*Belt et al., 2015)* is not as evident in Baffin Bay as observed in Barents Sea. The sea ice edge retreats completely from Baffin Bay in summer, however this retreat, as suggested by *Belt et al. (2015),* is not reflected in the HBI III distribution in this area. The Baffin Bay is strongly influenced by seasonal meltwater inflow from the Greenland Ice Sheet during late spring and summer, causing a strong stratification. During autumn, strong winds favour deep mixing and the upwelling of nutrients *(Humlum, 1985)*. This strong seasonality has a strong influence on phytoplankton blooms and communites. *Jensen and Christensen (2014)* observed strongly reduced diatom contributions to the phytoplankton community during spring (April, May, June) and September. Such a shift in the phytoplankton community may also influence the production of HBI III, produced by the marine diatom genera *Rhizosolenia (Belt et al., 2017)*.

For Hudson Strait, we observe high biomarker concentrations (Fig 3.2) that may be related to its seasonal sea ice cover *(Drinkwater, 1986)*. High accumulation rates and/or high nutrient supply from the hinterland may favour phytoplankton biomarker production.

High dinosterol and HBI III concentrations are observed in the Gulf of Saint Lawrence (Fig 3.2b, d), which is characterized by a brackish environment *(Le Fouest*

et al., 2005). In this brackish environment phytoplankton biomarkers might be also produced by freshwater algae. However, low IP_{25} concentrations, despite seasonal sea ice cover *(Le Fouest et al., 2005)*, may indicate an unfavourable environment for the marine and IP_{25}-producing sea ice diatoms *(Belt et al., 2007; Brown et al., 2014)*.

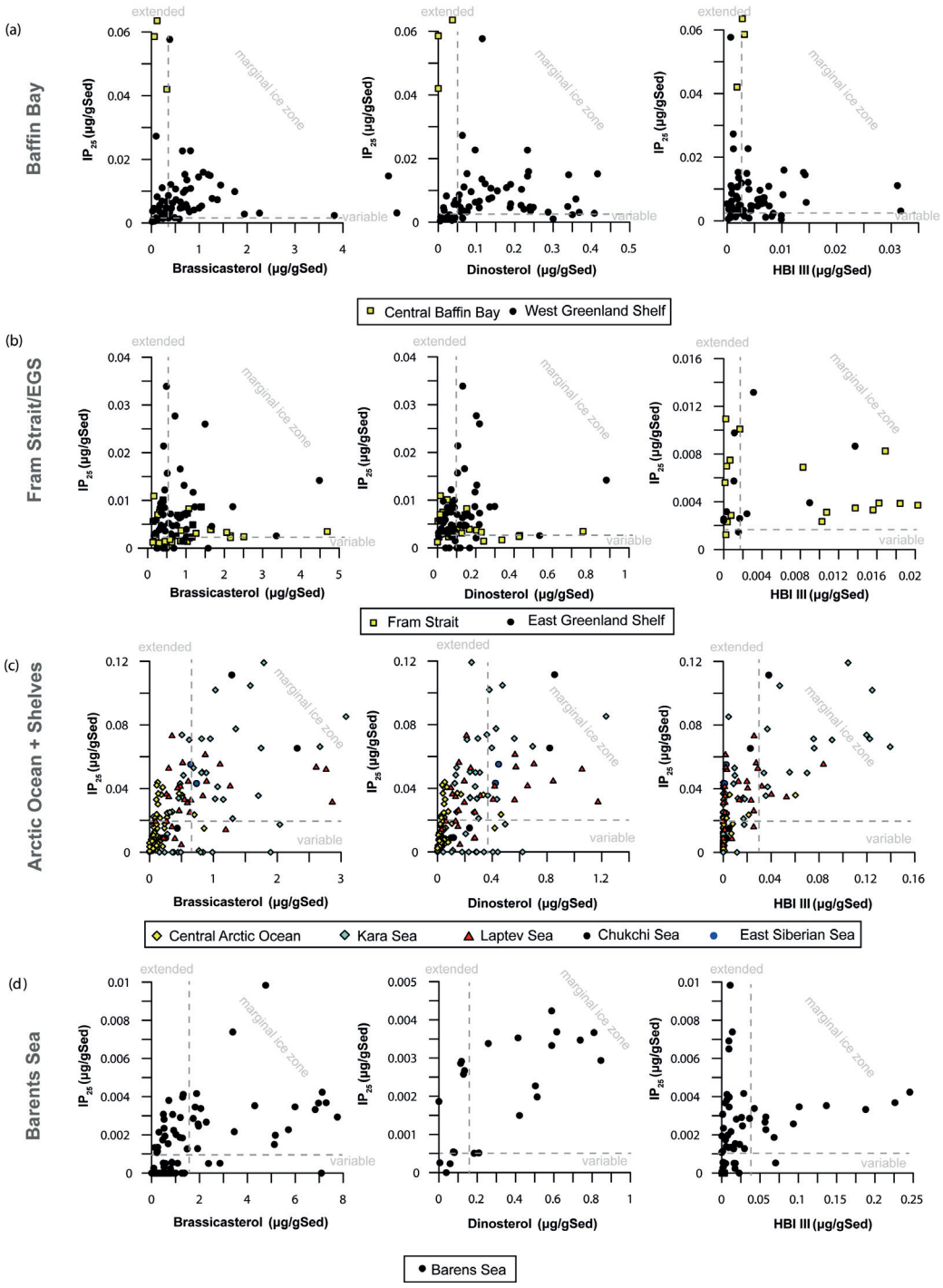

Fig 3. 4 Relationships of new and published IP_{25} to brassicasterol, dinosterol and HBI III in ***(a)*** Baffin Bay and West Greenland Shelf, ***(b)*** Fram Strait and the East Greenland Shelf (this study, *Müller et al., 2011; Navarro-Rodriguez et al., 2013; Xiao, et al., 2015a)*, ***(c)*** the Central Arctic Ocean and Russian marginal seas (this study, *Xiao, et al., 2013, 2015a)* and ***(d)*** in Barents Sea (this study, *Navarro-Rodriguez et al., 2013; Xiao, et al., 2015a; Belt et al., 2015; Smik et al., 2016)*. Classification of sea ice conditions is based on *Müller et al. (2011)*.

3.5.2. The PIP_{25} index and its implications for sea ice reconstructions

By the combination of phytoplankton markers with the sea ice marker IP_{25} (PIP_{25} index), sea ice biomarker surface sediments studies could achieve a better semi-quantitative reconstruction of modern sea ice than with IP_{25} alone *(Müller et al., 2011; Navarro-Rodriguez et al., 2013; Xiao et al., 2015a, Belt et al., 2015; Smik et al., 2016)*. However, the used phytoplankton marker and their (regional) applicability is strongly debated (for an overview see *Belt and Müller, 2013; Belt et al., 2015)*. With our comprehensive approach, we compare the PIP_{25} indices calculated by using the phytoplankton markers brassicasterol, dinosterol and HBI III respectively (Fig 3.3). For the first time, an over regional HBI III and $P_{III}IP_{25}$ data coverage is compared to satellite derived sea ice concentrations. The distribution of the P_BIP_{25} and P_DIP_{25} indices (Figs 3.2a, b) supports first findings of *Xiao et al. (2015a)* and reflect the spring sea ice conditions in Baffin Bay, Fram Strait and Barents Sea. In the Russian marginal seas and the Central Arctic Ocean values are closely related to the ice edge of perennial sea ice (Figs 3.3a, b; *Xiao et al., 2015a*). The $P_{III}IP_{25}$ index reflects the spring sea ice edge in Baffin Bay, Fram Strait and Barents Sea relatively good, in Laptev Sea however constant high values do not allow to distinguish between seasonally and permanent sea ice cover (Fig 3.3c). This may be caused by specific environmental conditions that restrict the production of HBI III in the seasonal sea ice covered regions of the Laptev Sea.

For the circum-Arctic dataset, as well as for specific regions, we find a positive correlation of IP_{25} to the phytoplankton markers brassicasterol, dinosterol and HBI III (Fig 3.4). The cross-plots of IP_{25} to the specific biomarker are helpful tools to differentiate between the different sea ice conditions (Fig 3.4). In line with the good spatial correlation of the PIP_{25} indices to spring sea ice (Fig 3.3), we find relatively good correlation of the PIP_{25} indices (P_DIP_{25} index ($r^2 = 0.49$), P_BIP_{25} ($r^2 = 0.48$) and $P_{III}IP_{25}$ ($r^2 = 0.53$); Appendix A3a).

With regard to specific areas, we find marked differences in the correlation of the different PIP_{25} indices to modern sea ice conditions (Appendix A3). We assume that regional environmental and seasonal differences, e.g., light conditions, nutrient availability, may play a role in the correlation of the different phytoplankton markers to modern sea ice. Further, the balance factor applied for the calculation of the P_BIP_{25}

and P_DIP_{25} is of concern and may strongly influence the accuracy of the index (for an overview see *Belt et al., 2015*). In order to test this hypothesis, the biomarker surface database, especially for HBI III and dinosterol, should be extended.

Our new comparative dataset indicates good correlations of all PIP_{25} indices for Baffin Bay and the West Greenland Shelf (r^2= 0.41-0.46) with modern spring sea ice (Appendix A3b). The relationship between IP_{25} to phytoplankton markers reflects the variable sea ice conditions in the area (Fig 3.4a). However, the $P_{III}IP_{25}$ index indicates much higher values than shown by P_BIP_{25} and P_DIP_{25} (Fig 3.3) and the relationship of HBI III to IP_{25} seem to partly overestimate the modern sea ice conditions (Fig 3.4a). Therefore, P_BIP_{25} and P_DIP_{25} seem to reflect the modern spring sea ice conditions better, despite the good correlation of $P_{III}IP_{25}$ to modern sea ice.

In the Fram Strait and on the East Greenland Shelf the relationship of IP_{25} to phytoplankton markers reflect mainly extended to marginal sea ice conditions. This is in line with satellite observations. However, we find only weak correlations of the PIP_{25} indices to spring sea ice concentrations in this area (Appendix A3c). This seems to be mainly caused by seven specific samples from a small area off northwest Svalbard (~5°W, ~80°N). These samples were analysed in three different studies (this study, *Navarro-Rodriguez et al., 2013; Xiao et al., 2015a)* and show extremely low PIP_{25} values that do not reflect the sea ice conditions (Fig 3.3). All samples were collected in a small area close to the spring sea ice edge and also within the inflow of Atlantic waters of the WSC (Fig 3.1). The inflowing Atlantic waters may create favourable conditions for phytoplankton growth causing high phytoplankton biomarker concentrations *(Nöthig et al., 2015)*, however IP_{25} concentrations are relatively low (Fig 3.2a), which may lead to the underestimation of the sea ice concentrations by the PIP_{25} index. We assume that biomarker concentrations in multi-annual surface samples from this area may be strongly affected by short-term WSC variability and associated rapid sea ice fluctuations as previously assumed for surface sediments on the West Svalbard shelf (*Smik and Belt, 2017)*. When removing these samples, the correlations can be improved significantly and are in the range as previously observed on a smaller dataset by *Müller et al., (2011)* (Appendix A3c).

In the Central Arctic Ocean, the relationship of IP_{25} to phytoplankton biomarkers reflects the enhanced sea ice conditions, with mostly extended and permanent sea ice cover (Fig 3.4c). However, we find no correlation of the calculated PIP_{25} indices to sea ice concentrations (Appendix A3d). This is line with previous findings by *(Xiao et al., 2013)*, who related this lack of correlation to sea ice transport and complex environmental conditions.

In the Barents Sea, the relationship of IP_{25} to the phytoplankton markers reflects the seasonal character of the modern sea ice conditions, with some areas of extended and permanent sea ice. Our dataset partly supports previous findings of relative good correlations of P_BIP_{25} to spring sea ice ($r^2 = 0.37$ Appendix A3e; *Navarro-Rodriguez et al., 2013*). Despite suggestions that HBI III may provide a higher sensitivity to ecological changes, we find similar correlations for the $P_{III}IP_{25}$ index ($r^2 = 0.32$; Appendix A3e), leading to the assumption that both indices reflect sea ice conditions to a similar extent. However, the correlations of the $P_{III}IP_{25}$ index in our comprehensive dataset display lower correlations than previously reported by *Smik et al. (2016)* for samples from Barents Sea and off northeast Svalbard. This may partly be caused by the bigger spatial distribution of our dataset, which includes a wider range of sea ice and environmental conditions (ice free, seasonal and permanent sea ice cover) whereas correlations reported by *Smik et al. (2016)* are mostly from samples from seasonal sea ice covered regions. Further in our dataset we included samples from West Svalbard, a region that is associated with rapid fluctuations in WSC intensity and associated sea ice fluctuation (*Smik and Belt, 2017*). It seems that highly variable sea ice conditions as found within the WSC inflow are a difficult area for sea ice concentration reconstructions based on surface sediments that may, based on sedimentation rates, represent several years to decades (*Navarro-Rodriguez et al., 2013* and references therein)

3.5.3. Comparison of sea ice proxies

3.5.3.1. PIP_{25} and MAT dinocyst sea ice reconstructions in the Northern Hemisphere

With the now acquired sea ice biomarker/PIP_{25} database, it is possible to compare it to one of the other common sea ice reconstructions based on the MAT dinocyst approach *(de Vernal et al., 2013c)*. Both proxies reflect important characteristics of modern sea ice in the marginal Arctic seas, i.e., in the Baffin Bay, the Fram Strait, the Barents Sea and the Bering Sea (Fig 3.3). Both approaches are to a good extent

able to distinguish between ice-free and variable sea ice conditions. However, the MAT dinocyst reconstructions are not able to distinguish between the seasonal and permanent sea ice covered regions of the Laptev and Kara Sea (Fig 3.3d). This may point towards the limits of the MAT dinocyst approach as environmental tolerances for dinocysts are not fully understood *(Zonneveld et al., 2013)* and regional differences of assemblage composition may strongly differ *(Heikkilä et al., 2014)*. Further no exclusive sea ice species could be identified so far *(Zonneveld et al., 2013)*.

However, we find weaker correlations to modern spring sea ice conditions for the PIP_{25} approach (highest for $P_{III}IP_{25}$ r^2 = 0.53) than those reported for the MAT dinocyst sea ice reconstruction (r^2 = 0.86; *de Vernal et al., 2013c*). We assume, that high correlation of the MAT dinocyst reconstruction may partly be caused by the wide spatial extent, including large perennial ice-free regions and missing the perennial sea ice covered Arctic regions, which seems a difficult region for proxy sea ice reconstructions, as dinocysts seem mostly absent under perennial sea ice (*de Vernal et al., 2013c)*. Further, different modern satellite sea ice databases and time intervals were used to calculate these correlations *(de Vernal et al., 2013c)*, which may limit the comparability of the correlation indices. In order to directly test the reliability of both sea ice reconstruction approaches, we selected 41 samples from the Baffin Bay and West Greenland area to compare both methods for the first time in a sample-to-sample approach (see Chapter 3.5.2.).

3.5.3.2. MAT dinocyst and PIP_{25} sea ice reconstruction in Baffin Bay

Our regional comparison of preliminary MAT dinocyst and PIP_{25} sea ice reconstructions, support the good correlation of the over regional Northern Hemisphere datasets. PIP_{25} as well as MAT dinocyst reconstructed sea ice concentrations reflect the northwestward extent of the spring sea ice margin and increasing sea ice conditions towards the northwest off Baffin Bay (Fig 3.5). All reconstruction approaches correlate strongest with spring sea ice conditions. Within the PIP_{25} approach, weakest correlations are observed for the P_BIP_{25} index (r^2=0.34), intermediate correlations for the P_DIP_{25} index (r^2=0.51) and good correlations for the $P_{III}IP_{25}$ index (r^2 =0.62). It should be noted, that a bigger dataset from this area showed slightly weaker but similar correlations for all PIP_{25} indices (see Chapter 5).

The preliminary MAT dinocyst reconstructions show a similar, positive correlation to modern spring sea ice concentration (r^2=0.42; Fig 3.5). Further, we find a positive correlation of MAT dinocyst sea ice reconstructions with the PIP_{25} indices (Appendix A2).

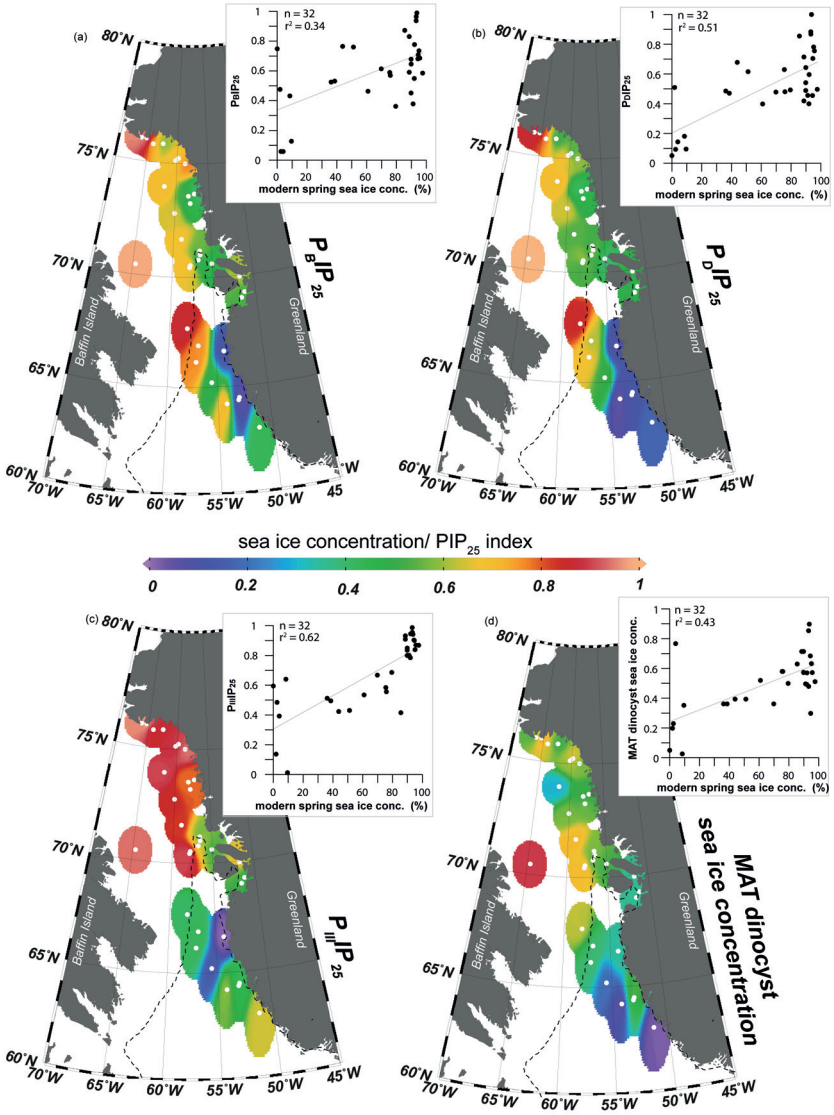

Fig 3. 5 Comparison of sea ice reconstructions in Baffin Bay using ***(a)*** P_BIP_{25}, ***(b)*** P_DIP_{25}, ***(c)*** $P_{III}IP_{25}$ and ***(d)*** preliminary results of the MAT dinocyst approach. The dashed line represents the spring sea ice extent. White points indicate location of surface samples. Upper right insets show correlations of the specific sea ice reconstruction to spring sea ice concentrations *(Cavalieri et al., 1996; updated 2015)*.

3.5.3.3. Diatom distributions and their relation to sea ice in Baffin Bay

Within this study we used 45 samples that were also analysed by *Krawczyk et al. (2017)* who determined good correlations of specific sea ice associated diatoms *(Jensen, 2003; Krawczyk et al., 2014)* to spring sea ice concentrations in the western

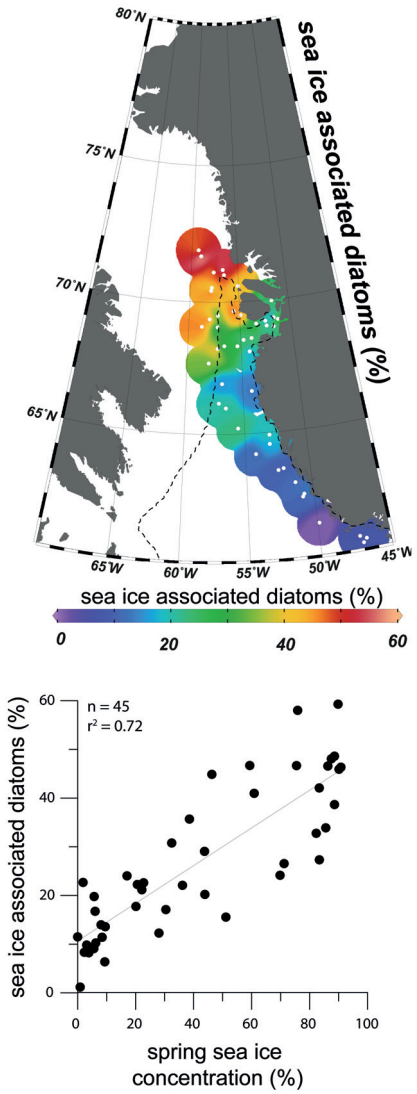

Fig. 3. 6 Distribution of sea ice associated diatoms in Baffin Bay. White points indicate location of surface samples. The dashed line represents the average spring sea ice extent. And the correlations of sea ice associated diatoms to spring sea ice concentrations *(Cavalieri et al., 1996; updated 2015)*.

Baffin Bay. The distribution of these sea ice associated diatoms, similar to PIP_{25} and preliminary MAT dinocyst results, can be closely related to the location of the spring ice edge (Fig 3.6). We find high correlations of the sea ice associated diatoms with modern spring sea ice conditions (r^2= 0.72; Fig 3.6). However, it should be noted, that the spatial distribution is different to those of the preliminary MAT dinocyst and PIP_{25} reconstructions, missing the northernmost part with highest modern sea ice concentrations. Hence we conclude, that the sea ice associated diatom assemblages seem to be a promising proxy to detect the position of the ice edge in Baffin Bay. Interestingly, sea ice associated diatoms show strongest correlations to IP_{25} but not to the PIP_{25} indices (Appendix A2). This might display the relation of the sea ice associate diatom group and the IP_{25} producing sea ice diatoms. As the IP_{25} producers *(Brown et al., 2014)* are not included in the sea ice diatom group used by *Krawczyk et al. (2017)* we suggest, that they may reflect similar environmental conditions. However, the small spatial distribution of the diatom database makes further assumptions difficult and an expansion of the diatom database would greatly contribute to the understanding of the relationship of both proxies. It further remains questionable if diatoms are applicable in an over regional approach, due to their vulnerability to dissolution and regional depositional differences *(Shemesh et al., 1989; Leventer, 1998)*.

3.5.3.4. Statistical approach

The relationship between our new biomarker/dinocyst surface record were analysed with a canonical correspondence analysis (CCA) in order to gain further insight to their relation to each other and specific environmental variables.

The ordination diagram of biomarker sea ice indices and environmental variables (Fig 3.7a) confirms the relationship of the PIP_{25} indices to sea ice. Our new samples include a wide variety of sea ice scenarios, perennial sea ice, seasonal sea ice and ice-free conditions and include crucial areas for sea ice reconstructions (as the Central Arctic Ocean, the Fram Strait, the Barents Sea and the Baffin Bay). The character of our dataset and the outcome of the CCA analysis reinforce previous assumptions about the reliability of this approach for sea ice reconstructions.

A multivariate analysis comparing specific biomarkers and dinocysts is shown in Fig 3.7b. IP_{25} correlates positive with CCA Axis 1. The dinocyst *I. minutum*, *P. dalei* and *Brigantedinium spp.* also show a close correlation with CCA Axis 1. *Brigantedinium spp.* is considered to be a cosmopolitan species, occurring in permanently sea ice covered regions as well as in the tropics *(Zonneveld et al., 2013)*. Similar. *P. dalei* is occurring widely within the Northern Hemisphere and not exclusively associated to cold or ice dominated conditions *(Zonneveld et al., 2013)*. Hence, we assume that the correlations to IP_{25} observed here are partly caused on the sample locations, i.e. mainly in ice dominated areas and conditions that are favourable for dinoflagellates as well as sea ice diatoms (as available light and nutrients).

Further, the correlation of *I. minutum* and IP_{25} may be related to the sea ice habitat of the producing organisms (cf. *Potvin et al., 2013*). Moreover, this heterotrophic species relies on prey, i.e., diatoms, and has been associated with high production areas in polynyas (cf. *Hamel et al., 2002*). Hence, this correlation may be related to the ecological relationship between IP_{25} producers, being the major food source, and *I. minutum*.

However, our statistical approach also shows a correlation of the *I. minutum* and *P. dalei* to brassicasterol (Fig 3.7b). This may have several reasons. Either those species are part of the source of brassicasterol (which is produced by a wide range of phytoplankton, e.g., *Volkman et al., 1993)*, or displaying a feeding relationship between heterotrophic *I. minutum* (cf. *Hamel et al., 2002*) and brassicasterol

producers, or the correlation indicate similar environmental requirements of the producing organisms.

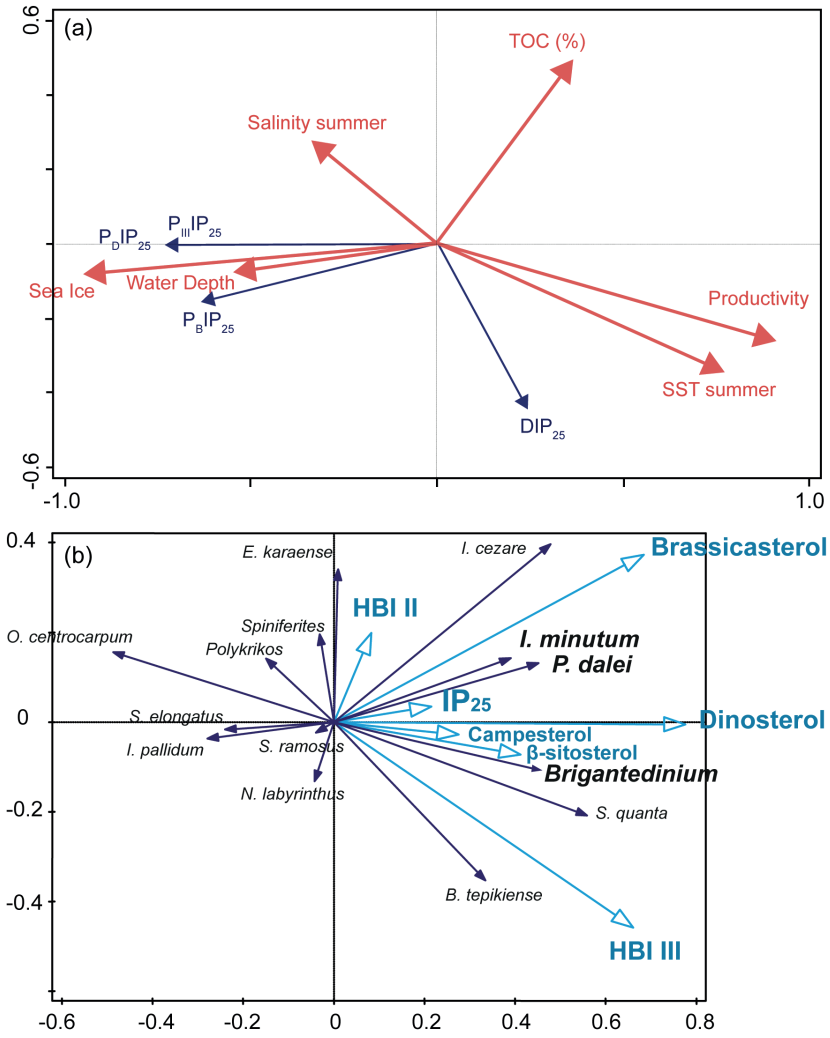

Fig 3. 7*(a)* Ordination diagram of biomarker indices, i.e., P_BIP_{25}, P_DIP_{25}, $P_{III}IP_{25}$, DIP_{25} and tested environmental variables, i.e. summer sea surface (SST), productivity ($gC/m^2/yr$), water depth (m), summer salinity and sea ice (month/yr). ***(b)*** Ordination diagram of specific dinocyst species with tested biomarkers, i.e. IP_{25}, HBI II, HBI III, brassicasterol, dinosterol, campesterol and β-sitosterol (in µg/gTOC).

Brigantedinium spp. shows also a correlation with terrigenous sterols (campesterol and β-sitosterol) which predominantly originate in land plants *(Jaffé et al., 1995; Bianchi, 2007)* and are associated with terrigenous input *(e.g., Huang and Meinschein, 1979; Volkman et al., 1993)*. This correlation may indicate a nutrient dependency of *Brigantedinium spp*..

Arising from these results, the CCA analysis reveals the complex mechanisms behind different proxies that need to be considered when comparing those.

3.6. Conclusions

With our new biomarker dataset and the combination with published surface records, we could confirm the circum-Arctic applicability of the biomarker approach for sea ice reconstructions. With regard to the PIP_{25} index, we showed that its applicability differs between regions, and shows good results for regions with seasonal sea ice cover, i.e., Baffin Bay and the Barents Sea. For regions with complex sea ice and environmental conditions, i.e., the Central Arctic Ocean and the Russian marginal seas, the direct correlation of PIP_{25} remains difficult.

For the first time, we could show that the use of the HBI III produces good correlations to spring sea ice in an over regional approach. However, its relationship to the marginal ice remains unclear for specific areas, i.e., the Russian shelf seas. In a statistical approach we could confirm the correlation of the PIP_{25} indices to sea ice.

We find that preliminary MAT dinocyst and biomarker sea ice reconstructions produce spatial good estimates of modern sea ice reconstructions in areas with seasonal sea ice cover. For the Baffin Bay, the PIP_{25} and preliminary MAT dinocyst approach as well as diatom assemblages reflect the spatial extent of the spring sea ice.

Acknowledgements

This study was funded by the Deutsche Forschungsgemeinschaft (DFG) through 'ArcTrain' (GRK 1904). The sediments used in this study were collected during several cruises and we wish to thank the captain and crew as well as the scientific parties. We thank W. Luttmer for laboratory support and M. Ungermann for helping with satellite sea ice data. Thanks to S.T. Belt and colleagues (Biogeochemistry Research Centre, University of Plymouth) for providing the internal standard for IP_{25} analysis.

4. Short-term variability in late Holocene sea ice cover on the East Greenland Shelf and its driving mechanisms

Henriette M. Kolling[a], Rüdiger Stein[a], Kirsten Fahl[a], Kerstin Perner[b], Matthias Moros[b]

[a] Alfred Wegener Institute, Helmholtz Centre for Polar and Marine Research

[b] Leibniz Institute for Baltic Sea Research Warnemünde, Department of Marine Geology, Germany

Published in Palaeogeography, Palaeoclimatology, Palaeoecology (June 2017)

Abstract

Arctic sea ice is a critical component of the climate system as it influences the albedo, heat, moisture and gas exchange between ocean and atmosphere as well as the ocean's salinity. An ideal location to study natural sea ice variability during pre-industrial times is the East Greenland Shelf that underlies the East Greenland Current (EGC), the main route of Arctic sea ice and freshwaters from the Arctic Ocean into the northern North Atlantic. Here, we present a new high-resolution biomarker record from the East Greenland Shelf (73°N), which provides new insights into the sea ice variability and accompanying phytoplankton productivity over the past 5.2 kyr. Our IP_{25} based sea ice reconstructions and the inferred PIP_{25} index do not reflect the wide-spread late Holocene Neoglacial cooling trend that follows the decreasing solar insolation pattern, which we relate to the strong influence of the polar EGC on the East Greenland Shelf and interactions with the adjacent fjord throughout the studied time interval. However, our reconstructions reveal several oscillations with increasing/decreasing sea ice concentrations that are linked to the known late Holocene climate cold/warm phases, i.e. the Roman Warm Period, Dark Ages Cold Period, Medieval Climate Anomaly and Little Ice Age. The observed changes seem to be connected to general ocean atmosphere circulation changes, possibly related to North Atlantic Oscillation and Atlantic Multidecadal Oscillation regimes. Furthermore, we identify a cyclicity of 73-74 years in sea ice algae and

phytoplankton productivity over the last 1.2 kyr, which may indicate a connection to Atlantic Multidecadal Oscillation mechanisms.

4.1. Introduction

4.1.1. Background

Arctic sea ice is a highly variable system, with drastic inter-annual changes *(Thomas & Dieckmann, 2010)*. It is a critical component of the climate system as it influences the albedo, heat, moisture and gas exchange between ocean and atmosphere as well as the ocean's salinity (*Rudels et al., 1996; Dieckmann & Hellmer, 2003*). Sea ice has declined in extent and thickness much more drastically during the past decades than predicted by any climate model *(e.g. Cavalieri et al., 1997; Johannessen et al., 2004; Francis et al., 2005; Stroeve et al., 2007;Comiso et al., 2008; Serreze and Barry, 2011*). It is expected that the on-going reduction of Arctic sea ice will amplify Arctic sea surface temperatures (SST) (*Manabe et al., 1992; Randall et al., 1998; Screen and Simmonds, 2010*), as the areas covered by bright snow and ice are replaced by dark ocean surface. Additionally, changes in freshwater and ice export from the Arctic Ocean to the adjacent seas, are expected to have a strong influence on the deep-water formation and the global thermohaline circulation *(Aagaard et al., 1985; Hakkinen, 1995, 1999; Holland et al., 2001; Arzel et al., 2008)*. Due to its critical influence on the climate system, Arctic sea ice has gathered a lot of attention, raising a debate whether the observed recent changes are within a natural variability or whether anthropogenic greenhouse gas emissions play a leading role causing the observed changes. Here, high-resolution records extending the direct measurements into the past may help to improve our understanding of the natural variability of sea ice and its driving mechanisms during pre-industrial times. Such records may allow to test and improve climate models, in order to predict future sea ice variability and to improve the accuracy of these climate models.

A particularly interesting phase to study pre-industrial sea ice changes is the late Holocene, as it is characterized by a general cooling trend, termed as 'Late Holocene Neoglacial' (*Wanner et al., 2011)*. During this time interval significant reductions of SST and increases of sea ice have been recorded in sedimentary archives from the northern North Atlantic *(Marchal et al., 2002; Jennings et al., 2002, 2011; Sicre et al., 2008; Andresen et al., 2012; Telesiński et al., 2014b; Cabedo-Sanz et al., 2016)*.

During this general cooling trend several extreme warm and cold intervals have been identified on the Northern Hemisphere; two phases of exceptional warmth, the Roman Warm Period (RWP, CE 1 – 300, *Ljungqvist, 2010*) and the Medieval Climate Anomaly (MCA, CE 950 – 1200; *Lamb, 1965, 1977; Stine, 1994)* as well as two distinct cooling episodes, the Dark Ages Cold Period (DACP, CE 300 – 800; *Ljungqvist, 2010*) and the Little Ice Age (LIA, CE 1300 – 1900; *Jones and Mann, 2004; Ljungqvist, 2010*). The transition from these cold to warm phases has been associated with changes in the mode of the North Atlantic Oscillation (NAO*; Nesje et al., 2001; Jackson et al., 2005; Funder et al., 2011; Darby et al., 2012; Olsen et al., 2012; Faust et al., 2016*), which describes the mode of atmospheric circulation in the North Atlantic region *(Dickson et al., 1996; Wanner et al., 2001)*. A positive (negative) NAO is associated with increased (reduced) northward advection of Atlantic Water and a decrease (increase) in sea ice in the Arctic *(Dickson et al., 1996; Thompson and Wallace, 1998)*. These changes will affect the sea ice export and recirculation of Atlantic Water and by this, impact the East Greenland Shelf.

4.1.2. Regional Setting

The East Greenland Shelf at 73° N is located underneath the EGC, which transports sea ice and cold, nutrient-poor, and low salinity (T: 0-1°C, S: <30) waters through Fram Strait southward along the margin of East Greenland towards Denmark Strait (Fig 4.1A; *Aagaard and Coachman, 1968a, b; Johannessen, 1986; Hopkins, 1991*). Waters of the EGC dominate the upper 250 m of the water column, subsurface waters originate in the Atlantic and are composed of waters from the Atlantic Intermediate Water (AIW, T: 0°C, S: 34 – 35, Fig 4.1A; *Rudels et al., 2005*) and the Return Atlantic Current (RAC, T: <2°C, S: 34 – 35; *Gladfelter, 1964*). A strong stratification separates the low-salinity polar waters at the surface and the more saline Atlantic Waters below *(Aagaard and Coachman, 1968a, b; Rudels et al., 2000)*. Nutrient concentrations in surface waters are relatively low and limit phytoplankton productivity *(e.g., Hirche et al., 1991)*.

Most of the sea ice on the East Greenland Shelf is formed in the Arctic Ocean during the winter months, and exported through Fram Strait via the Transpolar Drift with maximum export during March (*Michel et al., 2015*). The sea ice cover on the East

Greenland Shelf is highly dynamic throughout the year; during summer only the inner shelf remains ice-covered (Fig 4.1B, *NSIDC, Boulder, USA)*. Ice exported by the EGC reaches as far south as Iceland (*Ogilvie, 1996*). The eastward extent of the perennial sea ice cover on the East Greenland Shelf is described by the Polar Front (*Petersen, 2011*). Its position is important for bioproductivity (*Hald and Steinsund, 1992*). Further, the Polar Front is highly sensitive to changes in Arctic outflow on seasonal and geological time scales (*Petersen, 2011*).

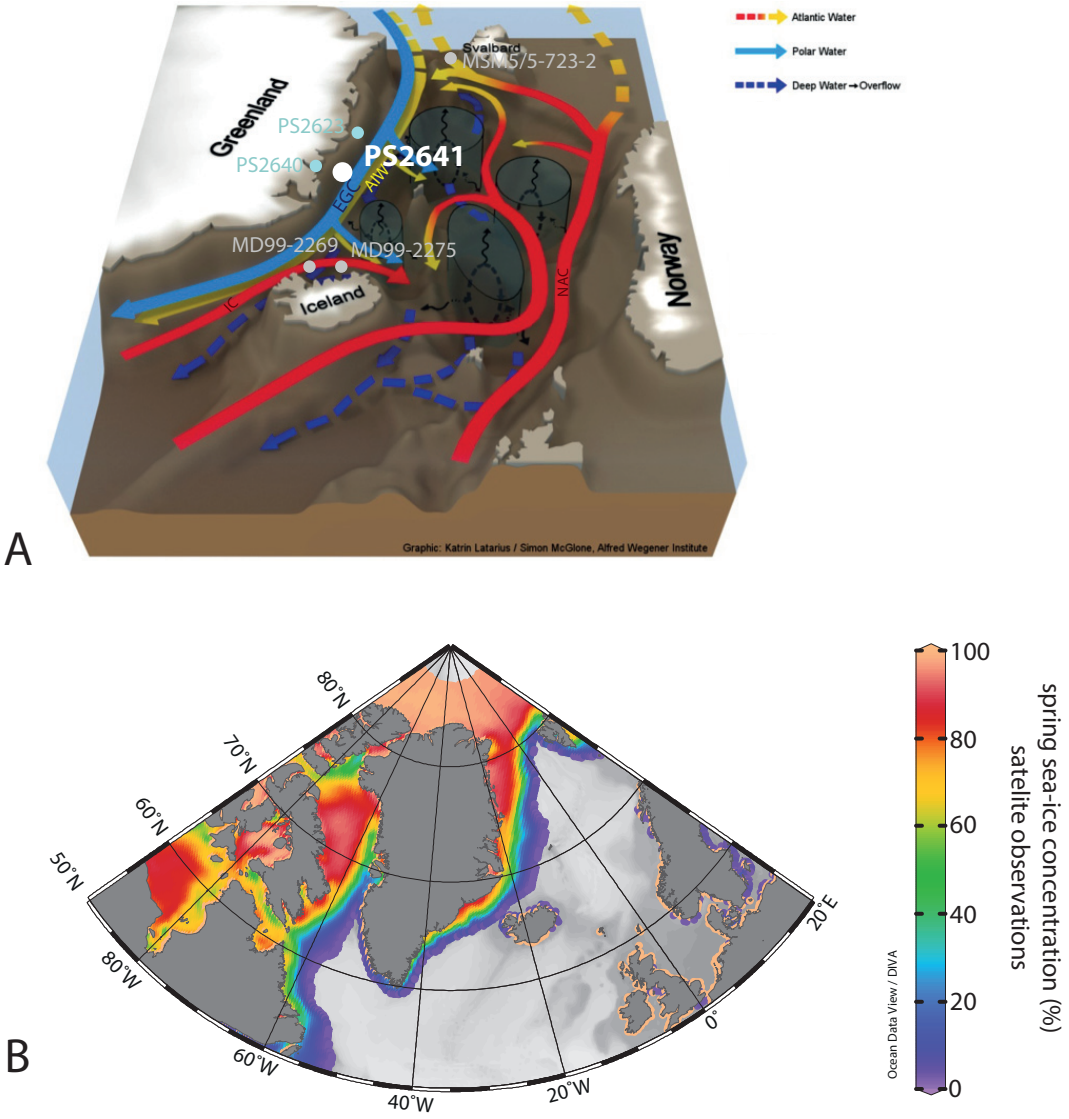

Fig 4. 1 *A*. Average spring sea ice concentration (April to June from 1978 to 2007, *http://nsidc.org/*). *B*. Map of the study area with the core site on the East Greenland Shelf (PS2641) and key locations on the East Greenland Shelf (PS2640, PS2623, *Andrews et al., 2016*), North Iceland Shelf (MD99-2269, *Cabedo-Sanz et al., 2016*; MD99-2275, *Massé et al., 2008*) and in Fram Strait (MSM5/5-723-2, *Müller et al., 2012*). Major currents of the region are the East Greenland Current (EGC), North Atlantic Current (NAC), Irminger Current (IC) and Atlantic Intermediate Water (AIW). Map adapted after *Latarius and Quadfasel, 2016*.

4.1.3. Approach for sea ice reconstructions

For our sea ice reconstruction study, we used a geochemical proxy for spring sea ice conditions, a highly-branched isoprenoid (HBI) alkene with 25 carbon atoms (i.e., IP_{25}) derived from specific sea ice diatoms *(Belt et al., 2007; Brown et al., 2014)*. This biomarker proxy has been proven as direct proxy for modern and Quaternary sea ice conditions in the Arctic *(e.g., Massé et al., 2008; Müller et al., 2009; Vare et al., 2009; Belt et al., 2010; Fahl and Stein, 2012; Cabedo-Sanz et al., 2016; Hörner et al., 2016)*. Furthermore, IP_{25} appears to be quite stable in sediments over millions of years *(Stein and Fahl, 2013; Knies et al., 2014; Stein et al., 2016)*.

To gain a more detailed picture of sea ice conditions and to avoid misleading interpretations of the absence of IP_{25}, which may result either from a lack of sea ice or a permanent, thick sea ice cover with too low light penetration for ice algae growth *(Horner and Schrader, 1982), Müller et al. (2009, 2011)* have introduced the so-called 'PIP_{25} index' (see 'Methods' for calculation). This index combines open-water phytoplankton biomarker proxies with the sea ice proxy IP_{25}. Brassicasterol and dinosterol *(cf. Volkman, 1986; Volkman et al., 1993)* have been used as phytoplankton biomarkers. The PIP_{25} index has been verified to represent sea ice concentration quite well through a comparison with satellite-derived values *(Müller et al., 2011)* and has been applied successfully in several studies in the Arctic Ocean and its marginal seas *(e.g., Fahl and Stein, 2012; Cabedo-Sanz et al., 2013; Müller and Stein, 2014; Xiao et al., 2015b; Hörner et al., 2016; Stein et al., 2016)*. Recently, *Smik et al. (2016)* have further developed the PIP_{25} approach by introducing a HBI-triene (HBI III) as phytoplankton biomarker. The HBI-diene (HBI II; $C_{25:2}$) has also been related to a possible sea ice source for the Arctic and Antarctic realm *(Belt et al., 2007; Vare et al., 2009; Massé et al., 2011)*. The role of the HBI-diene, however, is not fully understood and still under discussion. Some studies proposed that the ratio of the HBI-diene and IP_{25} might be related to sea-surface temperature *(Fahl and Stein, 2012; Stein et al., 2012; Xiao et al., 2013)* whereas *Cabedo-Sanz et al. (2013)* proposed that the ratio between the HBI-diene and IP_{25} might provide a useful indicator for the stability or variability of sea ice conditions.

In this study we aim for a continuous high-resolution climate record from the East Greenland Shelf Core PS2641, representing the last about 5 kyr. Recently, *Perner et al., (2015)* published a foraminifer reconstruction from the very same samples, which

gives the unique opportunity to compare not only trends but exact correlations between biomarker and micropaleontological proxies. Furthermore, a sedimentological record *(Andrews et al., 2016)* from the same core provides an ideal background to discuss sediment sources and draw conclusions about sea ice conditions.

4.2. Material and Methods

4.2.1. Material

For this study sediment material from gravity core (GC) PS2641-4 and box core (GKG) PS2641-5 (representing the near-surface undisturbed sediments) was analysed and interpreted as one composite data record named as core 'PS2641'. Both cores were taken on the central part of the East Greenland Shelf at about 73°09.35'N, 19°29.00'W in a water depth of 469 m during the 1994 ARK-X/2 *RV Polarstern* expedition (*Hubberten, 1995,* Fig 4.1A). Box core sediments consist of olive grey to dark olive grey clay with minor amounts of silt and sand, in the upper 2 cm tube worms were found, deeper parts show indications for bioturbation *(Hubberten, 1995)*. The investigated part of the gravity core (30-250 cm) consist of moderately bioturbated dark olive grey silty clay *(Hubberten, 1995)*. Bioturbation is characterized by pyritized chonditres and burrows *(Evans et al., 2002)*. The box core was sampled every 0.5 cm, the gravity core every 1 cm. Samples were stored in glass vials, freeze-dried and homogenized prior to biomarker analysis.

4.2.2.Chronology

The age model of core PS2641 is based on 24 AMS ^{14}C dates (Appendix B1). Distinct increases of ^{137}Cs and Hg content are associated with the onset of anthropogenic emissions around 1960 and applied as stratigraphic markers *(Perner et al., 2015)*. The age model of the GKG has been developed by linear interpolation between 1960, marked by Hg and ^{137}Cs increase, and 1994, the year of core recovery. A combined age model of GC and GKG was established based on the total benthic foraminifera content and overlapping AMS ^{14}C dates *(Perner et al., 2015)*.

Two horizons (66 – 82 cm, 202 – 228 cm depth) gave similar AMS ^{14}C ages for top and bottom samples for these horizons, further an overall low foraminiferal content was observed *(Perner et al., 2015)*. These intervals were excluded from the applied

age model developed by *Perner et al. (2015)*. Sedimentation rates show variations between 60 and 30 cm*kyr^{-1}, low values are observed from 3 to 4.7 kyr BP and 0.9 to 2.5 kyr BP. For further details about the age model we refer to *Perner et al. (2015)*.

The combination of gravity core PS2641-4 and box core PS2641-5 gives a continuous record from 5.2 kyr BP to CE 1994. With a resolution of 13 - 42 years per 1 cm for the gravity core and 2.5 - 20 years per 0.5 cm for the box core, the material yields high potential to have preserved short-scale climate changes.

4.2.3. Methods

For this study, we analysed the total organic carbon (TOC) content and concentrations of the IP_{25} monoene, the HBI-diene, 24-methylcholesta-5, 22-dien-3β-ol (brassicasterol), 4-23, 24 trimethyl-5α-cholest-22 E-en-3β-ol (dinosterol), 24-ethylcholest-5-en-3β-ol (β-sitosterol) and 24-methylcholest-5en-3β-ol (campesterol).

TOC was measured on 0.1 g of dried, homogenised sediment with a carbon-sulphur determinator (CS-125, Leco) after carbonates were removed by adding hydrochloric acid (500 µl). The machine was calibrated with a standard before measurements; accuracy of these measurements was controlled by additional standard measurements after every 10 samples, the error of our TOC measurements is at ±0.028%.

About 5 g of dried, homogenized sediment was used for biomarker extraction. Prior to extraction, the two internal standards, 7-HND (7-hexylnonadecane, 0.076 µg/sample) and cholesterol-D6 (cholest-5-en-3β-ol-D6, 11 µg/sample), were added for quantification purposes. The sediment was extracted by an Accelerated Solvent Extractor (DIONEX, ASE 200; 100°C, 5 min, 1000 psi), with dichloromethane:methanol (2:1 vol/vol) as solvent. The extracts were separated in different fractions by open-column chromatography, with SiO_2 as stationary phase. *N*-hexane (5 ml) was used for IP_{25}, and ethylacetate:*n*-hexane (20:80 vol/vol; 7 ml) for sterols. The sterol fraction was silylated using 200µl BSTFA (60°C, 2 h).

All biomarker concentrations were measured with a gas chromatograph (Agilent 6850 GC, 30m HP-1MS column, 0.25mm I.d. and 0.25µm film thickness) coupled to an Agilent 5975 C VL mass selective detector (Triple-Axis Detector, 70eV constant

ionization potential, Scan 50-550 m/z, 1 scan*s^{-1}, ion source temperature 230°C). The temperature program of the GC for hydrocarbons was set as follows: 60°C (3min), 150°C (rate: 15°C*min^{-1}), 320°C (rate 10° C*min^{-1}), 320°C (15° C*min^{-1}), 320°C (10° C*min^{-1}), 320°C (15min isothermal) and for sterols: 60°C (2min), 150°C (rate: 15° C*min^{-1}), 320 (rate: 3° C*min^{-1}), 320°C (20 min isothermal). The single compounds were identified by comparing the retention times with those of reference compounds. IP_{25} and the HBI-diene (IP_{25}: m/z 350; HBI-diene: m/z 348) were quantified in relation to the abundant fragment ion m/z 266 of the internal standard 7-hexylnonadecane. The sterols were quantified as trimethylsilyl ethers (brassicasterol: m/z 470, campesterol: m/z 472, β-sitosterol: m/z 486, dinosterol: m/z 500) in respect to the molecular ion of cholest-5-en-3b-ol-D6 (ion m/z 464). A detailed description of the quantification methods is given by *Fahl and Stein (2012)*. The concentrations of all biomarkers have been normalised to the extracted amount of sediment and TOC (both show nearly the same signal, we only show the data corrected against the amount of sediment referred to as μg*g^{-1}). We controlled the instrument stability by reruns of external standards several times during one analytical sequence and by replicate analyses for random samples.

P_BIP_{25} (using brassicasterol) and P_DIP_{25} (using dinosterol) ratios were calculated after *Müller et al. (2011)* using the following equation:

$$PIP_{25} = IP_{25} / (IP_{25} + (Sterol \times c)) \quad (1)$$

With c as a balance factor, being the ratio of mean IP_{25} concentration to mean sterol concentration, to counterbalance the higher concentrations of sterols compared to IP_{25}. As the PIP_{25} values based on brassicasterol and dinosterol are very similar, we only present and discuss the brassicasterol-based PIP_{25} values here.

As proxy for sea ice, we only used IP_{25} and PIP_{25}. The HBI-diene values, not fully understood in terms of origin and significance (see above), were not considered here. The data, however, are presented in Appendix B3.

As indicators for terrigenous input, β-sitosterol and campesterol, both mainly produced by vascular plants *(e.g. Huang & Meinschein, 1979; Volkman, 1986; Volkman et al., 1993; Yunker et al., 1995; Fahl & Stein, 1999)* are used.

For a statistic analysis of short-term oscillations, a MatLab code was applied to detrend the original data and the BTuckey function of AnalySeries *(Paillard et al., 1996)* was applied to produce a spectrum of the oscillations (confidence 99%, bandwidth: 0.1).

All data (including the biomarker data normalised to TOC and dinosterol-based PIP_{25} values) are online available on https://doi.pangaea.de/10.1594/PANGAEA.871904.

4.3. Results

TOC concentrations show a general increasing trend from about 0.5 to 0.7 % over the last 5.2 kyr. Values of 0.6 % to 0.7 % TOC occur from ca. 2 kyr BP towards the top of the core with some higher peaks reaching up to 0.85 % TOC (Fig 4.2G). The IP_{25} concentrations can be divided into three sections. The lowest section from 5.2 to 2.4 kyr BP shows values around 0.004 $\mu g*g^{-1}$. From 2.4 to 1.3 kyr BP concentrations reach minimum values of about 0.003 $\mu g*g^{-1}$. Afterwards IP_{25} increases to higher values reaching up to 0.01 $\mu g*g^{-1}$ around 1.2 kyr BP. At about 1 kyr BP minimum values of about 0.003 $\mu g*g^{-1}$ are reached. From 0.7 kyr BP IP_{25} concentrations reach the highest values of the records, reaching 0.009 $\mu g*g^{-1}$, these high concentrations are interrupted by two reductions two lower values around 0.5 kyr BP and 0.2 kyr BP (Fig 4.2F). Brassicasterol shows a three-step increase, with lowest values from 5.2 to 3 kyr BP followed by a minor rise until 1.6 kyr BP, from 0.2 $\mu g*g^{-1}$ to 0.4 $\mu g*g^{-1}$. From 1.6 kyr BP onwards, the concentrations increase continuously to the highest values, around 1-2 $\mu g*g^{-1}$. These high values show two reductions around 0.9 kyr BP and 0.5 kyr BP. The phytoplankton sterols show a short-term variability varying between high and low values over the last 1 kyr. (Fig 4.2E). In general, the terrigenous sterols show a similar trend as seen in the concentrations of the marine sterols – lowest and constant values (0.25 $\mu g*g^{-1}$) until 3 kyr BP, followed by a constant increase for the rest of the core section (reaching 1.0 $\mu g*g^{-1}$). A peak is observed at 1 kyr BP, reaching an extreme value of 2.5 $\mu g*g^{-1}$ (Fig 4.2B).

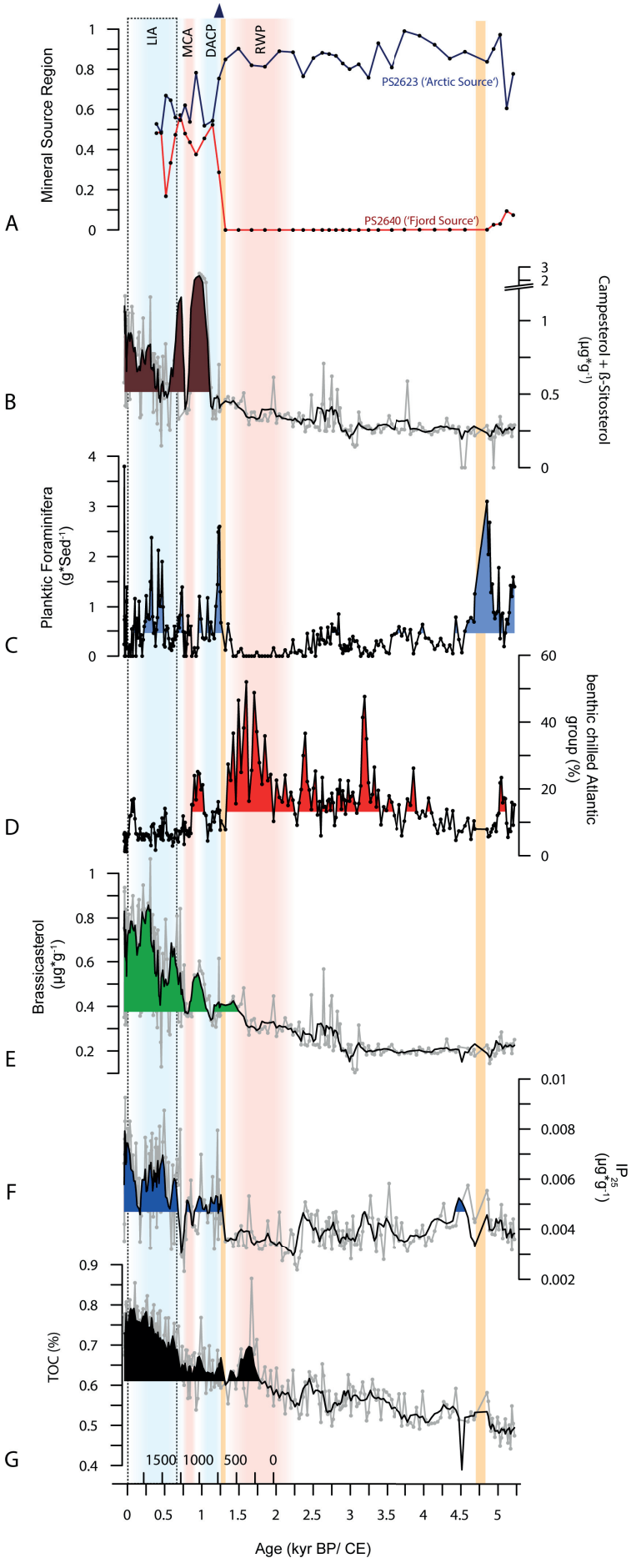

Fig 4. 2 Combined record of gravity core PS2641-4 and box core PS2641-5 (dash-lined box) with content of ***G.*** TOC (in %) and concentrations of ***F.*** IP_{25}, ***E.*** brassicasterol and ***B.*** terrigenous sterols (all in $\mu g*g^{-1}$). Abundances of ***D.*** benthic chilled Atlantic foraminifera and ***C.*** planktic foraminifera (both in %; *Perner et al., 2015*). ***A.*** Results from a principal component analysis, indicating the general mineral source region (*Andrews et al., 2016*). All plots are shown versus age before present (kyr BP), an additional age scale shows calendar ages Common Era (CE). Orange shaded areas indicate age model insecurities (*Appendix B1*, see 4.*2.2. Chronology*). The thick black line represents the 5-point average, the thin grey line the original data. Specific climate events are indicated in blue/red areas, Roman Warm Period (RWP) Dark Ages Cold Period (DACP), Medieval Climate Anomaly (MCA) and Little Ice Age (LIA). A dark blue triangle indicates a glacier advance on Greenland *(Solomina et al., 2015)*.

4.4. Discussion

This study focuses on changes of sea ice conditions and phytoplankton productivity on the East Greenland Shelf, an area highly influenced by the EGC and the adjacent Greenland Ice Sheet.

By the EGC the area is directly connected to the Arctic Ocean and is subject to changes in Arctic sea ice conditions. Periods with reduced sea ice cover in Fram Strait, are associated with changes in North Atlantic Current (NAC; *Müller et al., 2012)* strength and will most likely result in reduced amounts of sea ice exported towards the study area.

Fjords and tidewater glaciers along the coast of East Greenland form the connection between the Greenland Ice Sheet and the Shelf area. Changes in atmospheric conditions will affect the extent of glaciers and landfast ice. An atmospheric warming may cause a retreat of glaciers from tide waters and reduce their effect on sea ice *(Mugford and Dowdeswell, 2010; Alonso-Garcia et al., 2013)*.

A continuous presence of the sea ice and phytoplankton biomarkers indicates a continuous presence of seasonal sea ice on the East Greenland Shelf during the past 5200 years. However, there is evidence that extent and duration of this seasonal sea ice cover changed over the investigated time period.

4.4.1 Mid to Late Holocene climate change along the East Greenland continental margin

A first low-resolution biomarker record of gravity core PS2641-4 was already presented by *Müller et al. (2012)*. These authors found rather stable sea ice conditions over the past 8.5 kyr, with an increase in sea ice over the past 1000 years. Indications of the MCA and other small-scale events, however, were not evident in this low-resolution record.

Our new high-resolution biomarker record from Core PS2641 in Foster Bugt at 73° N provides crucial information on changes in sea ice conditions on the East Greenland Shelf over the past 5.2 kyr BP (Fig 4.2). This time interval is characterized by a continuous decrease in Northern Hemisphere solar insolation and a related cooling trend known as ‘late Holocene Neoglacial cooling’ *(Porter and Denton, 1967; Denton and Karlén, 1973; Wanner et al., 2011*).

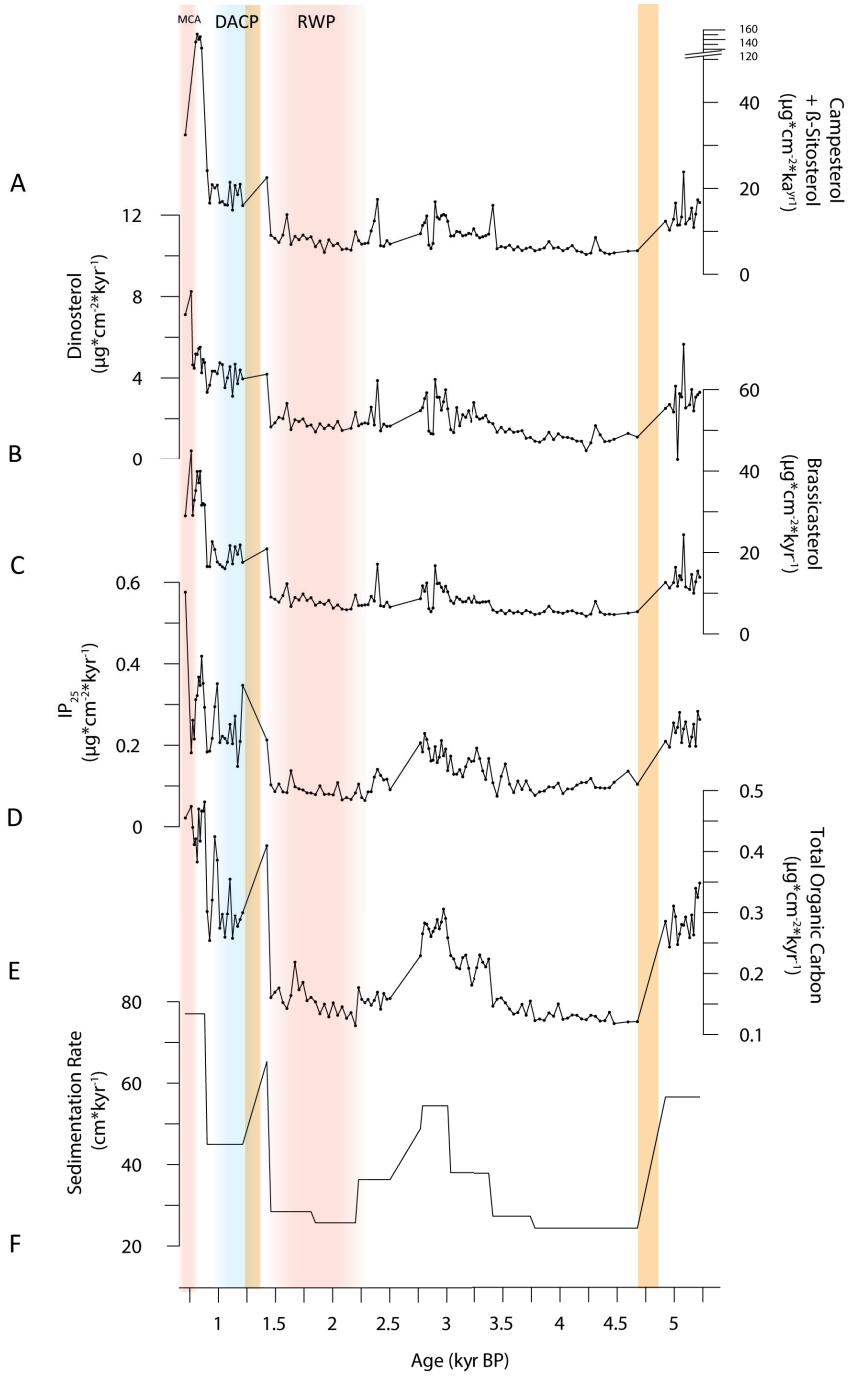

Fig 4. 3 ***F.*** Sedimentation rates (in cm*kyr^{-1}) and accumulation rates of ***E.*** Total Organic Carbon (TOC) ***D.*** IP_{25}, ***C.*** brassicasterol ***B.*** dinosterol and ***A.*** terrigenous sterols (campesterol + β-sitosterol) (all in µg*cm^{-2}*kyr^{-1}) for gravity core PS2641-4. Specific climate events are indicated by red and blue areas; Roman Warm Period (RWP), Dark Ages Cold Period (DACP) and Medieval Climate Anomaly (MCA). Orange shaded areas indicate age model insecurities (*Appendix B1*, see 4.*2.2. Chronology*).

This Neoglacial cooling is characterized by an increase in sea ice concentrations in the Canadian Arctic Archipelago, eastern Fram Strait, the Laptev Sea and the Chukchi Sea *(Hörner et al., 2016; Müller et al., 2012; Stein et al., 2017b; Vare et al., 2009)*. Furthermore, an increase in drift ice export via the EGC has been reported by several studies from the northern North Atlantic over the past 5 kyr BP *(Moros et*

al., 2006b), and a reduction in SSTs, primary production as well as an increase of polar water outflow to the Nordic Seas has been found over the past 3 kyr BP *(Koç et al., 1993; Calvo et al., 2002; Andersen et al., 2004b; Cabedo-Sanz et al., 2016)*. *Perner et al. (2015)* associated a major change in the benthic foraminiferal assemblages and a shift from a high to nearly absent planktic foraminifera content in Core PS2641 at 4.5 kyr BP with the onset of the Neoglacial. They relate this cooling to an overall strengthening of the EGC. Planktonic and benthic foraminiferal reconstructions provide information about the overall marine environment but only limited information about sea ice *(Seidenkrantz, 2013)*. With our high-resolution biomarker record we provide new vital information on sea ice variability and contribute to a more complete understanding of the environmental changes on the East Greenland Shelf.

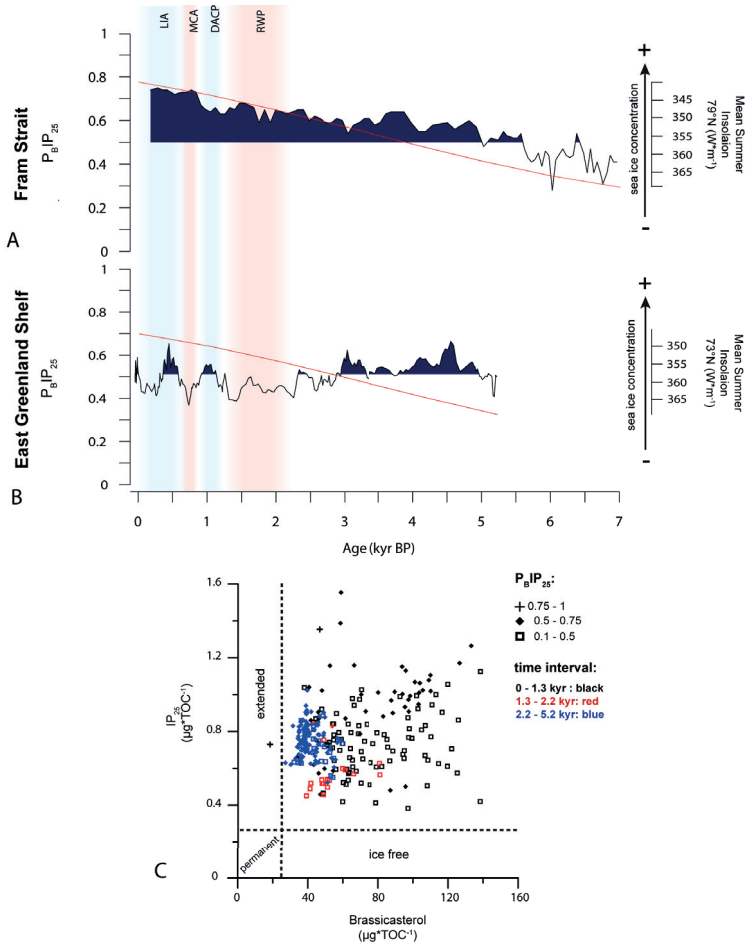

Fig 4. 4 P_BIP_{25} indices calculated for sediment cores ***A.*** MSM5/5-723-2 *(Müller et al., 2012)* and ***B.*** PS2641 (this study) with solar insolation at 73°N and 79°N (red curves; *Laskar et al., 2004)*, respectively (in W/m). Specific climate events are indicated in blue/red areas, Roman Warm Period (RWP) Dark Ages Cold Period (DACP), Medieval Climate Anomaly (MCA) and Little Ice Age (LIA). **C.** Correlation of IP_{25} versus brassicasterol and corresponding P_BIP_{25} indices. P_BIP_{25} values are indicated by different symbols (cross: 0.75-1; diamond: 0.5-0.75; square: 0.1-0.5). Different time intervals are indicated by different colours (black: 0-1.3 kyr, red: 1.3-2.2 kyr, blue: 2.2-5.2 kyr BP).

Our biomarker record of Core PS2641 from the East Greenland Shelf does not reflect a long-term Neoglacial cooling trend. Sea ice algae productivity, represented by IP_{25} only shows an increase after 1.3 kyr BP (Fig 4.2F) and sea ice concentrations, indicated by the PIP_{25} index, do not show a significant overall increase over the past 5 kyr (Fig 4.4B, C). We assume that the location on the inner East Greenland Shelf is both affected by fjord processes as well as EGC intensity, and associated Arctic sea ice export, which causes the observed relative constant seasonal sea ice conditions.

A direct comparison of sea ice records from the East Greenland Shelf, influenced by the cold EGC (Core PS2641), and the eastern Fram Strait, influenced by the warm West Spitsbergen Current (Core MSM5/5-723-2; *Müller et al., 2012*) shows a significant difference of sea ice development between both areas (Fig 4.4). The East Greenland Shelf experienced an average reduction of about 5% over the past 5 kyr (Fig 4.4B), whereas the eastern Fram Strait shows an increase of sea ice of about 19% over the same period *(Müller et al., 2012)* (Fig 4.4A). The record from the eastern Fram Strait shows increasing IP_{25} concentrations and a maximum IRD release during the past 3 kyr BP that are associated with the Neoglacial cooling *(Müller et al., 2012)*. The reason for this difference likely relate to the dominance of the EGC along the East Greenland Shelf, which does not have a warm surface-'counter current' as it is the case in the eastern Fram Strait. There, Arctic water outflow increases when the NAC is reduced, consequently the area gets cooler and local sea ice formation is strengthened *(Müller et al., 2012)*. On the East Greenland Shelf such a 'seesaw' between a warm and a cold surface current is missing.

Even under reduced EGC scenarios, the area is dominated by cold surface water and therefore stays cool, due to the lack of a warm surface current being able to deliver a critical amount of warm water to the area. The Irminger Current, transporting warm water masses through eastern Denmark Strait, has been reported to be strengthened during warm periods on the North Iceland Shelf *(e.g. Cabedo-Sanz et al., 2016; Sicre et al., 2008)*, but does not reach far enough northwest to become a dominant current, even if the EGC is strongly reduced. As previously suggested by *Müller et al. (2012)*, a broadening of the EGC towards the East during times of increased Arctic outflow might increase the ice flux via Fram Strait but not the delivery of ice to the core site on the inner shelf. Further, *Telesiński et al. (2014b)* indicate a general

change in the route of the EGC on the East Greenland Shelf after the onset of the Neoglacial, after 3 kyr BP.

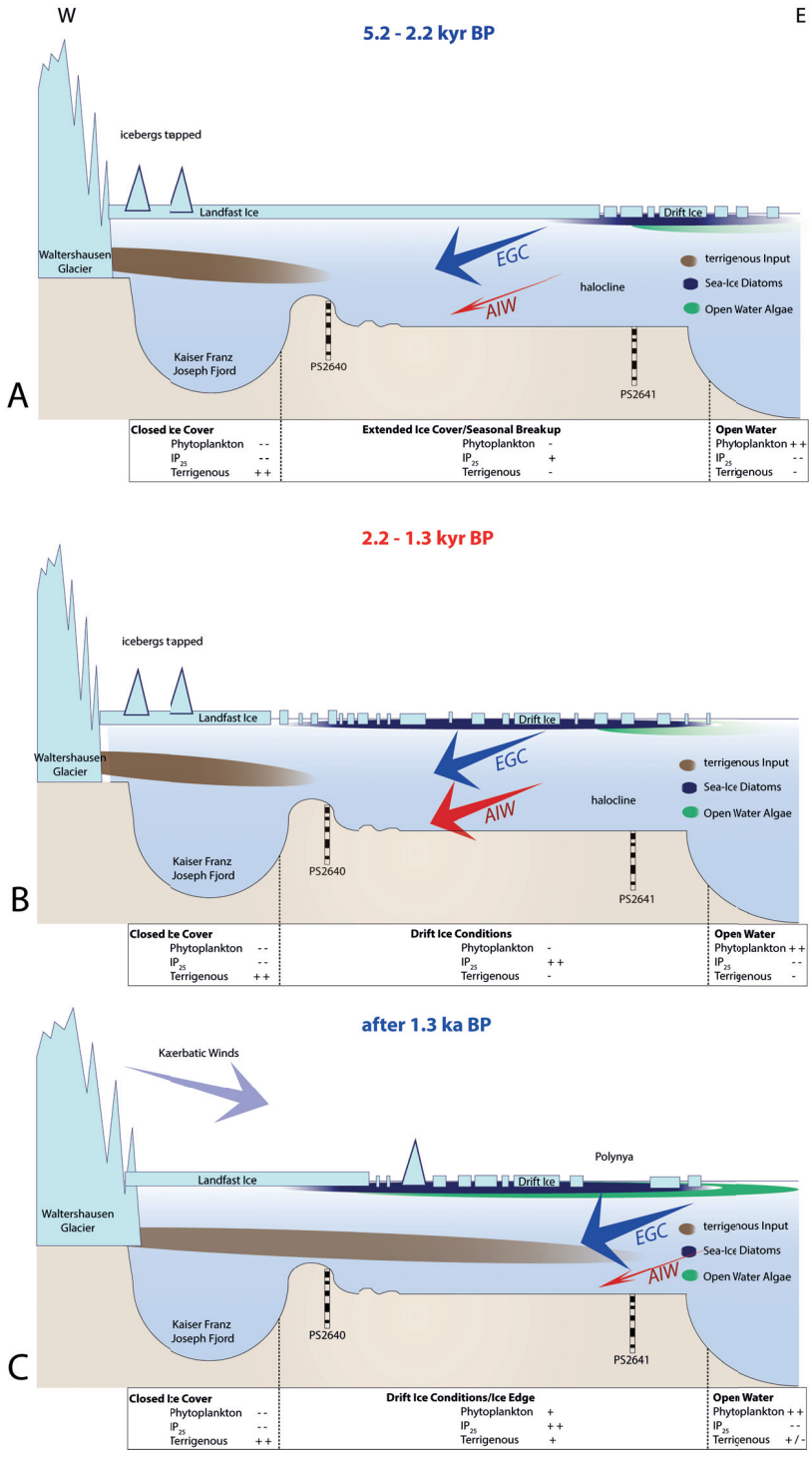

Fig 4. 5*:* Schematic W-E section across the East Greenland Shelf at 70°N ***A.*** from 5.2 – 2.2 kyr BP, ***B.*** from 2.2 – 1.3 kyr BP and ***B.*** after 1.3 kyr BP showing the production areas of IP_{25} (blue), and phytoplankton sterols (green). Brown sections indicate a suspended matter plume from Greenland and terrigenous sterols. Dominant currents are indicated by blue (EGC: East Greenland Current) and red (AIW: Atlantic Intermediate Water) arrows. Size of arrows indicates current influence (strength).

The vicinity to the Kaiser Franz Joseph Fjord to the core site on the East Greenland Shelf has also taken into account; glaciers and landfast ice have a more direct influence on this site than on the site in Fram Strait. In order to receive detailed information about the paleopathway of the EGC, more high-resolution records of the late Holocene located further east are needed. A detailed sea ice reconstruction from Kaiser Franz Joseph Fjord would also contribute to the understanding of the processes, as from our core only indirect assumptions about conditions in the fjord can be made.

In general, we propose that seasonal sea ice characterized the East Greenland Shelf. We found evidence for phases of changes in the intensity of the seasonal sea ice cover. The general over-regional solar forcing trend seems to be only indirectly recorded in sediments from our core site. Influences from the adjacent fjord and Greenland Ice Sheet, which is itself influenced by solar forcing, may overprint the general climatic trend. Our record seems to record small-scale, more regional climate events caused by a combination of changes in EGC intensity and in the fjord environment on rather small-scales. The changes of sea ice and specific short-term events will be subject of discussion in the following.

4.4.2. The late Holocene (5.2 – 1.3 kyr BP)

Relatively low ice algae and phytoplankton productivity during this phase (Fig 4.2E, F) are accompanied by generally low accumulation rates (Fig 4.3). Throughout this period the input of terrigenous sterols remains relatively low (Fig 4.2B). We take this as indicative for relative harsh seasonal sea ice conditions with a nearly closed sea ice cover in winter and seasonal break up during summer melt, allowing relatively low phytoplankton and intermediate ice algae productivity. This is supported by sea ice concentration calculated with the PIP_{25} index, showing relatively constant and high values (Fig 4.4B, C). Landfast ice from the fjord may have extended towards the core site and joined with relatively strong and constant sea ice inflow from the Arctic (Fig 4.5A). A strong EGC, and associated sea ice export, has been reported over the northwestern Atlantic for this period *(Jennings et al., 2002; Moros et al., 2004, 2006b; Funder et al., 2011; Darby et al., 2012; Perner et al., 2015)*. A strong stratification may have restrained phytoplankton productivity during times of

seasonal ice break up. Evidence for a strong halocline related to EGC strengthening has been found in Denmark Strait and at our core site during this period by *Perner et al. (2015, 2016)*. Permanent landfast ice in the fjord may have prevented the outflow of local terrigenous material (Fig 4.5A). A sediment source analysis from the same material (Fig 4.2A; *Andrews et al., 2016*) revealed a dominance of sediment transport from northward sources.. Further, the absence of IRD *(Evans et al., 2002)* indicates a strong landfast ice cover in the fjord, which may have trapped icebergs and prevented input of local and coarse-grained material *(Alonso-Garcia et al., 2013; Mugford and Dowdeswell, 2010)*

Increasing biomarker accumulation rates around 3.4 kyr BP (Fig 4.3) are followed by minor increases of terrigenous and phytoplankton sterol concentrations around 2.8 kyr BP (Figs 4.2B, E). This may indicate a slight shift to less harsh seasonal sea ice conditions. Here we speculate, that in respect to the local oceanography, that is characterized by nutrient depleted Arctic waters *(Aagaard and Coachman, 1968a, b; Johannessen, 1986; Hopkins, 1991; Perner et al., 2015)*, a low productivity ice edge might evolve during a southward movement of the Polar Front. Sea ice concentrations based on the PIP_{25} index show a slight decreasing trend from 3.0 kyr BP onwards (Fig 4.4B), this decrease may be connected to a shut-down of the so-called 'ice factory' in Storfjorden, Svalbard that occurred from 2.8 kyr to 0.5 yr BP *(Knies et al., 2017)*. The associated reduction in sea ice export to the core site on the East Greenland Shelf is in relative good agreement with our findings (Figs 4.2., 4.4B) and may support a reduction of seasonal ice cover and a south-westward retreat of the ice margin, moving it closer to our core site.

2.2 to 1.3 kyr BP – The Roman Warm Period

A reduction in IP_{25} concentration is accompanied by slightly increasing brassicasterol concentration around 2.2 kyr BP (Figs 4.2E, F, 4.4A), which may imply a phase of more open seasonal sea ice conditions. This is supported by the PIP_{25} index, which also supports a slight reduction of sea ice concentrations and shows values indicating less severe conditions within the still prevailing seasonal sea ice conditions (Fig 4.4B, C). Low accumulation rates of all biomarkers (Fig 4.3) seem to be contradictory to a reduction of sea ice cover. We assume that a strong stratification due to enhanced input of freshwater hampered surface water production in general,

leading to the observed low accumulation rates (Fig 4.5B). This may be supported by indications for high AIW inflow and higher subsurface temperatures at our core site *(Perner et al., 2015)* and in a fjord in southeast Greenland between 2.5 and 1.5 kyr BP *(Mernild et al., 2012; Perner et al., 2016)*. A strong AIW and subsurface warming during this phase (Fig 4.2D; *Perner et al., 2015*) may have favoured subsurface melting of sea ice and landfast ice in the adjacent fjords. Consequently, this might lead to increased input of freshwater to the core location on the inner shelf. A slight increase of terrigenous sterol concentration (Fig 4.2B) supports an increased input from fjords north of the core site, possibly related to enhanced landfast ice melting. Based on the absence of IRD during this phase *(Evans et al., 2002)* and a dominance of northern mineral sources (Fig 4.2A; *Andrews et al., 2016*), we assume that the Kaiser Franz Joseph fjord was still covered by landfast ice or had a stable sikussaq *(Syvitski et al., 1996)*, which trapped icebergs and prevented them from transporting coarse grained material to the core site (Fig 4.5B; *Mugford and Dowdeswell, 2010; Alonso-Garcia et al., 2013*). A strong, possible perennial stratification and halocline may prevent a noticeable heat and nutrient exchange between the water masses and would have created unfavourable conditions for primary productivity and therefore reducing accumulation rates in general.

Our findings of a reduction of seasonal sea ice cover, however, seem to be in conflict with the almost absence of planktic foraminifera (Fig 4.2C), interpreted as a signal for a cold and low productivity phase with harsher sea ice conditions, caused by an extended EGC leading to a strong stratification and a well-defined halocline *(Perner et al., 2015)*. Nevertheless, the strong stratification, indicated in the foraminiferal record, fits well to our interpretation of a strongly reduced primary production due to a freshening of surface waters. We assume that the planktic foraminifera signal is overprinted by high stratification and freshening of the surface waters.

This phase of less severe seasonal sea ice concentration (Fig 4.4B, C) correlates quite well with the RWP, a phase of atmospheric warming across the Northern Hemisphere accompanied by ocean warming culminating around 1.8 kyr BP (i.e. CE 150; *Ljungqvist, 2010*). The RWP is considered to be a possible pre-industrial equivalent for the modern warming *(Mann and Jones 2003; Ljungqvist, 2010)*. This phase of reduced sea ice on the East Greenland Shelf is in good agreement with other

records from the northern North Atlantic *(Jennings et al., 2002; Risebrobakken, 2003; Sarnthein et al., 2003; Giraudeau et al., 2004; Jiang et al., 2005; Sicre et al., 2008; Mernild et al., 2012; Moros et al., 2006b, 2012; Werner et al., 2015)*. Our interpretation of the biomarker data of Core PS2641 is also supported by a biomarker record north off Iceland where a pronounced negative excursion is seen in the IP_{25} record between 2.3 and 1.5 kyr BP *(Cabedo-Sanz et al., 2016)*.

An enhanced northward transport of warm Atlantic Waters has been found in several records after 2 to 2.5 kyr BP *(Nesje et al., 2001; Risebrobakken, 2003; Jackson et al., 2005; Funder et al., 2011; Darby et al., 2012; Mernild et al., 2012; Olsen et al., 2012; Perner et al., 2015)*. This may cause a retreat of sea ice in Fram Strait and a related decrease in southward export of sea ice *(Müller et al., 2012)* as well as increased recirculation rates of subsurface Atlantic Waters towards the East Greenland Shelf. Such a change in oceanography may lead to the signal observed on the East Greenland Shelf: reduced sea ice export, enhanced freshwater export in surface waters and increased inflow of warm subsurface Atlantic Water masses. A strong possible perennial stratification and halocline between surface and subsurface waters may prevent a noticeable heat exchange between the water masses and would have created unfavourable conditions for primary productivity and therefore reducing accumulation rates in general.

Perner et al. (2015) relate the RWP warming to either changes in the subpolar gyre circulation or shifts in the NAO mode. A shift towards a more positive NAO mode would be related to increased Atlantic Water inflow through Fram Strait and a reduction in sea ice formation *(Dickson, 1999; Kwok and Rothrock, 1999; Hurrell and Deser, 2009)*. Such a process may cause the reduced sea ice and increased freshwater export towards the East Greenland Shelf. Due to the proximity of the Greenland Ice Sheet and fjord systems it is likely that several mechanisms may contribute to the observed changes in sea ice. Due to the complexity of the investigated region, a combination of several effects, which might have caused the reduction of sea ice during the RWP, need to be considered.

4.4.3. The last Millennium (1.3 kyr BP to present)

The last Millennium is characterized by a general increase in ice algae and phytoplankton productivity; this trend continues towards the present and is superimposed by several short-term oscillations (Figs 2, 6). We relate these increases to severe seasonal sea ice conditions and the establishment of an ice edge or a polynya situation on the East Greenland Shelf (Fig 4.5C). This overall change in our biomarker record correlates with glacier advances in Greenland around 1.4 kyr (Fig 4.2, *Solomina et al., 2015*) and a constant strong EGC *(Perner et al., 2015)*, transporting more sea ice towards the core site. Katabatic winds from the advancing glacier may have favoured polynya formation *(Barber and Massom, 2007)*.

A change in mineral source, with a shift from a dominance of a more northward/Arctic source to a mixture of a northern/Arctic and local/Fjord source after 1.2 kyr BP (i.e. CE 700) (Fig 4.2A; *Andrews et al., 2016*) may be related to increased outflow from the fjord, carrying high amounts of terrigenous matter and nutrients to the shelf area. This change in mineral composition correlates with glacier advances in Greenland around 1.4 kyr (Fig 4.2, *Solomina et al., 2015)*. The glacier advance and high export rates of Arctic sea ice may have destabilized sea ice above the core site, causing more break up *(Mugford and Dowdeswell, 2010)*. Evidence for a destabilizing effect of the glacier advance on the landfast ice/sikussaq in the fjord may be provided by enhanced concentration of terrigenous sterols. Two extreme events around 1 and 0.75 kyr BP (Fig 4.2B) may be related to single break ups in landfast ice/sikussaq which caused the release of icebergs that have been trapped for several years in the fjord, which released massive amounts of local sourced terrigenous matter within a short period *(Mugford and Dowdeswell, 2010)*. The possible establishment of a seasonal ice edge close to the core site after 1.3 kyr BP created more favourable conditions for sea ice algae and phytoplankton productivity (Figs 4.2E, F). Generally cooler conditions over Greenland and a reduction of AIW inflow during this phase *(Alley et al., 2010; Perner et al., 2015)* may have reduced the meltwater input, favouring a seasonal break up of the stratification and the upwelling of nutrient enriched waters. The change in productivity during this phase is also represented in the increasing planktic foraminiferal abundances (Fig 4.2C; *Perner et al., 2015)*. This might either indicate that foraminifers could profit directly

from the change of water masses or that with increased phytoplankton productivity their food supply increased.

1.3 – 0.9 kyr – The Dark Ages Cold Period

A phase of extended seasonal sea ice concentration, reflected in increased IP_{25} and reduced phytoplankton productivity around 1.3 kyr BP (CE 650) (Figs 4.2, C), points towards a phase with enhanced export of sea ice towards the core site. Harsher seasonal sea ice conditions are supported by elevated PIP_{25} values (Fig 4.4B). An extremely high terrigenous sterol peak during this time (Fig 4.2B) may be related to an event where the landfast ice and possible icebergs trapped therein were released. Increasing accumulation rates (Fig 4.3) are most likely caused by a combination of a more active fjord system, increasing the downward drag of suspended material. An advance of the adjacent glaciers during this phase *(Solomina et al., 2015)* may have enhanced the break-up of landfast ice and the release of icebergs *(Mugford and Dowdeswell, 2010)*. Enhanced westerly winds during this period may have contributed wind stress to sea ice *(O'Brien et al., 1995)*, favouring polynya formation, favourable for ice algae productivity. We still assume a strong stratification, due to low phytoplankton productivity, which may have caused a low productivity polynya situation.

This phase of enhanced seasonal ice cover on the East Greenland Shelf correlates well with the well-known DACP, a phase of deteriorated climate in Northwest Europe *(Lamb, 1995)*. Although some differences are obvious in the exact timing and behaviour, cold phases with extended sea ice, coinciding with the DACP, are found in several other climate proxy records:

- A record from the Fram Strait displays cold conditions between CE 700 and 900, biomarkers indicate extended sea ice cover from CE 700 to 800 *(Werner et al., 2013; Cabedo-Sanz and Belt, 2016)*.
- The region north off Iceland experienced two periods with increased sea ice conditions (1.5 and 0.7 kyr BP, i.e. CE 450 and 1250; *Cabedo-Sanz et al., 2016)*.
- Two cooling episodes with enhanced EGC inflow at CE 960 and CE 1080 were found in Igaliku Fjord, South Greenland *(Jensen et al., 2004)*.

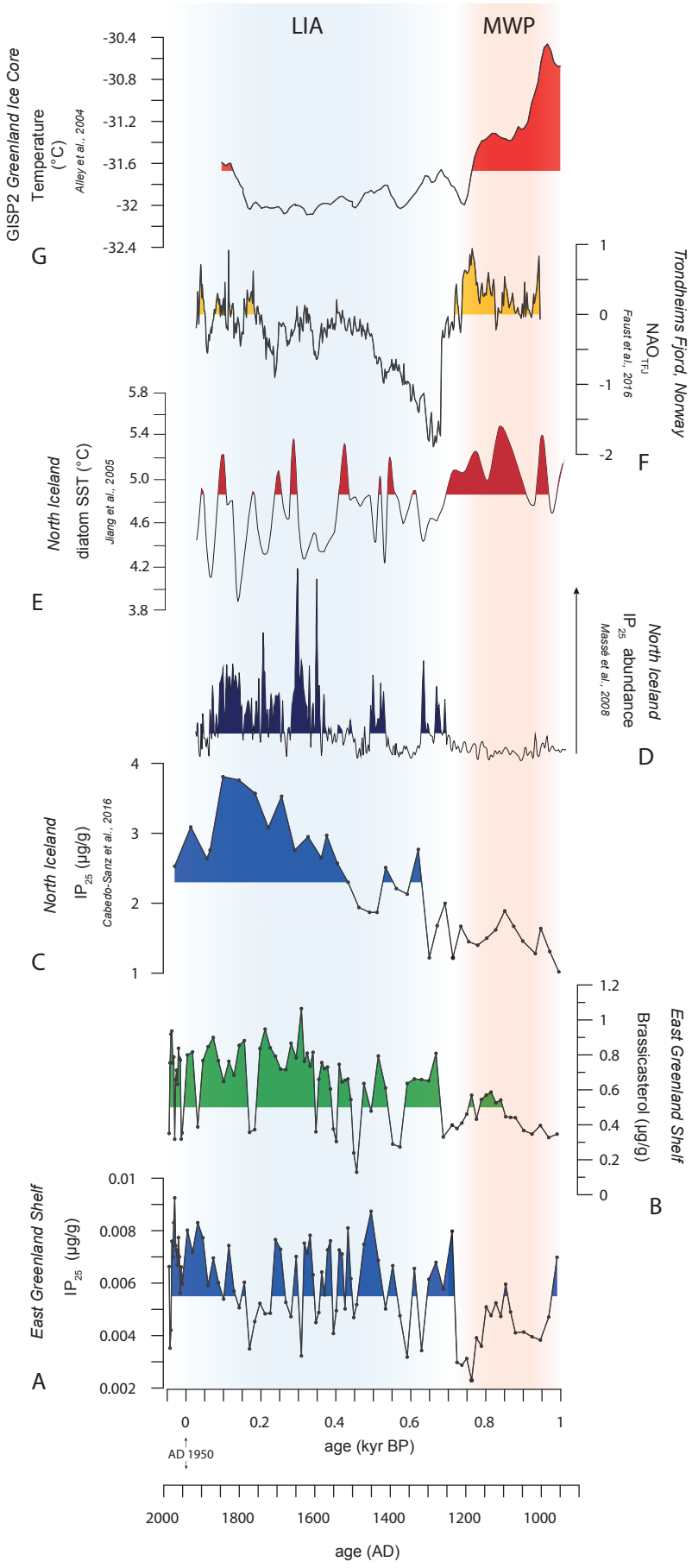

Fig 4. 6 IP_{25} and ***F.*** brassicasterol concentrations from the East Greenland Shelf (Core 2641, this study), and two IP_{25} records from the North Iceland Shelf ***(E.*** *Cabedo-Sanz et al., 2016,* ***D.*** *Massé et al., 2008)* and ***C.*** a sea surface temperature (SST) record based on diatoms, also from the North Iceland Shelf *(Jiang et al., 2005).* ***B.*** NAO reconstruction from the Trondheims Fjord *(Faust et al., 2016)* and ***A.*** atmospheric temperatures from the GISP2 ice core in Greenland *(Alley et al., 2010)*. The red area marks the Medieval Climate Anomaly (MCA), blue area represents the Little Ice Age (LIA).

The mechanisms behind this cooling period have been discussed by several authors *(Zielinski, 2000; Mayewski et al., 2004; Wanner et al., 2011),* no clear indications for a single forcing mechanism could be found. A negative excursion in the solar output (maximum in ^{10}Be) and an associated migration of the ITCZ as well as higher volcanic activity have been observed after CE 600 *(Zielinski, 2000; Mayweski et al., 2004; Wanner et al., 2011)*. This process could have caused a significant cooling in the Arctic leading to increased sea ice formation and export towards the East Greenland Shelf and increasing local sea ice formation and glacier advances.

1.0 – 0.7 kyr BP – The Medieval Climate Anomaly

The DACP ends around 1 kyr (CE 950) with an abrupt drop in IP_{25} concentrations, to values as low as observed during the RWP, accompanied by a strong increase in phytoplankton productivity (Figs 4.2 E, F). A short-lived but strong reduction in PIP_{25} based sea ice concentrations (Fig 4.4B) is taken as evidence for a short but strong reduction of sea ice transported to the East Greenland Shelf. High accumulation rates for the phytoplankton biomarkers and low rates for IP_{25} (Fig 4.3) support a short phase of reduced sea ice cover that favoured phytoplankton productivity. A biomarker study from the Fram Strait indicates less severe sea ice conditions from CE 800 to 1350 *(Cabedo-Sanz and Belt, 2016)* a retreat of sea ice in Fram Strait might be directly coupled to reduced ice export to the East Greenland Shelf.

This phase of reduced seasonal sea ice correlates with the European MCA (CE 950 - 1200, *(Lamb, 1977, 1965; Stine, 1994)*, which was characterized in several studies from the Northern Hemisphere by reduced sea ice cover and drift ice *(Andrews et al., 2009; Kinnard et al., 2011; Cabedo-Sanz et al., 2016),* warmer SSTs *(Helama et al., 2010; Mernild et al., 2012)*, enhanced northward advection of Atlantic Water *(Spielhagen et al., 2011)*, and low IRD *(Moros et al., 2006b)* between the 9th and 14th century.

The interpretation of the biomarker data from Core PS2641 is supported by foraminiferal data showing a minor peak in AIW culminating at 1 kyr BP (CE 950) (Fig 4.2D; *Perner et al., 2015)* that coincides with the onset of the MCA. This may point towards higher northward advection of warm Atlantic Water through Fram

Strait, an associated retreat of sea ice *(Müller et al., 2012)* and enhanced recirculation rates of subsurface Atlantic Water, leading to reduced sea ice export and enhanced inflow of subsurface Atlantic Water towards the East Greenland Shelf. Stronger westerly winds, enhancing the Atlantic Meridional Overturning Circulation (AMOC), a process that has also been associated with a positive NAO mode *(Trouet et al., 2009),* may have led to a reduction in sea ice export to the East Greenland Shelf. What caused the observed changes remains speculative.

According to *Perner et al. (2015)* the RWP was a more pronounced and warmer phase than the MCA due to the intensity of AIW inflow. In terms of sea ice variability, IP_{25} and the PIP_{25} index indicate a similar reduction of sea ice (Figs 4.2F, 4.4B, C). It seems that the amount of recirculated Atlantic Water is not directly connected to the amount of sea ice exported to the East Greenland Shelf.

0.65 to 0 kyr BP – The Little Ice Age

Around 0.65 kyr BP (CE 1300) sea ice concentrations and phytoplankton productivity strongly increase, reaching the highest values observed over the past 5.2 kyr (Figs 4.2, 4.4, 4.6). Sea ice concentrations, indicated by the PIP_{25} index (Fig 4.4B, C), show a return to marginal ice zone conditions, a polynya-like situation seems possible in respect to the strong increase in phytoplankton and ice algae productivity (Fig 4.2E, F). PIP_{25} based sea ice concentrations stay in a similar range as in the phase from 4.7 to 2.8 kyr BP, indicating a marginal ice zone situation on the East Greenland Shelf over the past 5 kyr (Fig 4.4B). Even though the PIP_{25} index indicates a similar sea ice situation during both phases, we see evidence for two different scenarios (Fig 4.5A, C). High local terrigenous input points towards a very active fjord outflow, supported by the mineral source analysis from the same core (Fig 4.2A; *(Andrews et al., 2016)*. Glacier advance has been associated with the destabilisation of sea ice *(Mugford and Dowdeswell, 2010)*, which could contribute to a higher variability within the increasing seasonal sea ice. Advancing glaciers may have led to increasing katabatic wind stress on sea ice over our core site, favouring the formation of a polynya like situation *(Barber and Massom, 2007)*.

Knies et al. (2017) assume a change towards an active 'sea ice factory' in the Arctic polynyas around 0.5 kyr BP, which allows the assumption that the increase in

seasonal sea ice cover on the East Greenland Shelf might be related to enhanced sea ice export from the Arctic. Further, a cooling of the EGC has been reported by several authors and is in line with our observations: a cooling of the EGC occurred for instance after CE 1200 off South East Greenland (based on the diatom record of *Jensen, 2003*), and is also observed around CE 1370 on the East Greenland Shelf at 68°N *(Jennings and Weiner, 1996)*. Several marine *(e.g. Andersson et al., 2003; Moros et al., 2006b; Bendle and Rosell-Melé, 2007; Sejrup et al., 2010; Spielhagen et al., 2011; Mernild et al., 2012; Cabedo-Sanz et al., 2016)* and terrestrial records *(e.g. Nesje et al., 2000; Seppä and Birks, 2002; Jansen et al., 2016)* additionally report a cooling over the past 600 to 700 years. Increased sea ice concentration in Fram Strait *(Müller et al., 2012; Werner et al., 2013; Cabedo-Sanz and Belt, 2016)* are in line with these findings, indicating high export-rates of sea ice. It has to be considered that a strengthened EGC may not consequently increase the sea ice transport to the core site as it may expand eastward as proposed by *Müller et al. (2012)*. This may explain the observed sea ice concentrations that show only a return to concentrations as observed before 2.8 kyr BP (Fig 4.4B). Nevertheless, it seems unlikely that our core site stays fully unaffected by enhanced but eastward-expanded EGC conditions. A combination of slightly strengthened EGC and sea ice transport and enhanced local sea ice formation might be considered for this time.

Even though the cold agglutinated foraminfers and IP_{25} show a similar trend for this phase they do not show a direct correlation (Appendix B4). This supports findings of *Seidenkrantz (2013)*, that benthic foraminifera are a good proxy for general trends of changes in surface waters but do not record a direct sea ice signal.

This phase of variable and severe seasonal sea ice conditions on the East Greenland Shelf can be related to the LIA, which describes the most recent atmospheric cooling, and glacier advances during the Late Holocene in most of the marine and continental Northern Hemisphere (*Denton and Karlén, 1973; Nesje and Dahl, 2003; Matthews and Briffa, 2005; Wanner et al., 2008)*.

Our LIA record from the East Greenland Shelf seems to show a twofold maximum of high IP_{25} concentrations interrupted by a strong IP_{25} minimum between 0.19 to 0.1 kyr BP (i.e. CE 1760 to 1850, Fig 4.6G). This pattern seems to be a widespread

signal as such a twofold division of the LIA has been reported in Greenland Ice Cores *(Dahl-Jensen, 1998; Johnsen et al., 2001)*, the Norwegian Sea *(Jansen and Koç, 2000)* and in the Fram Strait *(Werner et al., 2015)*. In Fram Strait severe sea ice conditions during the LIA are terminated around CE 1750 *(Cabedo-Sanz and Belt, 2016)*, coinciding with a decrease in sea ice algae productivity (IP_{25}) and concentrations (PIP_{25}). On the East Greenland Shelf, however, the values return to high values again at CE 1850. This might indicate that local ice formation and fjord processes may have contributed more to the sea ice conditions on the East Greenland Shelf.

In terms of timing, the transition from MCA to LIA is very well preserved in several IP_{25} records from the northern North Atlantic (Fig 4.6). Our record from the East Greenland Shelf and the two other existing biomarker records from north of Iceland *(Massé et al., 2008; Cabedo-Sanz et al., 2016)* show a first increase in IP_{25} concentrations between 0.62 and 0.69 kyr BP (CE 1330 and 1260) (Figs 4.6G, E, D). This transition correlates well with decreasing SSTs north of Iceland around 0.7 kyr BP (CE 1250) *(Jiang et al., 2005,* Fig 4.6C) and an increase of sea ice concentrations in the eastern Fram Strait *(Cabedo-Sanz and Belt, 2016)*. Other paleoceanographic records from more distant sites also correlate very well with the transition from MCA to LIA, e.g., Chesapeake Bay: CE 1400 *(Cronin et al., 2003),* Skagerrak: CE 1350 *(Hass and Kaminski, 1995)*, Fram Strait: CE 1350 *(Werner et al., 2011)*, Norwegian Sea: CE 1500 *(Sejrup et al., 2010)*.

The transition from MCA to LIA on the East Greenland Shelf seems to be related to a combination of atmospheric cooling causing a glacier advance *(Alley et al., 2010; Solomina et al., 2015)* and an increase in sea ice export from the Arctic Ocean. The nearly synchronous change in sea ice records over the central and western North Atlantic indicates a widespread phenomenon. A reorganization of the oceanographic system in the northern North Atlantic, associated with reduced heat and moisture transport towards the North, causing a general cooling and sea ice advance, seems to happen on rather short time scales and in an over regional manner. The transition from MCA to LIA has been associated with a combination of forcings, e.g., the reduction in solar irradiance, explosive volcanism and greenhouse gasses *(Gillett et al., 2003; Wanner et al., 2011; Miller et al., 2012; Faust et al., 2016)*. It has to be

taken into account that a cooling and associated glacier and sea ice retreat may set off the positive ice/albedo feedback, enhancing the cooling trend. A proxy reconstruction of NAO modes in the Trondheims Fjord (Norway) shows a clear shift just shortly before 0.7 kyr BP (CE 1250) from positive to negative NAO values *(Faust et al., 2016,* Fig 4.6B). This shift in NAO reconstructed in the Trondheims Fjord correlates very well with the observed transition from MCA to LIA in our and other biomarker records (Figs 4.6). The exact timing of the NAO shift is still under discussion *(Trouet et al., 2009; Olsen et al., 2012; Ortega et al., 2015; Faust et al., 2016)* and should not be over interpreted.

Our biomarker record shows a high and cyclic variability in IP_{25} and phytoplankton biomarkers for the last millennium (Figs 4.2, 4.6). A frequency analysis for the last 1.2 kyr BP of the biomarker record of Core PS2641 revealed a dominant periodicity of approximately 73-74 years (Fig 4.7). This cyclicity was found in IP_{25} as well as in the marine sterols (i.e., brassicasterol and dinosterol*;* Fig 4.7B) indicating a close connection between the driving mechanisms of sea ice and phytoplankton productivity. A similar period of 70 to 90 years has been found in numerous records from the North Atlantic *(e.g., Cronin et al., 2003; Jungclaus et al., 2005; Moros et al., 2006b; Knudsen et al., 2009; Kuijpers and Mikkelsen, 2009; Andresen et al., 2012; Miles et al., 2014)* and has been attributed to the Atlantic Multidecadal Oscillation (AMO), which represents variations in the intensity of the global thermohaline circulation *(Kerr, 2000)*. A warm AMO state is associated with increased heat flux towards the North Atlantic and a decrease in mean Arctic sea ice concentration *(Venegas and Mysak, 2000; Dijkstra et al., 2006)*. The formation and export mechanisms of Arctic sea ice via Fram Strait underlies complex mechanisms and is still not yet fully understood *(Venegas and Mysak, 2000)*. Nevertheless, it seems likely that the sea ice cover and primary production on the East Greenland Shelf is at least partly affected directly or indirectly by these changes in the reduction in Arctic sea ice extent, leading to changes in sea ice and freshwater export. Increased heat export towards the North Atlantic may lead to enhanced recirculation of relative warm AIW towards the study area, having a direct influence on water column properties and subsurface temperatures. The driving mechanisms of AMO variability are still under discussion and not yet understood.

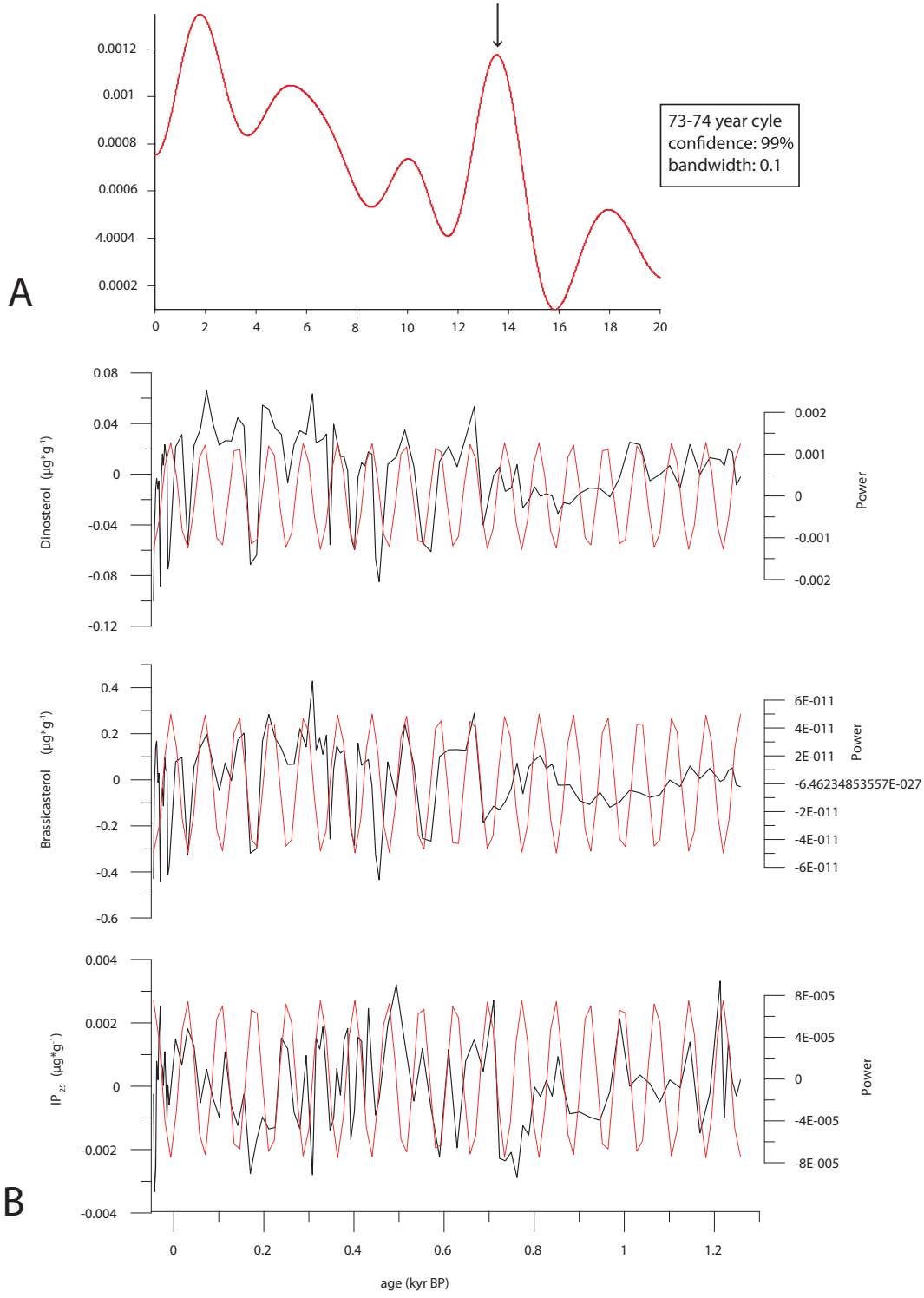

Fig 4. 7 ***A.*** Spectrum of spectral analysis, the frequency of the 73-74 year cycle is indicated by a black arrow. ***B.*** Comparison of the band-pass filtered 73-74 years cycle (red) and the linear detrended IP_{25}, brassicasterol and dinosterol record (black) (confidence 99%) of Core PS2641 over the past 1.2 kyr.

In respect to age model uncertainties the 88-year solar Gleissberg cycle *(Peristykh and Damon, 2003)* may be connected to the oscillation observed in our biomarker record. Changes in solar activity will lead to atmospheric and oceanic changes that

will affect the amount of sea ice that is exported from the Arctic to the East Greenland Shelf as well as the current system and related water masses *(Cubasch et al., 1997; Velasco and Mendoza, 2008)*. Additionally, phytoplankton and sea ice algae are photosynthetic organisms and depend on incoming solar radiation and may react to such changes as well.

4.5. Conclusions

Our detailed biomarker record obtained from Core PS2641 provide important information about the late Holocene sea ice and climate history:

- The East Greenland Shelf at 73° N does not directly reflect the solar insolation decrease and the related late Holocene Neoglacial cooling trend around 5 kyr BP as observed in other marine paleoclimatic records. The area was dominated by seasonal sea ice throughout the investigated time period.
- It is highly affected by Arctic sea ice conditions and North Atlantic oceanic and atmospheric circulation changes. The Greenland Ice Sheet and local fjord processes also affect the area.
- We find two phases of extended sea ice concentrations from 5.2 to 2.2 kyr BP and 1.3 kyr BP to present interrupted by a phase of reduced sea ice concentrations between 2.2 and 1.3 kyr BP.
- A pronounced short-term variability in sea ice extent during the past 2.2 kyr correlates with the warm and cold events RWP, DACP, MCA and LIA.
- Transitions between these events occurred rather fast and display a close connection of sea ice changes on the East Greenland Shelf and the Northern Hemisphere climate. These findings are crucial for our understanding of the recent reduction of Arctic sea ice. A better understanding of this naturally highly variable area may help to improve climate models and climate predictions.
- For further information about driving mechanisms, fjord conditions and EGC strength more high-resolution sea ice reconstructions from the area are needed.

Acknowledgments

Financial support was provided by the Deutsche Forschungsgemeinschaft through 'ArcTrain' (GRK 1904) and 'GreenClime' (PE2071/2-1). Furthermore we wish to thank the captain, crew and science party of RV Polarstern Expedition ARKTIS-X/2. Thanks to Simon Belt and colleagues (Biogeochemistry Research Centre, University of Plymouth) for providing the internal standard for IP_{25} analysis. The authors would like to thank two anonymous reviewers for their thorough and helpful comments to improve the manuscript.

5. New insights into sea ice changes over the past 2.2 kyr in Disko Bugt, West Greenland

Henriette M. Kolling[a], Ruediger Stein[a], Kirsten Fahl[a], Kerstin Perner[b], Matthias Moros[b]

[a] Alfred Wegener Institute, Helmholtz Centre for Polar and Marine Research, Am Alten Hafen 26, 27568 Bremerhaven, Germany
[b] Leibniz Institute for Baltic Sea Research Warnemuende, Seestraße 15, 18119 Rostock, Germany

Under review with *arktos – The Journal of Arctic Geosciences* (since November 2017)

Abstract

Past sea ice conditions and open water phytoplankton productivity were reconstructed using biomarker records determined in a sediment core from Disko Bugt. For a better interpretation of the paleorecord, biomarker concentrations of Baffin Bay surface sediments were compared to modern sea ice concentrations. Increased concentrations of the sea ice biomarker IP_{25} were observed under seasonal ice cover, whereas open water biomarker (i.e., brassicasterol, dinosterol and HBI III) concentrations could be related to the spring ice edge. The 'PIP_{25} index' correlates well with modern sea ice concentration, supporting that our biomarker approach is a reliable tool for paleo-sea ice reconstructions in the Baffin Bay.

The paleorecord indicates that Disko Bugt experienced a gradual expansion of seasonal sea ice over the past 2.2 kyr. Maximum sea ice conditions were reached during the Little Ice Age around 0.2 kyr BP. Superimposed on the general trend, a short-term oscillation in open water primary production and terrigenous input may be related the Atlantic Multidecadal Oscillation and solar activity as trigger mechanism. A multi-proxy comparison of our biomarker record to microfossil (i.e., benthic foraminifera, dinoflagellates and diatoms) and other geochemical proxies (i.e., alkenones) indicates that all proxies are influenced by the complex environmental system with pronounced seasonal changes and strong oceanographic

gradients, i.e., freshwater inflow from the Greenland Ice Sheet. We combine our new biomarker record with the available proxy data in a direct sample-to-sample comparison. Our results support the PIP_{25} index as the direct sea ice proxy, whereas other microfossils are more indirectly associated to sea ice.

5.1. Introduction

Sea ice plays an important role in the climate system by influencing the Earth's energy balance as well as the exchange between ocean and atmosphere. It is considered as one of the critical components in climate models *(Vinnikov et al., 1999),* and the underestimation of the recent sea ice loss *(Cavalieri et al., 1997; Serreze & Barry, 2011; Stroeve et al., 2012)* displays the need to extend our knowledge on natural sea ice dynamics. As reliable satellite observations are only available for the past ~40 years *(NSIDC, 2017)* high-resolution proxy reconstructions from regions characterized by highly dynamic sea ice conditions may provide vital information about pre-industrial sea ice variability.

An area that displays such seasonal sea ice variability is the Baffin Bay region, especially the Disko Bugt area at the central West Greenland coast (Fig 5.1). In autumn, the sea ice margin of the so-called 'Westice' expands southwards and reaches as far south as Kangerlussaq, just south of Disko Bugt during winter (Fig 5.2; *Buch, 2000*). During summer the ice margin retreats as far north as Nares Strait and leaves Disko Bugt ice free (Fig 5.2; *Tang et al., 2004*). Further, Disko Bugt is highly affected by outlet glaciers of the Greenland Ice Sheet and associated meltwater input *(Tang et al., 2004)*.

Due to the importance of this area, several studies have focused on paleoceanographic changes *(e.g., Moros et al., 2006a, 2016; Seidenkrantz et al., 2008; Lloyd et al., 2011; Perner et al., 2011, 2013; Krawczyk et al., 2012, 2013; Ribeio et al., 2012; Ouellet-Bernier et al., 2014; Cormier et al., 2016)* and variations of the Greenland Ice Sheet *(e.g., Weidick et al., 2007; Young et al., 2015)* during the mid- to late Holocene. Within these studies first assumptions about the sea ice distribution have been made, however, showing very different results. This displays the need for direct proxy reconstructions of sea ice.

Starting with new biomarker sea ice proxy data from Baffin Bay surface sediments and their correlation with satellite derived sea ice concentrations, we provide a high-resolution sea ice reconstruction based on the direct sea ice proxy IP_{25} and contribute important information about the natural variability of sea ice in this highly sensitive region over the past 2.2 kyr. Furthermore, we compare microfossil and geochemical proxies in order to provide a better understanding of the relationship of those proxies to sea ice and other environmental factors.

Application of Biomarkers for environmental reconstructions

Biomarker proxies for organic carbon sources

Specific sterols have been associated with terrigenous and marine organic matter input in paleoenvironmental reconstructions *(e.g., Meyers, 1997; Fahl & Stein, 1999, 2007*). Long chain n-alkanes (C_{25}, C_{27}, C_{29}, C_{31}) and lignin are established proxies for the reconstruction of organic matter input from vascular plants (e.g., *Prahl & Muehlhausen, 1989; Yunker, et al., 1995)*. Further, β-sitosterol and campesterol, which are applied in this study, have been proven as reliable proxies for higher land plants, i.e., terrigenous organic matter *(e.g., Huang & Meinschein, 1979; Volkman et al., 1993*).

For marine organic matter production reconstructions, specific short chain n-alkanes (C_{17}, $C_{19;}$ *Blumer et al., 1971; Prahl & Muehlhausen, 1989; Yunker et al., 1995)* and short chain fatty acids (e.g., *de Leeuw et al., 1983; Fahl & Stein, 1997; Nichols et al., 1984; Volkman et al., 1993*) have been successfully applied. Here, we use the sterols brassicasterol and dinosterol, which have been established as reliable phytoplankton biomarker proxies *(e.g., Volkman, 1986; Volkman et al., 1993*).

Biomarker proxies for sea ice

A highly-branched isoprenoid (HBI) alkene with 25 carbon atoms (i.e., IP_{25}) derived from specific sea ice diatoms *(Belt et al., 2007; Brown et al., 2014)* has been proven to be a direct proxy for Quaternary sea ice conditions in the Arctic and sub-Arctic region *(e.g., Massé et al., 2008; Müller et al., 2009; Varé et al., 2009; Belt et al., 2010; Fahl & Stein, 2012; Hörner et al., 2016; Kolling et al., 2017)*. For more detailed understanding of sea ice conditions and to avoid misleading

interpretations concerning the absence of IP_{25}, which may result either from a lack of sea ice or a permanent, thick sea ice cover with too low light penetration for ice algae growth *(Horner and Schrader, 1982), Müller et al. (2011)* have introduced the so-called 'PIP_{25} index' (see '*4.3.3. Methods'* for calculation). This index combines open water phytoplankton biomarker proxies with the sea ice proxy IP_{25}. As open water phytoplankton marker *Müller et al. (2012)* have used brassicasterol and dinosterol, which are produced by a wide range of algae groups *(e.g., Volkman, 1986; Volkman et al., 1993)*. The PIP_{25} index has been verified to represent sea ice concentration quite well through a comparison with satellite-derived values *(Müller et al., 2011)* and has been applied successfully in several studies in the Arctic Ocean and its marginal seas *(Fahl & Stein, 2012; Cabedo-Sanz et al., 2013; Müller & Stein, 2014; Xiao et al., 2015b; Hörner et al., 2016; Stein et al., 2016, 2017a)*. Recently, *Smik et al. (2016)* have modified the PIP_{25} approach by introducing a tri-unsaturated HBI alkene (HBI III, $C_{25:3,}$ z-isomere), associated to ice margin productivity, as open water phytoplankton biomarker. HBI III is produced by marine diatoms of the genera *Pleurosigma* and *Rhizosolenia (Rowland et al., 2001; Belt et al., 2017)*. So far however, this new approach has only been verified as promising proxy for modern and late Quaternary sea ice conditions in sedimentary records from the Barents Sea and its northern continental margin *(Belt et al., 2015; Smik et al., 2016; Berben et al., 2017; Stein et al., 2017b)* but not yet Arctic wide.

Another sea ice related compound seems to be the di-unsaturated HBI alkene (HBI II, $C_{25:2}$), which has been identified in Arctic and Antarctic sediments *(Belt et al., 2007; Vare et al., 2009; Massé et al., 2011)*. Following *Rowland et al. (2001)* who found a relationship between the degree of unsaturation in HBI molecules and temperature, the ratio of the HBI II to IP_{25} (termed 'DIP index'; *Cabedo-Sanz et al., 2013*) has been suggested as a possible index for sea surface temperature (SST; *Fahl & Stein, 2012; Stein et al., 2012; Xiao et al., 2013; Müller & Stein, 2014)*. Despite the good correlations in some regions, however other studies could not find such a correlation to temperature and proposed the DIP index as indicative for sea ice stability rather than SSTs (*Cabedo-Sanz et al., 2013*).

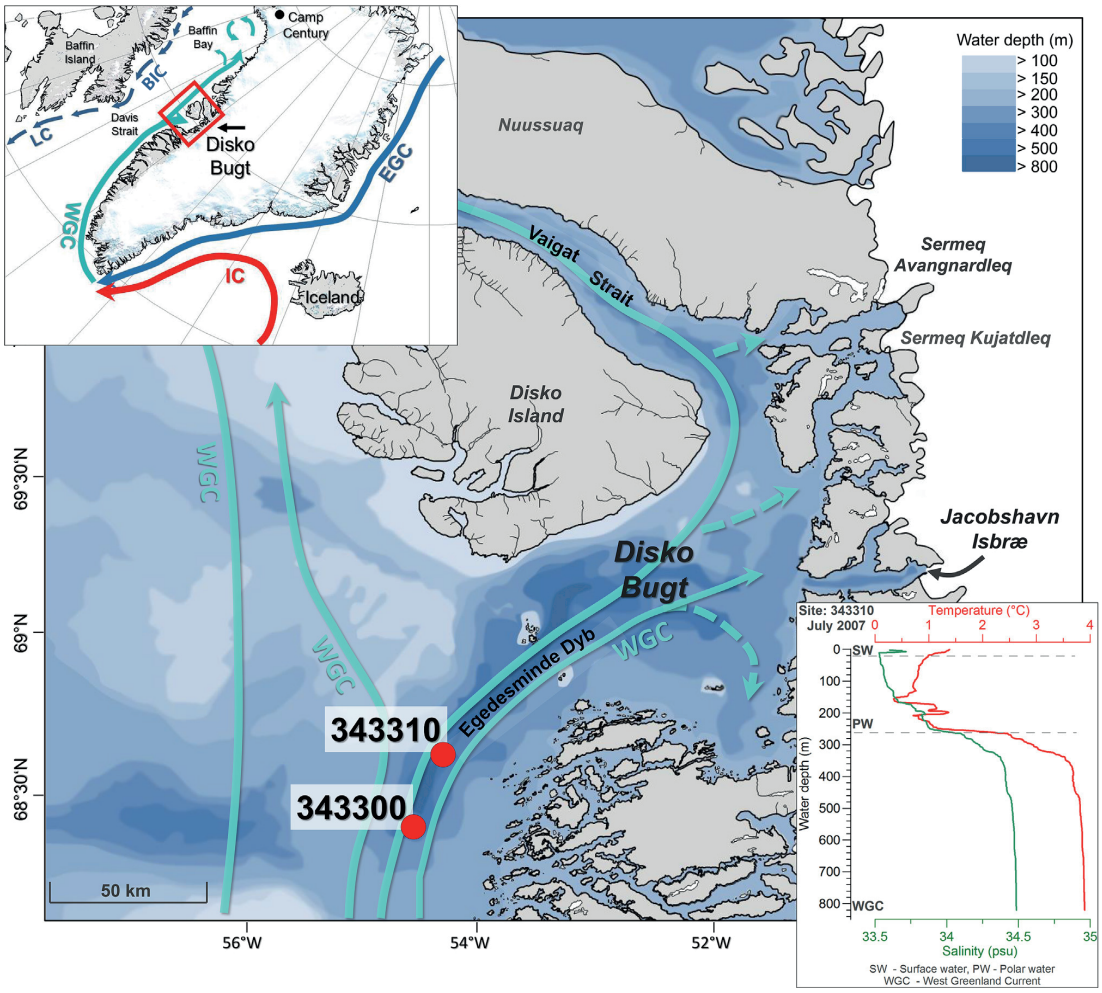

Fig 5. 1. Bathymetric map of Disko Bugt, adapted from *Jakobsson et al. (2008)* showing the present day oceanographic setting of the study area. The location of core 343300 at the southwest edge of Egedesminde Trough and of Core 343310 in the main Egedesminde Trough, are shown by red dots. The upper left map shows the oceanographic setting around Greenland. Lower right inset: Salinity and temperature profile at core site 343310 in July 2007. Abbreviations are as follows: EGC - East Greenland Current; IC - Irminger Current; WGC - West Greenland Current; BIC: Baffin Island Current; LC - Labrador Current

5.2. Physical Setting

Disko Bugt is a large open bay (40,000 km^2) off central West Greenland (Fig 5.1). It is strongly influenced by the West Greenland Current (WGC), which is composed of Atlantic/Irminger Current (IC) derived waters and waters of Polar/East Greenland Current (EGC) origin (Fig 5.1, *Tang et al., 2004*). The WGC inflow to Disko Bugt occurs mainly in the southern part of the bay, whereas the outflow occurs predominantly via Vaigat Strait in the northern part of the bay (Fig 5.1). The WGC penetrates deeper parts of the fjords and affects subglacial melting of tidewater glaciers (Fig 5.1; *Holland et al., 2008; Rignot et al., 2010)*. Further, meltwater originates from the Greenland Ice Sheet has strong seasonal influence on SSTs and salinity of the uppermost water layer *(Buch, 2000; Holland et al., 2008)*,

leading to a strong stratification of the upper 20 – 30 m of the water column *(Andersen, 1981)*. A strong seasonal shift in stratification is caused by enhanced wind activity during autumn and is favouring a well-mixed upper water layer *(Andersen, 1981)*.

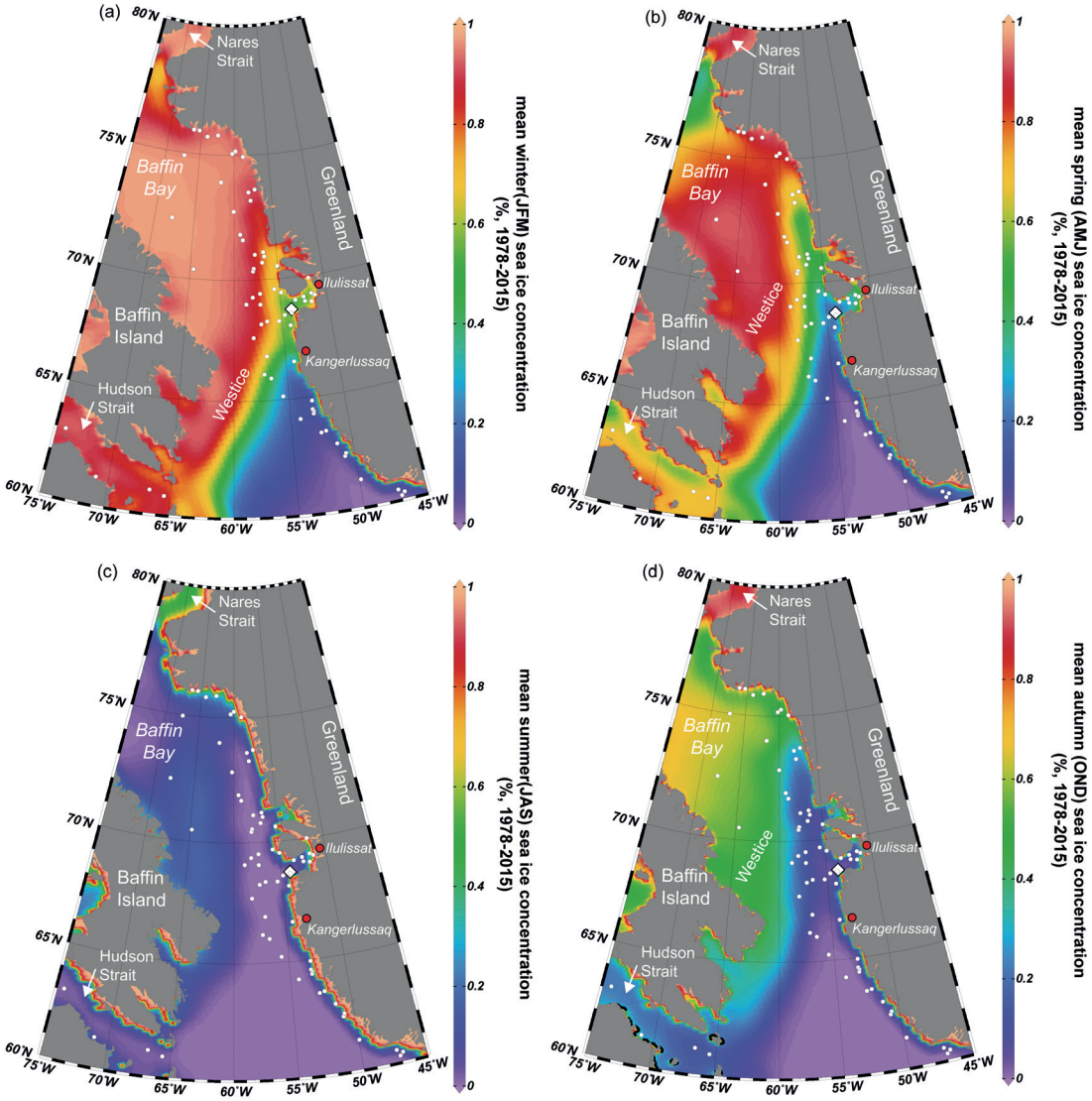

Fig 5. 2 Modern, satellite measured sea ice concentrations for ***(a)*** winter (January, February, March), ***(b)*** spring (April, May June), ***(c)*** summer (July, August, September) and ***(d)*** autumn (October, November, December) from 1978 to 2015 (in %; *Cavalieri et al., 1996; updated 2015*) in the Baffin Bay. The white diamond marks the location of Core 343310, white dots indicate locations of surface samples.

At present, the Baffin Bay and Disco Bugt are covered by sea ice for 3 to 5 months per year (Appendix C2; *Cavalieri et al., 1996, updated 2015; Nielsen et al., 2001)*. The so-called 'Westice' starts to extend southward in autumn with the maximum extend during winter months with all of the Baffin Bay, except Davis Strait, covered by ice (Fig 5.2; *Tang et al., 2004*). The inner Disko Bay, in particular, is also covered by land-fast ice (thickness: 0.7 m) during winter *(Buch, 2000)*. Disko

Bugt is considered a highly productive low arctic marine environment, with three annual maxima in phytoplankton activity during spring, mid-summer and autumn and distinct seasonal changes in the phytoplankton community (i.e., chrysiophytes, diliates, dinoflagellates, silicioflagellates, haptophytes and diatoms; *Jensen & Christensen, 2014)*. The interaction of the Greenland Ice Sheet and the establishment of the sea ice margin as well as its retreat have major impact on marine primary production *(Sakshaug, 2004; Perrette et al., 2011)*.

5.3. Material and Methods

5.3.1. Material

5.3.1.1. Surface Sediments

A total of 66 surface samples (uppermost 1 cm) were collected from *CCGS Hudson*, *R/V Marian S. Merian*, and *R/V Paamiut* along the West Greenland Shelf, inner Baffin Bay and Hudson Strait during three cruises from 2008 to 2015 (Fig 5.2; *Campbell & de Vernal, 2009; Dorschel et al., 2014; Krawczyk et al., 2017)*.

5.3.1.2. Sediment core

Sediment Core 343310 was collected in southwestern Disko Bugt (Fig 5.1; 68° 38' N, 53°49' W; water depth: 855 m) from Egedesminde Dyb, during Cruise MSM05/03 of the R/V *Maria S. Merian (Harff et al., 2007)*. Sediments consist of olive brown to olive grey organic rich silty clay with occasional shell fragments. The gravity core (940 cm) was sampled at 1cm steps; the multi core (32 cm) was sampled at 0.5 cm. This study uses the upper 580.5 cm of the gravity core and eight selected samples of the multi core.

5.3.2. Chronology

A robust age model was established based on 20 AMS ^{14}C dates for the gravity core and 10 AMS ^{14}C dates for the multi core, from benthic foraminifera and mollusc shells *(Lloyd et al., 2011; Perner et al., 2011)*. Ages were calibrated with Marine 09 *(Reimer et al., 2009)* using OxCal 4.1 *(Bronk-Ramsey, 2009)* and a marine reservoir age of $\Delta R = 140 \pm 35$ years. Additionally, the age model of the multi core was completed with ^{210}Pb/^{137}Cs measurements *(Lloyd et al., 2011)*. Due to gravity coring disturbance and sediment loss, there is a gap of ~100 years between gravity

and multi core. Further details about the age control are given by *Perner et al. (2011)* and *Lloyd et al. (2011)*.

5.3.3. Methods

The analysis of surface sediments and Core 343310 was carried out on freeze-dried and homogenised sediment. The sediment was analysed for total organic carbon (TOC) content and concentrations of IP_{25}, HBI II, HBI III, brassicasterol, dinosterol, β-sitosterol and campesterol (Table 5.1).

Compound	Short Name	Source	Reference
2,6,10,14-tetramethyl-7-(3-methylpent-4-enyl)pentadecane	IP_{25}	Sea ice diatoms; *Pleurosigma stuxbergii var. rhomboides*; *Haslea crucigeroides* (and/or *Haslea spicula*); *Haslea kjellmanii*.	Belt et al., 2007, Brown et al., 2014
2,10,14-Trimethyl-6-enyl-7-(3-methylpent-1-enyl)pentadecene	HBI II	Uncertain	Barrick et al., 1980; Yruela et al., 1990; Summons et al., 1993; Johns et al., 1999; Vare et al., 2009, Massé et al., 2011; He et al., 2016
(9Z)-2,6,10,14-Tetramethyl-7-(3-methylpent-4-enyliden)pentadeca-9-en	HBI III	polar and sub-polar marine diatoms, i.e., *Rhizosolenia*	Belt et al., 2000, 2017
24-methylcholesta-5, 22E-dien-3β-ol	Brassicasterol	Marine and freshwater phytoplankton	Nichols et al., 1984; Yunker et al., 1995, Belt et al., 2013
4 α, 23, 24 trimethyl-5α-cholest-22E-en- 3β -ol	Dinosterol	Marine and freshwater phytoplankton (dinoflagellates)	Nichols et al., 1984; Volkman, 1986; Volkman et al., 1993
24-ethylcholest-5-en-3β-ol	β-sitosterol	Predominantly terrestrial plants	Huang & Meinschein, 1979; Volkman et al., 1993; Jaffe et al., 1995, Bianchi, 2007
24-methylcholest-5en-3β-ol	Campesterol	Predominantly terrestrial plants	Huang & Meinschein, 1979; Volkman et al., 1993; Jaffe et al., 1995, Bianchi, 2007

Tab 5.1 Chemical compounds used in this study.

Homogenised subsamples (0.1 g) were analysed for TOC content with a carbon-sulphur determinator (ELTRA CS-125).

For surface sediment extraction, the internal standards, 7-HND (7-hexylnonadecane, 0.076 µg/sample) and 9 OHD (9-octylheptadec-8-ene, 11.5 µg/sample) were added prior to extraction. 3-5 g of sediment were extracted with sonication (3x15 min) with dichloromethane:methanol (2:1 vol/vol) as solvent.

For Core 343310, prior to the extraction, two internal standards, 7-HND (7-hexylnonadecane, 0.076 µg/sample) and cholesterol-D_6 (cholest-5-en-3β-ol-D_6, 11 µg/sample), were added for quantification purposes. The samples from Core 343310 were extracted with an Accelerated Solvent Extractor (DIONEX, ASE 200; 100°C, 5 min, 1000 psi). About 3-5 g of sediment was extracted with dichloromethane:methanol (2:1 vol/vol) as solvent.

During the course of this study, the extraction method was changed to sonication for the surface sediment dataset. To confirm the comparability of the results from both methods and to other studies, we extracted material from 20 samples with both methods. The following sample treatment has been identical to the description below. Both extraction methods show very similar results for IP_{25}, HBI II and HBI III (Appendix C1). For specific sterols, i.e., brassicasterol, dinosterol, campesterol and β-sitosterol, we find better extraction results with the ASE method (Appendix C1). This should be kept in mind when comparing absolute concentrations of these sterols and absolute values of P_BIP_{25} and P_DIP_{25} indices.

The extracts of surface sediments and Core 343310 were separated into different fractions by open-column chromatography, with SiO_2 as stationary phase. As solvent *n*-hexane (5 ml) was used for IP_{25}, and ethylacetate:*n*-hexane (20:80 vol/vol; 7 ml) for sterols. The sterol fraction was silylated using 200 µl BSTFA (60°C, 2 h).

Hydrocarbon concentrations were identified with a gas chromatograph Agilent Technologies 7890 GC (30 m HP-1MS column, 0.25 mm I.d. and 0.25 µm film thickness) coupled to an Agilent Technologies 5977 A mass selective detector. Sterol concentrations were identified with a gas chromatograph Agilent Technologies 6850 GC (30 m HP-1MS column, 0.25 mm I.d. and 0.25 µm film thickness) coupled to an Agilent Technologies 5975 A mass selective detector.

Measurement settings and identification of sterols and hydrocarbons (IP_{25}, HBI II, HBI III) were performed as described in *Fahl and Stein (2012)*. The concentrations of all biomarkers have been normalised to the amount of sediment and TOC. As both show nearly the same signal, we only present the data normalised to the amount of TOC referred to as µg/gTOC in the main text. Data normalised to the amount of sediment (µg/gSed) are shown in Appendix C. Instrument stability was controlled by several reruns of external standards several times during one analytical sequence and by replicate analyses for random samples.

The PIP_{25} indices were calculated after *Müller et al. (2011)*, using the following equation:

$$PIP_{25} = IP_{25}/ (IP_{25}+ (\text{phytoplankton marker x } c)) \quad (1)$$

c is a balance factor, i.e., the ratio of mean IP_{25} concentration to mean phytoplankton marker concentration, to counterbalance the higher concentrations of sterols compared to IP_{25}. As open water phytoplankton markers brassicasterol (P_BIP_{25}), dinosterol (P_DIP_{25}) and HBI III ($P_{III}IP_{25}$) were used.

For a statistic analysis of short-term oscillations, a MatLab code was applied to detrend the original data, and the BTuckey function of AnalySeries *(Paillard et al., 1996)* was applied to produce a spectrum of the oscillations (confidence 90%, bandwidth: 0.1).

All data are available on https://doi.pangaea.de/10.1594/PANGAEA.885107.

5.4. Results

Throughout the last 2.2 kyr TOC contents in Core 343310 remain relatively constant, averaging around 2%, with maximum values of 2.6 % and minimum values of 1.6 % (Fig 5.3f). IP_{25} concentrations remain relatively low and constant (0.06-0.1 µg/TOC) until 1.2 kyr BP, followed by a gradual increase towards higher values. Extremely high and variable concentrations are reached around 0.4 kyr BP, with highest concentrations around 0.2 kyr BP (~0.9 µg/gTOC; Fig 5.3e).

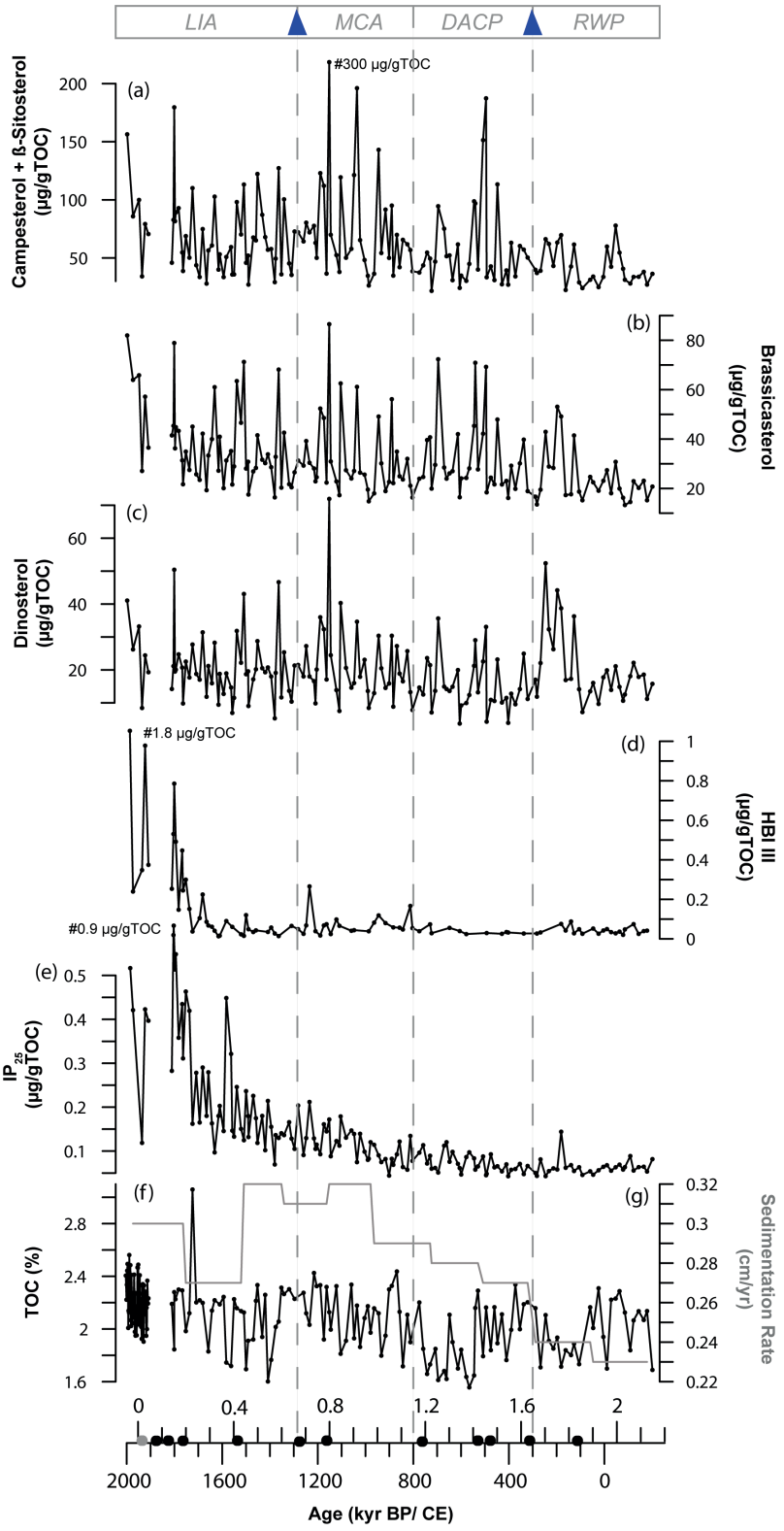

Fig 5. 3 Geochemical results of Core 343310. Biomarker concentrations ***(a)*** campesterol+β-sitosterol, ***(b)*** brassicasterol, ***(c)*** dinosterol, ***(d)*** HBI III, ***(e)*** IP_{25} (all in µg/gTOC), ***(f)*** total organic carbon content (TOC in %) and ***(g)*** sedimentation rates (in cm/yr). All plots are shown versus age before present (kyr BP), an additional age scale shows calendar ages Common Era (CE). Black dots represent AMS ^{14}C ages, grey dots indicate $^{210}Pb/^{137}Cs$ measurements. Abbreviations are as follows: RWP - Roman Warm Period, DACP - Dark Ages Cold Period, MCA - Medieval Climate Anomaly, LIA - Little Ice Age. Blue triangles indicates glacier advances on Greenland *(Levy et al, 2017)*. From the HBI III record, 60 samples were excluded due to high sulphur content.

HBI III concentrations are low (~0.05 µg/gTOC) from 2.2 to 0.2 kyr BP, after which concentrations increase to high concentrations around 1.8 µg/gTOC (Fig 5.3d). Within our record, brassicasterol and dinosterol concentrations remain relatively constant (30 µg/gTOC and 20 µg/gTOC respectively) from 2.2 to 0.1 kyr BP (Figs 5.3b, c). Campesterol+β-sitosterol show lowest concentrations (~50 µg/gTOC) from 2.2 to 1.2 kyr BP, with a pronounced peak around 1.35 kyr BP. From 1.2 to 0.7 kyr BP highest concentrations are observed with maximum values of ~300 µg/gTOC. After 0.7 kyr, concentrations decrease and reach values around 75 µg/gTOC (Fig 5.3a).

During the last 0.1 kyr all biomarker concentrations show an increase, brassicasterol and HBI III reach maximum values in the uppermost sample (80 µg/gTOC and 1.8 µg/gTOC, respectively; Figs 5.3b, d). Superimposed on the general trend, brassicasterol, dinosterol and campesterol+β-sitosterol concentrations show a high variability on a decadal time scale (Figs 5.3a, b, c).

5.5. Discussion

5.5.1. Biomarker distribution in surface sediments and sea ice conditions in the Baffin Bay region

In order to test the applicability of sea ice and open water phytoplankton biomarkers as well as the PIP_{25} indices in the paleorecord, we compare our results from Baffin Bay surface sediments to modern satellite observed sea ice concentrations (Figs 5.4 and 5.5).

Enhanced IP_{25} concentrations are found northwest of the autumn sea ice extent (Fig 5.4a), with highest concentration off Baffin Island, north of 70°, where sea ice remains longest until July and forms first in November (Fig 5.2; *Cavalieri et al., 1996, updated 2015*). The distribution of HBI III in the Baffin Bay shows highest concentrations close to the spring ice edge (Fig 5.4b), which seems to support the assumption of *Belt et al. (2015),* who related high HBI III concentrations to a retreating ice edge. The open water phytoplankton sterols brassicasterol and dinosterol show high concentrations along the autumn ice edge in the Baffin Bay (Figs 5.4c, d). As spring and the southern autumn ice edge are located within a

similar area we assume that open water phytoplankton sterols have their origin in spring and autumn bloom, during which favourable light and nutrient conditions at the ice edge favour phytoplankton growth *(Sakshaug, 2004; Jensen & Christensen, 2014)*.

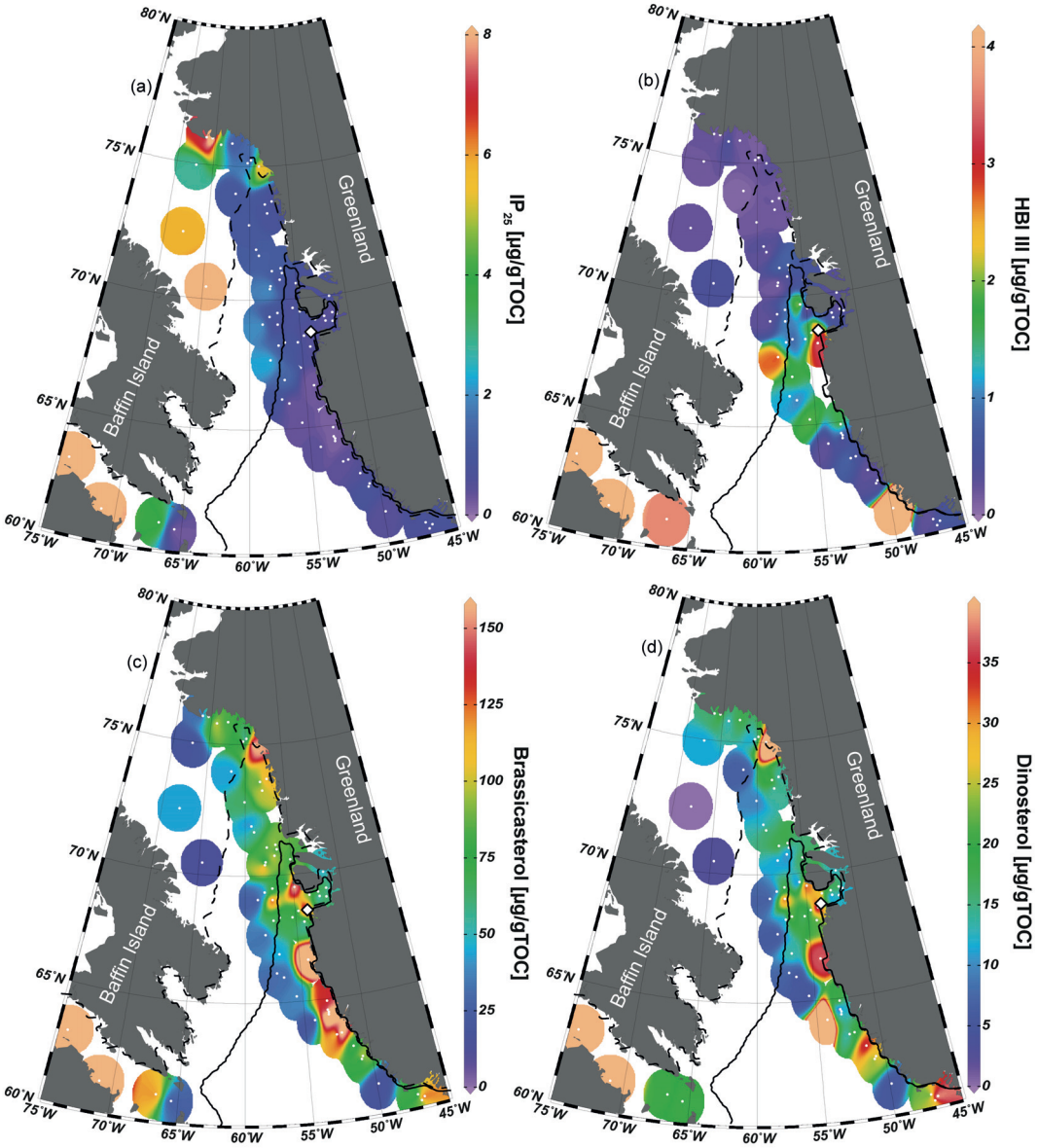

Fig 5. 4 Spatial distribution of biomarker concentrations, ***(a)*** IP_{25}, ***(b)*** HBI III, ***(c)*** brassicasterol and ***(d)*** dinosterol (all in µg/gTOC) in surface sediments from the Baffin Bay and the West Greenland Shelf. The dashed line represents the autumn sea ice edge; the solid black line represents the spring ice edge. White dots indicate sample locations; the white diamond represents the location of Core 343310.

As shown in previous studies (e.g., *Müller et al., 2011; Müller & Stein, 2014; Belt et al., 2015; Stein et al., 2017b)*, the PIP_{25} approach may yield more detailed information about sea ice conditions in the studied area. As the indices P_BIP_{25} and P_DIP_{25} show nearly the same values and distribution patterns (Fig 5.5), we concentrate on the P_DIP_{25} and $P_{III}IP_{25}$ index in the following discussion. All sea ice

indices reflect spring sea ice conditions and show the northwestward extent of sea ice in the Baffin Bay (Figs 5.5b, c). High IP_{25} concentrations and low phytoplankton marker concentration lead to highest P_DIP_{25} and $P_{III}IP_{25}$ values in the western Baffin Bay north of 70°N (Figs 5.5b, c). All sea ice indices show relatively good correlations to modern spring sea ice concentration for the Baffin Bay (Figs 5.5e, f; P_DIP_{25}: r^2=0.46; $P_{III}IP_{25}$: r^2 =0.41). However, the sea ice indices show correlations to modern sea ice concentrations except for the ice free summer season (for details see Appendix C5, C6, C7). This may support our previous assumption that our biomarker record from the Baffin Bay does not only record a spring signal but a mixture of possible spring and autumn, during which favourable light conditions allow phytoplankton blooms *(Sakshaug, 2004; Jensen & Christensen, 2014)*.

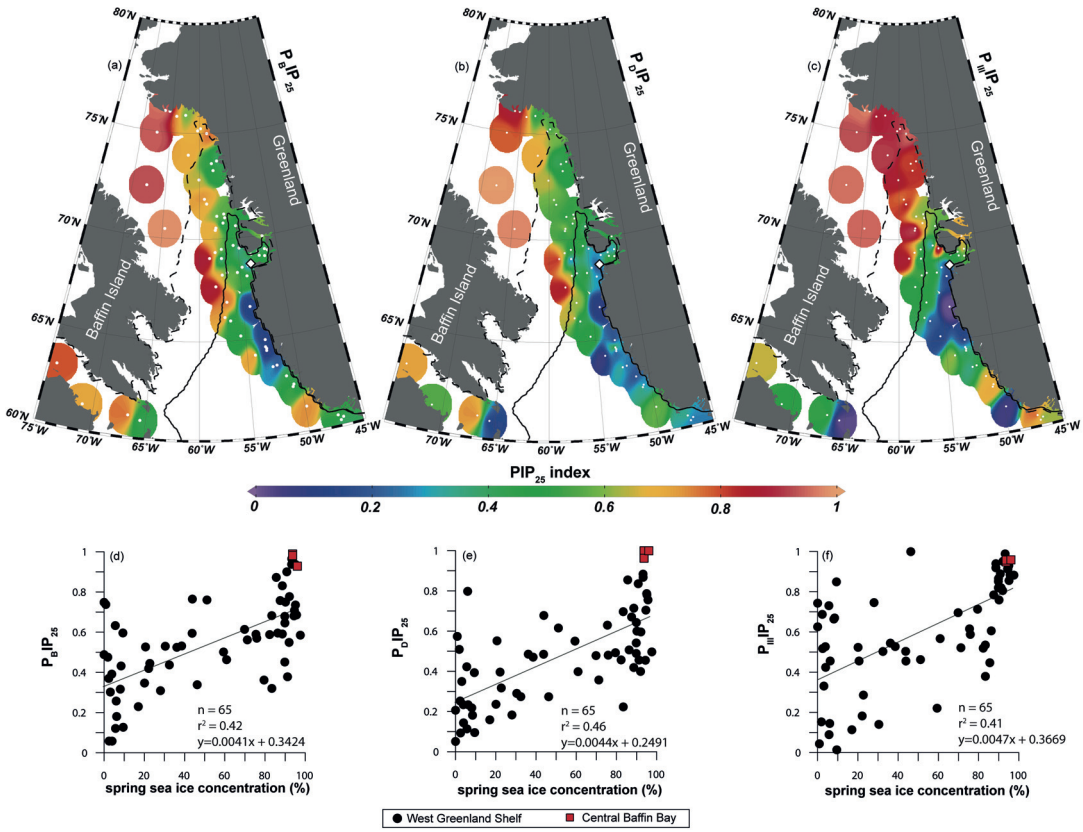

Fig 5. 5 Spatial distribution of sea ice indices ***(a)*** P_BIP_{25}, ***(b)*** P_DIP_{25}, ***(c)*** $P_{III}IP_{25}$ in the Baffin Bay and correlation of ***(d)*** P_BIP_{25}, ***(e)*** P_DIP_{25} and ***(f)*** $P_{III}IP_{25}$ with satellite measured spring (April, May, June) sea ice concentrations (*Cavalieri et al., 1996; updated 2015)*. The dashed black line represents the autumn ice edge; the solid black line represents the spring ice edge. White dots indicate surface sample stations; the white diamond indicates the location of Core 343310.

When comparing biomarker concentration from surface and down core records, higher biomarker concentrations are observed in the surface record, a difference

that might be related to degradation processes (Fig 5.6; e.g., *Fahl & Stein, 2012; Belt & Müller, 2013)*. It has also to be considered that surface sediments display a wide range of concentrations, possibly linked to environmental settings, i.e., sea ice conditions varying strongly from West to East, i.e., highest concentrations are found mainly in sediments north off 75° N (Fig 5.6). Close to the location of Core 343310 at ~68° N, IP_{25} concentrations observed in surface sediments are similar to those determined downcore at our study site (Fig 5.6). This provides further support to our assumption that there is a neglectable degradation influence on the IP_{25} signal. Similarly, dinosterol concentrations also remain in the same range in both surface and paleorecord (Fig 5.6b, e).

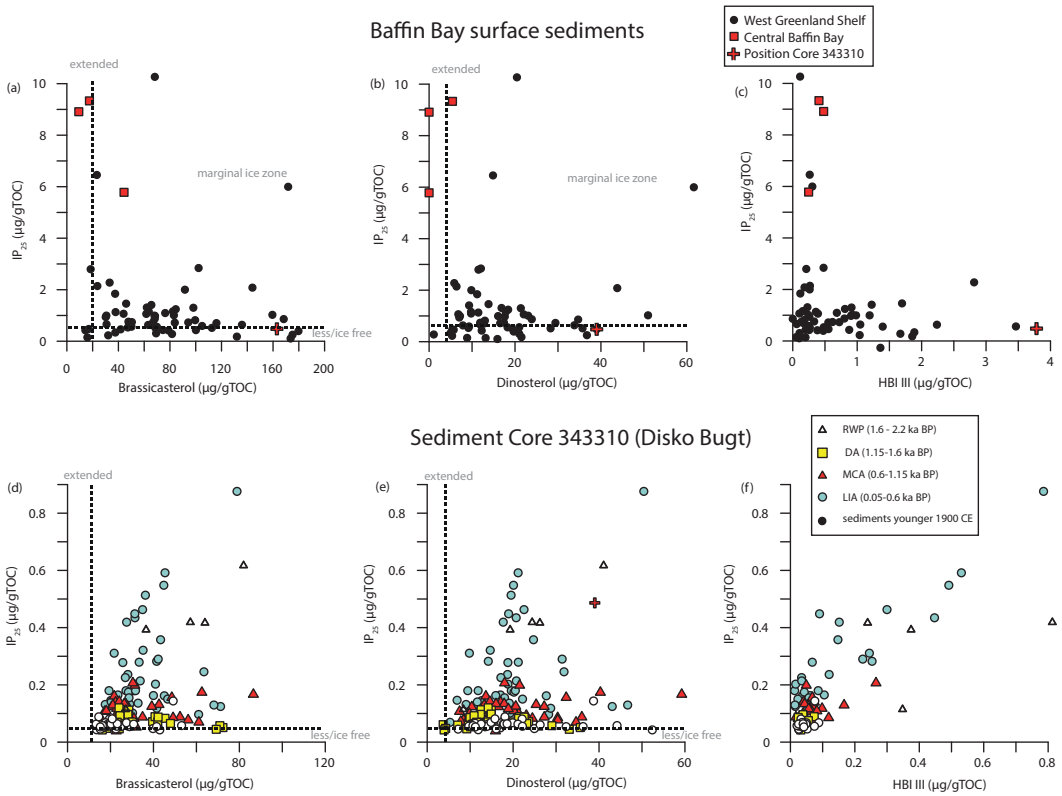

Fig 5. 6 Correlation of IP_{25} with ***(a)*** brassicasterol, ***(b)*** dinosterol and ***(c)*** HBI III (in µg/gTOC) from surface sediments in the Baffin Bay. For ***(a)*** and ***(b)*** different sea ice conditions based on *Müller et al. (2011)* are indicated. And correlation of IP_{25} with ***(d)*** brassicasterol, ***(e)*** dinosterol and ***(f)*** HBI III from Core 343310. Different symbols indicate different time intervals, Roman Warm Period (RWP), Dark Ages Cold Period (DACP), Medieval Climate Anomaly (MCA), and Little Ice Age (LIA).

However, phytoplankton marker concentrations of HBI III and brassicasterol are approximately twice as high in surface sediments from Disko Bugt compared to the paleorecord (Figs 5.6a, c, d, f). With regard to these concentration differences, compound specific degradation should be considered when comparing modern and sediment core concentrations as well as the effect on the PIP_{25} index.

Generally, IP_{25} and the associated PIP_{25} indices seem to be reliable sea ice proxies in the Baffin Bay fortifying its use to reconstruct paleo-sea ice conditions in this region. However, the combination of IP_{25} to phytoplankton biomarkers reveals clear differences in P_DIP_{25} and $P_{III}IP_{25}$ values (Figs 5.5, 5.6). Extremely high $P_{III}IP_{25}$ values in both the surface sediments and the paleorecord, seem partly to overestimate the sea ice conditions, whereas the P_DIP_{25} index shows intermediate values that correlate quite well with the modern situation (Figs 5.5, 5.6). Further, it seems that HBI III shows low sensitivity towards low sea ice concentrations, hence it was not possible to associate specific $P_{III}IP_{25}$ values to specific sea ice conditions in the Baffin Bay (Fig 5.6c). However, for P_DIP_{25} an association, as proposed by *Müller et al. (2011)*, could be attained (Fig 5.6b). Due to its good correlation with modern spring sea ice and being the only index obviously not affected by concentration shifts between surface and paleorecord, we propose that P_DIP_{25} is the most reliable sea ice index for the investigated region and time interval. Therefore, the P_DIP_{25} index will be used for sea ice interpretations in the following discussion.

5.5.2. Sea ice variability in Disko Bugt over the past 2.2 kyr BP

With our biomarker record we provide a direct sea ice reconstruction and are able to specify the interpretation of ecological changes and driving mechanisms of sea ice changes in Disko Bugt over the past two millennia. Furthermore, paleoenvironmental conditions have previously been reconstructed with a variety of microfossil proxies and alkenone geochemistry on Core 343310 *(Perner et al., 2011; Ribeiro et al., 2012; Krawczyk et al., 2013; Moros et al., 2016)*. This wide range of proxy records provides an ideal background to compare microfossil to geochemical proxies derived from the same sediment material.

5.5.2.1. The Roman Warm Period (2.2 – 1.7 kyr BP)

Fairly low sea ice algae productivity is taken as indicative for reduced sea ice conditions at the mouth of Disko Bugt (Fig 5.7c). This is also indicated by relatively low P_DIP_{25} indices (Fig 5.7d). Our interpretation support diatom assemblages from Core 343310 (Fig 5.7f*; Krawczyk et al., 2013*) that indicate lowered ice associated environmental conditions. Peaks in open water phytoplankton sterols, i.e., brassicasterol and dinosterol, around 1.75 kyr BP (Figs 5.7h, i), correlate with high influence of Atlantic derived waters (Fig 5.7n; *Perner*

et al., 2011). This Atlantic Water inflow, has been related to favour subsurface melting of Greenland outlet glaciers causing the observed increased meltwater contribution to the marine environment which has been associated with reduced SSTs (Figs 5.7k, l; *Moros et al., 2016*). High phytoplankton productivity has previously been associated with enhanced autumn mixing caused by increased winds *(Humlum, 1985; Krawczyk et al., 2013)*. Low sea ice cover during such times may have favoured the influence of wind on water column mixing. Further, the high contribution of meltwater may have caused a strong summer stratification *(Moros et al., 2016),* which presumably hampered phytoplankton productivity during summer. Hence, the observed increase in phytoplankton productivity may be associated with the autumn bloom.

This period of reduced sea ice conditions in Disko Bugt correlates with generally warm conditions over the Greenland Ice Sheet (Fig 5.7b; *Kobashi et al., 2017)*. A phase of relative atmospheric warming has been observed in NW Europe, termed Roman Warm Period (1.65 – 1.94 kyr BP; *Ljungqvist, 2010)*. This characteristic warming and reduction of sea ice during the Roman Warm Period has been recorded in several records along the West Greenland coast *(e.g., Seidenkrantz et al., 2008; Nørgaard-Pedersen & Mikkelsen, 2009; Erbs-Hansen et al., 2013; Larsen et al., 2015),* the Canadian Arctic *(Belt et al., 2010)* as well as the East Greenland Shelf and the northern North Atlantic *(Jennings et al., 2002; Risebrobakken, 2003; Moros, et al., 2006b, 2012; Sicre et al., 2008; Werner et al., 2015; Perner et al., 2016, 2018),* which indicates an over-regional signal in the northwestern Hemisphere.

5.5.2.2. The Dark Ages Cold Period (1.7 – 1.2 kyr BP)

Whilst sea ice conditions remain unchanged (Figs 5.7c, d), which is supported by diatom and dinoflagellate records from Core 343310 (Figs 5.7e, f, g; *Ribeiro et al., 2012; Krawczyk et al., 2013*) enhanced sedimentation rates and terrigenous sterol

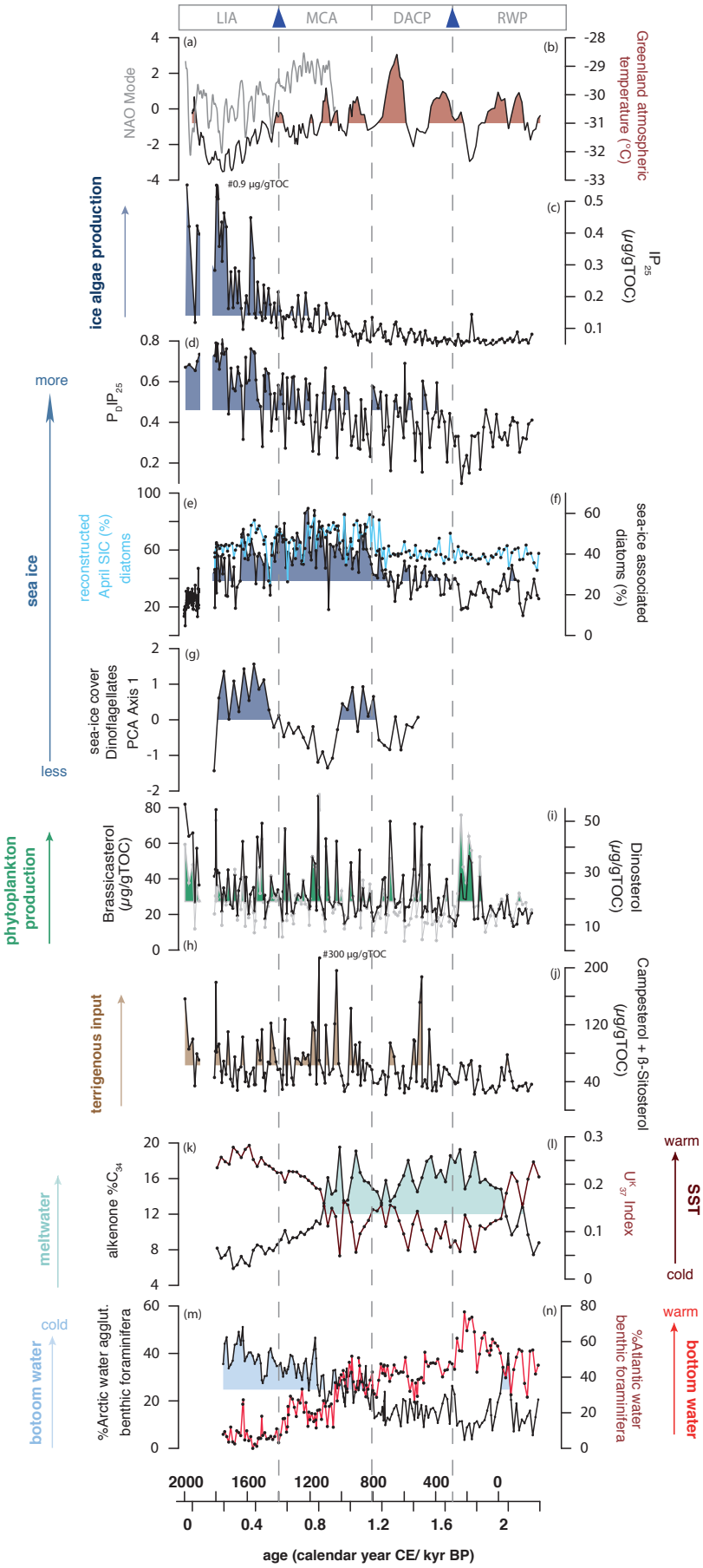

Fig. 5. 7 Comparison of different proxies from Disko Bugt. ***(a)*** Modelled NAO modes *(Trouet et al., 2009)* and ***(b)*** atmospheric temperatures derived from the GISP2 ice core (°C; *Kobashi et al., 2017*). ***(c)*** IP_{25} concentrations (µg/TOC; this study) ***(d)*** sea ice index P_DIP_{25} (this study). ***(e)*** reconstructed April sea ice concentrations (SIC) from diatoms *(%; Krawczyk et al., 2017)*, ***(f)*** abundances of sea ice associated diatoms (%; *Krawczyk et al., 2017) and* ***(g)*** principal component analysis based on dinoflagellates correlating with sea ice (*Ribeiro et al., 2012*). Concentrations of phytoplankton sterols ***(h)*** brassicasterol and ***(i)*** dinosterol and ***(j)*** terrigenous sterol concentrations (all in µg/TOC; this study), ***(k)*** alkenone $C_{37:4}$ (%, *Moros et al., 2016)* and ***(l)*** alkenone index U^K_{37} (*Moros et al., 2016*). ***(m)*** Atlantic water benthic foraminifera and ***(n)*** Arctic water agglutinated benthic foraminifers (both in %; *Perner et al., 2011*). Abbreviations are as follows: RWP - Roman Warm Period, DACP - Dark Ages Cold Period, MCA - Medieval Climate Anomaly, LIA - Little Ice Age. Blue triangles indicates glacier advances on Greenland (*Levy et al, 2017*).

concentrations are perceived during this interval (Fig 5.7j). This seems to correlate with slightly increasing open water phytoplankton productivity (Figs 5.7h, i). A re-advance of the Greenland Ice Sheet (Fig 5.7; *Levy et al., 2017; Schweinsberg et al., 2017)* may have resulted in an increased input of terrigenous material, which favoured open water phytoplankton productivity by enhanced nutrient supply.

The increase of open water primary production and terrigenous input correlates with the NW European Dark Ages Cold Period (DACP, 1.65 – 1.15 kyr BP; *Ljungqvist, 2010*). Several Disko Bugt records characterise the DACP as a phase of surface water cooling and propose an increase in sea ice *(Moros et al., 2006a; Seidenkrantz et al., 2008; Ouellet-Bernier et al., 2014; Sha et al., 2017)*, which has been related to an increased EGC contribution and a relative reduction of IC waters to the WGC *(Perner et al., 2011, 2013)*. It should be noted that these previous findings are based on microfossils, which are only indirectly related to sea ice cover/occurrence. Our direct, biomarker-based sea ice record does not indicate a notable change in seasonal sea ice conditions, instead we record enhanced and highly variable open water phytoplankton productivity during the DACP (Figs 5.7c, d). This may imply that a general cooling of surface waters does not necessarily directly relates to an increase in sea ice cover.

It has been found that winter SSTs are a critical factor for the formation of sea ice in the Baffin Bay area *(Tang et al., 2004)*. Based on our data, we suggest that the DACP was characterised by a strong seasonal temperature gradient and a summer cooling, rather than an overall cooling. We infer that cooler SSTs prevailed during the main open water phytoplankton bloom season (late spring – autumn) and relatively low seasonal sea ice conditions. Such a scenario may point towards the reduction of atmospheric summer temperatures due to volcanic eruptions, as proposed by *Kobashi et al., (2017)*. Further, a destabilizing effect of the advancing Greenland Ice Sheet, by adding pressure and causing more break-up of sea ice *(Mugford and Dowdeswell, 2010)* should also be considered as a mechanism contributing to the observed reduced seasonal sea ice concentrations.

5.5.2.3. The Medieval Climate Anomaly (1.2 – 0.7 kyr BP)

A gradual increase in sea ice algae productivity and sea ice concentration (Figs 5.7c, d) is taken as indicative for a minor increase in seasonal sea ice conditions, conceivably related to a temporal extent of 'Westice', which may have remained until mid-spring at Disko Bugt, causing a longer period of favourable light conditions and sea ice occurrence for sea ice algae bloom. HBI III concentrations remain at very low levels (Fig 5.3d). Such low levels may indicate that a prolonged, high productivity ice edge was not established (*Belt et al., 2015*).

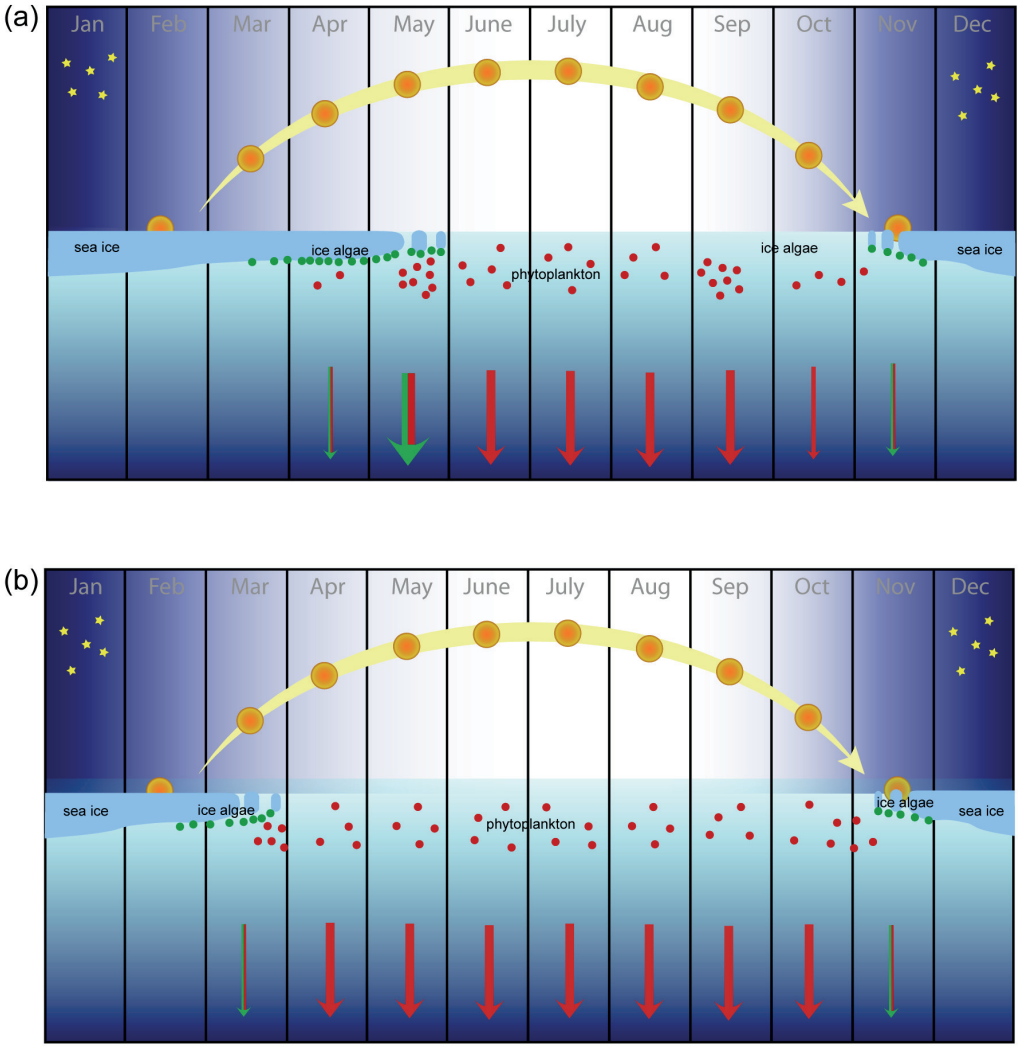

Fig 5. 8 Schematic illustration of seasonal light conditions, bloom development and downward export of sea ice algae derived IP_{25} (green arrows) and open water phytoplankton sterols (red arrows) in Disko Bugt during the past 2.2 kyr BP. ***(a)*** Conditions during the last ~ 0.3 kyr (0.2 yrs BP to present) with the ice edge reaching Disko Bugt in late spring with high daylight hours favouring ice algae productivity. And ***(b)*** conditions before 0.3 years BP (2.2 – 0.3 yrs BP), with the maximum sea ice extent in early spring with low light availability, hampering ice algae productivity. The width of the arrows indicates amount of deposited specific biomarkers. Modified from *Wassmann et al. (2011)*.

Open water phytoplankton productivity remains relatively high and variable (Figs 5.7h, i), which may be indicative for unstable environmental conditions. This instability may be linked to a strong summer stratification caused by strong meltwater inflow and low surface SSTs during summer (Figs 5.7k, l; *Moros et al., 2016*) and wind driven mixing during autumn favouring the upwelling of nutrient rich waters *(Humlum, 1985; Krawczyk et al., 2013)*. These highly variable seasonal environmental conditions may have caused the inconsistent signals reflected in dinoflagellate and diatom records from Core 343310 (Figs 5.7 e, f, g; *Ribeiro et al., 2012; Krawczyk et al., 2013)*.

This phase correlates with an atmospheric warming over Greenland (Fig 5.7b; *Kobashi et al., 2017*) and encompasses the European Medieval Climate Anomaly (MCA; 1.0 – 0.75 kyr BP; *Lamb, 1977*). Nevertheless, we do not find evidence for a reduction of sea ice following the atmospheric warming during the MCA. At Disko Bugt, such a warming has only been recorded in bottom water proxies i.e., benthic foraminifera (Figs 7m, n; *Perner et al., 2011*) whereas surface proxies, such as dinoflagellates and diatoms, support a cooling trend (Fig 5.7e. f, g; e.g., *Moros et al., 2006a; Seidenkrantz et al., 2008; Ribeiro et al., 2012; Krawczyk et al., 2013*). A temporal extent of sea ice during the MCA, indicated in our biomarker data, may be linked to a general change in oceanography, i.e., an intensification of Arctic outflow via the EGC and Baffin Island Current (BIC), transporting colder, polar water masses to the area.

Evidence for a strengthening of the EGC and a southward migration of the subarctic front as well as a reduction in SSTs during this time has been found at Reykjanes Ridge *(Solignac et al., 2004; Perner et al., 2018)*. Further, a lack of surface warming during the MCA in the Labrador Sea has been attributed to a constant strong Labrador Current (LC) along the Canadian coast over the past 1.6 kyr *(Keigwin et al., 2003)*. The LC originates from the BIC and WGC, which may point towards a strong Arctic contribution from both currents. The combination of enhanced cold Arctic water inflow from the Northwest and the South to the Baffin Bay may have caused the south-eastward expansion of 'Westice' *(Buch, 2000)*. Sea ice reconstruction from the Canadian Arctic, located at the gateway from the Arctic Ocean to the Baffin Bay, support a gradual increase of sea ice algae productivity during this phase *(Belt et al., 2010)*.

5.5.2.4. The Little Ice Age (0.7 – 0.2 kyr BP)

Strongly increasing sea ice algae production (Fig 5.7c) may point towards the presence of an ice edge at or close to our core site during spring, as it is also observed today (Fig 5.8b). Relatively high phytoplankton productivity and HBI III concentrations (Figs 5.3d; 5.7h,i) may represent the high productivity linked to an ice edge *(Sakshaug, 2004)*. Dinoflagellate data from Core 343310 are in line with this interpretation (Fig 5.7g; *Ribeiro et al., 2012)*. A relative reduction of meltwater inflow and a subsequent increase SSTs (due to lower inflow if cold meltwater and the subsequent reduction in stratification) since 0.7 kyr BP (Figs 5.7k, l; *Moros et al., 2016*) has been associated with a decrease of air temperatures over Greenland (Fig 5.7b; *Kobashi et al., 2017*) and advances of the Greenland Ice Sheet and its outlet glaciers, e.g., Jakobshavn Isbræ (Fig 5.7; *Lloyd et al., 2011; Levy et al., 2017)*. This atmospheric cooling likely favoured our reconstructed maximum sea ice concentrations (Fig 5.7d) and continuously high phytoplankton productivity (Figs 5.7h, i) as well as the presence of an ice edge until late spring in the Disko Bugt area (Fig 5.8a). The strongest increase in sea ice algae productivity and sea ice concentration (Figs 5.7c, d) correlates with the maximum of the Little Ice Age *(*LIA*; Ljungqvist, 2010)* around 0.2 kyr BP. Such a cooling and increase in sea ice conditions has been recorded along the West Greenland coast *(Jensen et al., 2004; Roncaglia & Kuijpers, 2004; Sha et al., 2012; Cormier et al., 2016)*, North Iceland *(Jiang et al., 2005; Massé et al., 2008; Cabedo-Sanz et al., 2016)* and the Canadian Arctic Archipelago *(Vare et al., 2009; Belt et al., 2010)* and seems to represent a widespread climatic phenomenon.

The extend of sea ice during the LIA may be related to a general increase in subsurface EGC contribution to the WGC *(Perner et al., 2011)*, causing a general cooling in the area. Further, a dominant westward Transpolar Drift, generating a strong cold LC inflow into the Baffin Bay *(Keigwin et al., 2003)*, may have favoured the temporal expansion of 'Westice'. The onset of the LIA has been associated with shifts in the NAO (Figs 5.7a; e.g., *Trouet et al., 2009*) and an increase in volcanic activity, which may have caused a short time reduction in atmospheric temperature, which itself may set off a sea ice feedback *(Kobashi et al., 2017)*.

5.5.2.5. The last century

A reduction in sea ice concentrations and a strong increase in phytoplankton productivity are observed after 0.2 kyr BP (Figs 5.7c, d, h, i). The youngest samples seem to indicate a strong increase of ice algae and phytoplankton productivity (Figs 5.7c, d, h, i), which are also observed in surface samples (Fig 5.6). Hence, we cannot exclude that lower phytoplankton biomarker concentrations in the downcore record were affected by diagenetic processes. However, findings from microfossil records from Core 343310 support a general reduction in sea ice during the last 0.2 kyr *(Ribeiro et al., 2012; Krawczyk et al., 2013)* and are in line with a general increase in atmospheric temperatures observed at the coast of Disko Bugt, e.g., in Ilulisaat *(Vinther et al., 2006)*. This warming has been associated with a decrease in mean annual sea ice cover since the 1990s *(Nielsen et al., 2001)*. Due to the low sample resolution in our biomarker record a detailed interpretation is not possible for this time period.

5.5.3. Cyclicity and driving mechanisms of sea ice conditions in Disko Bugt

Microfossil records from Disko Bugt and West Greenland sites found in parts of the late Holocene an antiphase correlation to the North Atlantic Oscillation (NAO) modes observed in the North Atlantic, i.e., a cooling during the positive NAO mode associated with the MCA and a warming during the negative NAO mode correlating with the LIA (Figs 5.7a, e, f, g; *Seidenkrantz et al., 2008; Krawczyk et al., 2010, 2013; Ribeiro et al., 2012)*. Our IP_{25} sea ice record does not reflect such an anti-correlation in sea ice variability (Figs 5.7a, c, d). It rather reflects a general increase in temporal sea ice extend following the decreasing solar insolation associated with the Neoglacial cooling, which culminates in the Little Ice Age. These different patterns may be caused due to the relatively short sea ice season that is observed over the past 2.2 kyr at Disko Bugt; hence sea ice may only record a short season whereas microfossils such as dinoflagellates, diatoms and foraminifera may represent a longer period and are able to record marked hydrographic variability *(Krawczyk et al., 2013)*. It should be noted that NAO reconstructions are still subject to discussion and the exact timing of late Holocene shifts in this atmospheric system are debated *(Trouet et al., 2009; Olsen et al., 2012; Ortega et al., 2015; Faust et al., 2016)*. Sea ice at the mouth of Disko Bugt seems to be mostly affected by over regional solar forcing. Open water

phytoplankton productivity and terrigenous sterols, on the other hand, seems to reflect short scale changes, that may point to specific mechanisms affecting environmental conditions favourable/unfavourable for open water phytoplankton growth (Fig 5.9).

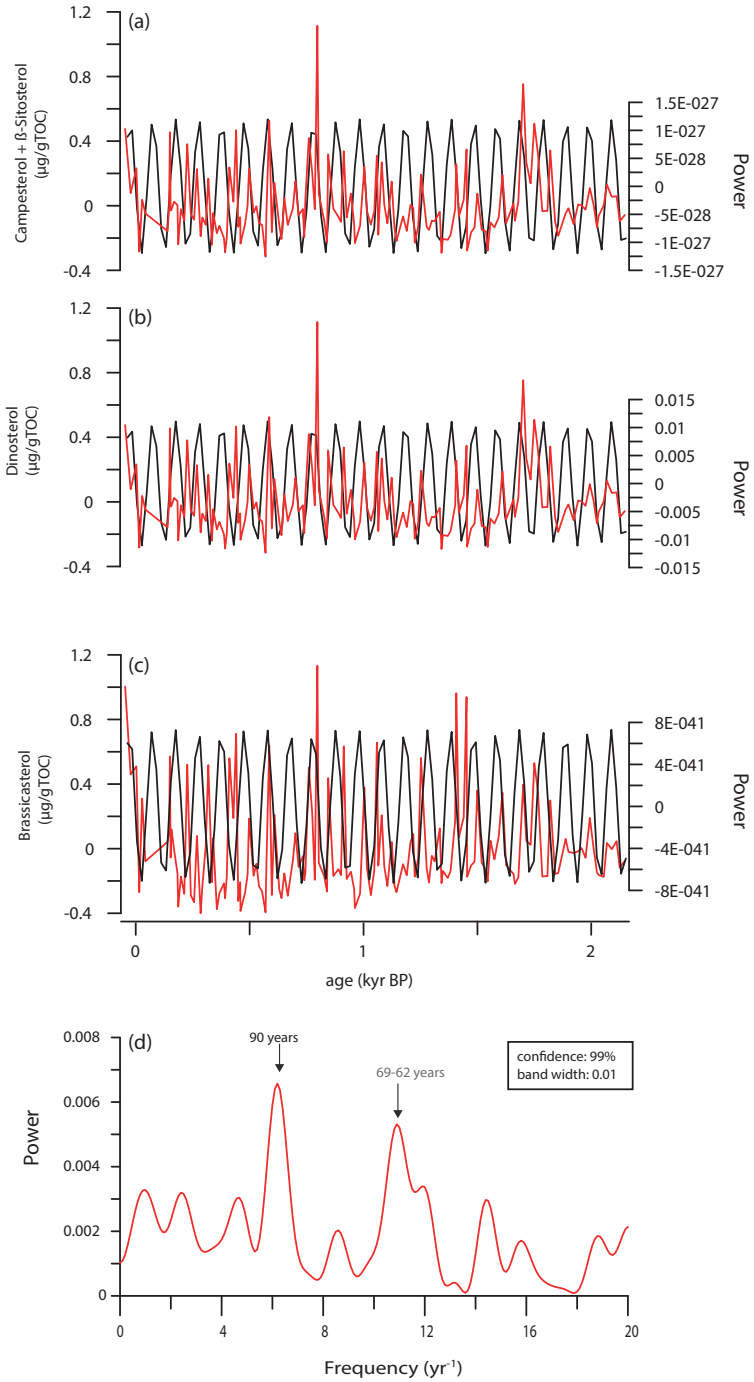

Fig 5. 9 Comparison of the band-pass filtered 69 years cycle (black) and the linear detrended ***(a)*** campesterol+β-sitosterol, ***(b)*** dinosterol and ***(c)*** brassicasterol records (red) (confidence 99%) of Core 343310 over the past 2.2 kyr. ***(d)*** Spectrum of spectral analysis, the frequency of the 69-62 and 90 year cycles are indicated by black arrows.

We find evidence for the sensitivity of open water phytoplankton productivity and terrigenous input into Disko Bugt to oceanic circulation patterns by spectral analysis (Fig 5.9). We observe a 63 to 90-year cycle in phytoplankton and terrigenous biomarker concentrations during the last 2.2 kyr (90% confidence; Fig 5.9). This cycle has previously been associated with the Atlantic Multidecadal Oscillation (AMO) frequency of ~50 to 70 years *(Knudsen et al., 2011)*.

Remarkably, a study focussing on the driving mechanisms of sea ice off West Greenland identified a very similar cyclicity in a sea ice diatom record, i.e., 50 to 70 years *(Sha et al., 2016)*. In our IP_{25} sea ice record we could not find evidence for such cyclicity. We assume that sea ice diatoms used by *Sha et al., (2016)* are influenced by similar mechanisms as phytoplankton sterols in our record. AMO variability has been associated to solar activity *(Knudsen et al., 2011)*, a change in incoming radiation may influence sea ice and the Greenland Ice Sheet *(Ruzmaikin et al., 2004)* and consequently will affect the freshwater inflow *(Schmith and Hansen, 2003)* and nutrient availability to the area. A self-amplifying system of a solar triggered Arctic sea ice melt *(Ruzmaikin et al., 2004)*, increasing freshwater inflow towards the North Atlantic causing a reduction in subpolar gyre activity and AMO *(Holland, et al., 2001; Schmith & Hansen, 2003)* as discribed by *Sha et al. (2016)* may cause distinct changes in WGC composition and meltwater input from the Greenland Ice Sheet that affects phytoplankton blooms.

However, others found evidence for volcanic eruptions being the main trigger for the aforementioned sea ice feedback mechanism *(*e.g., *Miller et al., 2012; Sigl et al., 2015; Kobashi et al., 2017)* that led to cold event, such as the LIA, during the late Holocene. It remains uncertain which, or if there is a single mechanism that drives sea ice extent on the Northern Hemisphere. It seems likely that a combination of external and internal forcing's and feedbacks, that may differ for each time interval, causes changes in atmospheric and oceanic systems that may lead to an expansion/reduction of sea ice extent during the late Holocene in the Baffin Bay *(cf. Kobashi et al., 2017)*.

6.5.4. Environmental reconstructions: biomarkers vs. microfossils

For Core 343310, a great variety of proxies have been compiled from the same sample set (for an overview see *Moros et al., 2016*), which provides ideal conditions for a direct proxy-to-proxy comparison that allows to gain further information about the correlation between microfossils and geochemical sea ice proxies and environmental factors controlling the signal formation (Fig 5.10).

Regarding sea ice, we find a relatively strong negative correlation of IP_{25} and the Atlantic/IC benthic foraminifera group (r^2 = -0.54; Fig 5.10a). With respect to the regional oceanography of the Baffin Bay, which is controlled by the composition of the WGC, higher contributions of IC derived Atlantic waters seem to occur during phases of reduced sea ice algae production, representing less severe seasonal sea ice conditions. A stronger IC/weaker EGC contribution to the WGC off West Greenland has been associated with atmospheric and oceanic warming *(Seidenkrantz et al., 2008; Perner et al., 2011, 2013)*.

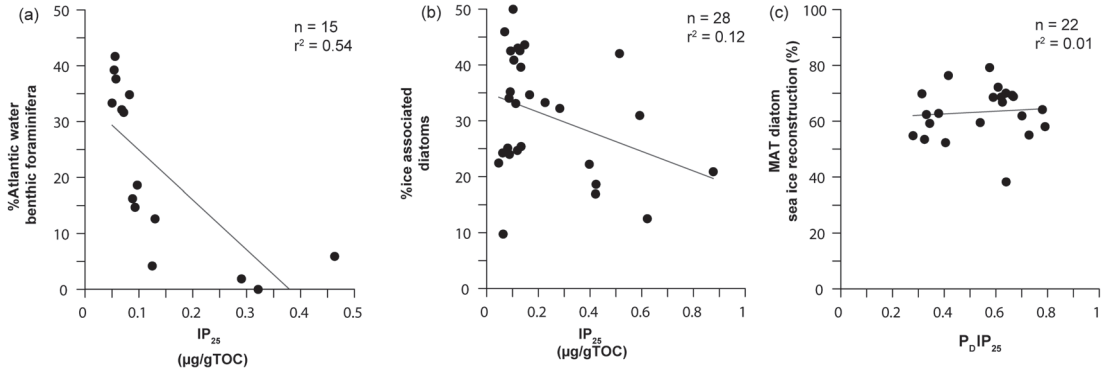

Fig 5. 10 Correlations of specific biomarkers and microfossil proxies. ***(a)*** Atlantic water benthic foraminifera (%; *Perner et al., 2011*) versus IP_{25} (µg/TOC). ***(b)*** sea ice associated diatoms (%; *Krawczyk et al., 2013*) versus IP_{25} (µg/TOC). ***(c)*** MAT diatom sea ice reconstruction (%; *Krawczyk et al., 2017*) versus P_DIP_{25}.

Sea ice diatoms have been used as a common sea ice proxy along West Greenland *(e.g., Jensen et al., 2004; Moros et al., 2006a; Krawczyk et al., 2010, 2013)*. Recently, *Krawczyk et al. (2017)* found a correlation of sea ice associated diatoms in surface sediment, collected along the West Greenland shelf, to satellite derived April sea ice conditions. In our downcore record, IP_{25} and sea ice associated diatoms do not show a direct correlation (r^2 = 0.12; Fig 5.10b). In previous studies, the diatoms included in the sea ice associated assemblage were only indirectly connected to the ice habitat, mainly by environmental conditions found close to sea

ice, e.g., meltwater, low SSTs *(Krawczyk et al., 2013)* whereas IP_{25} is produced by diatoms living inside the sea ice *(Brown et al., 2014)*. These different habitats and different factors controlling the abundance of the specific diatoms may cause the different signals recorded in the different proxies.

No correlation between P_DIP_{25} and the MAT diatoms sea ice reconstruction (Fig 5.10c; $r^2 = 0.01$; *Krawczyk et al., 2017*) could be found. Hence, we assume this may be caused by different environmental factors controlling sea ice associated and IP_{25} producing diatoms. It may be possible that sea ice associated diatoms and IP_{25} producers reflect different seasonal signals or underlie different deposition patterns, e.g., one species living mostly under the ice and another inside the ice.
Besides ecological factors, issues such as selective and no uniform depositional and post-depositional degradation of biomarkers *(Belt & Müller, 2013)* and species-selective dissolution/preservation as well as under-representation of sea ice species affecting the diatom assemblages *(Leventer, 1998)* have to be respected when comparing biomarkers, i.e., IP_{25}, and diatoms.

5.6. Conclusions

Surface sediment concentrations of specific biomarkers show a distinct spatial distribution in the Baffin Bay that can be related to modern sea ice concentrations during spring and autumn. Further, PIP_{25} indices correlate well with observed sea ice concentration supporting that these proxies are reliable tools for paleo-sea ice reconstructions.
Late Holocene sea ice conditions, open water phytoplankton productivity and terrigenous input in the southwest Disko Bugt area were reconstructed with a biomarker approach providing direct insights into sea ice variability and its driving mechanisms. Further, a multi-proxy comparison indicates different mechanisms behind phytoplankton and sea ice algae blooms.

Our results support the P_DIP_{25} index as a direct sea ice proxy, whereas other microfossils, e.g., diatoms are only indirectly associated to sea ice and strongly related to meltwater, atmospheric temperatures and nutrient availability.

We find that the Disko Bugt area was influenced by seasonal sea over the last 2.2

kyr BP. The overall sea ice trend indicates a development from a reduced sea ice cover during early spring, with sea ice algae productivity hampered by light availability to a gradual temporal extend of the sea ice cover from 1.2 kyr BP onwards. This temporal sea ice extend follows decreasing Northern Hemisphere atmospheric temperatures, culminating in the Little Ice Age around 0.2 kyr. We assume that modern conditions, with the presence of a stable ice edge at Disko Bugt, established around that time. A strong persistent Baffin Island Current and East Greenland Current may have contributed to this gradual increase in 'Westice' extent.

Sea ice seems to follow the overall longer-term atmospheric cooling trend in the Northern Hemisphere. Superimposed on longer-term trends, phytoplankton productivity and terrigenous input show a strong short-term variability, indicating a rapid response to water mass properties. These oscillations may be connected to the Atlantic Multidecadal Oscillation and to solar activity.

Acknowledgements

Financial support for this study was provided by the Deutsche Forschungsgemeinschaft through 'ArcTrain' (GRK 1904). We wish to thank the captain, crew and science party of the *R/V Maria S. Merian* expeditions MSM 05/03, 44 and 46, of the annual survey 2014 with the *R/V Paamiut* and of the 2008028 expedition with *CCGS Hudson*. We thank Diana W. Krawzcyk (Greenland Climate Research Centre, Greenland Institute of Natural Resources, Nuuk, Greenland) for providing surface sample from the *R/V Paamiut* expedition, and Walter Luttmer for laboratory support. Thanks to Simon Belt and colleagues (Biogeochemistry Research Centre, University of Plymouth) for providing the internal standard for IP_{25} analysis. Kerstin Perner has been funded through the DFG grant PE2071/2-2.

6. Conclusions and Outlook

6.1. Conclusions

Within in this thesis, new insights into the applicability of the biomarker approach are presented. Further, new vital information about late Holocene environmental changes, with special regard to sea ice variability on the East and West Greenland shelves are provided.

The new surface biomarker dataset and its combination with published surface records confirms the over regional applicability of the sea ice biomarker IP_{25} and the phytoplankton sterols brassicasterol and dinosterol. HBI III distribution could only be related to the marginal ice zone in specific regions and not on an over regional scale. In regard to the sea ice index PIP_{25}, a good correlation to modern sea ice extent on regional scales could be confirmed for seasonal sea ice covered regions of the Baffin Bay and Barents Sea. In other regions, characterized by more complex sea ice conditions, e.g., the Russian marginal seas, the direct correlation of PIP_{25} values to sea ice concentrations remains difficult.

A comparison of MAT dinocyst and biomarker sea ice reconstructions confirmed that both methods produce reliable results for regions with seasonal sea ice cover of the Baffin Bay, the Fram Strait and the Barents Sea. Both methods produce different results for regions with more complex sea ice conditions, such as the Russian marginal seas. In a regional comparison in the Baffin Bay, the PIP_{25} indices and preliminary MAT dinocyst reconstructions showed positive correlations to modern sea ice concentrations, with best results for the $P_{III}IP_{25}$ index. Further, sea ice associated diatom assemblages provide even better correlations to modern sea ice conditions in the Baffin Bay, however, the over regional application remains unclear.

The late Holocene sea ice studies from the East and West Greenland shelves revealed distinct changes in sea ice over the past 5.2 and 2.2 kyr BP, respectively, and provide important information about the late Holocene sea ice development.

On the East Greenland Shelf, sea ice conditions do not directly reflect the general Neoglacial cooling trend following the decreasing solar insolation. The core location seems highly sensitive to changes in the glacier/fjord system and sea ice export from

the Arctic Ocean. Sea ice export from the Arctic Ocean to the East Greenland Shelf seems to be closely related to changes oceanic and atmospheric circulation changes, especially for the last 2.5 kyr BP, and shows a high natural variability. Two phases of extended sea ice concentrations from 4.7 to 2.2 kyr BP and 1.3 kyr BP to present are observed and correlate with the Dark Ages Cold Period and Little Ice Age respectively. They were preceded by a phase of reduced sea ice conditions from 5.2 to 4.7 kyr BP, which correlates with the Roman Warm Period, and interrupted by a phase of reduced sea ice concentrations between 2.2 and 1.3 kyr BP, correlating with the Medieval Climate Anomaly. These shifts could be related to shifts in atmospheric circulation. The transitions between those events occurred rather fast and display a close connection of sea ice changes on the East Greenland Shelf and the Northern Hemisphere climate. These findings are crucial for our understanding of the recent reduction of Arctic sea ice. A spectral analysis revealed a cyclicity of 73-74 years in sea ice algae and phytoplankton productivity over the last 1.2 kyr, which is associated with Atlantic Multidecadal Oscillation variability.

Concerning the West Greenland Shelf, evidence was found that this region was influenced by seasonal sea ice over the last 2.2 kyr BP. The overall sea ice trend indicates a gradual development from a reduced sea ice cover during early spring, with sea ice algae production hampered by light availability to an extent of the sea ice cover from 1.2 kyr BP onwards. This temporal sea ice extent follows decreasing Northern Hemisphere atmospheric temperatures, culminating in the Little Ice Age around 0.2 kyr. We assume that modern conditions, with the presence of a stable ice edge at Disko Bugt, established around that time. A strong persistent Baffin Island Current and West Greenland Current may have contributed to this gradual increase in ‘Westice’ extent.

Sea ice on the West Greenland Shelf seems to follow the overall longer-term atmospheric cooling trend in the Northern Hemisphere. Superimposed on longer-term trends, phytoplankton productivity and terrigenous input show a strong short-term variability, indicating a rapid response to water mass properties. These oscillations may be connected to the Atlantic Multidecadal Oscillation and to solar activity.

6.2. Outlook

The surface biomarker record presented in this thesis provides important information about the distribution of the sea ice biomarker IP_{25}, specific phytoplankton biomarkers (i.e., brassicasterol, dinosterol and HBI III) and the application of the sea ice index PIP_{25} in surface sediments. However, the application of the biomarker approach for sea ice reconstructions and qualitative sea ice reconstructions may be improved by extending the surface sediment database. The biomarker surface dataset is missing crucial areas, i.e., North of Greenland, the Canadian Arctic Archipelago, Beaufort Sea and in the Nordic Seas. Specifically in regard to the phytoplankton markers dinosterol and HBI III the surface database needs to be expanded in specific areas, e.g., Barents Sea and the East Greenland Shelf to get an estimate about its applicability as a phytoplankton marker for the marginal ice zone *(Belt et al., 2015)*.
To further improve the understanding of the PIP_{25} indices and their relationship with sea ice concentrations, future surface studies should include all three sea ice indices, i.e., P_BIP_{25}, P_DIP_{25}, $P_{III}IP_{25}$.

The mid- to late Holocene biomarker paleorecords from the East and West Greenland shelves reveal new insights to small-scale variability in sea ice distribution around Greenland.
More high resolution records covering this time interval will improve the understanding of sea ice changes and their driving mechanisms, especially in regard to over regional atmospheric and oceanic oscillations, i.e., NAO and AMO. On the East Greenland Shelf sediment cores from the North and the East may provide records less affected by the adjacent fjords and Greenland Ice Sheet and give further insight to the sensitivity of sea ice in this area and EGC flow path and intensity. In the Baffin Bay, sediment cores from the Canadian Shelf, underlying the Baffin Island Current, reflecting the Arctic outflow through the Canadian Arctic Archipelago will provide important information regarding the variability and sensitivity of the 'Westice' extent. Further, sediment cores from the South and North on the West Greenland Shelf will provide useful insight to sea ice changes and interactions with the Greenland Ice Sheet.

The comparison of different sea ice proxies in modern and paleorecord showed that different sea ice proxies, i.e., biomarker, dinocysts and diatoms, often result in

different reconstructed sea ice conditions. In order to gain a better understanding of past sea ice conditions, it seems worthwhile to increase the knowledge of the signals preserved in the different sea ice proxies. A targeted sampling of sea ice, the water column and surface sediments in key areas during the different seasons and the analysis of phytoplankton and zooplankton assemblages may increase the knowledge on the ecology and environmental (seasonal) signals recorded in the different sea ice proxies. An enhanced precession of sea ice reconstructions may provide more accurate information about (seasonal) sea ice variability for climate models and increase the quality of future sea ice predictions.

7. References

Aagaard-Sørensen, S., Husum, K., Hald, M., Knies, J., 2010. Paleoceanographic development in the SW Barents Sea during the Late Weichselian–Early Holocene transition. Quat. Sci. Rev. 29, 3442–3456. doi:https://doi.org/10.1016/j.quascirev.2010.08.014

Aagaard, K., Carmack, E.C., 1989. The Role of Sea Ice and Other Fresh Water in the Arctic Circulation. J. Geophys. Res. 94.

Aagaard, K., Coachman, L.,1968b. The East Greenland Current North of Denmark Strait: Part II. Arctic 21, 267–290.

Aagaard, K., Coachman, L., 1968a. The East Greenland Current north of Denmark Strait: Part I. Arctic 21, 181–200.

Aagaard, K., Swift, J.H., Carmack, E.C., 1985. Thermohaline circulation in the Arctic Mediterranean Seas. J. Geophys. Res. 90, 4833. doi:10.1029/JC090iC03p04833

Alley, R.B., Andrews, J.T., Brigham-Grette, J., Clarke, G.K.C., Cuffey, K.M., Fitzpatrick, J.J., Funder, S., Marshall, S.J., Miller, G.H., Mitrovica, J.X., Muhs, D.R., Otto-Bliesner, B.L., Polyak, L., White, J.W.C., 2010. History of the Greenland Ice Sheet: paleoclimatic insights. Quat. Sci. Rev. 29, 1728–1756. doi:10.1016/j.quascirev.2010.02.007

Alley, R.B., Mayewski, P.A., Sowers, T., Stuiver, M., Taylor, K.C., Clark, P.U., 1997. Holocene climatic instability: A prominent, widespread event 8200 yr ago. Geology. doi:10.1130/0091-7613(1997)025<0483:HCIAPW>2.3.CO;2

Alonso-Garcia, M., Andrews, J.T., Belt, S.T., Cabedo-Sanz, P., Darby, D., Jaeger, J., 2013. A comparison between multiproxy and historical data (AD 1990–1840) of drift ice conditions on the East Greenland shelf (~66°N). The Holocene 23, 1672–1683. doi:10.1177/0959683613505343

Andersen, C., Koç, N., Jennings, A., Andrews, J.T., 2004a. Nonuniform response of the major surface currents in the Nordic Seas to insolation forcing: Implications for the Holocene climate variability. Paleoceanography. doi:10.1029/2002PA000873

Andersen, C., Koç, N., Moros, M., 2004b. A highly unstable Holocene climate in the subpolar North Atlantic: Evidence from diatoms. Quat. Sci. Rev. 23, 2155–2166. doi:10.1016/j.quascirev.2004.08.004

Andersen, O.G.N., 1981. The annual cycle of temperature, salinity, currents and water masses in Disko Bugt and adjacent waters, West Greenland. Comm. Sci. Res. Greenl. 5, 33.

Anderson, N.J., Leng, M.J., 2004. Increased aridity during the early Holocene in West Greenland inferred from stable isotopes in laminated-lake sediments. Quat. Sci. Rev. 23, 841–849. doi:https://doi.org/10.1016/j.quascirev.2003.06.013

Andersson, C., Pausata, F.S.R., Jansen, E., Risebrobakken, B., Telford, R.J., 2010. Holocene trends in the foraminifer record from the Norwegian Sea and the North Atlantic Ocean. Clim. Past 6, 179–193.

Andersson, C., Risebrobakken, B., Jansen, E., Dahl, S.O., 2003. Late Holocene surface ocean conditions of the Norwegian Sea (Vøring Plateau). Paleoceanography 18, 1–13.

Andreev, A.A., Schirrmeister, L., Meyer, H., Grosse, G., Kuznetsova, T. V., Derevyagin, A.Y., Bryantseva, A., Kuzmina, S.A., Bobrov, A.A., Tarasov, P.E., Novenko, E.Y., Kunitsky, V. V., Kienast, F., 2009. Weichselian and Holocene palaeoenvironmental history of the Bol'shoy Lyakhovsky Island, New Siberian Archipelago, Arctic Siberia. Boreas. doi:10.1111/j.1502-3885.2008.00039.x

Andresen, C., McCarthy, D. J., Dylmer, C. V., Seidenkrantz, M.-S., Kuijpers, A., Lloyd, J.M., 2010. Interaction between subsurface ocean waters and calving of the Jakobshavn Isbræ

during the late Holocene. The Holocene 21, 211–224.
Andresen, C., Hansen, M., Seidenkrantz, M.-S., Jennings, A., Knudsen, M., Norgaard-Pedersen, N., Larsen, N., Kuijpers, A., Pearce, C., 2012. Mid- to late-Holocene oceanographic variability on the Southeast Greenland shelf. The Holocene 23, 167–178. doi:10.1177/0959683612460789
Andresen, C.S., Straneo, F., Ribergaard, M.H., Bjørk, A.A., Andersen, T.J., Kuijpers, A., Nørgaard-Pedersen, N., Kjær, K.H., Schjøth, F., Weckström, K., Ahlstrøm, A.P., 2012. Rapid response of Helheim Glacier in Greenland to climate variability over the past century. Nat. Geosci. 5, 37–41. doi:10.1038/ngeo1349
Andrews, J.T., Jennings, A.E., Moros, M., Hillaire-Marcel, C., Eberl, D., 2006. Is there a pervasive Holocene ice-rafted debris (IRD) signal in the northern North Atlantic? The answer appears to be either no, or it depends on the proxy! PAGES Newsl. 14, 7–9.
Andrews, J.T., 2009. Seeking a Holocene drift ice proxy: non-clay mineral variations from the SW to N-central Iceland shelf: trends, regime shifts, and periodicities. J. Quat. Sci. 24, 664–676. doi:10.1002/jqs.1257
Andrews, J.T., Belt, S.T., Olafsdottir, S., Massé, G., Vare, L.L., 2009. Sea ice and marine climate variability for NW Iceland/Denmark Strait over the last 2000 cal. yr BP. The Holocene 19, 775–784. doi:10.1177/0959683609105302
Andrews, J.T., Bigg, G.R., Wilton, D.J., 2014. Holocene ice-rafting and sediment transport from the glaciated margin of East Greenland (67-70°N) to the N Iceland shelves: Detecting and modelling changing sediment sources. Quat. Sci. Rev. 91, 204–217. doi:10.1016/j.quascirev.2013.08.019
Andrews, J.T., Stein, R., Moros, M., Perner, K., 2016. Late Quaternary changes in sediment composition on the NE Greenland margin (~73° N) with a focus on the fjords and shelf. Boreas 45, 381–397. doi:10.1111/bor.12169
Armand, L.K., Leventer, A., 2010. Palaeo sea ice distribution and reconstruction derived fromthe geological record., in: Thomas, D.N., Dieckmann, G.S. (Ed.), Sea Ice. Blackwell Publishing, Oxford, p. 469–529.
Årthun, M., Eldevik, T., Smedsrud, L.H., Skagseth, Ø., Ingvaldsen, R.B., 2012. Quantifying the Influence of Atlantic Heat on Barents Sea Ice Variability and Retreat. J. Clim. 25, 4736–4743. doi:10.1175/JCLI-D-11-00466.1
Arzel, O., Fichefet, T., Goosse, H., Dufresne, J.L., 2008. Causes and impacts of changes in the Arctic freshwater budget during the twentieth and twenty-first centuries in an AOGCM. Clim. Dyn. 30, 37–58.
Barber, D.C., Dyke, A., Hillaire-Marcel, C., Jennings, A.E., Andrews, J.T., Kerwin, M.W., Bilodeau, G., McNeely, R., Southon, J., Morehead, M.D. and Gagnoni, J.-M., 1999. Forcing of the cold event of 8,200 years ago by catastrophic drainage of Laurentide lakes. Nature 400, 344–348.
Barber, D.G., Massom, R.A., 2007. Chapter 1 The Role of Sea Ice in Arctic and Antarctic Polynyas. Elsevier Oceanogr. Ser. 74, 1–54. doi:10.1016/S0422-9894(06)74001-6
Barrick, R.C., Hedges, J.I., Peterson, M.L., 1980. Hydrocarbon geochemistry of the Puget Sound region—I. Sedimentary acyclic hydrocarbons. Geochim. Cosmochim. Acta 44, 1349–1362. doi:10.1016/0016-7037(80)90094-0
Barry, R., 1996. The parameterization of surface albedo for sea ice and its snow cover. Prog. Phys. Geogr. doi:10.1177/030913339602000104
Bauch, H.A., Erlenkeuser, H., Spielhagen, R.F., Struck, U., Matthiessen, J., Thiede, K., Heinemeier, J., 2001b. A multiproxy reconstruction of the evolution of deep and surface

waters in the subarctic Nordic seas over the last 30,000 yr. Quat. Sci. Rev. 20, 659–678.

Bauch, H.A., Kassens, H., Erlenkeuser, H., Grootes, P.M., Thiede, J., 1999. Depositional environment of the Laptev Sea (Arctic Siberia) during the Holocene. Boreas. doi:10.1111/j.1502-3885.1999.tb00214.x

Bauch, H.A., Mueller-Lupp, T., Taldenkova, E., Spielhagen, R.F., Kassens, H., Grootes, P.M., Thiede, J., Heinemeier, J., Petryashov, V. V., 2001a. Chronology of the Holocene transgression at the north siberian margin. Glob. Planet. Change. doi:10.1016/S0921-8181(01)00116-3

Belchansky, G.I., Douglas, D.C., 2002. Seasonal comparisons of sea ice concentration estimates derived from SSM/I, OKEAN, and RADARSAT data. Remote Sens. Environ. doi:10.1016/S0034-4257(01)00333-9

Belt, S.T., Allard, W.G., Massé, G., Robert, J.M., Rowland, S.J., 2000. Highly branched isoprenoids (HBIs): Identification of the most common and abundant sedimentary isomers. Geochim. Cosmochim. Acta. doi:10.1016/S0016-7037(00)00464-6

Belt, S.T., Brown, T.A., Ampel, L., Cabedo-Sanz, P., Fahl, K., Kocis, J.J., Massé, G., Navarro-Rodriguez, A., Ruan, J., Xu, Y., 2014. An inter-laboratory investigation of the Arctic sea ice biomarker proxy IP_{25} in marine sediments: Key outcomes and recommendations. Clim. Past 10, 155–166. doi:10.5194/cp-10-155-2014

Belt, S.T., Brown, T.A., Ringrose, A.E., Cabedo-Sanz, P., Mundy, C.J., Gosselin, M., Poulin, M., 2013. Quantitative measurement of the sea ice diatom biomarker IP_{25} and sterols in Arctic sea ice and underlying sediments: Further considerations for palaeo sea ice reconstruction. Org. Geochem. 62, 33–45. doi:https://doi.org/10.1016/j.orggeochem.2013.07.002

Belt, S.T., Brown, T.A., Smik, L., Tatarek, A., Wiktor, J., Stowasser, G., Assmy, P., Allen, C.S., Husum, K., 2017. Identification of C25 highly branched isoprenoid (HBI) alkenes in diatoms of the genus Rhizosolenia in polar and sub-polar marine phytoplankton. Org. Geochem. 110, 65–72. doi:10.1016/j.orggeochem.2017.05.007

Belt, S.T., Cabedo-Sanz, P., Smik, L., Navarro-Rodriguez, A., Berben, S.M.P., Knies, J., Husum, K., 2015. Identification of paleo Arctic winter sea ice limits and the marginal ice zone: Optimised biomarker-based reconstructions of late Quaternary Arctic sea ice. Earth Planet. Sci. Lett. 431, 127–139. doi:10.1016/j.epsl.2015.09.020

Belt, S.T., Massé, G., Rowland, S.J., Poulin, M., Michel, C., LeBlanc, B., 2007. A novel chemical fossil of palaeo sea ice: IP_{25}. Org. Geochem. 38, 16–27. doi:10.1016/j.orggeochem.2006.09.013

Belt, S.T., Massé, G., Vare, L.L., Rowland, S.J., Poulin, M., Sicre, M.A., Sampei, M., Fortier, L., 2008. Distinctive ^{13}C isotopic signature distinguishes a novel sea ice biomarker in Arctic sediments and sediment traps. Mar. Chem. doi:10.1016/j.marchem.2008.09.002

Belt, S.T., Müller, J., 2013. The Arctic sea ice biomarker IP_{25} : a review of current understanding , recommendations for future research and applications in palaeo sea ice reconstructions. Quat. Sci. Rev. doi:10.1016/j.quascirev.2012.12.001

Belt, S.T., Smik, L., Brown, T.A., Kim, J.-H., Rowland, S.J., Allen, C.S., Gal, J.-K., Shin, K.-H., Lee, J.I., Taylor, K.W.R., 2016. Source identification and distribution reveals the potential of the geochemical Antarctic sea ice proxy $IPSO_{25}$. Nat. Commun. 7, 12655. doi:10.1038/ncomms12655

Belt, S.T., Vare, L.L., Massé, G., Manners, H.R., Price, J.C., MacLachlan, S.E., Andrews, J.T., Schmidt, S., 2010. Striking similarities in temporal changes to spring sea ice occurrence across the central Canadian Arctic Archipelago over the last 7000 years. Quat. Sci. Rev. 29, 3489–3504. doi:10.1016/j.quascirev.2010.06.041

Bendle, A.P., Rosell-Melé, A., 2007. High-resolution alkenone sea surface temperature variability on the North Icelandic Shelf: implications for Nordic Seas palaeoclimatic development during the Holocene. The Holocene 17, 9–24. doi:DOI: 10.1177/0959683607073269

Berben, S.M.P., Husum, K., Cabedo-Sanz, P., Belt, S.T., 2014. Holocene sub-centennial evolution of Atlantic water inflow and sea ice distribution in the western Barents Sea. Clim. Past 10, 181–198. doi:10.5194/cp-10-181-2014

Berben, S.M.P., Husum, K., Navarro-Rodriguez, A., Belt, S.T., Aagaard-Sørensen, S., 2017. Semi-quantitative reconstruction of early to late Holocene spring and summer sea ice conditions in the northern Barents Sea. J. Quat. Sci. 32, 587–603. doi:10.1002/jqs.2953

Berner, K.S., Ko, N., Godtliebsen, F., Divine, D., 2011. Holocene climate variability of the Norwegian Atlantic Current during high and low solar insolation forcing. Paleoceanography 26, 1–15. doi:10.1029/2010PA002002

Bianchi, T.S., 2007. Biogeochemistry of Estuaries. Oxford University Press, New York.

Birgel, D., Stein, R., Hefter, J., 2004. Aliphatic lipids in recent sediments of the Fram Strait/Yermak Plateau (Arctic Ocean): Composition, sources and transport processes. Mar. Chem. 88, 127–160. doi:10.1016/j.marchem.2004.03.006

Birks, C.J.A., Koç, N., 2002. A high-resolution diaton record of late-Quaternary sea-surface temperatures and oceanographic conditions from the eastern Norwegian Sea. Boreas 31, 323–344. doi:10.1080/030094802320942545

Blaschek, M., Renssen, H., 2013. The Holocene thermal maximum in the Nordic Seas: the impact of Greenland Ice Sheet melt and other forcings in a coupled atmosphere–sea-ice–ocean model. Clim. Past. doi:10.5194/cp-9-1629-2013

Blumer, M., Guillard, R.R.L., Chase, T., 1971. Hydrocarbons of marine phytoplankton. Mar. Biol. doi:10.1007/BF00355214

Bond, G., 1997. A Pervasive Millennial-Scale Cycle in North Atlantic Holocene and Glacial Climates. Science. 278, 1257–1266. doi:10.1126/science.278.5341.1257

Bond, G., Kromer, B., Beer, J., Muscheler, R., Evans, M.N., Showers, W., Hoffmann, S., Lotti-Bond, R., Hajdas, I., Bonani, G., 2001a. Persistent Solar Influence on North Atlantic Climate During the Holocene. Science. 294, 2130 LP-2136.

Bonnet, S., de Vernal, A., Hillaire-Marcel, C., Radi, T., Husum, K., 2010. Variability of sea-surface temperature and sea-ice cover in the Fram Strait over the last two millennia. Mar. Micropaleontol. 74, 59–74. doi:https://doi.org/10.1016/j.marmicro.2009.12.001

Boon, J. J., Rijpstra, W. I. C., de Lange, F., De Leeuw, J. W., Yoshioka, M., Shimizu, Y., 1979. Black Sea sterol—a molecular fossil for dinoflagellate blooms. Nature 277, 125–127.

Born, A., Stocker, T.F., 2013. Two Stable Equilibria of the Atlantic Subpolar Gyre. J. Phys. Oceanogr. 44, 246–264. doi:10.1175/JPO-D-13-073.1

Bronk-Ramsey, C., 2009. Bayesian Analysis of Radiocarbon Dates. Radiocarbon. doi:10.2458/azu_js_rc.v51i1.3494

Brown, T.A., Belt, S.T., Philippe, B., Mundy, C.J., Massé, G., Poulin, M., Gosselin, M., 2011. Temporal and vertical variations of lipid biomarkers during a bottom ice diatom bloom in the Canadian Beaufort Sea: Further evidence for the use of the IP_{25} biomarker as a proxy for spring Arctic sea ice. Polar Biol. 34, 1857–1868. doi:10.1007/s00300-010-0942-5

Brown, T. A., Belt, S.T., Tatarek, A., Mundy, C.J., 2014. Source identification of the Arctic sea ice proxy IP_{25}. Nat. Commun. 5, 4197. doi:10.1038/ncomms5197

Buch, E., 2002. Present Oceanographic Conditions in GreenlandWaters., in: Danish Meteorological Institute, Scientific Report 02-02. p. 1–39.

Buch, E., 2000. Air-sea-ice conditions off southwest Greenland, 1981-97. J. Northwest Atl. Fish. Sci. doi:10.2960/J.v26.a6

Cabedo-Sanz, P., Belt, S.T., 2016. Seasonal sea ice variability in eastern Fram Strait over the last 2000 years. Arktos 2, 22. doi:10.1007/s41063-016-0023-2

Cabedo-Sanz, P., Belt, S.T., Jennings, A.E., Andrews, J.T., Geirsdóttir, Á., 2016. Variability in drift ice export from the Arctic Ocean to the North Icelandic Shelf over the last 8000 years: A multi-proxy evaluation. Quat. Sci. Rev. 146, 99–115. doi:10.1016/j.quascirev.2016.06.012

Cabedo-Sanz, P., Belt, S.T., Knies, J., Husum, K., 2013. Identification of contrasting seasonal sea ice conditions during the Younger Dryas. Quat. Sci. Rev. 79, 74–86. doi:10.1016/j.quascirev.2012.10.028

Calvo, E., Grimalt, J., Jansen, E., 2002. High resolution U_{37}^{K} sea surface temperature reconstruction in the Norwegian Sea during the Holocene. Quat. Sci. Rev. 21, 1385–1394. doi:10.1016/S0277-3791(01)00096-8

Campbell, D.C., de Vernal, A., 2009. Marine Geology and Paleoceanography of Baffin Bay and Adjacent Areas: Nain, NL to Halifax, NS: August 28-September 23, 2008, Geological Survey of Canada.

Cappelen, J., Vinther, B.M., 2014. SW Greenland temperature data 1784-2013. Tech. Rep. 14–6.

Carmack; E.C., 2000. The Arctic Ocean's Freshwater Budget: Sources, Storage and Export, in: Lewis E.L., Jones E.P., Lemke P., Prowse T.D., W.P. (Ed.), The Freshwater Budget of the Arctic Ocean. NATO Science Series (Series 2. Environment Security), Vol 70. Springer, Dordrecht. doi:https://doi.org/10.1007/978-94-011-4132-1_5

Cavalieri, D. J., C. L. Parkinson, P. Gloersen, H.J.Z., 1996. Sea Ice Concentrations from Nimbus-7 SMMR and DMSP SSM/I-SSMIS Passive Microwave Data, Version 1. updated yearly. Boulder, Color. USA. NASA Natl. Snow Ice Data Cent. Distrib. Act. Arch. Cent. accessed august 2017. http://dx.doi.org/10.5067/8GQ8LZQVL0VL.

Cavalieri, D.J., Gloersen, P., Parkinson, C.L., Comiso, J.C., Zwally, H.J., 1997. Observed hemispheric asymmetry in global sea ice changes. Science. 278, 1104–1106.

Comiso, J.C., 2012. Large decadal decline of the arctic multiyear ice cover. J. Clim. 25, 1176–1193. doi:10.1175/JCLI-D-11-00113.1

Comiso, J.C., Cavalieri, D.J., Parkinson, C.L., Gloersen, P., 1997. Passive microwave algorithms for sea ice concentration: A comparison of two techniques. Remote Sens. Environ. 60, 357–384. doi:https://doi.org/10.1016/S0034-4257(96)00220-9

Comiso, J.C., Parkinson, C.L., Gersten, R., Stock, L., 2008. Accelerated decline in the Arctic Sea ice cover. Geophys. Res. Lett. 35. doi:Artn L01703\nDoi 10.1029/2007gl031972

Cormier, M.A., Rochon, A., de Vernal, A., Gélinas, Y., 2016. Multi-proxy study of primary production and paleoceanographical conditions in northern Baffin Bay during the last centuries. Mar. Micropaleontol. 127, 1–10. doi:10.1016/j.marmicro.2016.07.001

Cremer, H., 1999. Distribution patterns of diatom surface sediment assemblages in the Laptev Sea (Arctic Ocean). Mar. Micropaleontol. doi:10.1016/S0377-8398(99)00037-7

Cronin, T.M., Dwyer, G.S., Kamiya, T., Schwede, S., Willard, D.A., 2003. Medieval Warm period, Little Ice Age and 20th century temperature variability form Chesapeake Bay. Glob. Planet. Change 36, 17–29.

Cronin, T.M., Gemery, L., Briggs, W.M., Jakobsson, M., Polyak, L., Brouwers, E.M., 2010. Quaternary Sea-ice history in the Arctic Ocean based on a new Ostracode sea-ice proxy. Quat. Sci. Rev. 29, 3415–3429. doi:10.1016/j.quascirev.2010.05.024

Cronin, T.M., Polyak, L., Reed, D., Kandiano, E.S., Marzen, R.E., Council, E.A., 2013. A 600-ka Arctic sea-ice record from Mendeleev Ridge based on ostracodes. Quat. Sci. Rev. 79, 157–

167. doi:10.1016/j.quascirev.2012.12.010
Cubasch, U., Voss, R., Hegerl, G.C., Waszkewitz, J., Crowley, T.J., 1997. Climate Dynamics Simulation of the influence of solar radiation variations on the global climate with an ocean-atmosphere general circulation model. Clim. Dyn. 13, 757–767.
Cuny, J., Rhines, P.B., Kwok, R., 2005. Davis Strait volume, freshwater and heat fluxes. Deep. Res. Part I Oceanogr. Res. Pap. 52, 519–542. doi:10.1016/j.dsr.2004.10.006
Curry, R.G., McCartney, M.S., Joyce, T.M., 1998. Oceanic transport of subpolar climate signals to mid-depth subtropical waters. Nature 391, 575–577.
Dahl-Jensen, D., 1998. Past Temperatures Directly from the Greenland Ice Sheet. Science. 282, 268–271. doi:10.1126/science.282.5387.268
Darby, D. A., Ortiz, J.D., Grosch, C.E., Lund, S.P., 2012. 1,500-year cycle in the Arctic Oscillation identified in Holocene Arctic sea-ice drift. Nat. Geosci. 5, 897–900.
Dawson, A.G., Elliott, L., Mayewski, P., Lockett, P., Noone, S., Hickey, K., Holt, T., Wadhams, P., Foster, I., 2003. Late-Holocene North Atlantic climate "seesaws", storminess changes and Greenland ice sheet (GISP2) palaeoclimates. The Holocene 13, 381–392. doi:10.1191/0959683603hl631rp
de Leeuw, J.W., Rijpstra, W.I.C., Schenck, P.A., Volkman, J.K., 1983. Free, esterified and residual bound sterols in Black Sea Unit I sediments. Geochim. Cosmochim. Acta. doi:10.1016/0016-7037(83)90268-5
de Vernal, A., Henry, M., Matthiessen, J., Mudie, P.J., Rochon, A., Boessenkool, K.P., Eynaud, F., GrØsfjeld, K., Guiot, J., Hamel, D., Harland, R., Head, M.J., Kunz-Pirrung, M., Levac, E., Loucheur, V., Peyron, O., Pospelova, V., Radi, T., Turon, J.-L., Voronina, E., 2001. Dinoflagellate cyst assemblages as tracers of sea-surface conditions in the northern North Atlantic, Arctic and sub-Arctic seas: the new "n = 677" data base and its application for quantitative palaeoceanographic reconstruction. J. Quat. Sci. 16, 681–698. doi:10.1002/jqs.659
de Vernal, A., Turon, J.-L., Guiot, J., 1994. Dinoflagellate cyst distribution in high-latitude marine environments and quantitative reconstruction of sea-surface salinity, temperature, and seasonality. Can. J. Earth Sci. 31, 48–62. doi:10.1139/e94-006
de Vernal, A., Gersonde, R., Goosse, H., Seidenkrantz, M.S., Wolff, E.W., 2013a. Sea ice in the paleoclimate system: The challenge of reconstructing sea ice from proxies - an introduction. Quat. Sci. Rev. 79, 1–8. doi:10.1016/j.quascirev.2013.08.009
de Vernal, A., Hillaire-Marcel, C., Darby, D.A., 2005. Variability of sea ice cover in the Chukchi Sea (western Arctic Ocean) during the Holocene. Paleoceanography. doi:10.1029/2005PA001157
de Vernal, A., Hillaire-Marcel, C., Rochon, A., Fréchette, B., Henry, M., Solignac, S., Bonnet, S., 2013b. Dinocyst-based reconstructions of sea ice cover concentration during the Holocene in the Arctic Ocean, the northern North Atlantic Ocean and its adjacent seas. Quat. Sci. Rev. 79, 111–121. doi:10.1016/j.quascirev.2013.07.006
de Vernal, A., Rochon, A., Fréchette, B., Henry, M., Radi, T., Solignac, S., 2013c. Reconstructing past sea ice cover of the Northern Hemisphere from dinocyst assemblages: Status of the approach. Quat. Sci. Rev. 79, 122–134. doi:10.1016/j.quascirev.2013.06.022
de Vernal, A., Rochon, A., Turon, J.-L., Matthiessen, J., 1997. Organic-walled dinoflagellate cysts: Palynological tracers of sea-surface conditions in middle to high latitude marine environments. Geobios 30, 905–920. doi:https://doi.org/10.1016/S0016-6995(97)80215-X
Denton, G.H., Karlén, W., 1973. Holocene climatic variations-Their pattern and possible cause. Quat. Res. 3, 155–174.

Dethleff, D., Loewe, P., Kleine, E., 1998. The Laptev Sea flaw lead - detailed investigation on ice formation and export during 1991/1992 winter season. Cold Reg. Sci. Technol. doi:10.1016/S0165-232X(98)00005-6

Dickson, R., Lazier, J., Meincke, J., Rhines, P., Swift, J., 1996. Long-term coordinated changes in the convective activity of the North Atlantic. Prog. Oceanogr. 38, 241– 295.

Dickson, B., 1999. All change in the Arctic. Nature 389–391. doi:10.1038/17018

Dickson, R., Lazier, J., Meincke, J., Rhines, P., Swift, J., 1996. Long-term coordinated changes in the convective activity of the North Atlantic. Prog. Oceanogr. 38, 241–295. doi:10.1016/S0079-6611(97)00002-5

Dieckmann, G. S., Hellmer, H.H., 2010. The importance of sea ice: an overview, in: Thomas, D.N., Dieckmann, G.S. (Ed.), Sea Ice 2. Wiley-Blackwell, Oxford, UK, pp. 1–22.

Dieckmann, G. S. and Hellmer, H.H., 2003. The Importance of Sea Ice: An Overview, in: Dieckmann, D.N.T. and G.S. (Ed.), Sea Ice: An Introduction to Its Physics, Chemistry, Biology and Geology. Blackwell Science Ltd, Oxford, UK. doi:10.1002/9780470757161.ch1

Dijkstra, H.A., Te Raa, L., Schmeits, M., Gerrits, J., 2006. On the physics of the Atlantic Multidecadal Oscillation. Ocean Dyn. 56, 36–50. doi:10.1007/s10236-005-0043-0

Dima, M., Lohmann, G., 2007. A hemispheric mechanism for the Atlantic multidecadal oscillation. J. Clim. 20, 2706–2719.

Dokken, T.M., Nisancioglu, K.H., Li, C., Battisti, D.S., Kissel, C., 2013. Dansgaard-Oeschger cycles: Interactions between ocean and sea ice intrinsic to the Nordic seas. Paleoceanography 28, 491–502. doi:10.1002/palo.20042

Dorschel, B., Afanasyeva, V., Bender, M., Dreutter, S., Eisermann, H., Gebhardt, C., Hansen, K., Hebbeln, D., Jackson R., Jeltsch-Thömmes, A., Jensen, L., Kolling, H., Le Duc, C., Lenz, B., Lübben, B., Madaj, L., Martínez Méndez, G., Meyer-Schack, B., Sch, D.J., 2014. BAFFEAST Past Greenland Ice Sheet dynamics, Palaeoceanography and Plankton Ecology in the Northeast Baffin Bay. MARIA S. MERIAN-Berichte. doi:10.2312/cr

Drinkwater, K.F., 1996. Atmospheric and oceanic variability in the northwest Atlantic during the 1980s and early 1990s. J. Northwest Atl. Fish. Sci. 18, 77–97. doi:10.2960/J.v18.a6

Drinkwater, K. F., 1986. Physical oceanography of Hudson Strait and Ungava Bay, p. 237-264. In I. P. Martini (Ed.). Canadian Inland Seas. Elsevier, Amsterdam, 494 p.

Dyke, A. S., Hooper, J., Savelle, J.M., 1996. A history of sea ice in the Canadian Arctic Archipelago based on postglacial remains of the bowhead whale (Balaena mysticetus). Arctic 235–255.

Dyke, A.S., England, J., Reimnitz, E., Jetté, H., 1997. Changes in driftwood delivery to the Canadian Arctic Archipelago: The hypothesis of postglacial oscillations of the transpolar drift. Arctic. doi:10.14430/arctic1086

Eddy, J.A., 1976. The Maunder Minimum. Science. 192, 1189–1202.

Eicken, H., 2003. From the microscopic, to the macroscopic, to the regional scale: Growth, microstructure and properties of sea ice., in: In: Thomas, D.,N. Dieckmann, G.S,. (Ed.), Sea Ice: An Introduction to Its Physics, Chemistry, Biology and Geology. Blackwell, Oxford, p. 22–81.

Eldevik, T., Nilsen, J.E.O., Iovino, D., Anders Olsson, K., Sando, A.B., Drange, H., 2009. Observed sources and variability of Nordic seas overflow. Nat. Geosci 2, 406–410.

Erbs-Hansen, D.R., Knudsen, K.L., Olsen, J., Lykke-Andersen, H., Underbjerg, J.A., Sha, L., 2013. Paleoceanographical development off Sisimiut, West Greenland, during the mid- and late Holocene: A multiproxy study. Mar. Micropaleontol.

doi:10.1016/j.marmicro.2013.06.003
Evans, J., Dowdeswell, J. A., Grobe, H., Niessen, F., Stein, R., Hubberten, H.-W., Whittington, R.J., 2002. Late Quaternary sedimentation in Kejser Franz Joseph Fjord and the continental margin of East Greenland. Geol. Soc. London, Spec. Publ. 203, 149–179. doi:10.1144/GSL.SP.2002.203.01.09
Fahl, K., Stein, R., 2012. Modern seasonal variability and deglacial/Holocene change of central Arctic Ocean sea-ice cover: New insights from biomarker proxy records. Earth Planet. Sci. Lett. 351–352, 123–133. doi:10.1016/j.epsl.2012.07.009
Fahl, K., Stein, R., 2007. Biomarker records, organic carbon accumulation, and river discharge in the Holocene southern Kara Sea (Arctic Ocean). Geo-Marine Lett. doi:10.1007/s00367-006-0049-8
Fahl, K., Stein, R., 1999. Biomarkers as organic-carbon-source and environmental indicators in the late quaternary Arctic Ocean: Problems and perspectives. Mar. Chem. 63, 293–309. doi:10.1016/S0304-4203(98)00068-1
Fahl, K., Stein, R., 1997. Modern organic carbon deposition in the Laptev Sea and the adjacent continental slope: Surface water productivity vs. terrigenous input. Org. Geochem. doi:10.1016/S0146-6380(97)00007-7
Fahl K., Stein R., Gaye-Haake B., Gebhardt C., Kodina L. A., Unger D., I. V., 2003. Biomarkers in surface sediments from Ob and Yenisei estuaries and southern Kara Sea: evidence for particulate organic carbon sources, pathways, and degradation, in: Stein, R., Fahl, K., Fütterer, D.K., Galimov, E.M., Stepanets, O.V. (Ed.), Siberian River Run-off in the Kara Sea: Characterisation, Quantification, Variability, and Environmental Significance. Proceeding of Marine Science. Elsevier, Amsterdam, pp. 329–348.
Faust, J.C., Fabian, K., Milzer, G., Giraudeau, J., Knies, J., 2016. Norwegian fjord sediments reveal NAO related winter temperature and precipitation changes of the past 2800 years. Earth Planet. Sci. Lett. 435, 84–93. doi:10.1016/j.epsl.2015.12.003
Foster, K.L., Stern, G.A., Carrie, J., Bailey, J.N.L., Outridge, P.M., Sanei, H., Macdonald, R.W., 2015. Spatial, temporal, and source variations of hydrocarbons in marine sediments from Baffin Bay, Eastern Canadian Arctic. Sci. Total Environ. 506–507, 430–443. doi:10.1016/j.scitotenv.2014.11.002
Francis, J.A., Hunter, E., Key, J.R., Wang, X., 2005. Clues to variability in Arctic minimum sea ice extent. Geophys. Res. Lett. 32, 1–4.
Fronval, T., Jansen, E., 1997. Eemian and Early Weichselian (140-60 ka) Paleoceanography and paleoclimate in the Nordic Seas with comparisons to Holocene conditions. Paleoceanography. doi:10.1029/97PA00322
Funder, S., Goosse, H., Jepsen, H., Kaas, E., Kjær, K.H., Korsgaard, N.J., Larsen, N.K., Linderson, H., Lyså, A., Möller, P., Olsen, J., Willerslev, E., 2011. A 10,000-Year Record of Arctic Ocean Sea-Ice Variability-View from the Beach. Science. 333, 747–750. doi:10.1126/science.1202760
Geissler, W., 2013. Maria S. Merian ; Cruise No . MSM 31 Tromsø – Bremen Chief Scientist : Wolfram Geissler Captain : Matthias Günther Objectives Short cruise description. Short Cruise Rep. Maria S. Merian Cruise No. MSM 31 1–18.
Gibb, O.T., Hillaire-Marcel, C., de Vernal, A., 2014. Oceanographic regimes in the northwest Labrador Sea since Marine Isotope Stage 3 based on dinocyst and stable isotope proxy records. Quat. Sci. Rev. 92, 269–279. doi:10.1016/j.quascirev.2013.12.010
Gillett, N.P., Graf, H.F., Osborn, T.J., 2003. Climate Change and the North Atlantic Oscillation, in: The North Atlantic Oscillation: Climatic Significance and Environmental Impact.

doi:10.1029/134GM09

Giraudeau, J., Jennings, A.E., Andrews, J.T., 2004. Timing and mechanisms of surface and intermediate water circulation changes in the Nordic Seas over the last 10,000 cal years: A view from the North Iceland shelf. Quat. Sci. Rev. 23, 2127–2139. doi:10.1016/j.quascirev.2004.08.011

Gladfelter, W.H., 1964. Oceanography of the Greenland Sea: USS Atka (AGB-3) survey, summer 1962. Marine Sciences Dept., US Naval Oceanographic Office.

Gloersen, P., Campbell, W.J., Cavalieri, D.J., Comiso, J.C., Parkinson, C.L., Zwally, H.J., 1993. Satellite passive microwave observations and analysis of Arctic and Antarctic sea ice, 1978-1987. Ann. Glaciol. 17, 149–154. doi:10.1016/0021-9169(95)90010-1

Goad, L.J., Withers, N., 1982. Identification of 27-nor-(24R)-24-methylcholesta-5,22-dien-3β-ol and brassicasterol as the major sterols of the marine dinoflagellate Gymnodinium simplex. Lipids 17, 853–858. doi:10.1007/BF02534578

Gosselin, M., Levasseur, M., Wheeler, P.A., Horner, R.A., Booth, B.C., 1997. New measurements of phytoplankton and ice algal production in the Arctic Ocean. Deep. Res. Part II Top. Stud. Oceanogr. doi:10.1016/S0967-0645(97)00054-4

Gow, A.J., Tucker III, W.B., 1987. Physical properties of sea ice discharge from Fram Strait. Science. 236, 436–439.

Gowan, S.M., Ryves, D.B., Anderson, N.J., 2003. Holocene records of effective precipitation in West Greenland. The Holocene 13, 239–249. doi:10.1191/0959683603hl610rp

Gradinger, R., 2009. Sea-ice algae: Major contributors to primary production and algal biomass in the Chukchi and Beaufort Seas during May/June 2002. Deep. Res. Part II Top. Stud. Oceanogr. 56, 1201–1212. doi:10.1016/j.dsr2.2008.10.016

Gray, L.J., Beer, J., Geller, M., Haigh, J.D., Lockwood, M., Matthes, K., Cubasch, U., Fleitmann, D., Harrison, G., Hood, L., Luterbacher, J., Meehl, G. a., Shindell, D., van Geel, B., White, W., 2010. Solar influence on climate. Rev. Geophys. 48, RG4001. doi:10.1029/2009RG000282.1.INTRODUCTION

Grootes, P.M., Stuiver, M., White, J.W.C., Johnsen, S., Jouzel, J., 1993. Comparison of oxygen isotope records from the GISP2 and GRIP Greenland ice cores. Nature. doi:10.1038/366552a0

Grossi, V., Beker, B., Geenevasen, J.A.J., Schouten, S., Raphel, D., Fontaine, M.F., Sinninghe Damsté, J.S., 2004. C_{25} highly branched isoprenoid alkenes from the marine benthic diatom Pleurosigma strigosum. Phytochemistry. doi:10.1016/j.phytochem.2004.09.002

Häkkinen, S., 1999. A simulation of thermohaline effects of a great salinity anomaly. J. Clim. 12, 1781–1795.

Häkkinen, S., 1995. Simulated interannual variability of the Greenland Sea deep-water formation. J. Geophys. Res. 100, 4761–4770.

Hald, M., Andersson, C., Ebbesen, H., Jansen, E., Klitgaard-Kristensen, D., Risebrobakken, B., Salomonsen, G.R., Sarnthein, M., Sejrup, H.P., Telford, R.J., 2007. Variations in temperature and extent of Atlantic Water in the northern North Atlantic during the Holocene. Quat. Sci. Rev. doi:10.1016/j.quascirev.2007.10.005

Hald, M., Steinsund, P.I., 1992. Distribution of Surface Sediment Benthic Foraminifera in the Southwestern Barents Sea. J. Foraminifer. Res. 22, 347–362.

Hall, I.R., Bianchi, G.G., Evans, J.R., 2004. Centennial to millennial scale Holocene climate-deep water linkage in the North Atlantic. Quat. Sci. Rev. doi:10.1016/j.quascirev.2004.04.004

Hamel, D., Vernal, A. de, Gosselin, M., Hillaire-Marcel, C., 2002. Organic-walled microfossils and geochemical tracers: Sedimentary indicators of productivity changes in the North Water

and northern Baffin Bay during the last centuries. Deep. Res. Part II Top. Stud. Oceanogr. doi:10.1016/S0967-0645(02)00190-X

Hanebuth, T., 2009. Short Cruise Report: RV Maria S. Merian Cruise MSM 30. Short Cruise Report.https://www.ldf.uni-hamburg.de/merian/wochenberichte/wochenberichte-merian/msm29-msm31/msm30-scr.pdf

Hanna, E., Cappelen, J., 2003. Recent cooling in coastal southern Greenland and relation with the North Atlantic Oscillation. Geophys. Res. Lett. doi:10.1029/2002GL015797

Harff, J., Dietrich, R., Endler, R., Hentzsch, B., Jensen, J. B., K., A., Krauss, N., Leipe, T., Lloyd, J., Mikkelsen, N., M., M., Perner, K., Richter, A., Risgaard-Petersen, N., Rysgaard, S., Richter, T., Sandgren, P., Sheshenko, V., Snowball, I., Waniek, J., Weinrebe, W. Witkowski, A., 2007. Deglaciation history, Coastal Development, and environmental change during the Holocene in western Merian', Greenland. Cruise report MSM 05/03 R/V "Maria S. Merian." Balt. Sea Res. Institute, Rostock.

Hass, H.C., Kaminski, M.A., 1995. Change in atmospheric and oceanic circulation reflected in North Sea sediments during the late Holocene. Zbl. Geol. Paläont. Tl. 1 1994, 51–65.

Hátún, H., Payne, M.R., Beaugrand, G., Reid, P.C., Sandø, A.B., Drange, H., Hansen, B., Jacobsen, J.A., Bloch, D., 2009. Large bio-geographical shifts in the north-eastern Atlantic Ocean: From the subpolar gyre, via plankton, to blue whiting and pilot whales. Prog. Oceanogr. 80, 149–162. doi:10.1016/j.pocean.2009.03.001

He, D., Simoneit, B.R.T., Xu, Y., Jaffé, R., 2016. Occurrence of unsaturated C_{25} highly branched isoprenoids (HBIs) in a freshwater wetland. Org. Geochem. 93, 59–67. doi:10.1016/j.orggeochem.2016.01.006

Hebbeln, D., Berner, H., 1993. Surface sediment distribution in the Fram Strait. Deep Sea Res. Part I Oceanogr. Res. Pap. 40, 1731–1745. doi:10.1016/0967-0637(93)90029-3

Heikkilä, M., Pospelova, V., Forest, A., Stern, G.A., Fortier, L., Macdonald, R.W., 2016. Dinoflagellate cyst production over an annual cycle in seasonally ice-covered Hudson Bay. Mar. Micropaleontol. 125, 1–24. doi:10.1016/j.marmicro.2016.02.005

Heikkilä, M., Pospelova, V., Hochheim, K.P., Kuzyk, Z.Z.A., Stern, G.A., Barber, D.G., Macdonald, R.W., 2014. Surface sediment dinoflagellate cysts from the Hudson Bay system and their relation to freshwater and nutrient cycling. Mar. Micropaleontol. 106, 79–109. doi:10.1016/j.marmicro.2013.12.002

Helama, S., Jones, P.D., Briffa, K.R., 2017. Dark Ages Cold Period: A literature review and directions for future research. The Holocene 27, 1600–1606. doi:10.1177/0959683617693898

Helama, S., Fauria, M.M., Mielikäinen, K., Timonen, M., Eronen, M., 2010. Sub-Milankovitch solar forcing of past climates: Mid and late holocene perspectives. Bull. Geol. Soc. Am. 122, 1981–1988. doi:10.1130/B30088.1

Hillaire-Marcel, C., de Vernal, A., 2008. Stable isotope clue to episodic sea ice formation in the glacial North Atlantic. Earth Planet. Sci. Lett. 268, 143–150. doi:https://doi.org/10.1016/j.epsl.2008.01.012

Hirche, H.J., Baumann, M.E.M., Kattner, G., Gradinger, R., 1991. Plankton distribution and the impact of copepod grazing on primary production in Fram Strait, Greenland Sea. J. Mar. Syst. 2, 477–494. doi:10.1016/0924-7963(91)90048-Y

Hoff, U., Rasmussen, T.L., Stein, R., Ezat, M.,E., Fahl, K., 2016. Sea ice and millennial-scale climate variability in the Nordic seas 90kyr ago to present. Nat. Commun. 7. doi:10.1038/ncomms12247

Holland, D.M., Thomas, R.H., de Young, B., Ribergaard, M.H., Lyberth, B., 2008. Acceleration

of Jakobshavn Isbræ triggered by warm subsurface ocean waters. Nat. Geosci. doi:10.1038/ngeo316

Holland, M., Bitz, C., Eby, M., Weaver, A., 2001. The Role of Ice – Ocean Interactions in the Variability of the North Atlantic Thermohaline Circulation. J. Clim. 14, 656–675. doi:10.1175/1520-0442(2001)014<0656:TROIOI>2.0.CO;2

Holliday, N.P., Meyer, A., Bacon, S., Alderson, S.G., de Cuevas, B., 2007. Retroflection of part of the east Greenland current at Cape Farewell. Geophys. Res. Lett. 34, 1–5. doi:10.1029/2006GL029085

Hopkins, T.S., 1991. The GIN Sea-A synthesis of its physical oceanography and literature review 1972-1985. Earth Sci. Rev. 30, 175–318.

Horner, R., Schrader, G.C., 1982. Relative Contributions of Ice Algae, Phytoplankton, and Benthic Microalgae to Primary Production in Nearshore Regions of the Beaufort Sea. Arctic 35, 485–503. doi:10.14430/arctic2356

Hörner, T., Stein, R., Fahl, K., 2017. Evidence for Holocene centennial variability in sea ice cover based on IP 25 biomarker reconstruction in the southern Kara Sea (Arctic Ocean) 7. doi:10.1007/s00367-017-0501-y

Hörner, T., Stein, R., Fahl, K., Birgel, D., 2016. Post-glacial variability of sea ice cover, river run-off and biological production in the western Laptev Sea (Arctic Ocean) - A high-resolution biomarker study. Quat. Sci. Rev. 143, 133–149. doi:10.1016/j.quascirev.2016.04.011

Huang, W.Y., Meinschein, W.G., 1979. Sterols as ecological indicators. Geochim. Cosmochim. Acta 43, 739–745.

Hubberten, H.-W., 1995. Die Expedition ARKTIS-X/2 mit FS Polarstern (1994). (The Expedition ARKTIS-X/2 of RV Polarstern in 1994), in: Berichte Zur Polarforschung 174 (1995). Alfred Wegener Institute for Polar and Marine Research, Bremerhaven.

Humlum, O., 1985. The Glaciation Level in West Greenland. Arct. Alp. Res. 17, 311–319.

Hurrell, J.W., 1995. Decadal trends in the North Atlantic oscillation. Science. doi:10.1126/science.269.5224.676

Hurrell, J.W., Deser, C., 2009. North Atlantic climate variability: The role of the North Atlantic Oscillation. J. Mar. Syst. 78, 28–41. doi:10.1016/j.jmarsys.2008.11.026

IPCC, 2014. Climate Change 2014 - Synthesis Report, Headline statements from the Summary for Policymakers. doi:10.1017/CBO9781107415324

Isaksson, E., Kohler, J., Pohjola, V., Moore, J., Igarashi, M., Karlöf, L., Martma, T., Meijer, H., Motoyama, H., Vaikmäe, R., van de Wal, R.S.W., 2005. Two ice-core $\delta^{18}O$ records from Svalbard illustrating climate and sea-ice variability over the last 400 years. The Holocene. doi:10.1191/0959683605hl820rp

Jackson, M.G., Oskarsson, N., Trønnes, R.G., McManus, J.F., Oppo, D.W., Grönvold, K., Hart, S.R., Sachs, J.P., 2005. Holocene loess deposition in Iceland: Evidence for millenial-scale atmosphere-ocean coupling in the North Atlantic. Geology 33, 509–512. doi:10.1130/G21489.1

Jaffé, R., Wolff, G.A., Cabrera, A., Carvajal Chitty, H., 1995. The biogeochemistry of lipids in rivers of the Orinoco Basin. Geochim. Cosmochim. Acta. doi:10.1016/0016-7037(95)00246-V

Jakobsson, M., Grantz, A., Kristoffersen, Y., Macnab, R., 2004. The Arctic Ocean: Boundary conditions and background information, in: Stein, R., MacDonald, R.W. (Ed.), The Organic Carbon Cycle of the Arctic Ocean. Springer, Berlin, pp. 1–6.

Jakobsson, M., Macnab, R., Mayer, L., Anderson, R., Edwards, M., Hatzky, J., Schenke, H.W., Johnson, P., 2008. An improved bathymetric portrayal of the Arctic Ocean: Implications for ocean modeling and geological, geophysical and oceanographic analyses. Geophys. Res. Lett. doi:10.1029/2008GL033520

Jakobsson, M., Mayer, L.A., Coakley, B., Dowdeswell, J.A., Forbes, S., Fridman, B., Hodnesdal, H., Noormets, R., Pedersen, R., Rebesco, M., Schenke, H.-W., Zarayskaya Y., Accettella, D., Armstrong, A., Anderson, R.M., Bienhoff, P., Camerlenghi, A., Church, I., Edwards, M., Gardner, J.V., Hall, J.K., Hell, B., Hestvik, O.B., Kristoffersen, Y., Marcussen, C., M., R., Mosher, D., Nghiem, S.V., Pedrosa, M.T., Travaglini, P.G., Weatherall, P., 2012. The International Bathymetric Chart of the Arctic Ocean (IBCAO) Version 3.0. Geophys. Res. Lett. 39, L12609.

Jansen, E., Koc, N., 2000. Century to decadal scale records of Norwegian sea surface temperature variations of the past 2 millennia. PAGES Newsl. 8.1 13–14.

Jansen, H.L., Simonsen, J.R., Dahl, S.O., Bakke, J., Nielsen, P.R., 2016. Holocene glacier and climate fluctuations of the maritime ice cap Hogtuvbreen, northern Norway. The Holocene 0959683615618265-. doi:10.1177/0959683615618265

Jennings, A., Andrews, J., Wilson, L., 2011. Holocene environmental evolution of the SE Greenland Shelf North and South of the Denmark Strait: Irminger and East Greenland current interactions. Quat. Sci. Rev. 30, 980–998. doi:10.1016/j.quascirev.2011.01.016

Jennings, A.E., Knudsen, K.L., Hald, M., Hansen, V., Andrews, J.T., Hansen, C.V., Andrews, J.T., Hansen, V., Andrews, J.T., Hansen, C.V., Andrews, J.T., 2002. A mid-Holocene shift in Arctic sea-ice variability on the East Greenland Shelf. The Holocene 12, 49–58. doi:10.1191/0959683602hl519rp

Jennings, A.E., Weiner, N.J., 1996. Environmental change in eastern Greenland during the last 1300 years: evidence from foraminifera and lithofacies in Nansen Fjord, 68°N. The Holocene 6, 179–191. doi:doi: 10.1177/095968369600600205

Jensen, J.F., Petersen, E.B., Olsen, B., 1999. Sydostbugt Projekter. New Datings of the Paleo-eskimo Settlements in Qeqertarsuup Tunua (Disko Bugt), Greenland. Copenhagen Univ. Archeol. Notes p.2.

Jensen, J.F., 2006. Stone age of Qeqertarsuup Tunua (Disko Bugt) a regional analysis of the Saqqaq and Dorset cultures of central west Greenland. In:, in: Jensen (Ed.), Meddelelser Om Grønland/Monographs on Greenland. Man & Society, vol. 32. Danish Polar Centre, p. 272.

Jensen, K.G., 2003. Holocene hydrographic changes in Greenland coastal waters. Dissertation. Geol. Surv. Denmark Greenland, Denmark.

Jensen, K.G., 2003. Holocene hydrographic changes in Greenland coastal waters: reconstructing environmental change from sub-fossil and contemporary diatoms. Diss. University of Copenhagen.

Jensen, K.G., Kuijpers, A., Koç, N., Heinemeier, J., 2004. Diatom evidence of hydrographic changes and ice conditions in Igaliku Fjord, South Greenland, during the past 1500 years. The Holocene 14, 152–164. doi:10.1191/0959683604hl698rp

Jensen, L.M., Christensen, T.R., 2014. Nuuk Ecological Research Operations, 7 th Annual Report. Aarhus Univ. DCE - Danish Cent. Environ. Energy 94 pp.

Jiang, H., Eiríksson, J., Schulz, M., Knudsen, K.L., Seidenkrantz, M.S., 2005. Evidence for solar forcing of sea-surface temperature on the North Icelandic Shelf during the late Holocene. Geology 33, 73–76. doi:10.1130/G21130.1

Jiang, H., Seidenkrantz, M.S., Knudsen, K.L., Eiríksson, J., 2001. Diatom surface sediment assemblages around Iceland and their relationships to oceanic environmental variables. Mar.

Micropaleontol. 41, 73–96. doi:10.1016/S0377-8398(00)00053-0
Johannessen, O.M., 1986. Brief overview of the physical oceanography, in: Hurdle, B.G. (Ed.), The Nordic Seas. pp. 103–28.
Johannessen, O.M., Bengtsson, L., Alekseev, G. V., Nagurnyi, A.P., Zakharov, V.F., Bobylev, L.P., Petterson, L.H., Hasselmann, K., Cattle, H., 2004. Arctic climate change – observed and modeled temperature and sea ice. Tellus 56A, 328–341. doi:10.1111/j.1600-0870.2004.00060.x
Johannessen, O.M., Shalina, E. V., Miles, M.W., 1999. Satellite Evidence for an Arctic Sea Ice Cover in Transformation. Science. doi:10.1126/science.286.5446.1937
Johns, L., Wraige, E.J., Belt, S.T., Lewis, C.A., Massé, G., Robert, J.M., Rowland, S.J., 1999. Identification of a C25 highly branched isoprenoid (HBI) diene in Antarctic sediments, Antarctic sea-ice diatoms and cultured diatoms. Org. Geochem. 30, 1471–1475. doi:10.1016/S0146-6380(99)00112-6
Johnsen, S.J., Dahl-Jensen, D., Gundestrup, N., Steffensen, J.P., Clausen, H.B., Miller, H., Masson-Delmotte, V., Sveinbjörnsdottir, A.E., White, J., 2001. Oxygen isotope and palaeotemperature records from six Greenland ice-core stations: Camp Century, Dye-3, GRIP, GISP2, Renland and NorthGRIP. J. Quat. Sci. 16, 299–307.
Jones, P.D., Osborn, T.J., Briffa, K.R., 2001. The Evolution of Climate Over the Last Millennium. Science. 292, 662–667.
Jones, P.D., Harpham, C., B.M., W., 2014. Winter-respondingproxy temperature reconstructions and the North Atlantic Oscillation. J. Geophys. Res. Atmos. 119, 6497–6505. doi:10.1002/2014JD021561.Received
Jones, P.D., Mann, M.E., 2004. Climate over past millennia. Rev. Geophys. 42.
Jungclaus, Johann, H., Haak, Helmuth, Latif, Mojib, Mikolajewicz, U., 2005. Arctic – North Atlantic Interactions and Multidecadal Variability of the Meridional. J. Clim. 18, 4013–4031.
Justwan, A., Koç, N., 2008. A diatom based transfer function for reconstructing sea ice concentrations in the North Atlantic. Mar. Micropaleontol. 66, 264–278. doi:10.1016/j.marmicro.2007.11.001
Kanazwa, A., Yoshioka, M., Teshima, S.I., 1971. Occurence of Brassicasteril in Diatoms, Cyclotella-Nana and Nitzschia-Closterium. Bull. Japanese Soc. Sci. Fish. 37, 899.
Kaufman, D.S., Ager, T.A., Anderson, N.J., Anderson, P.M., Andrews, J.T., Bartlein, P.J., Brubaker, L.B., Coats, L.L., Cwynar, L.C., Duvall, M.L., Dyke, A.S., Edwards, M.E., Eisner, W.R., Gajewski, K., Geirsdóttir, A., Hu, F.S., Jennings, A.E., Kaplan, M.R., Kerwin, M.W., Lozhkin, A. V., MacDonald, G.M., Miller, G.H., Mock, C.J., Oswald, W.W., Otto-Bliesner, B.L., Porinchu, D.F., Rühland, K., Smol, J.P., Steig, E.J., Wolfe, B.B., 2004. Holocene thermal maximum in the western Arctic (0-180°W). Quat. Sci. Rev. doi:10.1016/j.quascirev.2003.09.007
Keigwin, L.D., Sachs, J. P., Rosentahl., Y., 2003. A 1600-year history of the Labrador Current off Nova Scotia. Clim. Dyn. 21, 53–62. doi:10.1007/s00382-003-0316-6
Keigwin, L.D., Pickart, R.S., 1999. Slope Water Current over the Laurentian Fan on Interannual to Millennial Time Scales. Science. 286, 520 LP-523.
Kerr, R.A., 2000. A North Atlantic Climate Pacemaker for the Centuries. Science. 288, 1984–1985. doi:10.1126/science.288.5473.1984
Killops, S., Killops, V., 2004. Introduction to Organic Geochemistry. Introd. to Org. Geochemistry. doi:10.1002/9781118697214
Kinnard, C., Zdanowicz, C.M., Fisher, D. A, Isaksson, E., de Vernal, A., Thompson, L.G., 2011.

Reconstructed changes in Arctic sea ice over the past 1,450 years. Nature 479, 509–12. doi:10.1038/nature10581

Kleiven, H.,F., Kissel, C., Laj, C., Ninnemann, U.S., Richter, T.O. and Cortijo, E., 2008. Reduced North Atlantic Deep Water Coeval with the Glacial Lake Agassiz Freshwater Outburst. Science. 319, 60–64.

Knies, J., Cabedo-Sanz, P., Belt, S.T., Baranwal, S., Fietz, S., Rosell-Melé, A., 2014. The emergence of modern sea ice cover in the Arctic Ocean. Nat Commun 5.

Knies, J., Pathirana, I., Cabedo-Sanz, P., Banica, A., Fabian, K., Rasmussen, T.L., Forwick, M., Belt, S.T., 2017. Sea-ice dynamics in an Arctic coastal polynya during the past 6500 years. Arktos 3, 1. doi:10.1007/s41063-016-0027-y

Knudsen, M.F., Riisager, P., Jacobsen, B.H., Muscheler, R., Snowball, I., Seidenkrantz, M.S., 2009. Taking the pulse of the Sun during the Holocene by joint analysis of ^{14}C and10Be. Geophys. Res. Lett. 36, 3–7. doi:10.1029/2009GL039439

Knudsen, M.F., Seidenkrantz, M.-S., Jacobsen, B.H., Kuijpers, A., 2011. Tracking the Atlantic Multidecadal Oscillation through the last 8,000 years. Nat. Commun. 2, 178. doi:10.1038/ncomms1186

Kobashi, T., Menviel, L., Jeltsch-Thömmes, A., Vinther, B.M., Box, J.E., Muscheler, R., Nakaegawa, T., Pfister, P.L., Döring, M., Leuenberger, M., Wanner, H., Ohmura, A., 2017. Volcanic influence on centennial to millennial Holocene Greenland temperature change. Sci. Rep. 7, 1441. doi:10.1038/s41598-017-01451-7

Koç, N., Jansen, E., 1994. Response of the high-latitude Northern Hemisphere to orbital climate forcing: Evidence from the Nordic Seas. Geology 22, 523–526.

Koç, N., Jansen, E., Haflidason, H., 1993. Paleoceanographic reconstructions of surface ocean conditions in the Greenland, Iceland and Norwegian seas through the last 14 ka based on diatoms. Quat. Sci. Rev. 12, 115–140. doi:10.1016/0277-3791(93)90012-B

Koerner, R. M., Fisher, D.A., 2002. Ice-core evidence for widespread Arctic glacier retreat in the Last Interglacial and the early Holocene. Ann. Glaciol. 35, 19–24.

Koerner, R.M., Fisher, D.A., 1990. A record of Holocene summer climate from a Canadian high-Arctic ice core. Nature 343, 630–631.

Koerner, R.M., Fisher, D.A., 2002. Ice-core evidence for widespread Arctic glacier retreat in the Last Interglacial and the early Holocene. Ann. Glaciol. doi:10.3189/172756402781817338

Kolling, H.M., Stein, R., Fahl, K., Perner, K., Moros, M., 2017. Short-term variability in late Holocene sea ice cover on the East Greenland Shelf and its driving mechanisms. Palaeogeogr. Palaeoclimatol. Palaeoecol. 485, 336–350. doi:10.1016/j.palaeo.2017.06.024

Krawczyk, D., Witkowski, A., Moros, M., Lloyd, J., Kuijpers, A., Kierzek, A., 2010. Late-Holocene diatom-inferred reconstruction of temperature variations of the West Greenland Current from Disko Bugt, central West Greenland. The Holocene. doi:10.1177/0959683610371993

Krawczyk, D.W., Witkowski, A., Lloyd, J., Moros, M., Harff, J., Kuijpers, A., 2013. Late-Holocene diatom derived seasonal variability in hydrological conditions off Disko Bay, West Greenland. Quat. Sci. Rev. 67, 93–104. doi:10.1016/j.quascirev.2013.01.025

Krawczyk, D.W., Witkowski, A., Moros, M., Lloyd, J.M., Høyer, J.L., Miettinen, A., Kuijpers, A., 2017. Quantitative reconstruction of Holocene sea ice and sea surface temperature off West Greenland from the first regional diatom data set. Paleoceanography 32, 18–40. doi:10.1002/2016PA003003

Krawczyk, D.W., Witkowski, A., Waniek, J.J., Wroniecki, M., Harff, J., 2014. Description of diatoms from the Southwest to West Greenland coastal and open marine waters. Polar Biol.

doi:10.1007/s00300-014-1546-2
Krawczyk, D.W., Witkowski, A., Wroniecki, M., Waniek, J., Kurzydłowski, K.J., Płociński, T., 2012. Reinterpretation of two diatom species from the West Greenland margin - Thalassiosira kushirensis and Thalassiosira antarctica var. borealis - hydrological consequences. Mar. Micropaleontol. doi:10.1016/j.marmicro.2012.02.004
Kuijpers, A., Mikkelsen, N., 2009. Geological records of changes in wind regime over south Greenland since the Medieval Warm Period: a tentative reconstruction. Polar Rec. (Gr. Brit). 45, 1–8. doi:10.1017/S0032247408007699
Kuijpers, A., Mikkelsen, N., Ribeiro, S., Seidenkrantz, M.-S., 2014. Impact of Medieval Fjord Hydrography and Climate on the Western and Eastern Settlements in Norse Greenland. J. North Atl. 6, 1–13.
Kwok, R., 2004. Fram Strait sea ice outflow. J. Geophys. Res. 109, C01009. doi:10.1029/2003JC001785
Kwok, R., Rothrock, D.A., 1999. Variability of Fram Strait ice flux and North Atlantic Oscillation. J. Geophys. Res. 104, 5177–5189.
Lamb, H.H., 1995. Climate history and the modern world, Second edi. ed. Routledge.
Lamb, H.H., 1977. Climate: Present, past and future. Volume 2. Methuen and Co. Ltd., London.
Lamb, H.H., 1965. The early medieval warm epoch and its sequel. Palaeogeogr. Palaeoclimatol. Palaeoecol. 1, 13–37.
Larsen, N.K., Kjær, K.H., Lecavalier, B., Bjørk, A.A., Colding, S., Huybrechts, P., Jakobsen, K.E., Kjeldsen, K.K., Knudsen, K.L., Odgaard, B. V., Olsen, J., 2015. The response of the southern Greenland ice sheet to the Holocene thermal maximum. Geology. doi:10.1130/G36476.1
Laskar, J., Robutel, P., Joutel, F., Gastineau, M., Correia, A. C.M., Levrard, B., 2004. A long-term numerical solution for the insolation quantities of the Earth. Astron. Astrophys. 428, 261–285.
Latarius, K., Quadfasel, D., 2016. Water mass transformation in the deep basins of the Nordic Seas: Analyses of heat and freshwater budgets. Deep. Res. Part I Oceanogr. Res. Pap. 114, 23–42.
Laxon, S.W., Giles, K.A., Ridout, A.L., Wingham, D.J., Willatt, R., Cullen, R., Kwok, R., Schweiger, A., Zhang, J., Haas, C., Hendricks, S., Krishfield, R., Kurtz, N., Farrell, S., Davidson, M., 2013. CryoSat-2 estimates of Arctic sea ice thickness and volume. Geophys. Res. Lett. 40, 732–737. doi:10.1002/grl.50193
Le Fouest, V., Zakardjian, B., Saucier, F.J., Starr, M., 2005. Seasonal versus synoptic variability in planktonic production in a high-latitude marginal sea: The Gulf of St. Lawrence (Canada). J. Geophys. Res. C Ocean. doi:10.1029/2004JC002423
Leventer, A., 1998. The fate of Antarctic “sea ice diatoms” and their use as paleoenvironmental indicators. Antarct. sea ice Biol. Process. Interact. Var. Antarct. Res. Ser. doi:10.1029/AR073p0121
Levy, L.B., Larsen, N.K., Davidson, T.A., Strunk, A., Olsen, J., Jeppesen, E., 2017. Contrasting evidence of Holocene ice margin retreat, south-western Greenland. J. Quat. Sci. doi:10.1002/jqs.2957
Lisitzin, A.P., 2002. Sea-ice and Iceberg Sedimentation in the Ocean, Recent and Past. Springer, Berlin.
Ljungqvist, F.C., 2010. A new reconstruction of temperature variability in the extra tropical Northern Hemisphere during the last two millennia. Geogr. Ann. Ser. A, Phys. Geogr. 92, 339–351. doi:10.1111/j.1468-0459.2010.00399.x

Lloyd, J., Moros, M., Perner, K., Telford, R.J., Kuijpers, A., Jansen, E., McCarthy, D., 2011. A 100 yr record of ocean temperature control on the stability of Jakobshavn Isbrae, West Greenland. Geology 39, 867–870. doi:10.1130/G32076.1

Loeb, V., Siegel, V., Holm-Hansen, O., Hewitt, R., Fraser, W., Trivelpiece, W., Trivelpiece, S., 1997. Effects of sea-ice extent and krill or salp dominance on the Antarctic food web. Nature 387, 897–900. doi:10.1038/43174

Lundholm, N., Hasle, G.R., 2010. Fragilariopsis (Bacillariophyceae) of the Northern Hemisphere – morphology, taxonomy, phylogeny and distribution, with a description of F. pacifica sp. nov. Phycologia. doi:10.2216/09-97.1

Macdonald, R.W., Sakshaug, E. and Stein, R., 2004. The Arctic Ocean: Modern Status and Recent Climate Change, in: Stein, R., Macdonald, R.W. (Ed.), The Organic Carbon Cycle In The Arctic Ocean. Springer, Berlin Heidelberg New York, pp. 6–20.

Macdonald, R.W., Harner, T., Fyfe, J., Loeng, H., Weingartner, T., 2003. AMAP Assessment 2002: The Influence of Global Change on Contaminant Pathways to, within, and from the Arctic, Arctic Monitoring and Assessment Programme (AMAP).

Manabe, S., Spelman, M.J., Stouffer, R.J., 1992. Transient responses of a coupled ocean-atmosphere model to gradual changes of atmospheric C02, Part II: Seasonal response. J. Clim. 5, 105–126. doi:10.1175/1520-0442(1992)005<0105:TROACO>2.0.CO;2

Mann, Michael E., Zhang, Zhihua, Rutherford, Scott, Bradley, Raymond, S., Hughes, Malcom, K., Shindell, Drew, Ammann, Caspar, Faluvegi, Greg, Ni, F., 2009. Global Signatures and Dynamical Origins of Little Ice Age and Medieval Climate Anomaly. Science. 78, 1256–1260. doi:10.1126/science.1166349

Mann, M.E. and Jones, P.D., 2003: Global surface temperatures over the past two millennia. Geophysical Research Letters, 30: 1820.

Marchal, O., Cacho, I., Stocker, T.F., Grimalt, J.O., Calvo, E., Martrat, B., Shackleton, N., Vautravers, M., Cortijo, E., Van Kreveld, S., Andersson, C., Koç, N., Chapman, M., Sbaffi, L., Duplessy, J.C., Sarnthein, M., Turon, J.L., Duprat, J., Jansen, E., 2002. Apparent long-term cooling of the sea surface in the northeast Atlantic and Mediterranean during the Holocene. Quat. Sci. Rev. 21, 455–483.

Martin, T., Wadhams, P., 1999. Sea-ice flux in the East Greenland Current. Deep Sea Res. Part II Top. Stud. Oceanogr. 46, 1063–1082. doi:https://doi.org/10.1016/S0967-0645(99)00016-8

Maslanik, J.A., Fowler, C., Stroeve, J., Drobot, S., Zwally, J., Yi, D., Emery, W., 2007. A younger, thinner Arctic ice cover: Increased potential for rapid, extensive sea-ice loss. Geophys. Res. Lett. doi:10.1029/2007GL032043

Massé, G., Belt, S.T., Crosta, X., Schmidt, S., Snape, I., Thomas, D.N., Rowland, S.J., 2011. Highly branched isoprenoids as proxies for variable sea ice conditions in the Southern Ocean. Antarct. Sci. 23, 487–498. doi:10.1017/S0954102011000381

Massé, G., Rowland, S.J., Sicre, M.A., Jacob, J., Jansen, E., Belt, S.T., 2008. Abrupt climate changes for Iceland during the last millennium: Evidence from high resolution sea ice reconstructions. Earth Planet. Sci. Lett. 269, 564–568. doi:10.1016/j.epsl.2008.03.017

Matthews, J.,A., Briffa, K.R., 2005. the “Little Ice Age”: Re-Evaluation of an Evolving Concept. Geogr. Ann. Ser. A, Phys. Geogr. 87, 17–36. doi:10.1111/j.0435-3676.2005.00242.x

Matthiessen, J., de Vernal, A., Head, M., Okolodkov, Y., Zonneveld, K., Harland, R., 2005. Modern organic-walled dinoflagellate cysts in Arctic marine environments and their (paleo-) environmental significance. Paläontologische Zeitschrift. doi:10.1007/BF03021752

Mayewski, P.A., Rohling, E.E., Stager, J.C., Karlén, W., Maasch, K.A., Meeker, L.D., Meyerson, E.A., Gasse, F., van Kreveld, S., Holmgren, K., Lee-Thorp, J., Rosqvist, G., Rack, F.,

Staubwasser, M., Schneider, R.R., Steig, E.J., 2004. Holocene climate variability. Quat. Res. 62, 243–255. doi:10.1016/j.yqres.2004.07.001

McGhee, R., 1996. Ancient People of the Arctic. UCB Press, Vancouver.

McGovern, T.H., 1991. Climate, correlation, and causation in Norse Greenland. Arctic Anthropol.

Méheust, M., Fahl, K., Stein, R., 2013. Variability in modern sea surface temperature, sea ice and terrigenous input in the sub-polar North Pacific and Bering Sea: Reconstruction from biomarker data. Org. Geochem. 57, 54–64. doi:10.1016/j.orggeochem.2013.01.008

Meldgaard, M., 2004. Ancient harp seal hunters of Disko Bay: subsistence and settlement at the Saqqaq culture site Qeqertasussuk (2400-1400 BC), west Greenland, Meddelelser om Gronland Man & Society. doi:10.1525/aa.2005.107.3.536.1

Mernild, S.H., Seidenkrantz, M.S., Chylek, P., Liston, G.E., Hasholt, B., 2012. Climate-driven fluctuations in freshwater flux to Sermilik Fjord, East Greenland, during the last 4000 years. Holocene 22, 155–164. doi:10.1177/0959683611431215

Meyers, P.A., 1997. Organic geochemical proxies of paleoceanographic, paleolimnologic, and paleoclimatic processes, in: Organic Geochemistry. doi:10.1016/S0146-6380(97)00049-1

Michel, C., Hamilton, J., Hansen, E., Barber, D., Reigstad, M., Iacozza, J., Seuthe, L., Niemi, A., 2015. Arctic Ocean outflow shelves in the changing Arctic: A review and perspectives. Prog. Oceanogr. 139, 66–88. doi:10.1016/j.pocean.2015.08.007

Miettinen, A., Divine, D., Koç, N., Godtliebsen, F., Hall, I.R., 2012. Multicentennial variability of the sea surface temperature gradient across the subpolar North Atlantic over the last 2.8 kyr. J. Clim. 25, 4205–4219. doi:10.1175/JCLI-D-11-00581.1

Miles, M.W., Divine, D. V, Furevik, T., Jansen, E., Moros, M., Ogilvie, A.E.J., 2014. A signal of persisten Atlantic multidecadal variaibility in Arctic sea ice. Geophys. Res. Lett. 41, 463–469. doi:10.1002/2013GL058084.Received

Miller, G.H., Brigham-Grette, J., Alley, R.B., Anderson, L., Bauch, H.A., Douglas, M.S.V., Edwards, M.E., Elias, S.A., Finney, B.P., Fitzpatrick, J.J., Funder, S.V., Herbert, T.D., Hinzman, L.D., Kaufman, D.S., MacDonald, G.M., Polyak, L., Robock, A., Serreze, M.C. Smol, J.P., Spielhagen, R.F., White, J.W.C., Wolfe, A.P., Wolff, E.W., 2010. Temperature and precipitation history of the Arctic. Quat. Sci. Rev. 29, 1679–1715.

Miller, G.H., Geirsdóttir, Á., Zhong, Y., Larsen, D.J., Otto-Bliesner, B.L., Holland, M.M., Bailey, D.A., Refsnider, K.A., Lehman, S.J., Southon, J.R., Anderson, C., Björnsson, H., Thordarson, T., 2012. Abrupt onset of the Little Ice Age triggered by volcanism and sustained by sea-ice/ocean feedbacks. Geophys. Res. Lett. 39, 1–5. doi:10.1029/2011GL050168

Miller, G.H., Wolfe, A.P., Briner, J.P., Sauer, P.E., Nesje, A., 2005. Holocene glaciation and climate evolution of Baffin Island, Arctic Canada. Quat. Sci. Rev. doi:10.1016/j.quascirev.2004.06.021

Miller, K.R., Chapman, M.R., Andrews, J.E., Koç, N., 2011. Diatom phytoplankton response to Holocene climate change in the Subpolar North Atlantic. Glob. Planet. Change 79, 214–225. doi:10.1016/j.gloplacha.2011.03.001

Moberg, A., Sonechkin, D.M., Holmgren, K., Datsenko, N.M., Karlén, W., 2005. Highly variable Northern Hemisphere temperatures reconstructed from low- and high-resolution proxy data. Nature. doi:10.1038/nature03265

Moros, M., Jensen, K., G., Kuijpers, A., 2006a. Mid- to late-Holocene hydrological and climatic variability in Disko Bugt, central West Greenland. The Holocene 3, 357–367.

Moros, M., Andrews, J.T., Eberl, D.D., Jansen, E., 2006b. Holocene history of drift ice in the

northern North Atlantic: Evidence for different spatial and temporal modes. Paleoceanography 21, 1–10. doi:10.1029/2005PA001214

Moros, M., Emeis, K., Risebrobakken, B., Snowball, I., Kuijpers, A., McManus, J., Jansen, E., 2004. Sea surface temperatures and ice rafting in the Holocene North Atlantic: Climate influences on northern Europe and Greenland. Quat. Sci. Rev. 23, 2113–2126. doi:10.1016/j.quascirev.2004.08.003

Moros, M., Jansen, E., Oppo, D.W., Giraudeau, J., Kuijpers, A, 2012. Reconstruction of the late-Holocene changes in the Sub-Arctic Front position at the Reykjanes Ridge, north Atlantic. Holocene 22, 877–886.

Moros, M., Lloyd, J.M., Perner, K., Krawczyk, D., Blanz, T., de Vernal, A., Ouellet-Bernier, M.M., Kuijpers, A., Jennings, A.E., Witkowski, A., Schneider, R., Jansen, E., 2016. Surface and sub-surface multi-proxy reconstruction of middle to late Holocene palaeoceanographic changes in Disko Bugt, West Greenland. Quat. Sci. Rev. 132, 146–160. doi:10.1016/j.quascirev.2015.11.017

Mugford, R.I., Dowdeswell, J.A., 2010. Modeling iceberg-rafted sedimentation in high-latitude fjord environments. J. Geophys. Res. Earth Surf. 115, 1–21. doi:10.1029/2009JF001564

Müller, J., Massé, G., Stein, R., Belt, S.T., 2009. Variability of sea-ice conditions in the Fram Strait over the past 30,000 years. Nat. Geosci. 2, 772–776. doi:10.1038/ngeo665

Müller, J., Stein, R., 2014. High-resolution record of late glacial and deglacial sea ice changes in Fram Strait corroborates ice-ocean interactions during abrupt climate shifts. Earth Planet. Sci. Lett. 403, 446–455. doi:10.1016/j.epsl.2014.07.016

Müller, J., Wagner, A., Fahl, K., Stein, R., Prange, M., Lohmann, G., 2011. Towards quantitative sea ice reconstructions in the northern North Atlantic: A combined biomarker and numerical modelling approach. Earth Planet. Sci. Lett. 306, 137–148. doi:10.1016/j.epsl.2011.04.011

Müller, J., Werner, K., Stein, R., Fahl, K., Moros, M., Jansen, E., 2012. Holocene cooling culminates in sea ice oscillations in Fram Strait. Quat. Sci. Rev. 47, 1–14. doi:10.1016/j.quascirev.2012.04.024

Murray, J.W., 1991. Ecology and palaeoecology of benthic foraminifera. Longman, London.

Myers, P., Kulan, N., H. Ribergaard, M., 2007. Irminger Water variability in the West Greenland Current, Geophys. Res. Lett. doi:10.1029/2007GL030419

Navarro-Rodriguez, A., Belt, S.T., Knies, J., Brown, T.A., 2013. Mapping recent sea ice conditions in the Barents Sea using the proxy biomarker IP_{25}: Implications for palaeo sea ice reconstructions. Quat. Sci. Rev. 79, 26–39. doi:10.1016/j.quascirev.2012.11.025

Nesje, A., Dahl, S.O., 1993. Lateglacial and Holocene glacier fluctuations and climate variations in western Norway: A review. Quat. Sci. Rev. 12, 255–261. doi:10.1016/0277-3791(93)90081-V

Nesje, A., Dahl, S.O., 2003. The “Little Ice Age” - only temperature? The Holocene 13, 139–145. doi:10.1191/0959683603hl603fa

Nesje, A., Lie, Ø., Dahl, S.O., 2000. Is the North Atlantic Oscillation reflected in Scandinavian glacier mass balance records? J. Quat. Sci. 15, 587–601.

Nesje, A., Matthews, J.A., Dahl, O., Berrisford, M.S., Andersson, C., 2001. Holocene glacier fluctuations of Flatebreen and winter-precipitation changes in the Jostedalsbreen region, western Norway, based on glaciolacustrine sediment records. The Holocene 11, 267–280. doi:10.1191/095968301669980885

NGRIP-Members, 2004. High-resolution record of Northern Hemisphere climate extending into the last interglacial period. Nature 431, 147–151.

Nichols, P.D., Jones, G.J., De Leeuw, J.W., Johns, R.B.B., 1984. The fatty acid and sterol

composition of two marine dinoflagellates. Phytochemistry. doi:10.1016/S0031-9422(00)82605-9

Nielsen, N., Humlum, O., Hansen, B.U., 2001. Meteorological Observations in 2000 at the Arctic Station, Qeqertarsuaq (69°15'N), Central West Greenland. Geogr. Tidsskr. J. Geogr. doi:10.1080/00167223.2001.10649458

Nørgaard-Pedersen, N., Mikkelsen, N., 2009. 8000 year marine record of climate variability and fjord dynamics from Southern Greenland. Mar. Geol. 264, 177–189. doi:10.1016/j.margeo.2009.05.004

Nöthig, E.M., Bracher, A., Engel, A., Metfies, K., Niehoff, B., Peeken, I., Bauerfeind, E., Cherkasheva, A., Gäbler-Schwarz, S., Hardge, K., Kilias, E., Kraft, A., Kidane, Y.M., Lalande, C., Piontek, J., Thomisch, K., Wurst, M., 2015. Summertime plankton ecology in fram strait-a compilation of long-and short-term observations. Polar Res. 34. doi:10.3402/polar.v34.23349

O'Brien, S.R., Mayewski, P.A., Meeker, L.D., Meese, D.A., Twickler, M.S., Whitlow, S.I., 1995. Complexity of Holocene Climate as Reconstructed from a Greenland Ice Core. Science. 270, 1962–1964. doi:10.1126/science.270.5244.1962

Ogilvie, A., 1996. Sea-ice conditions off the coasts of Iceland A. D. 1601-1850 with special reference to part of the Maunder Minimum period (1675-1715), AmS-Varia.

Olsen, J., Anderson, N.J., Knudsen, M.F., 2012. Variability of the North Atlantic Oscillation over the past 5,200 years. Nat. Geosci. 5, 1–14.

Ortega, P., Lehner, F., Swingedouw, D., Masson-Delmotte, V., Raible, C.C., Casado, M., Yiou, P., 2015. A model-tested North Atlantic Oscillation reconstruction for the past millennium. Nature 523, 71–74. doi:10.1038/nature14518

Ouellet-Bernier, M.M., de Vernal, A, Hillaire-Marcel, C., Moros, M., 2014. Paleoceanographic changes in the Disko Bugt area, West Greenland, during the Holocene. Holocene 24, 1573–1583. doi:10.1177/0959683614544060

Paillard, D., Labeyrie, L., Yiou, P., 1996. Macintosh Program performs time-series analysis. Eos, Trans. Am. Geophys. Union 77, 379. doi:10.1029/96EO00259

Parkinson, C.L., 2008. Satellite passive-microwave measurements of sea ice, in: Steele, H.,J., Thorpe, A.S., Turekian, K.K. (Ed.), Encyclopedia of Ocean Sciences. Academic Press, Oxford, pp. 80–90.

Parkinson, C.L., 2014. Global Sea Ice Coverage from Satellite Data: Annual Cycle and 35-Yr Trends. J. Clim. 27, 9377–9382. doi:10.1175/JCLI-D-14-00605.1

Parkinson, C.L., Cavalieri, D.J., Gloersen, P., Zwally, H.J., Comiso, J.C., 1999. Arctic sea ice extents, areas, and trends, 1978-1996. J. Geophys. Res. C Ocean. doi:10.1029/1999JC900082

Peristykh, A.N., Damon, P.E., 2003. Persistence of the Gleissberg 88-year solar cycle over the last ~12,000 years : Evidence from cosmogenic isotopes 108, 1–15. doi:10.1029/2002JA009390

Perner, K., Jennings, A.E., Moros, M., Andrews, J.T., Wacker, L., 2016. Interaction between warm Atlantic-sourced waters and the East Greenland Current in northern Denmark Strait (68 ° N) during the last 10 600 cal a BP. J. Quat. Sci. 31, 472–483. doi:10.1002/jqs.2872

Perner, K., Moros, M., Jansen, E., Kuijpers, A., Troelstra, S.R., Prins, M.A., 2018. Subarctic Front migration at the Reykjanes Ridge during the mid- to late Holocene: Evidence from planktic foraminifera. Boreas. doi:10.1111/bor.12263

Perner, K., Moros, M., Jennings, A.E., Lloyd, J.M., Knudsen, K.L., 2013. Holocene palaeoceanographic evolution off West Greenland. The Holocene 23, 374–387.

doi:10.1177/0959683612460785
Perner, K., Moros, M., Lloyd, J.M., Jansen, E., Stein, R., 2015. Mid to late Holocene strengthening of the East Greenland Current linked to warm subsurface Atlantic water. Quat. Sci. Rev. 129, 296–307. doi:10.1016/j.quascirev.2015.10.007
Perner, K., Moros, M., Lloyd, J.M., Kuijpers, A., Telford, R.J., Harff, J., 2011. Centennial scale benthic foraminiferal record of late Holocene oceanographic variability in Disko Bugt, West Greenland. Quat. Sci. Rev. 30, 2815–2826. doi:10.1016/j.quascirev.2011.06.018
Perovich, D.K., Grenfell, T.C., Light, B., Elder, B.C., Harbeck, J., Polashenski, C., Tucker, W.B., Stelmach, C., 2009. Transpolar observations of the morphological properties of Arctic sea ice. J. Geophys. Res. Ocean. 114, n/a-n/a. doi:10.1029/2008JC004892
Perrette, M., Yool, A., Quartly, G.D., Popova, E.E., 2011. Near-ubiquity of ice-edge blooms in the Arctic. Biogeosciences. doi:10.5194/bg-8-515-2011
Petersen, 2011. DMI, 2012-Danish Meteorological Institute and National snow and ice data Center, in: Underhill, V., Fetterer, F. (Ed.), Arctic Sea Ice Charts from Danish Meteorological Institute. Boulder, Colorado, p. 18931995. doi:http://dx.doi.org/10.7265/N56D5QXC.
Petrich, C., Eicken, H., 2010. Growth, Structure and Properties of Sea Ice, in: Thomas, D.N., Dieckmann, G.S. (Ed.), Sea Ice. Wiley-Blackwell, Oxford, UK, pp. 23–78. doi:10.1002/9781444317145.ch2
Pfirman, S.L., Kogeler, J., Anselme, B., 1995. Coastal environments of the western Kara and eastern Barents Seas. Deep Sea Res. Part II Top. Stud. Oceanogr. 42, 1391–1412.
Pflaumann, U., Sarnthein, M., Chapman, M., d'Abreu, L., Funnell, B., Huels, M., Kiefer, T., Maslin, M., Schulz, H., Swallow, J., van Kreveld, S., Vautravers, M., Vogelsang, E., Weinelt, M., 2003. Glacial North Atlantic: Sea-surface conditions reconstructed by GLAMAP 2000. Paleoceanography 18, n/a-n/a. doi:10.1029/2002PA000774
Pieńkowski, A.J., Gill, N.K., Furze, M.F.A., Mugo, S.M., Marret, F., Perreaux, A., 2017. Arctic sea-ice proxies: comparisons between biogeochemical and micropalaeontological reconstructions in a sediment archive from Arctic Canada. The Holocene 27, 665–682. doi:10.1177/0959683616670466
Pisaric, M.F.J., MacDonald, G.M., Velichko, A.A., Cwynar, L.C., 2001. The Lateglacial and Postglacial vegetation history of the northwestern limits of Beringia, based on pollen, stomate and tree stump evidence. Quat. Sci. Rev. 20, 235–245. doi:10.1016/S0277-3791(00)00120-7
Pollehne, F., 2015. Short Cruise Report Maria S. Merian MSM 46 Halifax - 25.08.2015 St. John's – 26.09.2015. https://www.ldf.uni-hamburg.de/merian/wochenberichte/wochenberichte-merian/msm44-msm46/msm46-scr.pdf
Polyak, L., Andrews, J.T., Brigham-Grette, J., Darby, D., Funder, S., Holland, M., Jennings, A., Savelle, J., Serreze, M., Wolff, E., 2009. History of Arctic sea ice. In: Past Climate Variability and Change in the Arctic and at High Latitudes. A Rep. by U.S. Clim. Chang. Sci. Progr. Subcomm. Glob. Chang. Res. U.S. Geol. Surv. Reston, VA, 159–184.
Polyak, L., Alley, R.B., Andrews, J.T., Brighamgrette, J., Cronin, T.M., Darby, D.A., Dyke, A.S., Fitzpatrick, J.J., Funder, S., Holland, M., Jennings, A.E., Miller, G.H., Regan, M.O., Savelle, J., Serreze, M., St, K., White, J.W.C., Wolff, E., 2010. History of sea ice in the Arctic. Quat. Sci. Rev. 29, 1757–1778. doi:10.1016/j.quascirev.2010.02.010
Polyak, L., Mikhailov, V., 1996. Post-glacial environments of the southeastern Barents Sea: foraminiferal evidence. Geol. Soc. London, Spec. Publ. doi:10.1144/GSL.SP.1996.111.01.21

Porter, S.C., Denton, G.H., 1967. Chronology of neoglaciation in the North American Cordillera. Am. J. Sci. 265, 177–210. doi:10.2475/ajs.265.3.177

Portis, D.H., Walsh, J.E., El Hamly, M., Lamb, P.J., 2001. Seasonality of the North Atlantic Oscillation. J. Clim. doi:10.1175/1520-0442(2001)014<2069:SOTNAO>2.0.CO;2

Potvin, É., Rochon, A., Lovejoy, C., 2013. Cyst-theca relationship of the arctic dinoflagellate cyst Islandinium minutum (Dinophyceae) and phylogenetic position based on SSU rDNA and LSU rDNA. J. Phycol. doi:10.1111/jpy.12089

Poulin, M., Daugbjerg, N., Gradinger, R., Ilyash, L., Ratkova, T., von Quillfeldt, C., 2011. The pan-Arctic biodiversity of marine pelagic and sea-ice unicellular eukaryotes: a first-attempt assessment. Mar. Biodivers. 41, 13–28. doi:10.1007/s12526-010-0058-8

Prahl, F. G., Muehlhausen, L.A., 1989. Lipid biomarkers as geochemical tools for paleoceanographic study. Product. Ocean Present past 27, 1–289.

Prange, M., Lohmann, G., 2003. Effects of mid-Holocene river runoff on the Arctic ocean/sea-ice system: a numerical model study. The Holocene. doi:10.1191/0959683603hl626rp

Radi, T., de Vernal, A., 2008. Dinocysts as proxy of primary productivity in mid–high latitudes of the Northern Hemisphere. Mar. Micropaleontol. 68, 84–114. doi:https://doi.org/10.1016/j.marmicro.2008.01.012

Ran, L., Jiang, H., Knudsen, K.L., Eiríksson, J., Gu, Z., 2006. Diatom response to the Holocene climatic optimum on the North Icelandic shelf. Mar. Micropaleontol. doi:10.1016/j.marmicro.2006.05.002

Randall, D., Curry, J., Battisti, D., Flato, G., Grumbine, R., Häkkinen, S., Martinson, D., Preller, R., Walsh, J., Weatherly, J., 1998. Status of and outlook for large-scale modeling of atmosphere-ice-ocean interactions in the Arctic. . Bull. Am. Meteorol. Soc. 79, 197–219.

Rasmussen, S.O., Andersen, K.K., Svensson, A.M., Steffensen, J.P., Vinther, B.M., Clausen, H.B., Siggaard-Andersen, M.L., Johnsen, S.J., Larsen, L.B., Dahl-Jensen, D., Bigler, M., Röthlisberger, R., Fischer, H., Goto-Azuma, K., Hansson, M.E., Ruth, U., 2006. A new Greenland ice core chronology for the last glacial termination. J. Geophys. Res. Atmos. doi:10.1029/2005JD006079

Rasmussen, T.L., Thomsen, E., Ślubowska, M.A., Jessen, S., Solheim, A., Koç, N., 2007. Paleoceanographic evolution of the SW Svalbard margin (76°N) since 20,000 14C yr BP. Quat. Res. doi:10.1016/j.yqres.2006.07.002

Rayner, N.A., Parker, D.E., Horton, E.B., Folland, C.K., Alexander, L. V, Rowell, D.P., Kent, E.C., Kaplan, A., 2003. Global analyses of sea surface temperature, sea ice, and night marine air temperature since the late nineteenth century. J. Geophys. Res. Atmos. 108, n/a-n/a. doi:10.1029/2002JD002670

Reimer, P.J., Baillie, M.G.L., Bard, E., Bayliss, A., Beck, J.W., Blackwell, P.G., Bronk Ramsey, C., Buck, C.E., Burr, G.S., Edwards, R.L., Friedrich, M., Grootes, P.M., Guilderson, T.P., Hajdas, I., Heaton, T.J., Hogg, A. G., Hughen, K. a., Kaiser, K.F., Kromer, B., McCormac, F.G., Manning, S.W., Reimer, R.W., Richards, D. a., Southon, J.R., Talamo, S., Turney, C.S.M., van der Plicht, J., Weyhenmeyer, C.E., 2009. INTCAL 09 and MARINE09 aadiocarbon age calibration curves, 0-50,000 years Cal BP. Radiocarbon. doi:10.2458/azu_js_rc.51.3569

Renssen, H., Goosse, H., Muscheler, R., 2006. Coupled climate model simulation of Holocene cooling events: oceanic feedback amplifies solar forcing. Clim. Past. doi:10.5194/cp-2-79-2006

Renssen, H., Seppä, H., Crosta, X., Goosse, H., Roche, D.M., 2012. Global characterization of the Holocene Thermal Maximum. Quat. Sci. Rev. 48, 7–19.

doi:10.1016/j.quascirev.2012.05.022
Ribeiro, S., Moros, M., Ellegaard, M., Kuijpers, A., 2012. Climate variability in West Greenland during the past 1500 years: Evidence from a high-resolution marine palynological record from Disko Bay. Boreas 41, 68–83. doi:10.1111/j.1502-3885.2011.00216.x
Rignot, E., Koppes, M., Velicogna, I., 2010. Rapid submarine melting of the calving faces of West Greenland glaciers. Nat. Geosci. doi:10.1038/ngeo765
Rigor, I.G., Wallace, J.M., Colony, R.L., 2002. Response of sea ice to the Arctic Oscillation. J. Clim. 15, 2648–2663.
Risebrobakken, B., 2003. A high-resolution study of Holocene paleoclimatic and paleoceanographic changes in the Nordic Seas. Paleoceanography 18, 1017.
Risebrobakken, B., Dokken, T., Smedsrud, L.H., Andersson, C., Jansen, E., Moros, M., Ivanova, E. V., 2011. Early Holocene temperature variability in the Nordic Seas: The role of oceanic heat advection versus changes in orbital forcing. Paleoceanography. doi:10.1029/2011PA002117
Risebrobakken, B., Moros, M., Ivanova, E. V., Chistyakova, N., Rosenberg, R., 2010. Climate and oceanographic variability in the SW Barents Sea during the Holocene. The Holocene. doi:10.1177/0959683609356586
Rochon, A. , Vernal, A. d. , Turon, J. L. , Matthießen, J., Head, M.J., 1999. Distribution of recent dinoflagellate cysts in surface sediments from the North Atlantic Ocean and adjacent seas in relation to sea-surface parameters. Am. Assoc. Stratigr. Palynol. Contrib. Ser. 35, 1–146.
Rogers, J.C., 1984. The Association between the North Atlantic Oscillation and the Southern Oscillation in the Northern Hemisphere. Mon. Weather Rev. doi:10.1175/1520-0493(1984)112<1999:TABTNA>2.0.CO;2
Rohling, E.J., Pälike, H., 2005. Centennial-scale climate cooling with a sudden cold event around 8,200 years ago. Nature. doi:10.1038/nature03421
Roncaglia, L., Kuijpers, A., 2004. Palynofacies analysis and organic-walled dinoflagellate cysts in late-Holocene sediments from Igaliku Fjord, South Greenland. The Holocene. doi:10.1191/0959683604hl700rp
Rontani, J.F., Charrière, B., Sempéré, R., Doxaran, D., Vaultier, F., Vonk, J.E., Volkman, J.K., 2014. Degradation of sterols and terrigenous organic matter in waters of the Mackenzie Shelf, Canadian Arctic. Org. Geochem. doi:10.1016/j.orggeochem.2014.06.002
Rothrock, D. A., Y. Yu, Maykut, G.A., 1999. Thinning of Arctic sea- ice,. Geophys. Res. Lett. 26, 3469–3472.
Rowland, S.J., Allard, W.G., Belt, S.T., Massé, G., Robert, J.M., Blackburn, S., Frampton, D., Revill, A.T., Volkman, J.K., 2001. Factors influencing the distributions of polyunsaturated terpenoids in the diatom, Rhizosolenia setigera. Phytochemistry 58, 717–728. doi:10.1016/S0031-9422(01)00318-1
Rowland, S.J., Robson, J.N., 1990. The widespread occurrence of highly branched acyclic C_{20}, C_{25} and C_{30} hydrocarbons in recent sediments and biota—A review. Mar. Environ. Res. 30, 191–216. doi:https://doi.org/10.1016/0141-1136(90)90019-K
Rudels, B., Anderson, L.G., Jones, E.P., 1996. Formation and evolution of the surface mixed layer and halocline of the Arctic Ocean. J. Geophys. Res. 101, 8807–8821.
Rudels, B., Björk, G., Nilsson, J., Winsor, P., Lake, I., Nohr, C., 2005. The interaction between waters from the Arctic Ocean and the Nordic Seas north of Fram Strait and along the East Greenland Current: Results from the Arctic Ocean-02 Oden expedition. J. Mar. Syst. 55, 1–30. doi:10.1016/j.jmarsys.2004.06.008
Rudels, B., Meyer, R., Fahrbach, E., Ivanov, V. V., Østerhus, S., Quadfasel, D., Schauer, U.,

Tverberg, V., Woodgate, R.A., 2000. Water mass distribution in Fram Strait and over the Yermak Plateau in summer 1997. Ann. Geophys. 18, 0687–0705.

Rudels, B., Quadfasel, D., 1991. Convection and deep water formation in the Arctic Ocean-Greenland Sea System. J. Mar. Syst. doi:10.1016/0924-7963(91)90045-V

Ruzmaikin, A., Feynman, J., Jiang, X., Noone, D.C., Waple, A.M., Yung, Y.L., 2004. The pattern of northern hemisphere surface air temperature during prolonged periods of low solar output. Geophys. Res. Lett. 31, 2–5. doi:10.1029/2004GL019955

Rytter F, Knudsen K-L, Seidenkrantz M-S., Eiríksson, J., 2002. Modern distribution on benthic foraminifera on the North Icelandic shelf and slope. J. Foraminifer. Res. 32, 217–244.

Saabye, H.E., 1942. Brudstykker af en Dagbog holden i Grönland i Aarene 1770–1778. Meddelelser om Grønland 129.

Sakshaug, E., 2004. Primary and secondary production in the Arctic Seas, in: Stein, R., Macdonald, R.W. (Eds.), The Organic Carbon Cycle in the Arctic Ocean. pp. 57–81. doi:10.1007/978-3-642-18912-8

Sarnthein, M., 2003a. Past extent of sea ice in the northern North Atlantic inferred from foraminiferal paleotemperature estimates. Paleoceanography 18. doi:10.1029/2002PA000771

Sarnthein, M., Van Kreveld, S., Erlenkeuser, H., Grootes, P.M., Kucera, M., Pflauman, U., Schulz, M., 2003b. Centennial-to-millennial-scale periodicities of Holocene climate and sediment injections off the western Barents shelf, 75°N. Boreas 32, 447–461. doi:10.1111/j.1502-3885.2003.tb01227.x

Schauer, U., Muench, R.D., Rudels, B., Timokhov, L., 1997. Impact of Eastern Arctic shelf waters on the Nansen Basin intermediate layers. J. Geophys. Res. 102, 3371–3382.

Schiltzer, R., 2017. Ocean Data View. https://odv.awi.de

Schmith, T., Hansen, C., 2003. Fram strait ice export during the nineteenth and twentieth centuries reconstructed from a multiyear sea ice index from southwestern Greenland. J. Clim. 16, 2782–2791. doi:10.1175/1520-0442(2003)016<2782:FSIEDT>2.0.CO;2

Schröder-Adams, C.J., Mudie, P.J., Cole, F.E., Medioli, F.S., 1990. Late Holocene benthic formainifera beneath perennial sea ice on an Arctic continental shelf. Mar. Geol. doi:10.1016/0025-3227(90)90085-X

Schulz, M., Paul, A., Timmermann, A., 2004. Glacial-interglacial contrast in climate variability at centennial-to-millennial timescales: Observations and conceptual model, in: Quaternary Science Reviews. doi:10.1016/j.quascirev.2004.08.014

Schweinsberg, A.D., Briner, J.P., Miller, G.H., Bennike, O., Thomas, E.K., 2017. Local glaciation in West Greenland linked to North Atlantic ocean circulation during the Holocene. Geology 45, 195–198. doi:10.1130/G38114.1

Scott, D.B., Schell, T., Rochon, A., Blasco, S., 2008. Benthic foraminifera in the surface sediments of the Beaufort Shelf and slope, Beaufort Sea, Canada: Applications and implications for past sea-ice conditions. J. Mar. Syst. doi:10.1016/j.jmarsys.2008.01.008

Scott, D.B., Schell, T., St-Onge, G., Rochon, A., Blasco, S., 2009. Foraminiferal assemblage changes over the last 15,000 years on the Mackenzie-Beaufort Sea Slope and Amundsen Gulf, Canada: Implications for past sea ice conditions. Paleoceanography. doi:10.1029/2007PA001575

Screen, J.A., Simmonds, I., 2010. The central role of diminishing sea ice in recent Arctic temperature amplification. Nature 464, 1334–1337.

Seidenkrantz, M.-S., Aagaard-Sørensen, S., Sulsbrück, H., Kuijpers, A., Jensen, K.G., Kunzendorf, H., 2007a. Hydrography and climate of the last 4400 years in a SW Greenland

fjord: implications for Labrador Sea palaeoceanography. The Holocene. doi:10.1177/0959683607075840

Seidenkrantz, M.-S., Aagaard-Sorensen, S., Sulsbruck, H., Kuijpers, A., Jensen, K.G., Kunzendorf, H., 2007b. Hydrography and climate of the last 4400 years in a SW Greenland fjord: implications for Labrador Sea palaeoceanography. The Holocene 17, 387–401. doi:10.1177/0959683607075840

Seidenkrantz, M.S., 2013. Benthic foraminifera as palaeo sea-ice indicators in the subarctic realm - examples from the Labrador Sea-Baffin Bay region. Quat. Sci. Rev. 79, 135–144. doi:10.1016/j.quascirev.2013.03.014

Seidenkrantz, M.S., Roncaglia, L., Fischel, A., Heilmann-Clausen, C., Kuijpers, A., Moros, M., 2008. Variable North Atlantic climate seesaw patterns documented by a late Holocene marine record from Disko Bugt, West Greenland. Mar. Micropaleontol. 68, 66–83. doi:10.1016/j.marmicro.2008.01.006

Sejrup, H.P., Birks, H.J.B., Klitgaard Kristensen, D., Madsen, H., 2004. Benthonic foraminiferal distributions and quantitative transfer functions for the northwest European continental margin. Mar. Micropaleontol. 53, 197–226. doi:https://doi.org/10.1016/j.marmicro.2004.05.009

Sejrup, H.P., Lehman, S.J., Haflidason, H., Noone, D., Muscheler, R., Berstad, I.M., Andrews, J.T., 2010. Response of Norwegian Sea temperature to solar forcing since 1000 A.D. J. Geophys. Res. Ocean. 115, 1–10. doi:10.1029/2010JC006264

Seppä, H., Birks, H.J.B., 2002. Holocene climate reconstructions from the fennoscandian tree-line area based on pollen data from Toskaijavri. Quat. Res. 57, 191–199. doi:10.1006/qres.2001.2313

Serreze, M.C., Barry, R.G., 2011. Processes and impacts of Arctic amplification: A research synthesis. Glob. Planet. Change 77, 85–96.

Serreze, M.C., Holland, M., Stroeve, J.C., 2007. Perspectives on the Arctic's shrinking sea-ice cover. Science. doi:10.1126/science.1139426

Sha, L., Jiang, H., Knudsen, K.L., 2012. Diatom evidence of climatic change in Holsteinsborg Dyb, west of Greenland, during the last 1200 years. The Holocene 22, 347–358. doi:10.1177/0959683611423684

Sha, L., Jiang, H., Seidenkrantz, M.S., Knudsen, K.L., Olsen, J., Kuijpers, A., Liu, Y., 2014. A diatom-based sea-ice reconstruction for the Vaigat Strait (Disko Bugt, West Greenland) over the last 5000yr. Palaeogeogr. Palaeoclimatol. Palaeoecol. 403, 66–79. doi:10.1016/j.palaeo.2014.03.028

Sha, L., Jiang, H., Seidenkrantz, M.S., Li, D., Andresen, C.S., Knudsen, K.L., Liu, Y., Zhao, M., 2017. A record of Holocene sea-ice variability off West Greenland and its potential forcing factors. Palaeogeogr. Palaeoclimatol. Palaeoecol. 475, 115–124. doi:10.1016/j.palaeo.2017.03.022

Sha, L., Jiang, H., Seidenkrantz, M.S., Muscheler, R., Zhang, X., Knudsen, M.F., Olsen, J., Knudsen, K.L., Zhang, W., 2016. Solar forcing as an important trigger for West Greenland sea-ice variability over the last millennium. Quat. Sci. Rev. 131, 148–156. doi:10.1016/j.quascirev.2015.11.002

Shemesh, A., Burckle, L.H., Froelich, P.N., 1989. Dissolution and preservation of Antarctic diatoms and the effect on sediment thanatocoenoses. Quat. Res. doi:10.1016/0033-5894(89)90010-0

Sicre, M.A., Jacob, J., Ezat, U., Rousse, S., Kissel, C., Yiou, P., Eiríksson, J., Knudsen, K.L., Jansen, E., Turon, J.L., 2008. Decadal variability of sea surface temperatures off North

Iceland over the last 2000 years. Earth Planet. Sci. Lett. 268, 137–142. doi:10.1016/j.epsl.2008.01.011

Sigl, M., Winstrup, M., McConnell, J.R., Welten, K.C., Plunkett, G., Ludlow, F., Büntgen, U., Caffee, M., Chellman, N., Dahl-Jensen, D., Fischer, H., Kipfstuhl, S., Kostick, C., Maselli, O.J., Mekhaldi, F., Mulvaney, R., Muscheler, R., Pasteris, D.R., Pilcher, J.R., Salzer, M., Schüpbach, S., Steffensen, J.P., Vinther, B.M., Woodruff, T.E., 2015. Timing and climate forcing of volcanic eruptions for the past 2,500 years. Nature. doi:10.1038/nature14565

Ślubowska-Woldengen, M., Rasmussen, T.L., Koç, N., Klitgaard-Kristensen, D., Nilsen, F., Solheim, A., 2007. Advection of Atlantic Water to the western and northern Svalbard shelf since 17,500 cal yr BP. Quat. Sci. Rev. doi:10.1016/j.quascirev.2006.09.009

Smik, L., Belt, S.T., 2017. Distributions of the Arctic sea ice biomarker proxy IP_{25} and two phytoplanktonic biomarkers in surface sediments from West Svalbard. Org. Geochem. 105, 39–41. doi:10.1016/j.orggeochem.2017.01.005

Smik, L., Cabedo-Sanz, P., Belt, S.T., 2016. Semi-quantitative estimates of paleo Arctic sea ice concentration based on source-specific highly branched isoprenoid alkenes: A further development of the PIP_{25} index. Org. Geochem. 92, 63–69. doi:10.1016/j.orggeochem.2015.12.007

Solanki, S.K., Usoskin, I.G., Kromer, B., Schussler, M., Beer, J., 2004. Unusual activity of the Sun during recent decades compared to the previous 11,000 years. Nature 431, 1084–1087.

Solignac, S., De Vernal, A., Hillaire-Marcel, C., 2004. Holocene sea-surface conditions in the North Atlantic - Contrasted trends and regimes in the western and eastern sectors (Labrador Sea vs. Iceland Basin). Quat. Sci. Rev. 23, 319–334. doi:10.1016/j.quascirev.2003.06.003

Solomina, O.N., Bradley, R.S., Hodgson, D.A., Ivy-ochs, S., Jomelli, V., Mackintosh, A.N., Nesje, A., Owen, L.A., Wanner, H., Wiles, G.C., Young, N.E., 2015. Holocene glacier fluctuations. Quat. Sci. Rev. 111, 9–34. doi:10.1016/j.quascirev.2014.11.018

Spielhagen, R.F., Baumann, K.-H., Erlenkeuser, H., Nowaczyk, N.R., Nørgaard-Pedersen, N., Vogt, C., Weiel, D., 2004. Arctic Ocean deep-sea record of northern Eurasian ice sheet history. Quat. Sci. Rev. 23, 1455–1483. doi:https://doi.org/10.1016/j.quascirev.2003.12.015

Spielhagen, R.F., Erlenkeuser, H., Siegert, C., 2005. History of freshwater runoff across the Laptev Sea (Arctic) during the last deglaciation. Glob. Planet. Change. doi:10.1016/j.gloplacha.2004.12.013

Spielhagen, R.F., Werner, K., Sørensen, S.A., Zamelczyk, K., Kandiano, E., Budeus, G., Husum, K., Marchitto, T.M., Hald, M., 2011. Enhanced modern heat transfer to the Arctic by warm Atlantic Water. Science 331, 450–453.

Stein, R., 2008. Arctic Ocean Sediments: Processes, Proxies, and Paleoenvironment. (Vol. 2). Elsevier.

Stein, R., Macdonald, R.W., 2004. The Organic Carbon Cycle in the Arctic Ocean. Springer, Berlin.

Stein, R., 2016. The Expedition PS93.1 of the Research Vessel POLARSTERN to the Greenland Sea and the Fram Strait in 2015. Berichte zur Polar- und Meeresforschung 2016. doi:10.2312/BzPM_0702_2016

Stein, R., 2015. The Expedition PS87 of the Research Vessel POLARSTERN to the Arctic Ocean in 2014. Berichte zur Polar- und Meeresforschung.

Stein, R., Boucsein, B., Fahl, K., Garcia de Oteyza, T., Knies, J., Niessen, F., 2001. Accumulation of particulate organic carbon at the Eurasian continental margin during late Quaternary times: Controlling mechanisms and paleoenvironmental significance. Glob. Planet. Change. doi:10.1016/S0921-8181(01)00114-X

Stein, R., Fahl, K., 2013. Biomarker proxy shows potential for studying the entire Quaternary Arctic sea ice history. Org. Geochem. 55, 98–102. doi:10.1016/j.orggeochem.2012.11.005

Stein, R., Fahl, K., Gierz, P., Niessen, F., Lohmann, G., 2017a. Arctic Ocean sea ice cover during the penultimate glacial and the last interglacial. Nat. Commun. 8, 373. doi:10.1038/s41467-017-00552-1

Stein, R., Fahl, K., Müller, J., 2012. Proxy reconstruction of Cenozoic Arctic Ocean sea-ice history - From IRD to IP_{25}-. Polarforschung 82, 37–71.

Stein, R., Fahl, K., Schade, I., Manerung, A., Wassmuth, S., Niessen, F., Nam, S. Il, 2017b. Holocene variability in sea ice cover, primary production, and Pacific-Water inflow and climate change in the Chukchi and East Siberian Seas (Arctic Ocean). J. Quat. Sci. 32, 362–379. doi:10.1002/jqs.2929

Stein, R., Fahl, K., Schreck, M., Knorr, G., Niessen, F., Forwick, M., Gebhardt, C., Jensen, L., Kaminski, M., Kopf, A., Matthiessen, J., Jokat, W., Lohmann, G., 2016. Evidence for ice-free summers in the late Miocene central Arctic Ocean. Nat. Commun. 7, 11148.

Stein, R., Nam, S.-I., Schubert, G., Voqt, C., Fütterer, D., Heinemeier, J., 1994. The last deglaciation event in the Eastern central Arctic Ocean. Science. 264, 5159.

Stine, S., 1994. Extreme and persistent drought in California and Patagonia during mediaeval time. Nature 369, 546–549. doi:10.1038/369546a0

Stoynova, V., Shanahan, T.M., Hughen, K.A., de Vernal, A., 2013. Insights into Circum-Arctic sea ice variability from molecular geochemistry. Quat. Sci. Rev. 79, 63–73. doi:10.1016/j.quascirev.2012.10.006

Stroeve, J., Holland, M.M., Meier, W., Scambos, T., Serreze, M., 2007. Arctic sea ice decline: Faster than forecast. Geophys. Res. Lett. 34, 1–5. doi:10.1029/2007GL029703

Stroeve, J.C., Serreze, M.C., Holland, M.M., Kay, J.E., Malanik, J., Barrett, A.P., 2012. The Arctic's rapidly shrinking sea ice cover: A research synthesis. Clim. Change. doi:10.1007/s10584-011-0101-1

Stuiver, M., 1961. Variations in radiocarbon concentration and sunspot activity. J. Geophys. Res. 66.

Stuiver, M., Grootes, P.M., 2000. GISP2 Oxygen Isotope Ratios. Quat. Res. 53, 277–284. doi:DOI: 10.1006/qres.2000.2127

Stuiver, M., Grootes, P.M., Braziunas, T.F., 1995. The GISP2 $\delta^{18}O$ Climate Record of the Past 16,500 Years and the Role of the Sun, Ocean, and Volcanoes. Quat. Res. doi:10.1006/qres.1995.1079

Summons, R.E., Capon, R.J., Stranger, C., Barrow, R.A., 1993. The structure of a new C_{25} isoprenoid alkene biomarker from diatomaceous microbial communities. Aust. J. Chem. doi:10.1071/CH9930907

Sundby, S., Drinkwater, K., 2007. On the mechanisms behind salinity anomaly signals of the northern North Atlantic. Prog. Oceanogr. 73, 190–202.

Svendsen, J.I., Alexanderson, H., Astakhov, V.I., Demidov, I., Dowdeswell, J.A., Funder, S., Gataullin, V., Henriksen, M., Hjort, C., Houmark-Nielsen, M., Hubberten, H.W., Ingylfsson, У., Jakobsson, M., Kjær, K.H., Larsen, E., Lokrantz, H., Lunkka, J.P., Lyså, A., Mangerud, J., Matiouchkov, A., Murray, A.S., Möller, P., Niessen, F., Nikolskaya, O., Polyak, L., Saarnisto, M., Siegert, C., Siegert, M.J., Spielhagen, R.F., Stein, R., 2004. Late Quaternary ice sheet history of northern Eurasia. Quat. Sci. Rev. doi:10.1016/j.quascirev.2003.12.008

Svendsen, J.I., Mangerud, J., 1997. Holocene glacial and climatic variations on Spitsbergen, Svalbard. The Holocene. doi:10.1177/095968369700700105

Swart, N., 2017. Natural causes of Arctic sea-ice loss. Nat. Clim. Chang. 7, 239.

Syvitski, J.P.M., Andrews, J.T., Dowdeswell, J. a., 1996. Sediment deposition in an iceberg-dominated glacimarine environment, East Greenland: basin fill implications. Glob. Planet. Change 12, 251–270. doi:10.1016/0921-8181(95)00023-2

Tang, C.C.L., Ross, C.K., Yao, T., Petrie, B., DeTracey, B.M., Dunlap, E., 2004. The circulation, water masses and sea-ice of Baffin Bay. Prog. Oceanogr. 63, 183–228. doi:10.1016/j.pocean.2004.09.005

Tarussov, A., 1992. The Arctic from Svalbard to Severnaya Zemlya: climatic reconstructions from ice cores, in: Bradley, R.S. and Jones, P.D. (Ed.), Climate since A.D. 1500. Routledge, London, New York, pp. 505–516.

Telesiński, M.M., Bauch, H.A., Spielhagen, R.F., Kandiano, E.S., 2015. Evolution of the central Nordic Seas over the last 20 thousand years. Quat. Sci. Rev. 121, 98–109. doi:10.1016/j.quascirev.2015.05.013

Telesiński, M.M., Spielhagen, R.F., Bauch, H.A., 2014. Water mass evolution of the Greenland sea since late glacial times. Clim. Past 10, 123–136. doi:10.5194/cp-10-123-2014

Telesiński, M.M., Spielhagen, R.F., Lind, E.M., 2014. A high-resolution Lateglacial and Holocene palaeoceanographic record from the Greenland Sea. Boreas 43, 273–285. doi:10.1111/bor.12045

ter Braak, C.J.F., Šmilauer, P., 2002. CANOCO Reference Manual and CanoDraw for Windows User's Guide: Software for Canonical Community Ordination (Version 4.5). Sect. Permut. Methods. Microcomput. Power, Ithaca, New York. doi:citeulike-article-id:7231853

Ternois, Y., Kawamura, K., Keigwin, L., Ohkouchi, N., Nakatsuka, T., 2001. A biomarker approach for assessing marine and terrigenous inputs to the sediments of sea of Okhotsk for the last 27,000 years. Geochim. Cosmochim. Acta. doi:10.1016/S0016-7037(00)00598-6

Thomas, D.N., Dieckmann, G.S., 2010. Sea Ice. Blackwell Publishing, Oxford.

Thomas, D.N., 2012. Sea ice, in: Bell, M.E. (Ed.), Life in Extremes: Environments, Organisms and Strategies for Survival. Oxford, U.K.

Thompson, D.W.J., Wallace, J.M., 1998. The Arctic oscillation signature in the wintertime geopotential height and temperature fields. Geophys. Res. Lett. 25, 1297. doi:10.1029/98GL00950

Thorndike, A.S., 1986. Kinematics of sea ice, in: Untersteiner, N. (Ed.), The Geophysics of Sea Ice. NATOASI Series, Series B, Physics. Plenum Press, New York, p. 489–549.

Tremblay, J.-E., Smith Jr., W.O., 2007. Chapter 8 Primary Production and Nutrient Dynamics in Polynyas. Elsevier Oceanogr. Ser. Volume 74, 239–269. doi:10.1016/S0422-9894(06)74008-9

Trouet, V., Esper, J., Graham, N.E., Baker, A., Scourse, J.D., Frank, D.C., 2009. Persistent positive North Atlantic oscillation mode dominated the Medieval Climate Anomaly. Science 324, 78–80. doi:10.1126/science.1166349

Tsamados, M., Feltham, D., Petty, A., Schroder, D., Flocco, D., 2015. Processes controlling surface, bottom and lateral melt of Arctic sea ice in a state of the art sea ice model. Philos. Trans. R. Soc. A 17, 10302. doi:10.1098/rsta.2014.0167

Tsukernik, M., Deser, C., Alexander, M., Tomas, R., 2010. Atmospheric forcing of Fram Strait sea ice export: A closer look. Clim. Dyn. 35, 1349–1360.

Uenzelmann-Neben, G., 2009. Cruise Report RV MARIA S . MERIAN Cruise MSM12-2 Reykjavik - Reykjavik. doi: 10.2312/cr_msm12_2

van Loon, H., Rogers, J.C., 1978. The Seesaw in Winter Temperatures between Greenland and Northern Europe. Part I: General Description. Mon. Weather Rev. doi:10.1175/1520-0493(1978)106<0296:TSIWTB>2.0.CO;2

Vare, L.L., Massé, G., Gregory, T.R., Smart, C.W., Belt, S.T., 2009. Sea ice variations in the central Canadian Arctic Archipelago during the Holocene. Quat. Sci. Rev. 28, 1354–1366. doi:10.1016/j.quascirev.2009.01.013

Velasco, V.M., Mendoza, B., 2008. Assessing the relationship between solar activity and some large scale climatic phenomena 42, 866–878. doi:10.1016/j.asr.2007.05.050

Venegas, S.A., Mysak, L.A., 2000. Is there a dominant timescale of natural climate variability in the Arctic? J. Clim. 13, 3412–3434. doi:10.1175/1520-0442(2000)013<3412:ITADTO>2.0.CO;2

Vinnikov, K.Y., Robock, A., Stouffer, R.J., Walsh, J.E., Parkinson, C.L., Cavalieri, D.J., Mitchell, J.F.B., Garrett, D., Zakharov, V.F., 1999. Global Warming and Northern Hemisphere Sea Ice Extent. Science. doi:10.1126/science.286.5446.1934

Vinther, B.M., Clausen, H.B., Johnsen, S.J., Rasmussen, S.O., Andersen, K.K., Buchardt, S.L., Dahl-Jensen, D., Seierstad, I.K., Siggaard-Andersen, M.L., Steffensen, J.P., Svensson, A., Olsen, J., Heinemeier, J., 2006. A synchronized dating of three Greenland ice cores throughout the Holocene. J. Geophys. Res. Atmos. 111, 1–11. doi:10.1029/2005JD006921

Vogt, C., Knies, J., Spielhagen, R.F., Stein, R., 2001. Detailed mineralogical evidence for two nearly identical glacial/deglacial cycles and Atlantic water advection to the Arctic Ocean during the last 90,000 years. Glob. Planet. Change 31, 23–44. doi:10.1016/S0921-8181(01)00111-4

Volkman, J.K., 2006. Lipid markers for marine organic matter, in: Volkman, J.K. (Ed.), Handbook of Environmental Chemistry. Springer-Verlag, Berlin, Heidelberg, pp. 27–70.

Volkman, J.K., 1986. A review of sterol markers for marine and terrigenous organic matter. Org. Geochem. 9, 83–99.

Volkman, J.K., Barrett, S.M., Dunstan, G.A., 1994. C_{25} and C_{30} highly branched isoprenoid alkenes in laboratory cultures of two marine diatoms. Org. Geochem. doi:10.1016/0146-6380(94)90202-X

Volkman, J.K., Barrett, S.M., Dunstan, G.A., Jeffrey, S.W., 1993a. Geochemical significance of the occurrence of dinosterol and other 4-methyl sterols in a marine diatom. Org. Geochem. 20, 7–15.

Volkman, J.K., Farrington, J., Gagosian, R.B., Wakeham, S.G., 1983. Lipid composition of coastal marine sediments from the Peru upwelling region, in: Advances in Organic Geochemistry 1981. pp. 228–240.

Volkman, J.K., Revill, A.T., Holdsworth, D.G., Fredericks, D., 2008. Organic matter sources in an enclosed coastal inlet assessed using lipid biomarkers and stable isotopes. Org. Geochem. doi:10.1016/j.orggeochem.2008.02.014

von Quillfeldt, C.H., 2004. The diatom Fragilariopsis cylindrus and its potential as an indicator species for cold water rather than for sea ice. Vie Milieu.

von Quillfeldt, C.H., Ambrose, W.G., Clough, L.M., 2003. High number of diatom species in first-year ice from the Chukchi Sea. Polar Biol. doi:10.1007/s00300-003-0549-1

Walsh, J. E., Chapman, W.L., 2001. 20th-century sea-ice variations from observational data. Ann. Glaciol. 33, 444–448.

Walsh, J.J., 1989. Arctic carbon sinks: Present and future. Global Biogeochem. Cycles. doi:10.1029/GB003i004p00393

Wang, J., Ikeda, M., 2000. Arctic oscillation and Arctic Sea-Ice oscillation. Geophys. Res. Lett. 27, 1287–1290.

Wanner, H., Beer, J., Bütikofer, J., Crowley, T.J., Cubasch, U., Flückiger, J., Goosse, H., Grosjean, M., Joos, F., Kaplan, J.O., Küttel, M., Müller, S.A., Prentice, I.C., Solomina, O.,

Stocker, T.F., Tarasov, P., Wagner, M., Widmann, M., 2008. Mid- to Late Holocene climate change: an overview. Quat. Sci. Rev. 27, 1791–1828. doi:10.1016/j.quascirev.2008.06.013

Wanner, H., Brönnimann, S., Casty, C., Luterbacher, J., Schmutz, C., David, B., 2001. North Atlantic Oscillation-Concepts and Studies. Surv. Geophys. 22, 321–382. doi:10.1023/A:1014217317898

Wanner, H., Solomina, O., Grosjean, M., Ritz, S.P., Jetel, M., 2011. Structure and origin of Holocene cold events. Quat. Sci. Rev. 30, 3109–3123. doi:10.1016/j.quascirev.2011.07.010

Wassmann, P., Duarte, C.M., Agustí, S., Sejr, M.K., 2011. Footprints of climate change in the Arctic marine ecosystem. Glob. Chang. Biol. 17, 1235–1249. doi:10.1111/j.1365-2486.2010.02311.x

Weckström, K., Massé, G., Collins, L.G., Hanhijärvi, S., Bouloubassi, I., Sicre, M.A., Seidenkrantz, M.S., Schmidt, S., Andersen, T.J., Andersen, M.L., Hill, B., Kuijpers, A., 2013. Evaluation of the sea ice proxy IP_{25} against observational and diatom proxy data in the SW Labrador Sea. Quat. Sci. Rev. 79, 53–62. doi:10.1016/j.quascirev.2013.02.012

Weidick, A., Bennike, O., Grafisk, S., 2007. Quaternary glaciation history and glaciology of Jakobshavn Isbrae and the Disko Bugt region, West Greenland: a review. Geol. Surv. Denmark Greenl. Bull. 14, 26–49.

Werner, A., 1993. Holocene moraine chronology, Spitsbergen, Svalbard: lichenometric evidence for multiple Neoglacial advances in the Arctic. The Holocene 3, 128–137.

Werner, K., Müller, J., Husum, K., Spielhagen, R.F., Kandiano, E.S., Polyak, L., 2016. Holocene sea subsurface and surface water masses in the Fram Strait – Comparisons of temperature and sea-ice reconstructions. Quat. Sci. Rev. 147, 194–209. doi:10.1016/j.quascirev.2015.09.007

Werner, K., Müller, J., Husum, K., Spielhagen, R.F., Kandiano, E.S., Polyak, L., 2015. Holocene sea subsurface and surface water masses in the Fram Strait - Comparisons of temperature and sea-ice reconstructions. Quat. Sci. Rev. doi:10.1016/j.quascirev.2015.09.007

Werner, K., Spielhagen, R.F., Bauch, D., Hass, H.C., Kandiano, E., 2013. Atlantic Water advection versus sea-ice advances in the eastern Fram Strait during the last 9 ka: Multiproxy evidence for a two-phase Holocene. Paleoceanography 28, 283–295. doi:10.1002/palo.20028

Werner, K., Spielhagen, R.F., Bauch, D., Hass, H.C., Kandiano, E., Zamelczyk, K., 2011. Atlantic Water advection to the eastern Fram Strait - Multiproxy evidence for late Holocene variability. Palaeogeogr. Palaeoclimatol. Palaeoecol. 308, 264–276. doi:10.1016/j.palaeo.2011.05.030

Willmes, S., Heinemann, G., 2016. Sea-ice wintertime lead frequencies and regional characteristics in the Arctic, 2003-2015. Remote Sens. 8, 2003–2015. doi:10.3390/rs8010004

Wohlfahrt, J., Harrison, S.P., Braconnot, P., 2004. Synergistic feedbacks between ocean and vegetation on mid- and high-latitude climates during the mid-Holocene. Clim. Dyn. 22, 223–238. doi:10.1007/s00382-003-0379-4

Wollenburg, E, Kuhnt, W., Mackensen, A., 2001. in Arctic Ocean paleoproductivity and hydrography summer East Greenland Current - passage of outflowing Arctic. Paleoceanography 16, 65–77.

Wollenburg, J.E., Knies, J., Mackensen, A., 2004. High-resolution paleoproductivity fluctuations during the past 24 kyr as indicated by benthic foraminifera in the marginal Arctic Ocean. Palaeogeogr. Palaeoclimatol. Palaeoecol. 204, 209–238. doi:https://doi.org/10.1016/S0031-0182(03)00726-0

Xiao, X., Fahl, K., Müller, J., Stein, R., 2015a. Sea-ice distribution in the modern Arctic Ocean: Biomarker records from trans-Arctic Ocean surface sediments. Geochim. Cosmochim. Acta 155, 16–29. doi:10.1016/j.gca.2015.01.029

Xiao, X., Fahl, K., Stein, R., 2013. Biomarker distributions in surface sediments from the Kara and Laptev seas (Arctic Ocean): Indicators for organic-carbon sources and sea-ice coverage. Quat. Sci. Rev. 79, 40–52. doi:10.1016/j.quascirev.2012.11.028

Xiao, X., Stein, R., Fahl, K., 2015b. MIS 3 to MIS 1 temporal and LGM spatial variability in Arctic Ocean sea ice cover: Reconstruction from biomarkers. Paleoceanography 30, 969–983. doi:10.1002/2015PA002814

Xiao, X., Zhao, M., Luise, K., Sha, L., Eiríksson, J., Gudmundsdóttir, E., Jiang, H., Guo, Z., 2017. Deglacial and Holocene sea – ice variability north of Iceland and response to ocean circulation changes. Earth Planet. Sci. Lett. 472, 14–24. doi:10.1016/j.epsl.2017.05.006

Xu, Y., Jaffé, R., Wachnicka, A., Gaiser, E.E., 2006. Occurrence of C_{25} highly branched isoprenoids (HBIs) in Florida Bay: Paleoenvironmental indicators of diatom-derived organic matter inputs. Org. Geochem. doi:10.1016/j.orggeochem.2006.02.001

Young, N.E., Schweinsberg, A.D., Briner, J.P., Schaefer, J.M., 2015. Glacier maxima in Baffin Bay during the Medieval Warm Period coeval with Norse settlement. Sci. Adv. 1, e1500806–e1500806. doi:10.1126/sciadv.1500806

Yruela, I., Barbe, A., Grimalt, J.O., 1990. Determination of double bond position and geometry in linear and highly branched hydrocarbons and fatty acids from gas chromatography-mass spectrometry of epoxides and diols generated by stereospecific resin hydration. J. Chromatogr. Sci. doi:10.1093/chromsci/28.8.421

Yunker, M.B., Macdonald, R.W., Snowdon, L.R., Fowler, B.R., 2011. Alkane and PAH biomarkers as tracers of terrigenous organic carbon in Arctic Ocean sediments. Org. Geochem. 42, 1109–1146. doi:10.1016/j.orggeochem.2011.06.007

Yunker, M.B., Macdonald, R.W., Veltkamp, D.J., Cretney, W.J., 1995. Terrestrial and marine biomarkers in a seasonally ice-covered Arctic estuary - integration of multivariate and biomarker approaches. Mar. Chem. 49, 1–50. doi:10.1016/0304-4203(94)00057-K

Zielinski, G.A., 2000. Use of paleo-records in determining variability within the volcanism-climate system. Quat. Sci. Rev. 19, 417–438. doi:10.1016/S0277-3791(99)00073-6

Zonneveld, K.A.F., Marret, F., Versteegh, G.J.M., Bogus, K., Bonnet, S., Bouimetarhan, I., Crouch, E., de Vernal, A., Elshanawany, R., Edwards, L., Esper, O., Forke, S., Grøsfjeld, K., Henry, M., Holzwarth, U., Kielt, J.F., Kim, S.Y., Ladouceur, S., Ledu, D., Chen, L., Limoges, A., Londeix, L., Lu, S.H., Mahmoud, M.S., Marino, G., Matsouka, K., Matthiessen, J., Mildenhal, D.C., Mudie, P., Neil, H.L., Pospelova, V., Qi, Y., Radi, T., Richerol, T., Rochon, A., Sangiorgi, F., Solignac, S., Turon, J.L., Verleye, T., Wang, Y., Wang, Z., Young, M., 2013. Atlas of modern dinoflagellate cyst distribution based on 2405 data points. Rev. Palaeobot. Palynol. doi:10.1016/j.revpalbo.2012.08.003

ldeo.columbia.edu/res/pi/NAO/ Visbeck, M.; Lamont-Doherty Earth Observatory, Columbia University; http://www.ldeo.columbia.edu/res/pi/NAO/

meereisportal.de; http://www.meereisportal.de

npolar.no; Norsk Polarinsitutt; http://www.npolar.no/no/

nsidc.org; NSIDC; National Snow and Sea Ice Data Center; https://nsidc.org

NODC; National Oceanographic Data Center; https://www.nodc.noaa.gov

Quote on Page v taken from “The Sea Ice Never Stops – Circumpolar Inuit Reflections on Sea Ice use & Shipping Routes in Inuit Nunaat”, Inuit Circumpolar Council, Canada, 2014

9. Appendix

Appendix A - Chapter 3

A.1 Relationship of IP_{25}, to brassicasterol, dinosterol and HBI III (in µg/gSed) for the complete surface sediment biomarker dataset.

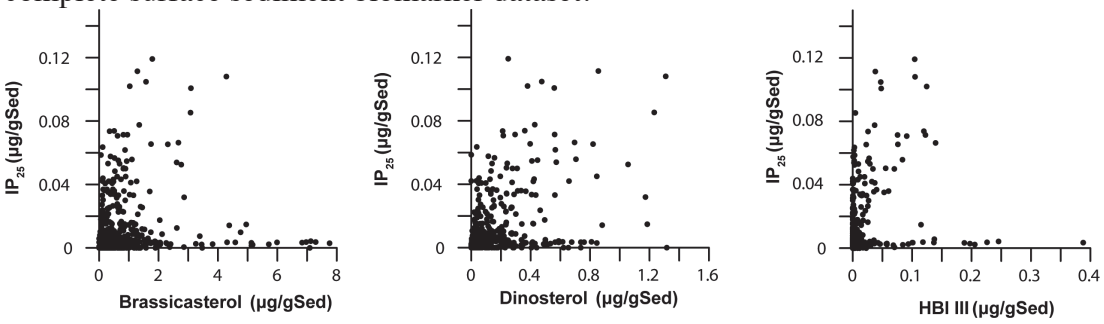

A.2 Correlations of P_BIP_{25}, P_DIP_{25} and $P_{III}IP_{25}$ with sea ice associated diatoms and preliminary MAT dinocyst sea ice reconstructions in Baffin Bay.

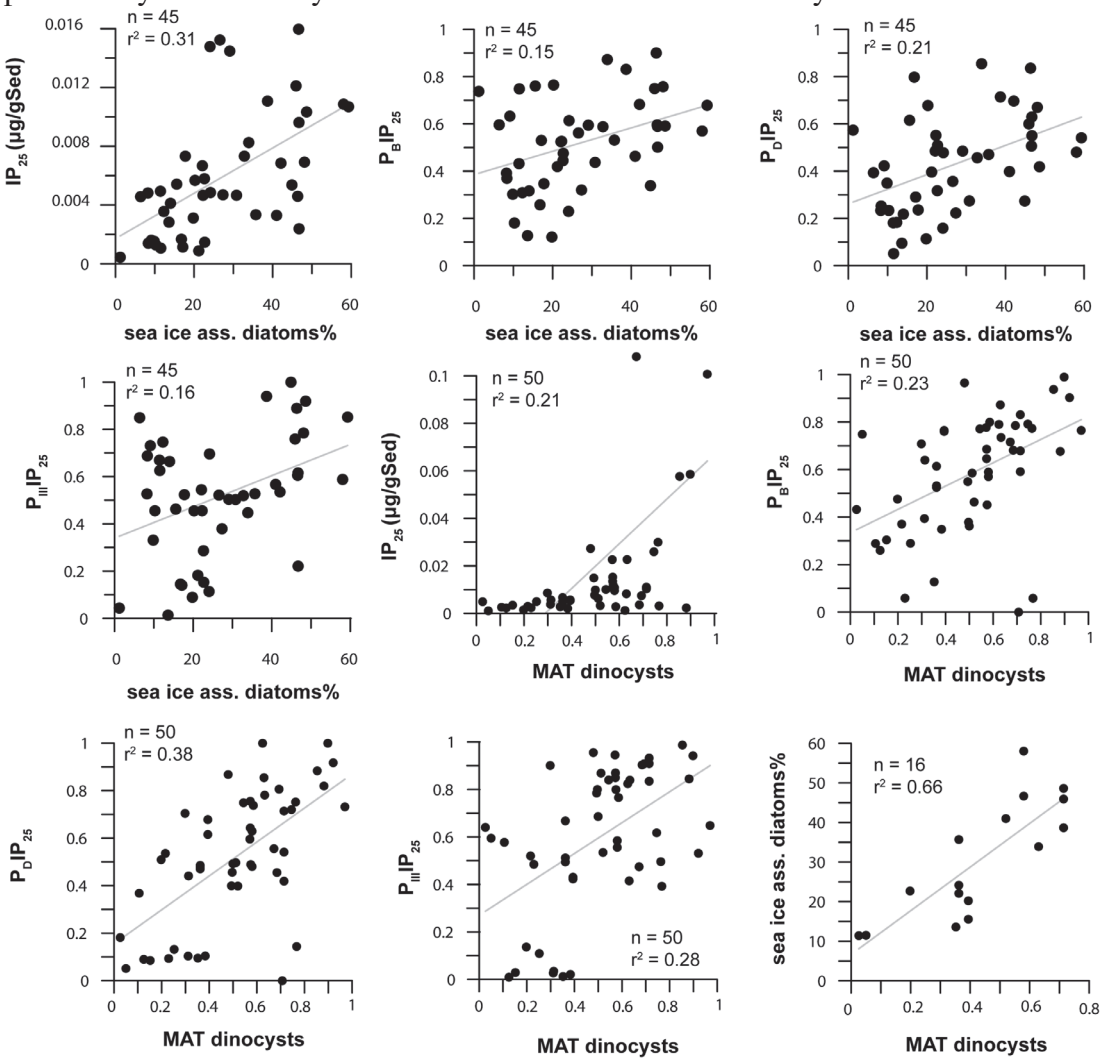

A3. Correlations of IP_{25}, P_BIP_{25}, P_DIP_{25} and $P_{III}IP_{25}$ with modern spring sea ice concentrations (1978-2015; *Cavallieri et al., 1996; updated 2015*) for ***(a)*** the complete dataset, ***(b)*** Baffin Bay and the West Greenland Shelf, ***(c)*** Fram Strait and the East Greenland Shelf (this study, *Müller et al., 2011; Navarro-Rodriguez et al., 2013; Xiao, et al., 2015a)*, ***(d)*** the Arctic Ocean and Russian marginal seas (this study, *Xiao, et al., 2013, 2015a)* and ***(e)*** Barents Sea and the Norwegian Sea (this study, *Navarro-Rodriguez et al., 2013; Belt et al., 2015; Xiao, et al., 2015a; Smik et al., 2016)*.

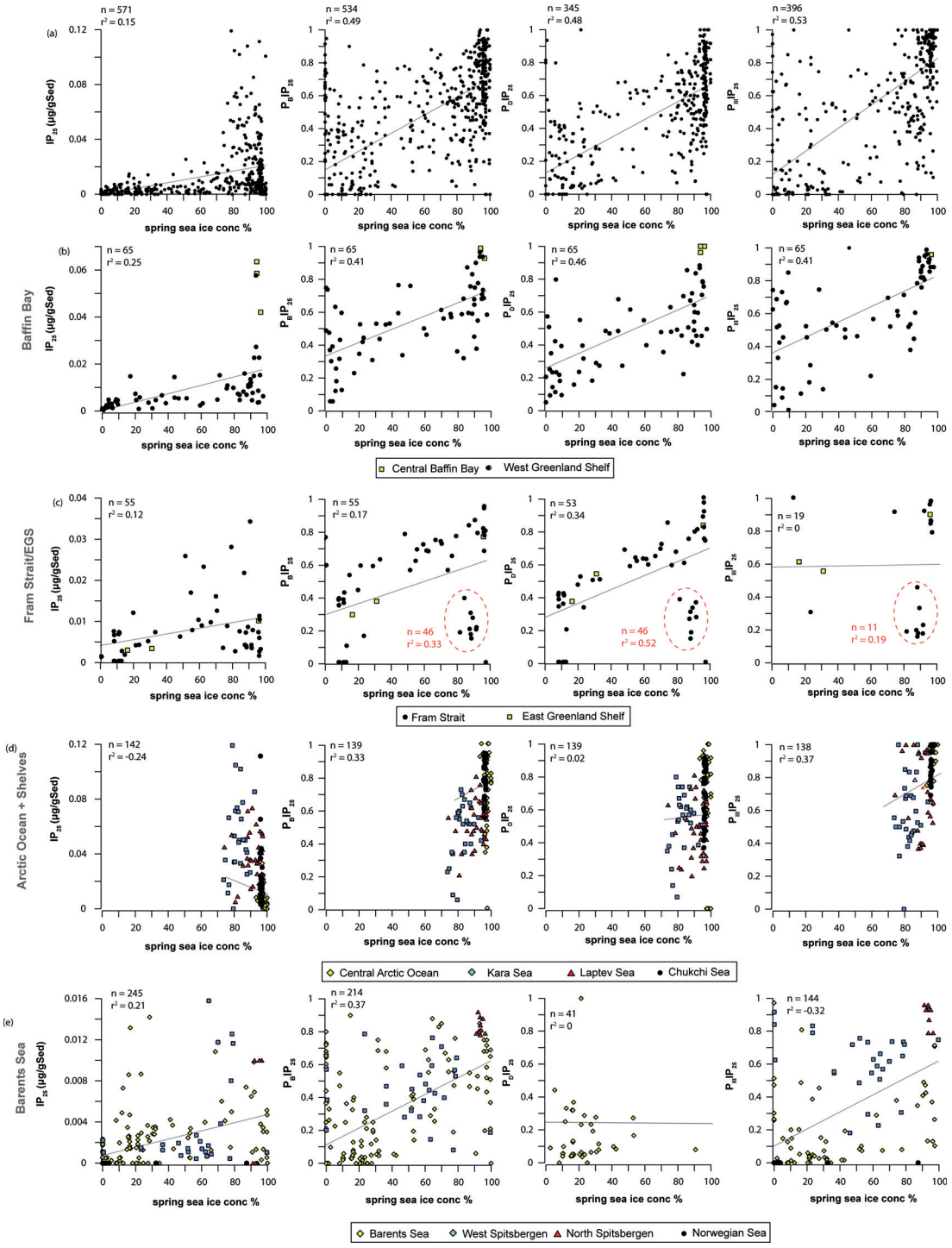

Appendix B – Chapter 4

B1. Age-depth plot of AMS ^{14}C ages of ***A.*** box core PS2641-5 and ***B.*** gravity core PS2641-4. Orange areas indicate core sections with age model uncertainties (See *2.2. Chronology*). All AMS ^{14}C ages were corrected for a reservoir age of 400 years. For details see *Perner et al., 2015*.

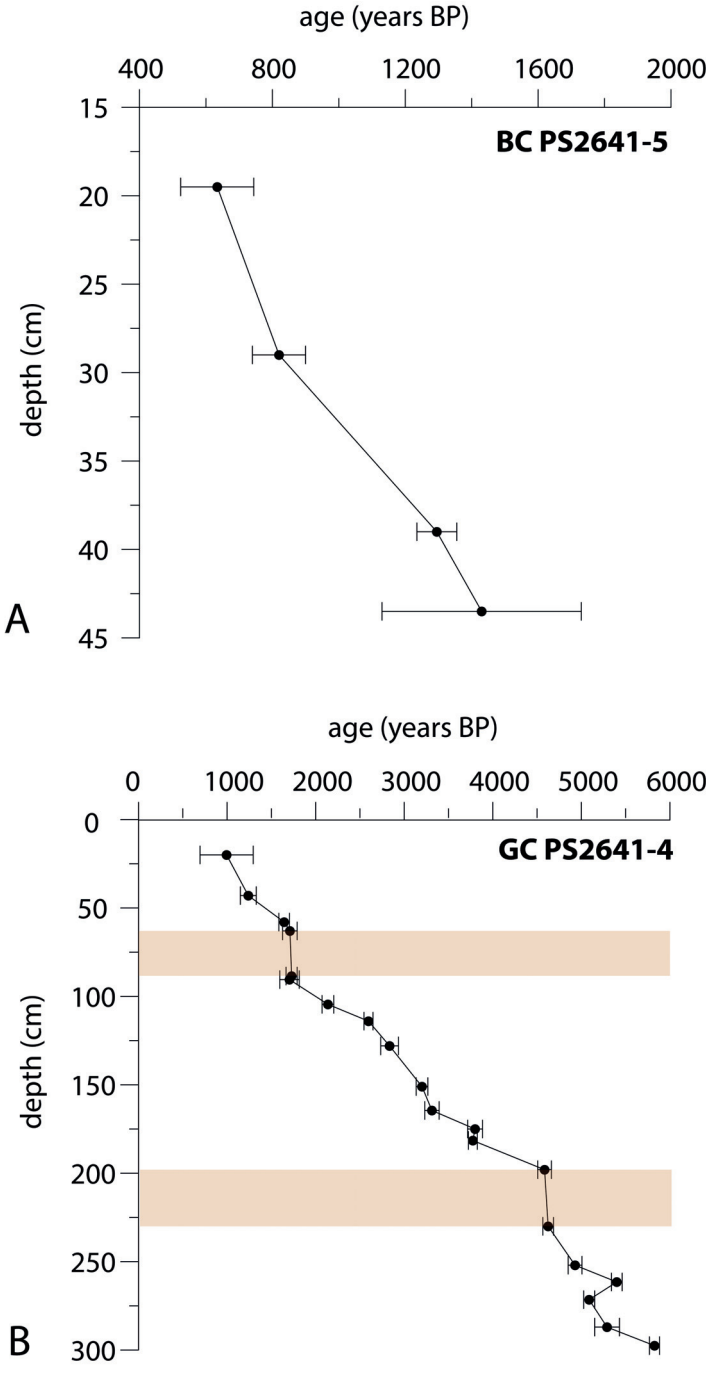

B2. ***A.*** Total organic carbon content (TOC, in weight %) and biomarker concentrations (in $\mu g*g^{-1}$) of gravity core PS2641-4 versus depth (in cm). **B.** Total Organic Carbon content (in weight %) and biomarker concentrations of box core PS2641-5 versus depth (in cm). The thick black line represents the 5-point average, the thin grey line represents the original data, points indicate measurements. Orange shaded areas indicate core sections with age model insecurities (*see 2.2. Chronology*, for details *Perner et al., 2015*)

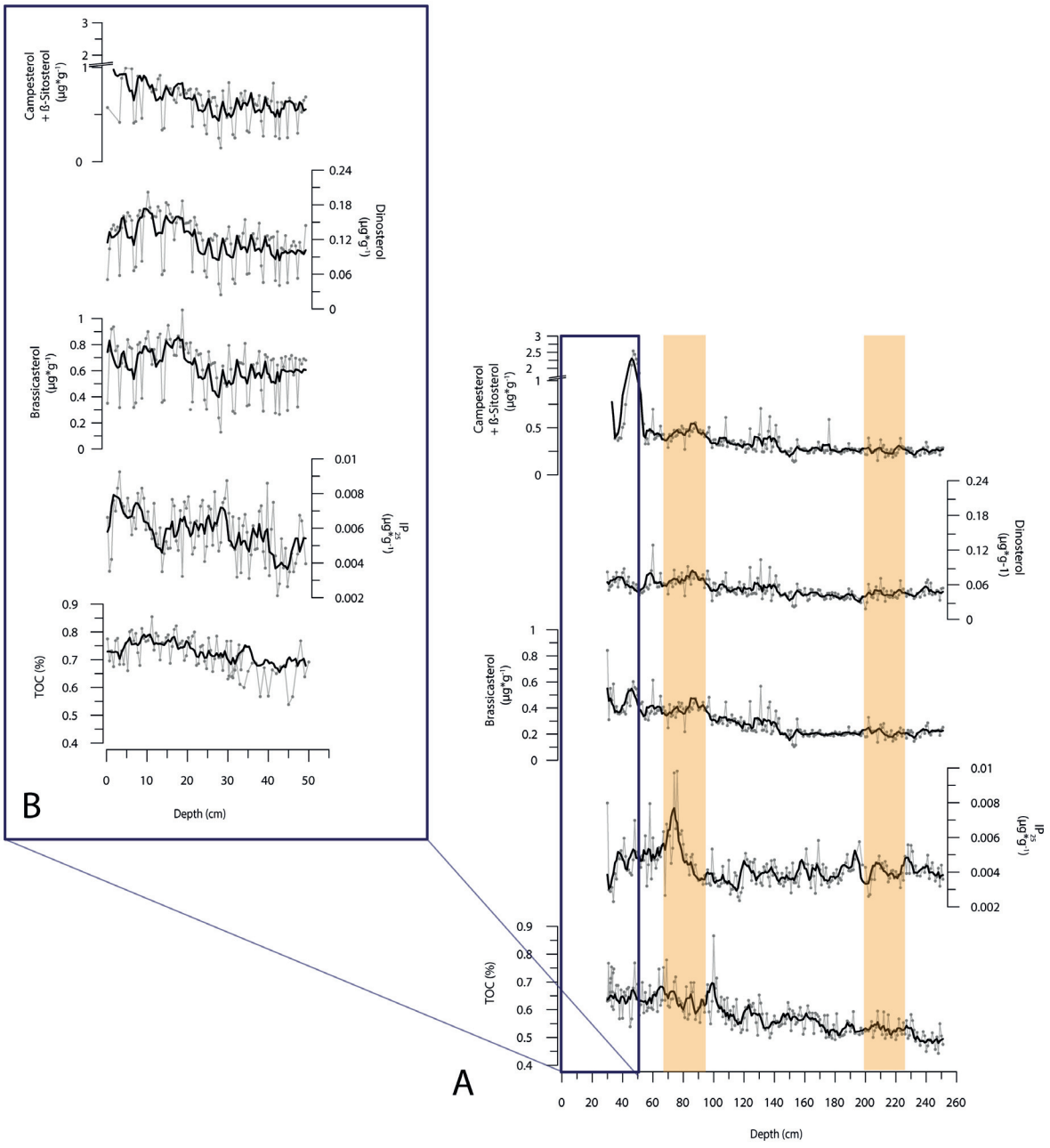

B3. ***A.*** Correlation of IP_{25} and the HBI-diene (in µg* g^{-1}), showing a relatively good correlation (r = 0.68). Concentrations of ***B.*** HBI diene and ***C.*** IP_{25} and (in µg* g^{-1}) against age (kyr BP).

Except for the uppermost part of the record the IP_{25} and the HBI-diene concentrations display a quite similar trend and variability and both compounds show a relatively good direct correlation. This may suggest that both compounds originate from the same source, i.e. sea ice diatoms *(cf. Vare et al., 2009)*. The HBI diene, however, has also been found in more temperate regions and fresh-water wetlands *(e.g. Summons et al., 1993, He et al., 2016*), i.e. non-ice covered regions Therefore, this molecule might not be an ultimate proxy for Arctic sea ice like IP_{25}. Thus, we will not further use the HBI diene in the interpretation of our biomarker records.

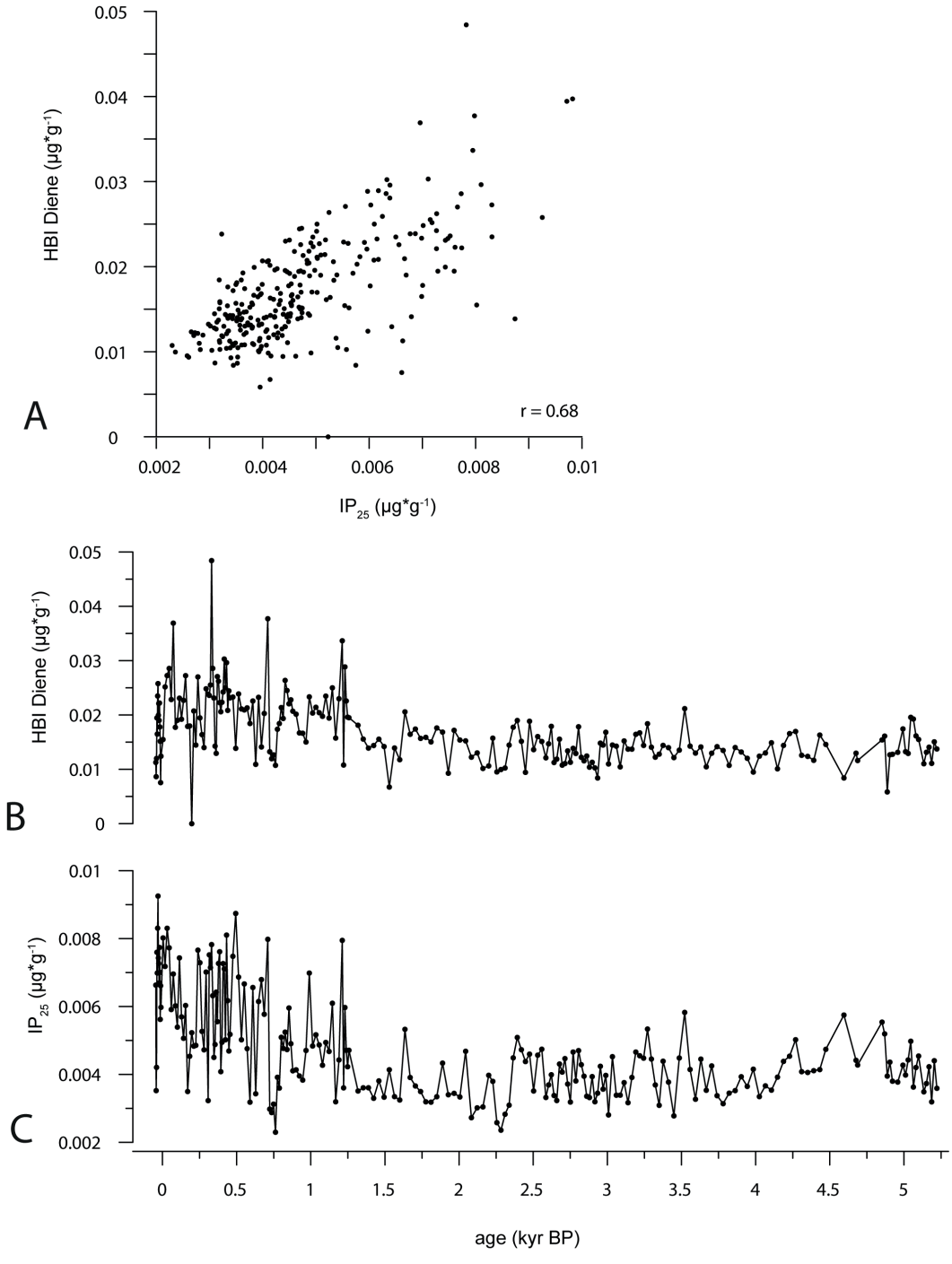

B4. ***A.*** Concentration of terrigenous sterols (in µg*g^{-1}) versus abundances of cold agglutinated foraminifera group (%) over the past 600 years. ***B.*** IP_{25} concentrations (in µg*g^{-1}) versus abundances of cold agglutinated foraminifera group (%) over the past 600 years.

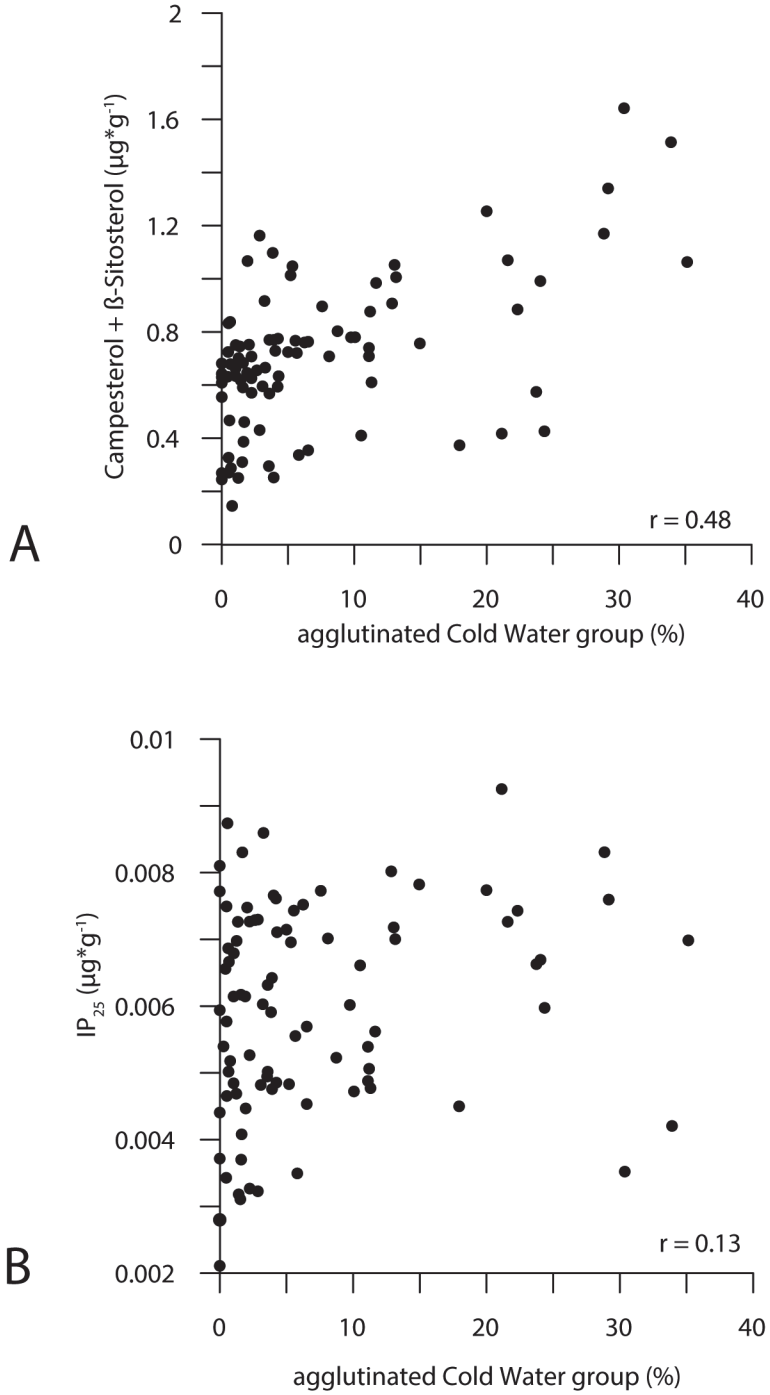

Appendix C – Chapter 5

C1. Comparison of different biomarker extraction methods, ASE and sonication and resulting biomarker indices. The red line with black dots indicates results of sonication; the black line with black triangles indicates results of ASE extraction.

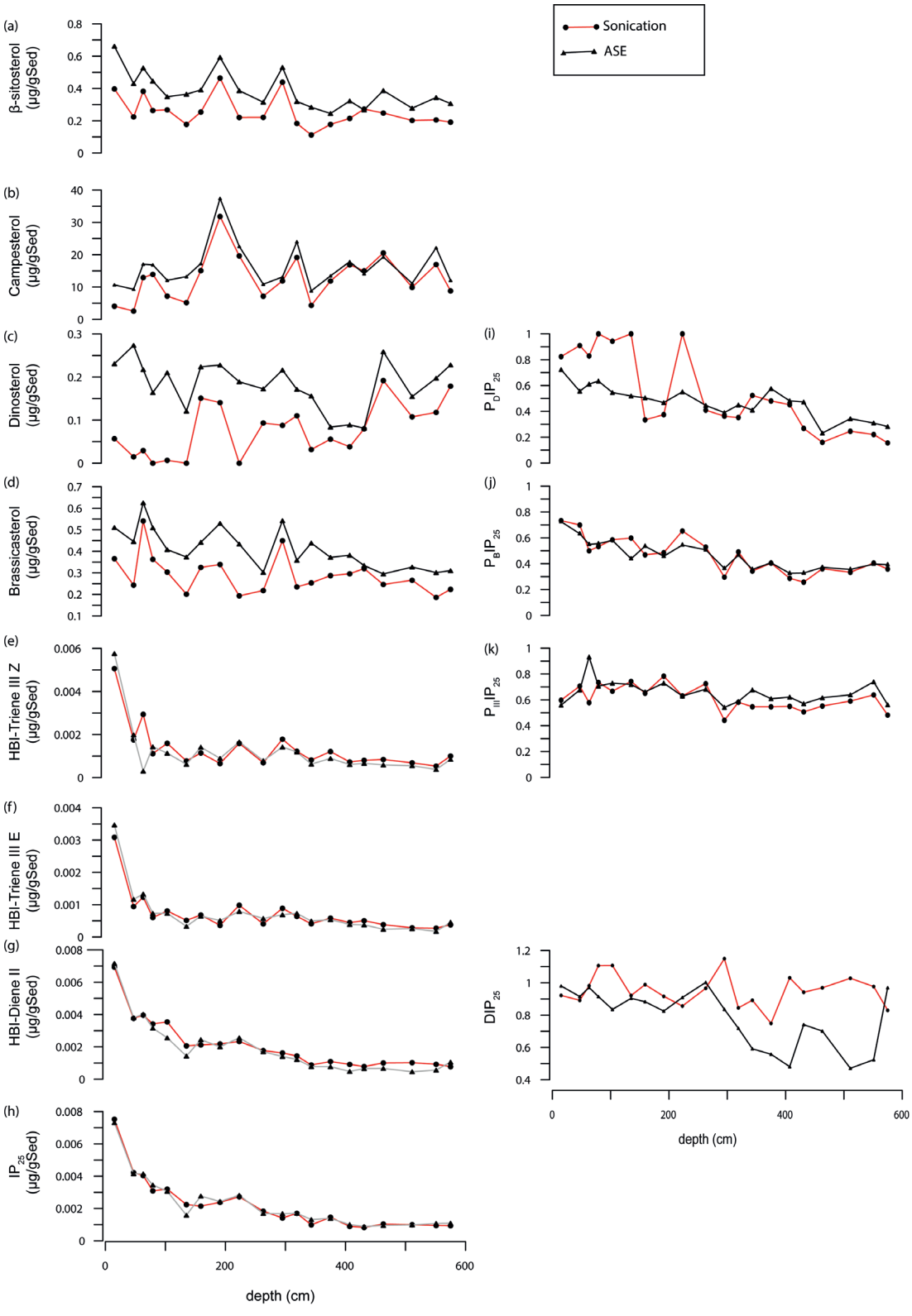

C2. Satellite measured monthly sea ice concentrations in Baffin Bay from 1978-2015 (*Cavalieri et al., 1996; updated 2015*). The white diamond indicates the position of Core 343310.

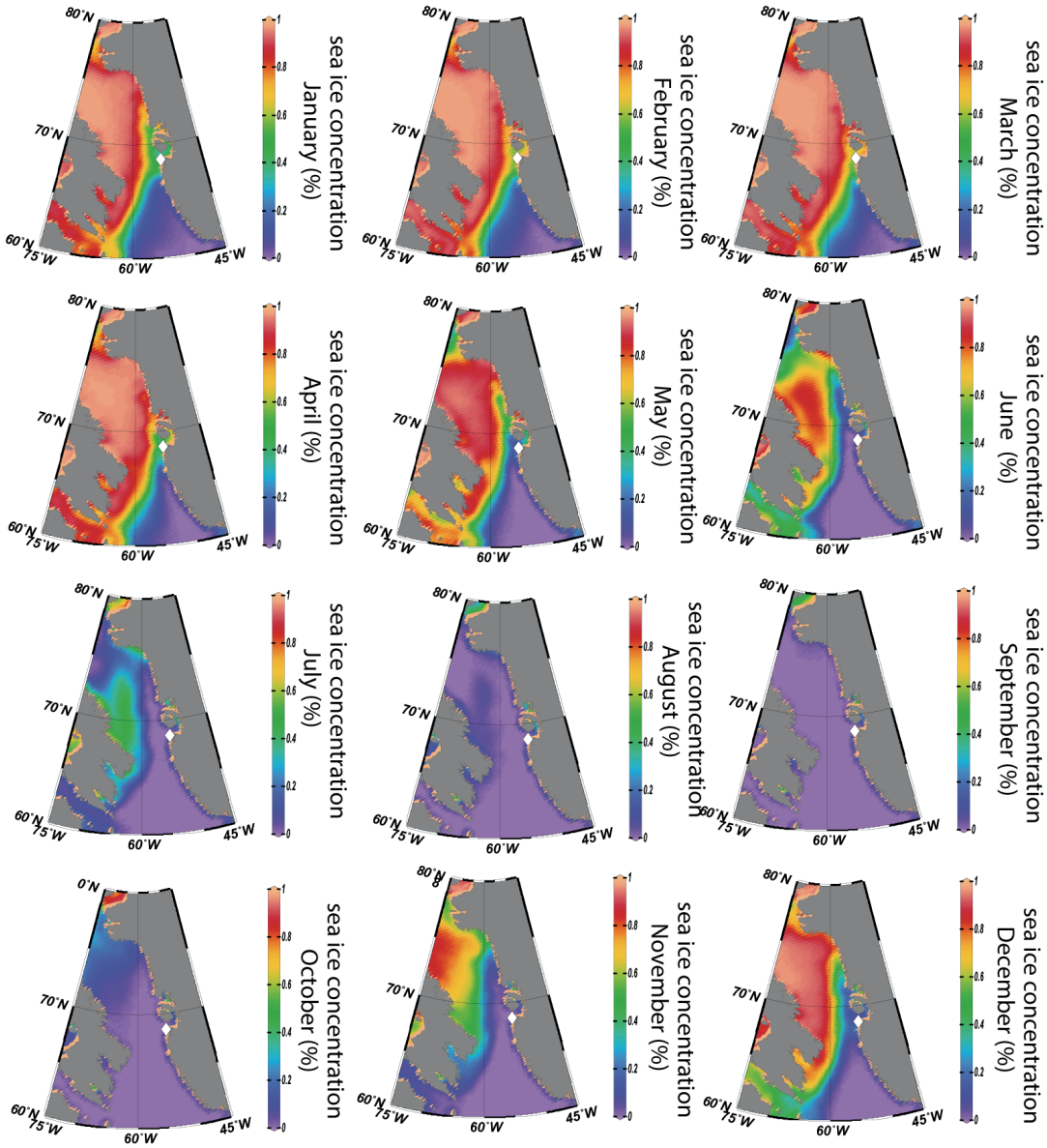

C3. Biomarker concentrations ***(a)*** campesterol+β-sitosterol, ***(b)*** dinosterol, ***(c)*** brassicasterol, ***(d)*** HBI III, ***(e)*** HBI II, ***(f)*** IP_{25} (all in µg/g sediment) and total organic carbon content (TOC; in %) of Core 343310 against depth (cm).

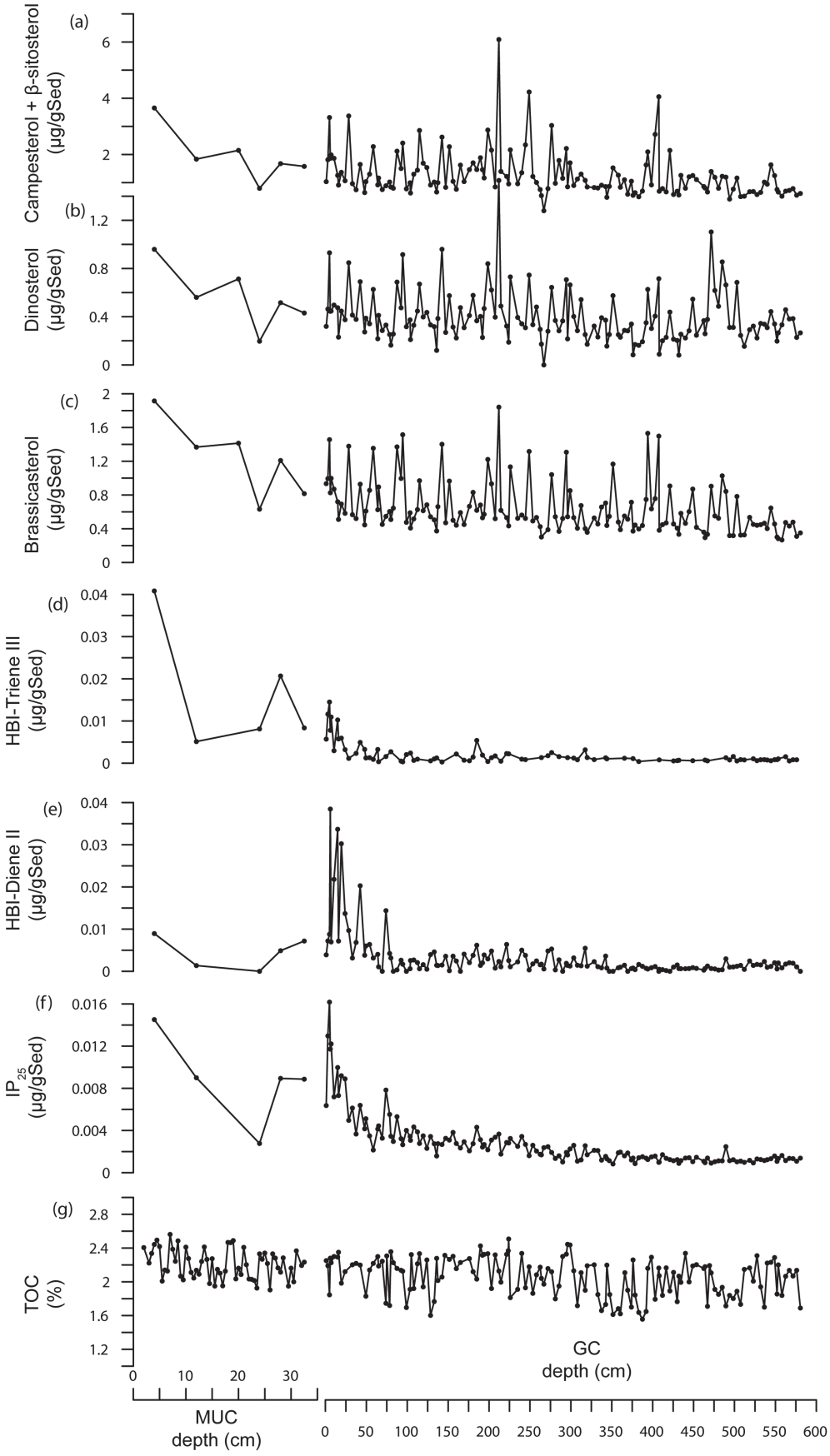

C4. Comparison of the sea ice indices $P_{III}IP_{25}$, P_BIP_{25} and P_DIP_{25} (red line) from Core 343310. P_BIP_{25} and P_DIP_{25} showing nearly identical values.

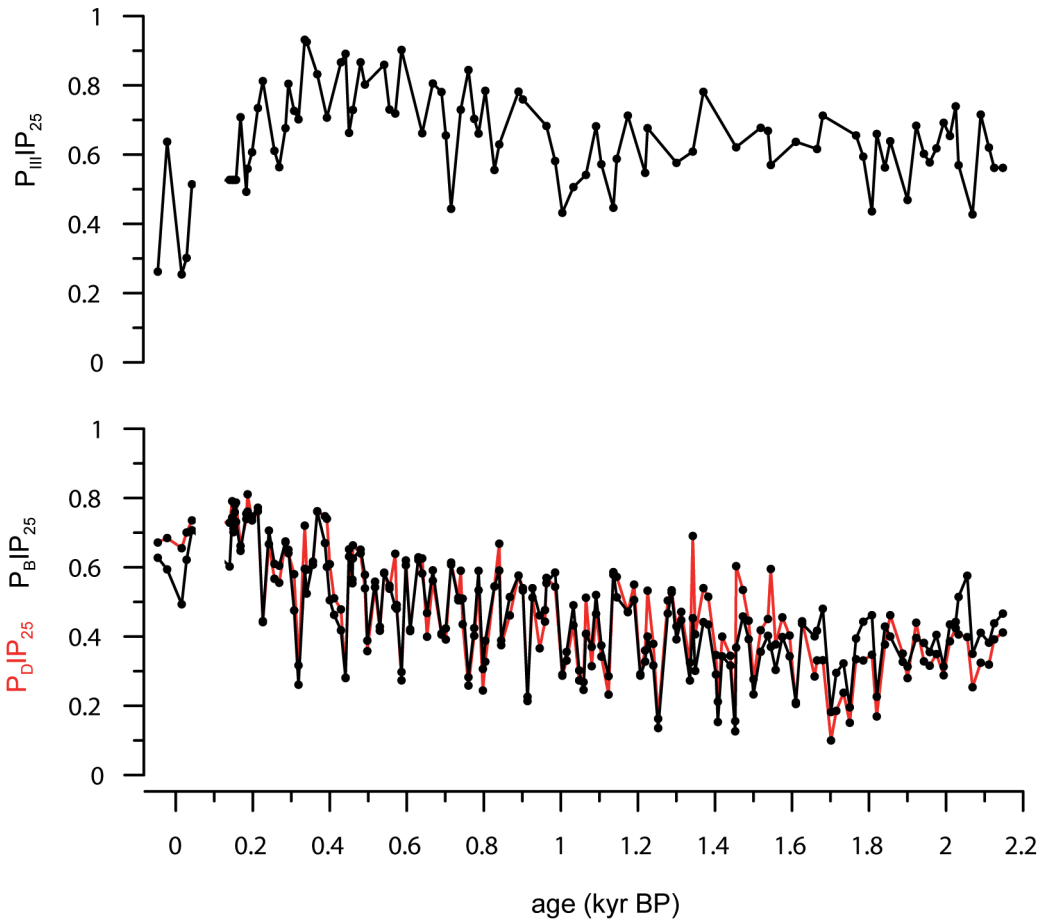

C5. Correlations of sea ice concentrations (1978-2015; *Cavalieri et al., 1996; updated 2015*) and $P_{III}IP_{25}$ for each month.

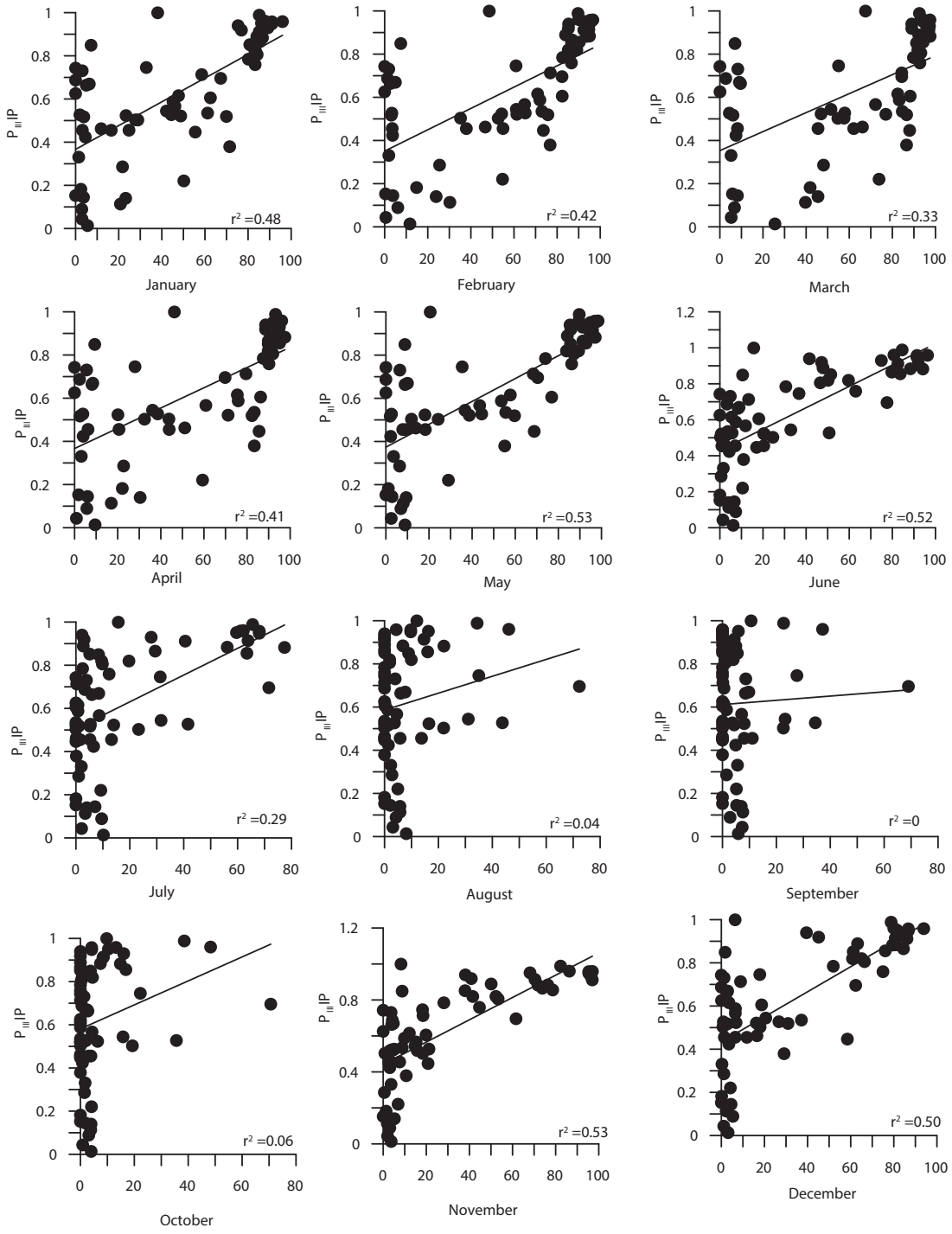

C6. Correlations of sea ice concentrations (1978-2015; *Cavalieri et al., 1996; updated 2015*) and P_DIP_{25} for each month.

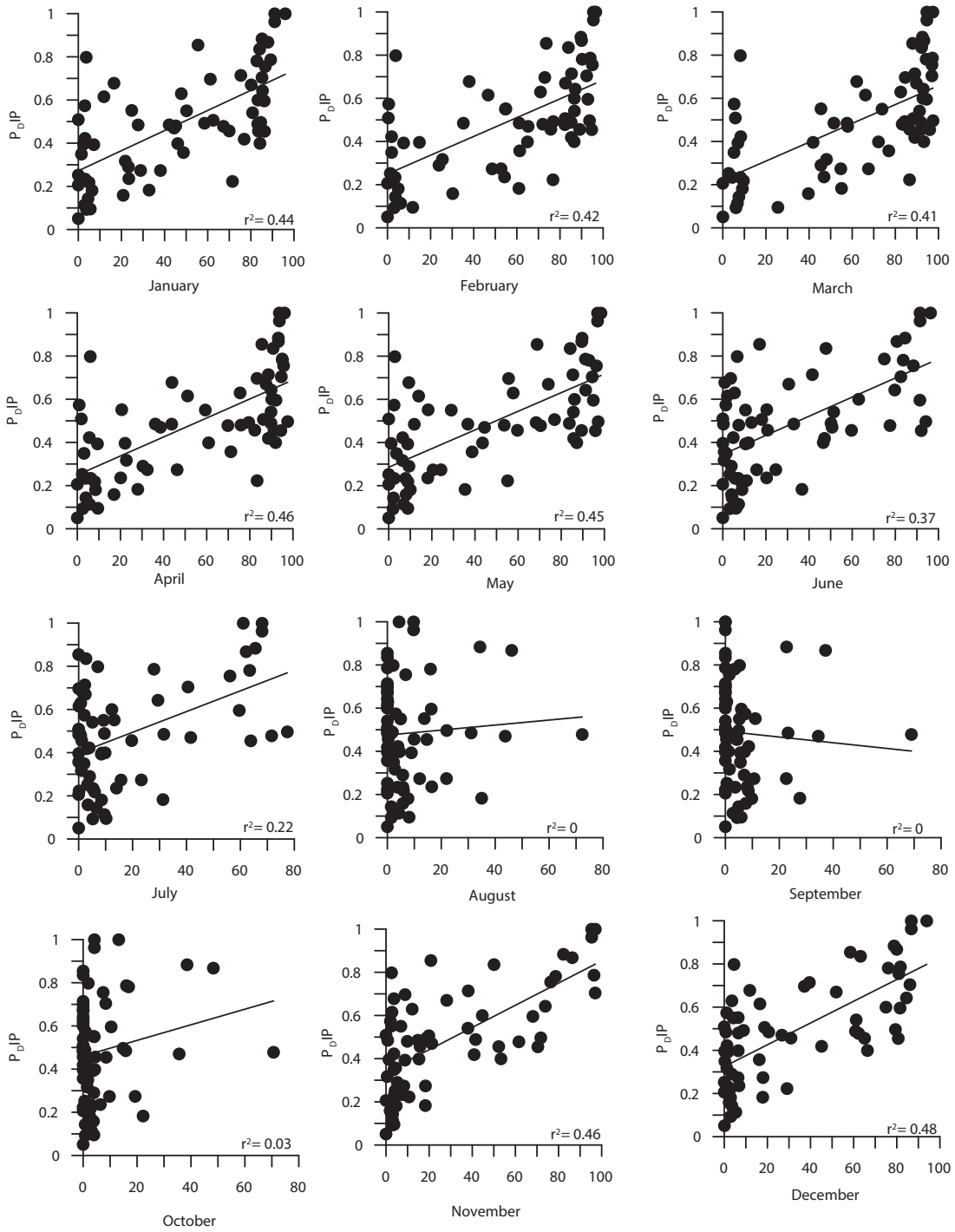

C7. Correlations of sea ice concentrations (1978-2015; *Cavalieri et al., 1996; updated 2015*) and P_BIP_{25} for each month.